Characterization of high-density prion protein oligomers in rapid progressive and sporadic Alzheimer's disease

Dissertation

for the award of the degree

"Doctor rerum naturalium" (Dr. rer. nat.)

of the Georg-August-Universität Göttingen

within the doctoral program "Biology"

of the Georg-August University School of Science (GAUSS)

Submitted by

MOHSIN SHAFIQ

from Lahore, Pakistan

Göttingen, 2019

Thesis Committee

Anleiter/in: **Dr. rer. nat. Saima Zafar**

Prion research group, Department of Neurology, UMG, Göttingen.

Betreuer and Referent: **Prof. Dr. Thomas Meyer**

Department of Psychosomatic Medicine and Psychotherapy, UMG, Göttingen.

Betreuer and Korreferent: **PD Dr. Michael Hoppert**

Department of General Microbiology, Georg August University Göttingen.

Members of the Examination Board

Prof. E. A. Wimmer

Department of Developmental Biology, Göttingen Center for Molecular Biosciences, Göttingen.

Prof. Dr. Stefan Jacobs

Department of NanoBiophotonics, Max Planck Institute for Biophysical Chemistry, Göttingen.

Dr. Dieter Klopfenstein

Department of Biophysics, University of Göttingen, Göttingen.

Prof. Dr. Uwe Groß

Institute for Medical Microbiology, University Medical Center Göttingen.

Date of oral examination: 14-Jan-2019

DECLARATION

I hereby declare that the Ph.D. thesis entitled “Characterization of high-density prion protein oligomers in rapid progressive and sporadic Alzheimer’s disease” is exclusively my own work. It is written solely by me and it does not contain any already published / written material except quoted with references

Mohsin Shafiq Göttingen, December 18th, 2018

Dedicated to

My loving parents

Contents

1 Introduction *1*

1.1 Alzheimer's disease **1**

1.2 Clinical presentation **1**

1.2.1 Senile plaques and neurofibrillary tangles 2

1.2.1.1 Amyloid precursor protein and biosynthesis of amyloid-β 2

1.2.1.2 Tau tangles and their biosynthesis 4

1.3 Genetic and non-genetic risk factors of Alzheimer's disease **5**

1.3.1 Non-genetic risk factors 5

1.3.2 Genetic risk factors 5

1.3.3 *APOE* polymorphism 5

1.4 Diagnosis **6**

1.4.1 Neuropsychological assessments 6

1.4.2 Neuroimaging 7

1.4.3 Biomarkers for Alzheimer's disease 7

1.5 Neuropathological profiling of Alzheimer's disease **8**

1.6 Subtypes classification of Alzheimer's disease **9**

1.6.1 Atypical pathological presentation in Alzheimer's disease 10

1.7 Rapidly progressive Alzheimer's disease **11**

1.7.1 History 11

1.7.2 Clinical features 11

1.7.3 Biomarkers and genetic linkages 12

1.7.4 Biochemistry of rpAD 13

1.8 Proteopathic oligomers and neurodegeneration **14**

1.9 Alzheimer's disease and Prion protein **15**

1.9.1 Prion protein -structure, functions, trafficking and pathological strains 15

1.9.1.1 Structure and biosynthesis 15

1.9.1.2 Signaling mediated by the PrP^{C} 17

1.9.1.3 Prion diseases and conversion of PrP^{C} into PrP^{Sc} 17

1.9.2 Involvement of prion protein in Alzheimer's disease 20

1.9.2.1 Prion-like behavior of Aβ and tau 20

1.9.2.2 PrP^{C} inhibition of BACE1 20

1.9.2.3 PrP^{C} as a receptor for Aβ oligomers 20

1.9.2.4 PrP^{C} alpha- cleavage shedding by ADAMs, controlling the fibrillation of Aβ 21

1.9.2.5 Codon 129 polymorphism and onset of AD 21

1.10 Study objectives 22

2 Materials and methods 23

2.1 Materials 23

2.1.1 Antibodies 23
2.1.2 Chemicals 24
2.1.3 Kits 24
2.1.4 Laboratory equipment and other materials 24
2.1.5 Software 25
2.1.6 Stock Solutions 25

2.2 Methods 27

2.2.1 Sample collection and processing 27
2.2.2 Pathological profiles 28
2.2.3 Ethics statement 29
2.2.4 Protein extraction 30
2.2.5 Protein concentration estimation 30
2.2.6 SDS-PAGE and immunoblot analysis 31
2.2.7 Co-immunoprecipitation from frontal cortex lysates 31
2.2.8 Sub-cellular (extracellular, intracellular and membrane) proteins enrichment 32
2.2.9 Sucrose-gradient ultracentrifugation 33
2.2.10 Preparation of protein and peptide pools from high-density gradient fractions 34
2.2.11 Co-immunoprecipitation of density variant fractions 34
2.2.12 Proteinase K digestion 34
2.2.13 Silver staining 34
2.2.14 Real-time quaking-induced cyclic amplification (RT-QuIC) 35
2.2.15 Staining of cryopreserved and formalin-fixed paraffin-embedded (FFPE) tissues 35
2.2.16 Confocal laser scanning and image quantification 36
2.2.17 Mass spectrometry-spectral counting 37
2.2.17.1 Peptide digestion and extraction 37
2.2.17.2 Peptide identification 37
2.2.18 SWATH-MS (Sequential Windowed Acquisition of All Theoretical Fragment Ion Mass Spectra)-based global proteomics 38
2.2.18.1 Library preparation 38
2.2.18.2 Quantitative SWATH measurement 39
2.2.19 Statistical analysis 39
2.2.20 Bioinformatic analysis 40

3 Results 41

3.1 Characterization of the rpAD cohort 41
3.1.1 Localization of amyloid plaques and Tau tangles 41
3.1.1.1 Amyloid plaques 41
3.1.1.2 Tau tangles 42
3.1.2 Expressions of amyloid-β and hyperphosphorylated Tau 44
3.1.3 Differential kinome 45
3.2 Differential regulation of prion protein metabolism 46
3.2.1 Subtype-specific alterations in PrP expression 46
3.2.2 Differential localization of PrP isoforms in cerebral tissue 47
3.2.3 Characteristic PrP^C interactome identification in spAD and rpAD human brains 49
3.2.4 Confirmation of unique rpAD-specific PrP interactors 53
3.3 Identification of disease-specific PrP oligomers 54
3.3.1 Proteinase-K (PK) resistance and absence of seeding activity 56
3.4 Proteomic characterization of disease subtype-specific high-density fractions 58
3.4.1 Disease subtype-specific clustering 59
3.4.2 Subtype-specific reference global proteome 61
3.4.3 Evaluated physiological domains 61
3.4.3.1 Proteopathic burden 62
3.4.3.2 Protein degradation machinery 63
3.4.3.3 Ras-related proteins 64
3.4.3.4 Cytoskeletal proteins 66
3.4.3.5 Subtype-specific changes in chaperones 68
3.5 Identification of binding interactors for high-density prion oligomers (HDPs) 69
3.5.1 Rapidly progressive Alzheimer's disease-specific high-density PrP interactors 70
3.5.2 The physiological coherence of subtype-specific high-density PrP binding proteins 72
3.6 Growth arrest-specific 2-like 2 (G2L2) and potential interaction to HDPs 73
3.6.1 Expression of G2L2 and associated proteins in Alzheimer's subtypes 73
3.6.2 Colocalization of G2L2 and associated proteins in brain frontal cortex 74
3.6.2.1 Neuronal co-localization of G2L2 and PrP 74
3.6.2.2 G2L2 and EB-1 binding 75
3.6.2.3 G2L2/tubulin-α colocalization 77
3.6.2.4 G2L2/actin-β colocalization 78
3.6.2.5 Actin-β/tubulin-α integration 79
4 Discussion 81
4.1 Amyloid plaques and Tau tangles 81

4.2 Differential signal transduction 82

4.3 Prion protein metabolism (differential glycoforms and distribution) 83

4.4 Subtype-specific PrP^C interactors 84

4.5 Prion protein oligomers in rpAD 86

4.6 Differentially distributed proteins in high-density fractions 86

4.6.1 Proteopathic proteins and protein degradation machinery 86

4.6.2 Ras-related proteins 87

4.6.3 Cytoskeletal components 88

4.6.4 Chaperones 88

4.7 Interactors of high-density prion (HDP) oligomers 89

4.7.1 G2L2 and cytoskeletal machinery 90

4.8 Conclusion 92

5 Summary ***94***

6 Annexure ***97***

6.1 Interacting partners of high-density prion (HDP) oligomers 99

7 Bibliography ***118***

8 Abbreviations ***153***

Acknowledgements ***156***

Curriculum vitae ***157***

1 Introduction

1.1 Alzheimer's disease

Alzheimer's disease (AD) is the most common form of neurodegenerative dementia and contributes to 60–70% of all the dementia cases. By 2015, the global occurrence of AD was 27 million people, and the number is expected to double by 2050 (GBD 2015 Disease, Incidence, Prevalence Collaborators, 2016). Higher prevalence and incidence rates are reported in the age group over 60 years from North America and Western Europe followed by those from Latin America and China and its western-Pacific neighbors (Reitz & Mayeux, 2014). Age can be considered as a principal risk factor for AD. The incidence of the disease doubles every 5 years after 65 years of age, with the diagnosis of 1275 new cases per year per 100,000 persons older than 65 years of age (Querfurth & LaFerla, 2010). However, genetic subtypes of AD (~5% of the total AD patients) show earlier clinical manifestation of the pathology, for example, from around the age of 45 (Mendez, 2017).

1.2 Clinical presentation

The clinical presentation of AD comprises symptoms related to cognitive decline particularly those related to the memory domain. Severity of the symptoms gradually increases with the disease progression, starting with mild cognitive decline (short-term memory deficits) in pre-dementia phases. Mild cognitive decline then develops into the early phase of dementia with difficulties in perception, language (vocabulary and speech fluency), and motor coordination. These clinical symptoms result from the deterioration of selective cognitive domains, particularly those related to memory. Memory decline initially manifests as a loss of episodic memory, which is considered a subcategory of declarative memory. The dysfunction in episodic memory impedes recollection of recent events including autobiographical activities. Elucidating the underlying molecular determinants that trigger the disruption of recent episodic memory, and eventually the decline in the other cognitive domains, is among the most crucial unanswered questions in the AD field. Moderate and final stage AD cases exhibit an even higher magnitude of linguistic and motor symptoms, long-term memory loss and

exhaustion. Overall, the decline in cognition makes the patient vulnerable to secondary illnesses such as ulceration and infections (Förstl & Kurz, 1999; Lopez, 2008).

1.2.1 Senile plaques and neurofibrillary tangles

Alzheimer's disease is pathologically characterized by the occurrence of senile amyloid-β (Aβ) plaques and presence of intraneuronal neurofibrillary tangles (NFTs) of abnormally hyperphosphorylated Tau protein. Presence of plaques and tangles was first reported by Alois Alzheimer in 1907 (Alzheimer, 1907) and their biochemical nature was first characterized in the 1980s. Although both Aβ plaques and Tau tangles are considered to be the specific hallmarks for Alzheimer's disease, but the establishment of AD pathology is complicated and includes many underlying alterations, mostly inflammatory response and oxidative stress resulting in defects in energy metabolism and synaptic dysfunction (Markesbery, 1997; Rozemuller, Eikelenboom, & Stam, 1986; Simard et al., 2006; Wyss-Coray, 2006).

1.2.1.1 Amyloid precursor protein and biosynthesis of amyloid-β

The senile plaques prevalent in brain tissues of AD patients predominantly are concentrations of amyloid β peptides with a length of 42 amino acid residues ($A\beta_{42}$). Whereas multiple variants (ranging from 36 to 43 amino acids in length) of Aβ itself are produced as cleavage products of the amyloid precursor protein (APP), monomers of $A\beta_{40}$ are much more abundant physiologically than those of aggregation-prone and toxic $A\beta_{42}$ species.

The amyloid precursor protein is a single-pass transmembrane protein with a large extracellular domain. Alternate splicing of APP generates eight splice variants, of which three are most abundant: a 695 amino acid variant, which is expressed predominantly in the CNS, a further two variants with 751 and 770 amino acids are more ubiquitously expressed (Bayer et al., 1999; O'Brien & Wong, 2011). Various Aβ species are produced because of endoproteolytic cleavages of the parental APP. Three different types of enzyme complexes are involved in the endoproteolytic cleavages, namely α-, β- and γ-secretases. Three enzymes with α-secretase activity have been identified. These α-secretases belong to ADAM (a disintegrin- and metalloproteinase-family enzyme) family of enzymes: ADAM9, ADAM10, and ADAM17 (Melo, Morgan, Monahan-Earley, Dvorak, & Weller, 2014). The β-secretase is a membrane integral β-site APP-cleaving enzyme 1 (BACE1), belonging to the pepsin family of proteases

(Vassar et al., 1999). The γ-secretase has been identified as a complex consisting of presenilin 1 or 2, (PS1 and PS2), nicastrin, anterior pharynx defective and presenilin enhancer 2 (De Strooper, Iwatsubo, & Wolfe, 2012). APP proteolysis can be classified into two categories, i.e. non-amyloidogenic and amyloidogenic pathways. The non-amyloidogenic pathway includes a cleavage of APP by α-secretase at the 83rd aa-residue position from the C-terminus, resulting in a larger N-terminus ectodomain (sAPPα) released in the extracellular matrix. The C83 fragment remains in the membrane and is subsequently cleaved by γ-secretase resulting in a p3 fragment which is released in the intracellular lumen. Importantly, the α-cleavage occurs in the Aβ region of APP, thereby eliminating the chances of Aβ formation. In comparison, in amyloidogenic pathway APP undergoes a BACE1-mediated β-cleavage, at the 99th aa-residue position from C-terminus, resulting in sAPPβ released into the extracellular space, leaving a membranous 99-amino-acid C-terminus stub, known as C99. The C99 fragment undergoes another cleavage event carried out by γ-secretase somewhere between the 38th and 43rd amino acid residues, liberating Aβ-peptide variants of different lengths (LaFerla, Green, & Oddo, 2007).

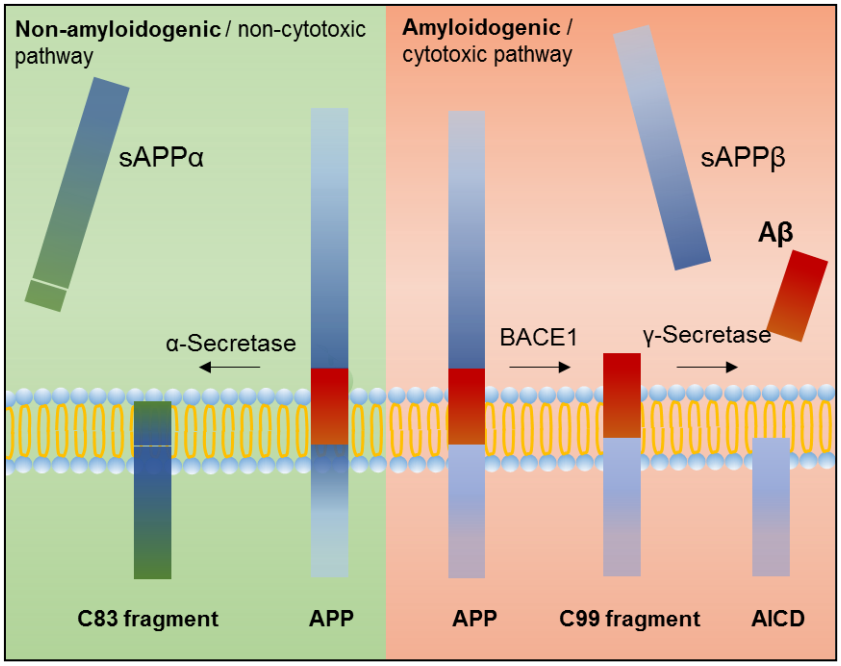

Figure 1: Amyloidogenic and non-amyloidogenic processing of the amyloid precursor protein. Non-amyloidogenic cleavage is conducted by ADAM family proteinases and results in shed-APP and C83 fragment, which is cleaved further by γ-secretase to give rise to an intracellular P3 fragment. Amyloidogenic cleavage, on the other hand, is initiated by BACE1 at the 83rd aa-residue from the C-terminal domain resulting in the C83 fragment, which after the second cleavage by γ-secretase results in Aβ peptide and an amyloid intracellular domain. Adapted from: LaFerla, Green and Oddo, 2007.

1.2.1.2 Tau tangles and their biosynthesis

Microtubule-associated protein Tau is an abundantly occurring soluble protein, associated with the cytoskeleton. Their abnormal hyperphosphorylation results in the switching of its soluble nature to a more hydrophobic one. These hydrophobic hyperphosphorylated Tau molecules are no longer attached to the microtubules and this results in self-association in the form of paired helical filaments (PHFs), which tend to further aggregate ultimately forming the inclusion bodies of Tau. The Tau tangles are not only characteristic of AD but are also present in many other neurodegenerative disorders, categorized as tauopathies. Like Aβ oligomers, the intermediate forms of Tau oligomers are considered cytotoxic and potentially causative in memory loss. Insoluble helical filaments are believed to sequester the toxic Tau oligomers and prove to be inert to the neuron. Six isoforms of Tau are expressed in the adult human brain, and this isoform variation is a consequence of alternative splicing of exon 2 (E2), 3 (E3) and 10 (E10). Exon 2 (E2) expresses N-terminal insert-N1, and E3 expresses N-terminal insert-N2. Three N-terminal variations are possible, due to the presence or absence of either insert. Tau isoforms are categorized depending on the presence of three or four carboxy-terminal repeat domains (3R or 4R, respectively); the second repeat is encoded by E10 and is not included in 3R Tau (Querfurth & LaFerla, 2010).

A battery of kinases and phosphatase is in action for the regulation of these site-specific phosphorylations in Tau protein molecules. Most of the kinases including PKA, CaMKII, PKC, and MAPKs (p38, ERK, SAPK and JNK) are transiently activated by exogenous and endogenous stimuli that result in the phosphorylation of Tau in healthy neurons. However, several Ser-Pro and Thr/-Pro sites are constitutively phosphorylated regulated by house-keeping kinase-protein kinases (Iqbal, Liu, Gong, & Grundke-Iqbal, 2010; Sengupta, Grundke-Iqbal, & Iqbal, 2006; Wang et al., 2012; Wang & Mandelkow, 2016). Mutations in the Tau gene (chromosome 17) are not reported to have any association with the severity of neuronal loss in Alzheimer's disease (Goedert & Jakes, 2005; Gómez-Isla et al., 1997). Nevertheless, increased p-Tau and Tau levels in the cerebrospinal fluid (CSF) correlate with cognitive decline and serve as reliable biomarkers in the MCI phase of the AD (Andreasen, et al., 2003).

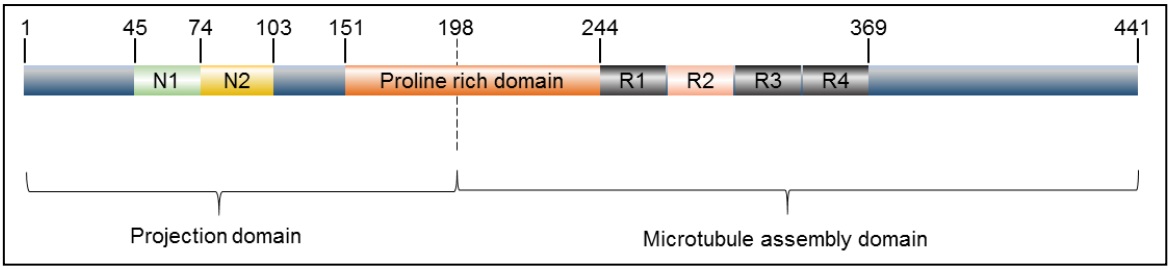

Figure 2: Structure of Tau protein: Tau protein can be subdivided into two major domains. The assembly domain in the C-terminal region comprising the amino acid repeats (is responsible for binding to microtubules (MTs) and for Tau aggregation). The N-terminal domain is a projection domain and projects away from the MTs. The middle region of Tau (aa-residues 151–243) contains multiple Thr-Pro or Ser-Pro motifs that are hyperphosphorylation targets of proline-directed kinases in tauopathies. Adapted from Wang and Mandelkow, 2016

1.3 Genetic and non-genetic risk factors of Alzheimer's disease

Alzheimer's disease-associated risk factors can be classified into two categories. The non-genetic risk factors (the factors having no established gene linkages to the AD) and genetic risk factors (including the genes, that have been proved to be associated with various aspects of Alzheimer's disease).

1.3.1 Non-genetic risk factors

Non-genetic risk factors include, most conspicuously, cerebrovascular diseases, hypertension (associated disintegration of blood-brain barrier), type 2 diabetes, plasma lipid levels, general health condition and traumatic injury to the head (Reitz & Mayeux, 2014).

1.3.2 Genetic risk factors

Several genetic risk factors have been identified that are associated with different aspects of Alzheimer's disease, mainly APP, Tau and cholesterol metabolism, immune response, endocytosis, and axon cytoskeleton. Highly linked genes include *ADAM10, TREM2, PLD3, DSG2, CD2AP,* and *APOE* (Karch & Goate, 2015). Among these AD-associated genes, *APOE* polymorphism has been one of the most frequently studied risk factors.

1.3.3 *APOE* polymorphism

Apolipoprotein *E* (*APOE*) polymorphism is a well-established risk factor for Alzheimer's disease. *APOE* is polymorphic with three major alleles in human population ε2, ε3, and ε4. About 25% of the human population carries the ε4 allele, and 50-65% of the

AD patients are carriers of the ε4-allele. Presence of at least one ε4 is associated with a reduction in the age of onset. *APOE-ε4* allele homozygous carriers are reported to develop AD at least ten years earlier than the non-carriers. Nonetheless, early onset Alzheimer's disease can develop in the absence of *APOE-ε4*. In contrast, some protection is provided by the presence of the rarer *APOE-ε2* (Liu, et al., 2013; Strittmatter & Roses, 1995).

1.4 Diagnosis

The progression of Alzheimer's disease is characterized using three major clinical methods, i.e., neuropsychological assessments, neuroimaging, and biomarkers.

1.4.1 Neuropsychological assessments

Neuropsychological assessments comprising a battery of tests, based on language skills, motor coordination, memory (learning and executive), intelligence and visual-reception. These neuropsychological tests provide a rough estimation of disease severity. Different testing strategies have been formulated, to estimate varying neuropsychological deficits e.g. *General Practitioner Assessment of Cognition, Mental Attributes Profiling System, Mental Status Examination (MSE), Montreal Cognitive Assessment, NIH Stroke Scale, Abbreviated Mental Test Score, Mini-Mental State Examination (MMSE)* and the Consortium to Establish a Registry for Alzheimer's Disease (*CERAD)-neuropsychological assessment* (Morris et al., 1989; Peterson and Lantz, 2001). *CERAD-neuropsychological assessment* consists of a battery of tests including verbal fluency, a modified Boston naming test, mini-mental state, language and constructional praxis (Morris et al., 1989). However, the most commonly used method for the neuropsychological assessment of AD is MMSE, for multiple reasons; foremost the simplicity of its application (Arevalo-Rodriguez et al., 2015; Pozueta et al., 2011; Tombaugh, McDowell, Kristjansson, & Hubley, 1996). The MMSE is a 30-score testing system that engages different cognitive and motor domains. A score of 24 or more points out of 30 is considered normal. A score below 24 can indicate a mild (19–23 points), moderate (10–18 points) or severe (≤9 points) cognitive impairment (Mungas, 1991; Roselli et al., 2009). Certain statistical corrections are applied to surpass differences in the educational background of the patients (Crum, Anthony, Bassett, & Folstein, 1993). The advantage of utilizing MMSE scoring for Alzheimer's assessment is

that a repeated temporal testing profile can reflect the progression rate of the disease (Musicco et al., 2009).

1.4.2 Neuroimaging

An endorsement to the neuropsychological examination is made by utilizing neuroimaging approaches. A variety of neuroimaging methods have been designed to provide specific insights into different structural or functional aspects of the brain. The table below provides a summary of these imaging techniques and their respective applications.

Table 1: Neuroimaging as a diagnostic approach in patients with suspected Alzheimer's disease.

Imaging modalities	Acquired information	Alterations observed in AD
sMRI	Provides information regarding the general structure and distribution of white matter, gray matter and CSF in the brain	Medial temporal lobe atrophies, hippocampal atrophy. A compensatory increase in the prefrontal cortex has also been reported by some authors (Lehéricy et al., 1994; Scahill, Schott, Stevens, Rossor, & Fox, 2002).
fMRI	Provides insight into the synaptic activity dependent on the alterations of blood flow and oxy/deoxyhemoglobin ratios (Kwong et al., 1992; Ogawa, Lee, Nayak, & Glynn, 1990)	Decreased hippocampal activity is observed in AD patients while performing episodic memory tasks (Hämäläinen et al., 2007; Rombouts et al., 2000)
CT	Gross brain anatomical study	Used as a confirmation technique for MRI (Ferreira & Busatto, 2011)
SPECT	Regional brain perfusion (Ferreira & Busatto, 2011)	
FDG-PET	This is a version of positron emission tomography that utilizes fluorescence-tagged glucose (F-fluorodeoxyglucose) and assesses the synaptic activity directly by measuring the glucose consumption in different brain regions (Johnson, Fox, Sperling, & Klunk, 2012).	Hypometabolism in the limbic and associated region (De Santi et al., 2001)
Amyloid-PET	Deposition of amyloid fibrils is assessed in the brain using a radioactive compound that intercalates in amyloid fibrils (Ikonomovic et al., 2008)	Utilized in both diagnosis and research settings, various groups have reported 96% of AD patients as positive for the amyloids (Johnson et al., 2007; Perani, 2014)

sMRI = structural magnetic resonance imaging; fMRI = function magnetic resonance imaging; CT = computerized tomography; PET = positron emission tomography, FDG-PET = ^{18}F-fluorodeoxyglucose-PET; SPECT = single photon emission tomography.

1.4.3 Biomarkers for Alzheimer's disease

Alterations occurring in the brain due to neurodegeneration cast a disease-specific biochemical signature over cerebrospinal fluid (CSF), blood and urine. These

biochemical alterations can be utilized to depict and confirm the disease subtypes and stages. Biomarkers have been crucial in the differential diagnosis of neurodegenerative diseases. To characterize a certain disease, it is common to rely on a set of biomarkers. In the case of differential diagnosis of the AD, CSF biomarkers are considered the most reliable. Commonly measured biomarkers include $A\beta_{40}$, $A\beta_{42}$, Tau and p-Tau as their levels correspond to the amyloidosis and Tau pathologies respectively (Schaffer et al., 2015). The decrease in the $A\beta_{42}$ marks an increase in amyloid plaque burden in the cerebral tissues. Conversely, $A\beta_{42}$ levels alone cannot be relied for the differential diagnosis, as decrease in the $A\beta_{42}$ is also observed in the subjects with mild cognitive impairment and even in the non-demented controls (Llorens, Schmitz, Ferrer, & Zerr, 2016). Increase in the CSF levels of Tau indicates an increase in the Tau protein and a higher degree of tangle formation in the brain (Humpel, 2011). Some studies also consider other subsidiary CSF biomarkers, including YKL-40, carnosinase I, chromogranin A, and NrCAM (neuronal cell adhesion molecule) to increase the assay potential of Aβ and Tau levels (Schaffer et al., 2015).

1.5 Neuropathological profiling of Alzheimer's disease

Current neuropathological assessment and staging for the AD are exercised according to the guidelines updated by the National Institute of Aging – NIA (Montine et al., 2012). NIA guidelines further take into account Aβ plaque scoring (Thal, Rüb, Orantes, & Braak, 2002), NFT staging (Braak & Braak, 1991) and CERAD scoring (Neuropathological staging of Alzheimer-related changes) (Mirra et al., 1991). Thus, the neuropathological findings are ranked along three parameters (Amyloid, Braak, CERAD) to obtain an ABC score (Montine et al., 2012). The table below summarizes the A, B, and C scoring patterns used in NIA-AD staging.

Table 2: A, B and C scoring used in the staging of Alzheimer's disease according to National Institute of Aging guidelines.

'A' Aβ plaque score	'B' NFT stage	'C' Neuritic plaque score (modified from CERAD)
A0: no Aβ	B0: no NFTs	C0: no neuritic plaques
A1: Thal phase 1 or 2	B1: Braak stage I or II	C1: CERAD score: sparse
A2: Thal phase 3	B2: Braak stage III or IV	C2: CERAD score: moderate
A3: Thal phase 4 or 5	B3: Braak stage V or VI	C3: CERAD score: frequent

The Thal Aβ plaque phases are defined by the presence of the senile plaques in different brain regions, from neocortex to dentate nucleus (Thal et al., 2002).

Braak stages describe the spread of NFT lesions in diverse brain areas. Lesion profiles are described in Table 3. The CERAD stages are defined based on the frequency of plaques in the middle frontal cortex region of the brain. The stages range from no plaques to sparse, moderate and finally to frequent plaques (Mirra et al., 1991).

Table 3: Lesion profiles of neurofibrillary tangles in diverse brain regions

Braak stages	Centers of NFT lesions
I	Transentorhinal region
II	Entorhinal region
III	Neocortex of the fusiform and lingual gyri
IV	Wider neocortical association areas
V	Frontal, superolateral, and occipital directions, reaching the peristriate region
VI	Secondary and primary neocortical areas and, in the occipital lobe, extends into the striate area

1.6 Subtypes classification of Alzheimer's disease

Subtype classification of the AD can be based on two major factors, namely genetic background and the age of onset. Cases of genetic or early-onset familial AD (eFAD) account for only 1% of the total Alzheimer's cases, where AD presentation is associated with the autosomal dominant mutations in three genes *PSEN1, PSEN2,* and *APP*. AD cases without any characterized associated genetic mutations are categorized as sporadic AD (Mendez, 2017).

Both familial and sporadic cases prevail in two classes, based on their onset age. Sporadic AD cases are predominantly late-onset type, and the familial cases belong mainly to the early onset AD. Although cut-offs for the age of onset are arbitrary, the risk of developing AD is quoted to increase with the age. Based on the onset of disease, AD is subdivided into early-onset AD (EOAD), cases developing AD earlier than 65 years of age (45-50 years of age) and late-onset Alzheimer's disease (LOAD), i.e. 95% of all the AD cases presenting the symptoms after 65 years of age (Newens et al., 1993).

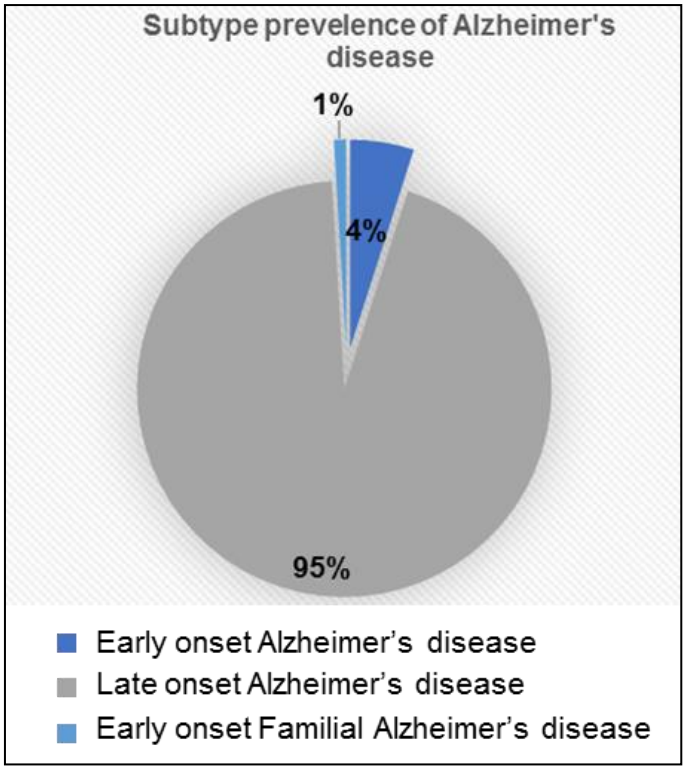

Figure 3: Epidemiology of Alzheimer's disease subtypes. Late-onset Alzheimer's disease constitutes the largest percentage of the patients suffering from AD which is 95% of the total AD cases. About 4% of the AD cases are early-onset Alzheimer's disease, and 1% of all the AD cases are early-onset familial AD cases.

1.6.1 Atypical pathological presentation in Alzheimer's disease

Alzheimer's disease is a slowly progressive neurodegenerative disease. Disease course typically is associated with gradually developing symptoms related to the hippocampal abnormalities – cognitive decline. However, some atypical AD cases pose variation in the pathological centers in the brain leading to a higher disease progression (Jack et al., 1998; Mueller et al., 2010). Giannakopoulos, Bouras, and Hof (1994) have reported an AD case with a higher extent of cortical degeneration compared to the hippocampal damage. Greater damage in occipital-parietal cortex relative to frontal and temporal cortices has been reported in a cohort of AD cases by Hof, Bouras, Constandinidis, and Morrison (1989). Likewise, two distinct groups of AD cases have been classified by Murray et al. (2011). The study discusses a group of Alzheimer's disease with relative sparing of hippocampal regions (these cases with hippocampal sparing were observed to have a higher degree of Lewy body disease as well). The second group described in the study presents Alzheimer's pathology centered in the limbic region instead of the primary cortex (Murray et al., 2011).

1.7 Rapidly progressive Alzheimer's disease

Alzheimer's disease is a slowly progressive neurodegenerative disease and typically spans a period of 8 years with gradually developing severity of symptoms, hence easily differentiable from the rapidly progressive dementia cases. The neuropsychological decline, when assessed by a Mini Mental State Examination, averages a drop of less than 6 MMSE units per year. Some atypical cases of AD, on the other hand, exhibit a neuropsychological profile that resembles the rapidly progressive dementias. In these cases, the average cognitive decline is more than 6 MMSE units per year. The prevalence of and reports on such cases are low. The post-diagnostic survival time in these cases is around 4 years in comparison to 8 years in typical spAD cases. Due to the atypical disease progression, such AD cases are often misdiagnosed as Creutzfeldt-Jakob-disease in the dementia centers, and post-mortem pathological observations then later confirmed the Alzheimer's pathology (Schmidt et al., 2011).

1.7.1 History

The literature is still sparse with its accounts of rpAD. The first case of rapidly progressive AD (rpAD) mimicking CJD was reported in 1989 (Mann, Mohr, & Chase, 1989), followed by another report in 2004 with detection of 14-3-3 in CSF and subsequent classification of the patient as a CJD case, where postmortem pathological examination revealed the occurrence of AD pathology (Reinwald, Westner, & Niedermaier, 2004). Protein 14-3-3 presence in CSF has been associated to CJD and is considered a very crucial differential biomarker for the detection of CJD (Aksamit, Preissner, & Homburger, 2001; Green et al., 2001; Zerr et al., 2000). A case of rapidly progressive AD was again reported to be positive for 14-3-3 by Jayaratnam and coworkers (Jayaratnam, Khoo, & Basic, 2008).

1.7.2 Clinical features

Detailed clinical features of rpAD have been studied by Schmidt et al. (2010). The study encompassed various aspects related to the disease, including the age of disease onset, gender, CSF biomarkers, clinical presentation and genotypes for *APOe* and *PRNP.* The disease duration from clinical examination was reported 26.4 months (median) and the age at death was reported to be 73 years (median). The gender ratio was observed to be equal in the disease cohort. Neuropathological features of prion

dementia were not reported, whereas the pathology was in accordance with Alzheimer's pathology. Two cases were reported with a very low degree of Lewy body pathology. The most frequent signs included myoclonus (75%), gait disturbance (66%), a positive Babinski's sign (66%), rigidity (50%), aphasia (66%), falls (50%) and hallucinations (44%). Especially aphasia, myoclonus, and rigidity were symptoms predominantly appearing in advanced disease stages, while depression, disturbed gait and impaired concentration occurred rather early in the disease course (Schmidt et al., 2010). Neuropsychological predictors have been revisited for rpAD cases, based on MMSE scoring by Tosto and coworkers. The study indicates that a decline in the executive/language tasks is a significant predictive criterion for the rpAD cases, in contrast to spAD (Tosto et al., 2015).

1.7.3 Biomarkers and genetic linkages

In rpAD cases, CSF Tau levels were slightly lower than that of the AD and for CSF-$A\beta_{42}$ levels, no difference was seen in comparison with the typical AD cases. Approximately one third (31%) of the rpAD cases were positive for 14-3-3. For *APOE* genotypes, no ε4/ε4 homozygous subjects were found for the study cohort, ε2/ε4 combination was prevalent in 6% of the subjects, 31% of the cohort was reported to be ε3/ε4 heterozygous, 6% were heterozygous for ε2/ε3 and the ε3/ε3 genotype was seen in the majority (56%) of the test group. *PRNP* codon 129 genotype did not influence the disease onset or clinical course. However, a statistically significant association of hallucinations with methionine homozygous individuals and that of epileptic seizures to the non-MM individuals was noticed in the cohort (Schmidt et al., 2010). Same clinical findings including CSF 14-3-3 positivity (42% in the studied cohort), higher prevalence of MM-*PRNP* genotype, and absence of *APOE* ε4/ε4 homozygosity, were augmented by a multicenter update including cohorts from France, Germany, Japan, and Spain later in 2012 (Schmidt et al., 2012). The similar CSF biomarker profiles were re-established for rpAD alongside an increase in p-tau/tau for rpAD in another cohort more recently (Ba et al., 2017). Table 4 provides a summary of CSF biomarker profile for differential diagnosis of Alzheimer's disease subtypes (rapidly progressive forms and sporadic cases) and sporadic Creutzfeldt-Jakob disease.

Table 4: An outlook of CSF biomarkers in variants of AD and CJD as indicated by Schmidt et al., 2010, 2011, 2012.

CSF Biomarkers	rpAD	spAD	sCJD
Tau	↑	↑	×
p-Tau/Tau	↑↑	↑	×
Aβ1-42	↓	↓	×
Aβ1-40	—	—	×
Tau/Aβ1-42	↑	×	×
14-3-3	↑	×	↑↑
Synuclein-Alpha	—	—	↑↑
IL-8	—	—	↑
MCP-1	—	↑	↑

A signature elevation in proinflammatory cytokines (IL-6, IL-13, TNF-α, and G-CSF) exclusively in the serum of rpAD patients has been reported, suggesting a difference in immune activation mechanism in rpAD pathology (Stoeck, Schmitz, Ebert, Schmidt, & Zerr, 2014). Table 5 summarizes the serum pro-inflammatory biomarkers in rpAD, spAD and sCJD.

Table 5: Pro-inflammatory cytokines significantly elevated in the serum of rpAD cases compared with spAD and CJD, as indicated by Stoeck et al., 2014.

Serum Cytokines	rpAD	spAD	sCJD
IL-13	↑↑	—	—
TNF-α	↑↑	—	—
G-CSF	↑↑	—	—
IL-6	↑	—	—

1.7.4 Biochemistry of rpAD

The difference in the progression rate in rpAD cases compared to the spAD cases has also been associated with distinct physicochemical oligomeric species of Aβ characterized in the brain by Cohen et al. (2015). The study provides evidence of the existence of $A\beta_{42}$ species composed of about 100 monomers that are stable to chaotropic denaturation. However, the discrepancy in oligomerization between rpAD and spAD has not been discussed (Cohen et al., 2015).

Significant proteomic alterations in amyloid plaques have been discussed in a recent study by Drummond et al. (2017). The difference in the plaque proteomic makeup represents the distinction of rpAD from spAD. However, no such protein candidates were found in either group to highlight supposedly different mechanisms involved in the pathogenesis of spAD and rpAD. Synaptic proteins were mainly associated with

the plaques from rpAD cases, suggesting the higher degree of synaptic dysfunction in the AD cases with rapid progression (Drummond et al., 2017).

1.8 Proteopathic oligomers and neurodegeneration

Neurodegenerative diseases are characterized by the development of pathological hallmarks, consisting of fibrillar structures of seeding proteins. In AD pathology, these are Aβ plaques and Tau tangles, in prion diseases these plaques consist of PrP^{Sc}, whereas in Parkinson's and Lewy body dementia these fibrillar plaques are made up of α-synuclein. The formation of these pathological hallmarks is a sequential multi-phasic process, starting from the misfolding of physiological forms of respective proteins. This misfolding ability is commonly associated with mutations/polymorphisms in the protein (gene) sequences, innate dysregulation of protein-cleaving machinery or both. Misfolding of these proteins is associated with acquiring a β sheets-rich conformation, and these β sheets-rich molecules, in turn, develop the capability of converting other physiological molecules to β sheets-rich molecules. The misfolded molecules have the tendency to polymerize in a variety of oligomeric species, i.e. dimers, trimers, tetramers, and so on, ultimately forming relatively stable fibrillar structures. The intermediate soluble oligomers are biologically active and are believed to be cytotoxic species. According to this hypothesis, the fibrils (contrary to initial beliefs) are the inert end products of the polymerization chain (Meredith, 2005). There is increasing evidence of the toxicity of various amyloid oligomers.

Animal experiments have demonstrated the toxic effects of the Aβ oligomers (AβOs) *in vivo,* resulting in memory loss and loss of synaptic plasticity (Cleary et al., 2005) He et al., 2012). Inhibition of long-term potentiation (LTP) has also been noted in response to naturally occurring AβOs (Walsh et al., 2002). Synaptic calcium currents in the cellular models have also been altered in cell models when treated with AβOs (Nimmrich et al., 2008). Furthermore, two major populations of AβOs (type 1 and type 2) have been identified that are capable of plaque formation and neurotoxicity, respectively. The relative amounts of these specific types are also found to be different *in vivo* along with their differential immunoreactivity (Liu et al., 2015). The Aβ-dimers derived from AD brains have also been able to cause synaptic toxicity in rat models (Shankar et al., 2008). In AD patients, AβOs levels also correlate with the degree of synaptic loss (Lesné et al., 2013; Pham et al., 2010). Likewise, Tau oligomer species have been

associated with the neurotoxicity (Goedert, Masuda-Suzukake, & Falcon, 2017; Usenovic et al., 2015). Toxicity caused by other proteopathic proteins has also been reported for other neurodegenerative diseases. Oligomerization prone α-synuclein species have been associated with synaptotoxicity (Kalia, Kalia, McLean, Lozano, & Lang, 2013; Pieri, Madiona, & Melki, 2016; Stöckl, Zijlstra, & Subramaniam, 2013) and dysregulation of the kinesin-microtubule system (Prots et al., 2013). Similarly, various species of prion oligomers have been identified, affecting the disease progression rates and the disease subtypes (Choi et al., 2009; Haldiman et al., 2013; Safar et al., 2015; Kim et al., 2011).

1.9 Alzheimer's disease and Prion protein

1.9.1 Prion protein -structure, functions, trafficking and pathological strains

The cellular form of prion protein (also known as CD230) is a glycoprotein encoded by *PRNP* gene on the chromosome number 20 in humans (Basler et al., 1986; Oesch et al., 1985). The expression of the protein is ubiquitous in the body with higher expression in the nervous tissues, specifically the brain, immune cells, and lymphoid organs (Linden et al., 2008). In nervous tissue, the localization of the PrP^{C} is observed at the pre-synaptic and post-synaptic membranes and is reported to be necessary for normal synaptic function (Collinge et al., 1994; Herms et al., 1999).

1.9.1.1 Structure and biosynthesis

The primary sequence of prion protein consists of 253 amino acid residues containing two signal peptides, at the COOH-terminal and the NH_2-terminal. Post-translational modification results in the physiological form of prion protein with a length of 208 amino acid residues. A physiological form of prion protein, PrP^{C} occurs primarily along with low amounts of truncated, transmembrane PrP^{Ctm} (with C-terminal facing towards ER lumen) and PrP^{Ntm} (with N-terminal facing the ER lumen) (Hegde et al., 1998; Hegde, Voigt, & Lingappa, 1998). A GPI-anchor is attached to PrP^{C} during its life cycle in the cell (Taylor & Hooper, 2006). Newly synthesized PrP^{C} enters the ER lumen with the assistance of an N-terminal signal peptide where core GPI-anchor is added after the removal of the C-terminal signal peptide followed by an assemblage of PrP^{C} molecules in the lipid rafts. Association of PrP^{C} to the raft is necessary for its proper folding and glycosylation which include glycosylation at two asparagine residues 181 and 197

(Haraguchi et al., 1989), and formation of a disulfide bond between two cysteine residues at amino acid residues 179 and 214 in human PrP^C (Turk et al., 1988) in ER and Golgi apparatus respectively (Campana, Sarnataro, & Zurzolo, 2005; Sarnataro, Campana, & Paladino, 2004). In addition, mature PrP^C contains 5 octapeptide repeats with a PHGGGWGQ sequence near the NH_2-terminal.

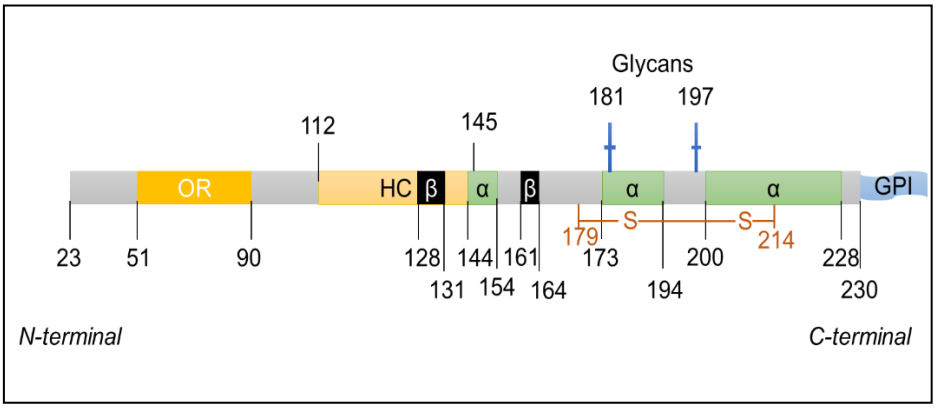

Figure 4: Structure of mature physiological prion protein (PrP^C). Disulfide linkage is presented between aa residues 179 and 214. Two glycan bodies are attached at aa residues 181 and 197. A GPI (glycophosphoinositol) anchor is added at the 230th aa residue. OR = octa-repeats region; HC = hydrophobic core; α = alpha helix domain; β = beta sheet domains. Adapted from Zahn et al., 2000 and Linden et al., 2008.

In neurons, the cell surface retentivity is very short-lived, like other classical membrane receptors, i.e. a $t_{1/2}$ of 3-5 min. The endocytosis is rather enigmatic. In different cells and different physiological conditions, internalization via both clathrin- and non-clathrin-coated vesicles has been reported (Sunyach, 2003).

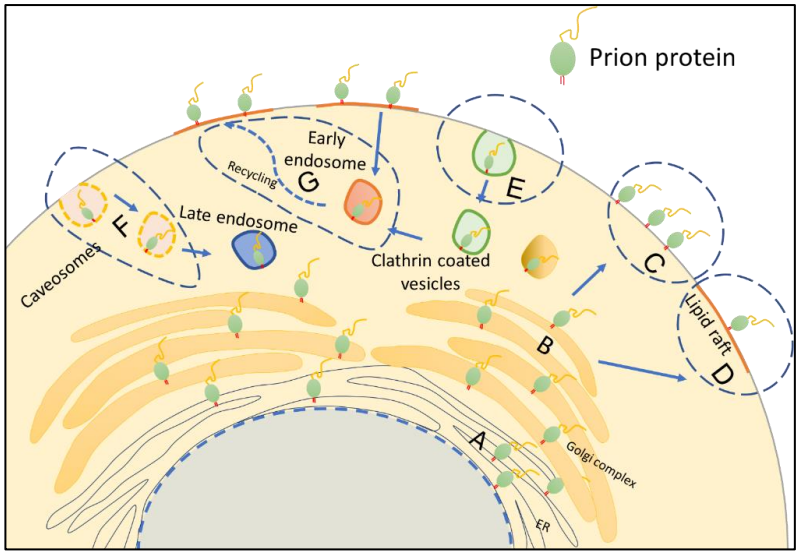

Figure 5: Biosynthesis and trafficking of the cellular prion protein. PrP^C is synthesized in the ER (A) and is translocated via the Golgi apparatus (B) to the cell surface, residing at the membrane for a short time (C) predominantly at lipid rafts (D). PrP^C endocytosis is

mediated either via clathrin-coated pits (E) or caveolae (yellow) (F), or PrP^C is transported back to the cell surface being part of recycling endosomes (brown) (G). Adapted from: Lewis & Hooper, 2011.

1.9.1.2 Signaling mediated by the PrP^C

The expression of the prion protein on the cell surface implies its avid function as a cell receptor. PrP^C is discussed to be involved in many signaling pathways. A controversial signaling pathway involves the caveolin-mediated signaling induced by PrP^C. The cascade is hypothesized to work via N-CAM, which in turn activates the Fyn pathway (He & Meiri, 2002). PrP^C is also involved in modulating the cAMP/PKA pathway with significant biological consequences, with various possibilities of cAMP phosphorylation being discussed, including heterotrimeric G proteins engaged by G protein-coupled receptors (GPCR) (Cooper & Crossthwaite, 2006; He & Meiri, 2002; Kamenetsky et al., 2006). Likewise, Erk activation, via the activation of Ras GTPases, is also achieved by the interaction with the PrP^C (both forms, membrane-anchored and extracellular forms). Ras GTPases after their activation by binding of Grb2 adaptor protein to phosphorylated cytosolic domains of receptor tyrosine kinases, result in the changes of cellular Ca^{2+} levels (Spielhaupter & Schätzl, 2001; Stork & Schmitt, 2002). PrP^C is also reported to promote the cellular influx of Ca^{2+} via a voltage-gated calcium channel (Fuhrmann et al., 2006; Herms et al., 2000). PrP^C crosslinking promotes the Ca^{2+}influx, which in turn acts as feedback for the lateral distribution of surface proteins including PrP^C itself. Crosslinking of PrP^C also recruits the non-receptor tyrosine kinases including Fyn (discussed earlier) and lymphocyte-specific protein tyrosine kinase to PrP^C-containing membrane rafts (Stuermer et al. 2004). Protein kinase C is also reported to be activated by the PrP^C, but the mechanism of activation is poorly understood (Dekker, Palmer, & Parker, 1995). A PrP^C mediated neuroprotective role of PI3 kinase/Akt signaling is suggested to protect the neurons against oxidative stress (Vassallo et al., 2005; Weise et al., 2006). Interaction of PrP^C with neural cell adhesion molecule (NrCAM) (Schmitt-Ulms et al., 2001) induces neurite formation.

1.9.1.3 Prion diseases and conversion of PrP^C into PrP^{Sc}

The physiological conformation of cellular prion protein contains about 40% alpha-helical structure and 3% β-sheets, and this proportion of secondary structures is complementary for PrP^C to perform cellular functions. In transmissible spongiform encephalopathies, misfolding of physiological prion results in a predominant β-sheet

conformation (43% β-sheets and 30% alpha helix) and the misfolded form of prion protein is referred to as the scrapie form (PrP^{Sc}). The PrP^{Sc} is extremely resistant to proteolysis and tends to have the ability to convert other PrP^{C} molecules to PrP^{Sc} forms (Prusiner, Groth, Bolton, Kent, & Hood, 1984; Prusiner, Scott, DeArmond, & Cohen, 1998). The process of PrP^{C} to PrP^{Sc} conversion is also accompanied by oligomerization of the PrP^{Sc} species, resulting in its cytotoxicity. These oligomers are finally converted into the amyloid fibrils and plaques which are characteristics of prion dementias (Figure 6).

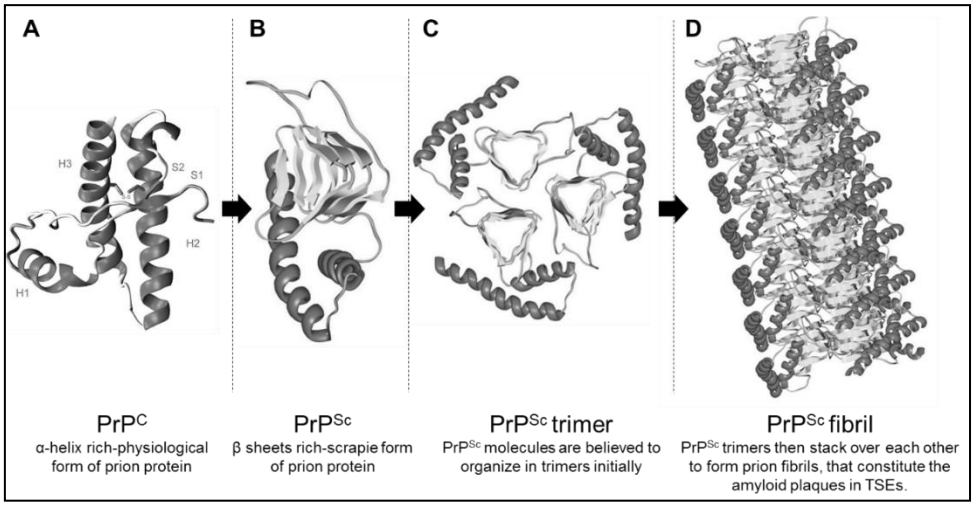

Figure 6: Conformation changes in prion protein. Conversion of α-helix-rich PrP^{C} (A) to β-sheets rich PrP^{Sc} (B), marks the beginning of pathological events in prion neurodegeneration. PrP^{Sc} molecules are then hypothesized to form planer trimers (C) and the trimers stack up over each other to form the fibrils (D). Modified from Stroylova et al., 2014.

Multiple types of *transmissible spongiform encephalopathies* (TSEs) in humans and animals are associated with prion protein strains. The pathological hallmarks are spongiosis and formation of PrP^{Sc} plaques in the brain. Human prion diseases are detailed in Table 6.

Table 6**: Classification of human prion disease.** Modified from Gambetti et al., 2003.

Disease group	Phenotypes	Cause
Familial (inherited)	Familial Creutzfeldt-Jakob-disease (fCJD)	Mutations in *PRNP* gene
	Fatal Familial Insomnia (FFI)	
	Gerstmann-Sträussler-Scheinker disease (GSS)	
	Mixed or undefined forms	
Sporadic	CJD (sporadic)	No association with the mutations in *PRNP* gene, but the phenotypes are affected by the PRNP codon 129 polymorphism (MM, VV, MV), and type of PrPSc strain (1 or 2, defined by proteinase-K digestion) (Cali et al., 2009; Gambetti et al., 2003)
	Typical (MM1 and MV1)	
	Early onset (VV1)	
	Long duration (MM2)	
	Kuru plaques (MV2)	
	Ataxic (VV2)	
	Sporadic Familial Insomnia (sFI)	
Acquired	Kuru	Exposure to human brain material
	Iatrogenic CJD (iCJD)	Exposure to PrP^{Sc} during transfusion
	Variant CJD (vCJD)	Acquired from the bovine spongiform encephalopathy material

Animal prion diseases comprise a large group of diseases targeting various animal species, detailed in Table 7.

Table 7: Animal prion diseases and proposed etiologies. Source: modified from Imran and Mahmood, 2011.

Disease	Host	Proposed Etiology
Scrapie	Sheep, Goats	Infection with prions of unknown origin
Transmissible Mink Encephalopathy (TME)	Mink	Infection with prions of either sheep or cattle origin
Chronic wasting disease (CWD)	Cervids	Infection with prions of unknown origin
Bovine spongiform encephalopathy (BSE)	Cattle	Infection with prions of unknown origin
Exotic ungulate spongiform encephalopathy (EUE)	Nyala, Kudu	Infection with prions of BSE origin
Feline spongiform encephalopathy (FSE)	Cats	Infection with prions of BSE origin
TSEs in non-human primates	Lemurs	Infection with prions of BSE origin

1.9.2 Involvement of prion protein in Alzheimer's disease

1.9.2.1 Prion-like behavior of Aβ and tau

Primary interest to study the prion protein in association with Alzheimer's pathology arose due to the similarities between the mechanisms of misfolding, transformation and spread of prion protein, Aβ and Tau. Toxicity in Alzheimer's disease is primarily due to the conversion of alpha-rich molecules of Aβ and Tau to the β-sheets-rich molecules, much like the prion conversion to PrP-scrapie forms (Frost & Diamond, 2010; Goedert, Clavaguera, & Tolnay, 2010; Jucker & Walker, 2011). Much like the PrP^{Sc}, the Aβ and Tau also exhibit the seeding activity, i.e. misfolded molecules can transform other normal Aβ and Tau forms to the toxic forms, in turn starting a spread chain (Braak and Del Tredici 2011; Brettschneider et al. 2015; de Calignon et al. 2012; Harris et al. 2010). Transmissibility has also been observed for AD. Brain homogenates from AD patients, when inoculated into the hippocampus of mice, initiated an Aβ deposition in mice. The spread of the Aβ and Tau in the brain also resembles the spread of PrP^{Sc} (Kim & Holtzman, 2010; Novak, Prcina, & Kontsekova, 2011; Prusiner, 1984).

1.9.2.2 PrP^{C} inhibition of BACE1

The N-terminal domain of membrane-anchored PrP^{C} is reported to regulate the formation of Aβ, by inhibiting BACE1 cleavage activity subjected on APP. BACE1 inhibition activity is associated with the localization of PrP^{C} to the membrane rafts, as the activity is lost in the PrP^{C} variants which are not associated with the rafts. Membrane raft-associated mutant forms of PrP^{C}, formed in familial prion diseases, are reported to lose their BACE1 inhibition, suggesting that structural integrity and sequence conservation are also important factors required for BACE1 inhibition activity in PrP^{C} (Parkin et al., 2007). Likewise, loss of BACE1 inhibition is also reported in the scrapie-infected humanized mice, resulting in subsequent higher levels of $A\beta_{40}$ and $A\beta_{42}$ (Parton, Joggerst and Simons, 1994; Sunyach, 2003; Linden et al., 2008).

1.9.2.3 PrP^{C} as a receptor for Aβ oligomers

The cellular prion PrP^{C} is a well-characterized receptor for of amyloid-β oligomers. Hippocampal CA1 long-term potentiation is suppressed under the effect of nanomolar concentrations of Aβ treatment. However, this LTP suppression is not observed in the hippocampi of PrP knock out mice (Laurén et al., 2009). Likewise, mice with the

APPswe/PSen1DeltaE9 transgenes in $PrP^{-/-}$ condition do develop the amyloid plaques but memory functions are conserved, suggesting the involvement of PrP^{C} in amyloid toxicity (Parton et al., 1994). PrP^{C} after the attachment of Aβ is believed to initiate the Fyn signaling cascade resulting in the phosphorylation of the NR2B subunit of N-methyl-D-aspartic acid receptors resulting in a transient increase in surface NR2B and subsequent excitotoxicity and destabilization of dendritic spines. Activated Fyn also acts as a kinase for Tau phosphorylation (Roberson et al., 2011).

1.9.2.4 PrP^{C} alpha- cleavage shedding by ADAMs, controlling the fibrillation of Aβ

The N-terminus of the PrP^{C} is responsible for the attachment of Aβ to the prion protein (Fluharty et al., 2013). Physiologically, under the action of ADAM-10, PrP^{C} undergoes alpha-cleavage between amino acids 111/112, resulting in the formation of N1 and C1 fragments, both resultant fragments keep their neuroprotective roles in the AD and CJD, respectively (Altmeppen et al., 2012). A detachment of the N1 fragment from the PrP^{C} eliminates the possibility of Aβ anchorage to the PrP molecules, hence no subsequent Fyn signaling cascade operates in the cell. On the other hand, the release of N1 fragments in the outer cellular space, allows the sequestering of Aβ-oligomers, sequentially minimizing the chances of their attachment to cell surface PrP^{C}. ADAM-10 is also responsible for the shedding of PrP^{C} from the cell surface which in turn behaves as a bait for the soluble Aβ-oligomers (Altmeppen et al., 2011, 2012; Roberson et al., 2011).

1.9.2.5 Codon 129 polymorphism and onset of AD

A linkage between the polymorphism at codon 129 and early onset of the AD has been discovered in various studies. A higher risk of developing AD with early onset has been associated with codon 129 valine homozygosity in patients from Dutch and Polish cohorts (Dermaut et al., 2003; Golanska et al., 2004), whereas a higher risk of developing early AD-associated to *PRNP* codon 129 methionine homozygosity is reported from a German cohort (Riemenschneider et al., 2004). However, no such associations could be seen from the patients from Spain, Italy or Japan. These linkage differences can be explained by a strong effect of ethnicity. In any case, there is a dose-dependent relation between memory decline in the AD and *PRNP* codon 129 valine (Casadei et al., 2001; Combarros et al., 2000; Del Bo et al., 2006).

1.10 Study objectives

The progression rate in rpAD cases mimics the characteristics of prion diseases. Likewise, rapid progressive Alzheimer's disease has also been attributed to distinct prion-like oligomers of Aβ (Cohen, Appleby, and Safar, 2016). However, the mechanistic details of progression rate variations in rpAD have not been studied previously.

The current study primarily focusses on defining differential signal transduction pathways, physiological regulation of prion protein in rpAD and oligomer metabolism. Experiments in the current study, utilize cerebral cortex samples from patients with spAD, rpAD, age-matched controls and other rapid dementias as positive controls. Details of the cohort are discussed in the "Methods" section.

Objectives of the study were

1. to characterize pathological hallmarks of Alzheimer's disease (Aβ plaques and tangles),

2. to identify and characterize differential signal transduction mechanisms involved in the progression rate variations,

3. to study the differential metabolism of prion protein and subtype-specific interacting partners in rpAD and spAD,

4. to isolate and characterize the oligomers of prion protein and other proteopathic proteins and their influence on progression rate, and

5. to study the mechanism of proteopathic oligomer toxicity in rpAD.

2 Materials and methods

2.1 Materials

2.1.1 Antibodies

Antibodies used for immunofluorescence (IF), immunoprecipitation (IP), immunoblotting (IB), and are listed in Tables 1 and 2.

Table 8 : List of primary antibodies and their applications in the current study

Primary Antibody	Origin	Dilution (IB/IP)	Dilution (IF)	Company / Cat. No.
SAF 70 (anti PrP antibody)	Mouse IgG2b	1:1000/1:100	1:100	SPIbio / A03206
Actin-beta	Mouse IgM	1:10000	1:100	Sigma / A5441
Zinc Alpha 2 Glycoprotein	Mouse IgG1	1:1000/ 1:100	1:100	Abcam / ab117275
Peroxiredoxin-1	Rabbit IgG	1:1000	-	Abcam / ab15571
GAPDH	Mouse IgM	1:10000	-	Sigma / G8795
AKT	Rabbit IgG	1:1000	-	CST / 9272
Phospho-Akt (Ser473)	Rabbit IgG	1:1000	-	CST / 4060
GSK3-B	Rabbit IgG	1:1000	-	CST / 12456
Phospho-GSK-3β (Ser9)	Rabbit IgG	1:1000	-	CST / 5558
ERK 1/2 MAPK	Rabbit IgG	1:1000	-	CST / 4695
Phospho-ERK 1/2 MAPK	Rabbit IgG	1:1000	-	CST / 4370
p38 MAPK	Rabbit IgG	1:1000	-	CST / 8690
Phospho-p38 MAPK	Rabbit IgG	1:1000	-	CST / 4631
Tau	Rabbit IgG	1:1000	-	Abcam / ab64193
Tau phospho (S199)	Rabbit IgG	1:5000	1:100	Abcam / ab4749
Tau phospho (S199 + S202)	Rabbit IgG	-	1:100	GeneTex / GTX24864
6E10 (anti amyloid beta antibody)	Mouse IgG	1:1000	1:100	Biolegend / 803001
4G8 (anti amyloid beta antibody)	Mouse IgG	1:1000	1:100	Biolegend / 800701
G2L2	Rabbit IgG	1:1000	1:100	Abcam / ab170275
EB-1	Rabbit IgG	1:1000	1:100	Invitrogen / PA5-25913
Tubulin-alpha	Mouse IgG	1:1000	1:100	Santacruz biotech. / sc-58667

Table 9: List of secondary antibodies and their applications in current study

Secondary antibody	Origin	Dilution (IB)	Dilution (IF)	Company/ Cat. No.
α-Mouse-HRP	Goat	1:10000	-	JacksonIR Lab / 115-035-062
α-Rabbit-HRP	Goat	1:10000	-	JacksonIR Lab / 111-035-144
α-Goat-HRP	Goat	-	1:200	JacksonIR Lab / 705-035-003
α-Mouse-A488	Goat	-	1:200	Thermo Fischer Sci. / A32723
α-Rabbit-A488	Goat	-	1:200	Thermo Fischer Sci. / A-11034
α-Mouse-A546	Goat	-	1:200	Thermo Fischer Sci. / A-11003
α-Rabbit-A546	Goat	-	1:200	Thermo Fischer Sci. / A-11010

2.1.2 Chemicals

Chemicals used in the study were purchased from Sigma-Aldrich, Fluka (Deisenhofen, Germany), Merck (Haar, Germany), Roth (Karlsruhe, Germany), BioRad (München, Germany) and Amersham (Freiburg, Germany), or are otherwise mentioned in the text.

2.1.3 Kits

Kits used for the study included

i) High throughput Co-IP kits (catch and release HT immunoprecipitation kit, Cat. No.17-501, Merck)
ii) Pierce High pH Reversed-Phase Peptide Fractionation Kit, Thermo Fisher Scientific

2.1.4 Laboratory equipment and other materials

The table below lists the instruments and other materials used in the study.

Table 10: Instruments and other materials used in the study

Appliance	Model / Description	Company
Tissue lyser LT	85600	Qiagen, Hilden, Germany
Tabletop ultracentrifuge	Optima™ TL 100	Beckman coulter, Krefeld, Germany
Refrigerated centrifuge	5415 C	Eppendorf, Hamburg, Germany
Speedvac	SPD111V	Sigma-Aldrich, Savant
Picofrit reversed phase-C18 column	0.075 mm ID × 200 mm	New Objective, Woburn, USA
Hybrid quadrupole/orbitrap mass spectrometry system	Q Exactive	Thermo Fisher Scientific, Dreieich, Germany
Nanoflow chromatography system	Eksigent nanoLC425	AB Sciex, Darmstadt, Germany
Mass spectrometer	TripleTOF 5600+	AB Sciex, Darmstadt, Germany
Protean i12 IEF system	164-6000	Bio-Rad, Munich, Germany
Floor ultracentrifuge	Optima™ TL 60	Beckman coulter, Krefeld, Germany
Swinging bucket rotor	SW-55ti	Beckman coulter, Krefeld, Germany
Thin wall Polyallomer tubes	13 x 51mm	Beckman coulter, Krefeld, Germany
ChemiDoc ™ XRS+ system	170-8265	Bio-Rad, Munich, Germany
Mini-PROTEAN Tetra Cell	1658004EDU	Bio-Rad, Munich, Germany
PVDF membrane	Amersham Hybond P 0.2	GE Healthcare Life Sciences
Nitrocellulose membrane	Amersham Protran 0.2 NC	GE Healthcare Life Sciences
Semi-Dry transfer cell	Transblot Turbo transfer system	Bio-Rad, Munich, Germany
Power supply	Power Pac 300	Bio-Rad, Munich, Germany
Thermomixer	5436	Eppendorf, Hamburg, Germany
Microscope	Leica TCS SPE	Leica, Wetzlar, Germany

2.1.5 Software

The following software were used in the study.

Table 11: List of software used in study

Software	Use	References
LabImage 2.7.1	Densitometric analysis	Kapelan GmbH, Halle, Germany
ImageJ 1.51j8	Co-localization analysis	National institutes of Health, USA
Raw2 MSM v1.10 software	Instructing Mass spectrometer	Thermo Fisher Scientific, Dreieich, Germany
Excalibur v2.4 software	Instructing Mass spectrometer	AB Sciex, Darmstadt, Germany
Scaffold 4.8.4	MS/MS data analysis	Proteome Software, Inc
Perseus	MS/MS data analysis	MPI of Biochemistry, Martinsried, Germany
Zeiss LSM 4.2.0.121	Immunofluorescence	MicroImaging GmbH, Göttingen, Germany
R version 3.4.3	Statistical analysis	
Graphpad Prism 6	Statistical analysis	GraphPad Software, Inc. California, USA

2.1.6 Stock Solutions

Lysis Buffer I: 2 M thiourea, 7 M urea, 4% CHAPS, 66 mM DTT and 0.5% ampholytes

Tissue-Lysis Buffer II: 2% sarkosyl in PBS (without Ca^{2+} and Mg^{2+})

Lysis Buffers for subcellular protein enrichment:

NP-40 lysis buffer: 50 mM Tris HCl, pH 7.6, 0.01% NP-40, 150 mM NaCl, 2 mM EDTA and 0.1% SDS

TNT lysis buffer: 50 mM Tris HCl, pH 7.4, 150 mM NaCl and 0.1% Triton X-100

RIPA buffer: 50 mM Tris HCl, pH 7.4, 150 mM NaCl, 0.5% Triton X-100, 1 mM EDTA, 3% SDS and 1% deoxycholate

Rt-QuIC reaction Buffer: 162 mM phosphate buffer (pH 6.9), 170 mM NaCl, 1 mM EDTA, 10 µM thioflavin-T, 0.1 mg/mL recPrP.

Citrate buffer (pH 6.0): 10mM sodium citrate (pH 6.0)

Laemmli Buffer (4x): 2.0 mL 1M Tris-HCl pH 6.8, 1.0 mL 0.5 M EDTA, 4.0 mL 100% glycerol, 0.4 mL 14.7 M β-mercaptoethanol, 0.8 g SDS, 8 mg bromophenol Blue.

Tris-glycine electrophoresis buffer 10x (1L): 144 g Glycin, 30 g Tris, 10 g SDS, ddH2O

Resolving gel buffer: 1.5M Tris, 2% SDS (pH 8.8), ddH_2O

Transblot buffer 10x: 48 mM TRIS, 39 mM Glycin, 1 mM SDS

TBS-T: TBS and 0.1% of Tween-20

Blocking solution for immunoblotting: 5% Milk Powder in TBS-T

Silver staining solutions

Developing solution: 6% Na2CO3, 0.0185% formaldehyde, 16 µM Na2S2O3 in ddH2O

Fixation solution: 50% methanol, 12% acetic acid in ddH2O

Sensitizing solution: 0.8 mM Na2S2O3 in ddH2O

Silver nitrate solution: AgNO3 0.2% and 0.026% formaldehyde in ddH2O

Peptide digestion and extraction solutions

Reducing buffer: DTT (10 mM in 100 mM NH_4HCO_3)

Alkylation buffer: IAA (55 mM in 100 mM NH_4HCO_3)

Porcine trypsin: 12.5 ng/µL in 50 mM NH_4HCO_3, 5 mM $CaCl_2$

2.2 Methods

An overview of methods used in the current study is given in Figure 7. The detailed methods are discussed below.

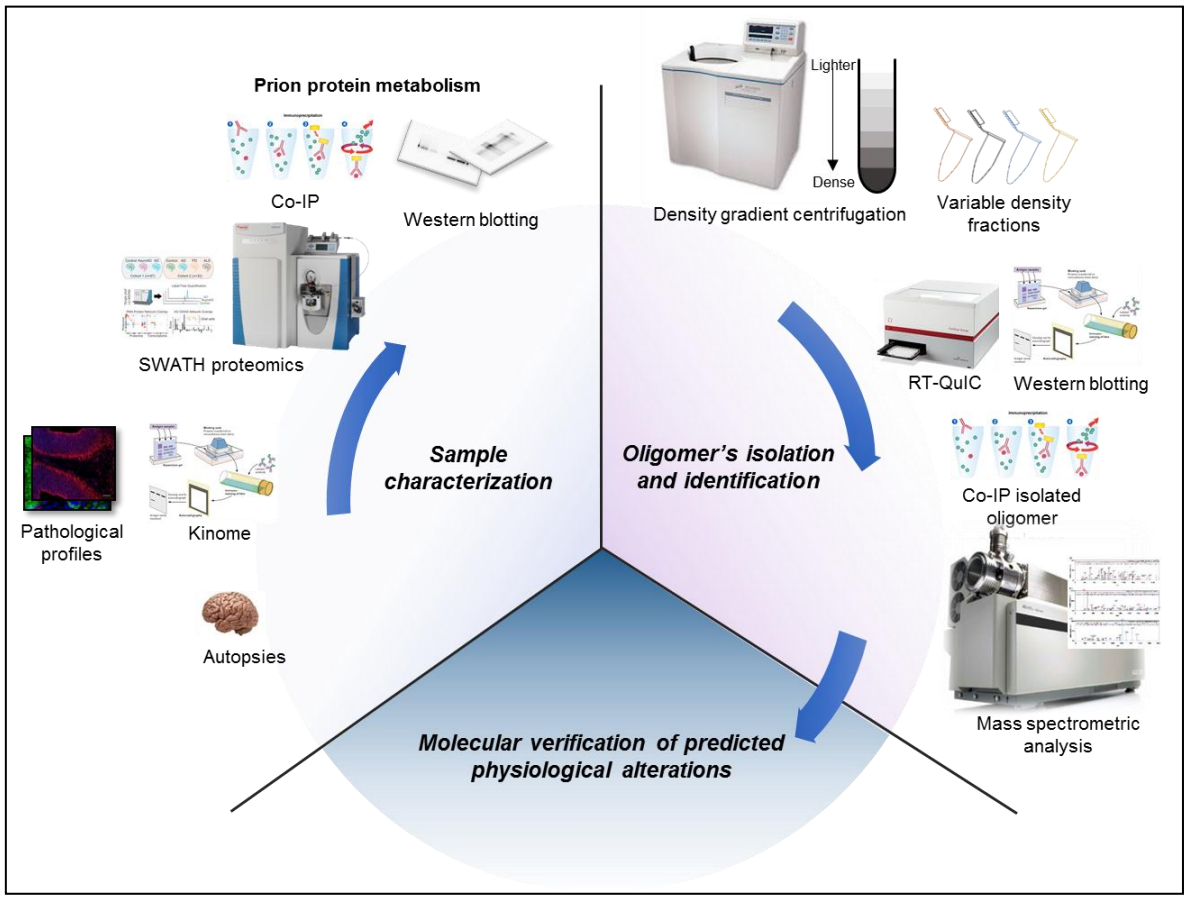

Figure 7: Overview of methodology. The first phase of the study included the sample collection (brain autopsies), characterization for various pathological features and assessment of biochemical regulations of kinases that are involved in the neurodegenerative diseases. The prion protein metabolism was then studied. In the second phase, high-density, molecular species of PrP were isolated (using ultracentrifugation) and their biochemical composition was demonstrated using Co-IP. Additionally, other high-density molecules were studied using high-resolution mass spectrometry. Finally, the predicted interactors were studied for their physiological relevance in the disease cases.

2.2.1 Sample collection and processing

Frontal cortex samples from cohorts with spAD, rpAD, small vessel disease (SVD), rapidly progressive dementia with Lewy bodies (rDLB), dementia with Lewy bodies (DLB) and dementia with frontotemporal lobar degeneration, were provided by the Brain Bank of Institute of Neuropathology (HUB-ICO-IDIBELL Biobank) and Biobank of Hospital Clinic-IDIBAPS Spain. Frontal cortex samples from patients with sporadic

Creutzfeldt-Jakob disease (sCJD) subtypes were obtained from the Department of Neurology at the University Medical Center, Göttingen, Germany.

A rapidly progressive Alzheimer's disease cohort was composed of those patients who strictly fulfilled the following inclusion criteria:

1. Initial classification as prion disease based on clinical parameters
2. Neuropathological diagnosis of Alzheimer's disease, due to an indication of AD pathological features, i.e., higher Braak and CERAD stages justifying AD diagnosis whereas assessment and diagnosis of the examining neuropathologist were accepted as an adequate neuropathological diagnosis in cases of unavailability of the data on CERAD / Braak staging).
3. Exclusion of prion disease and other relevant, potential causes of rapid dementia (i.e., extensive cortical Lewy body pathology (Braak stage ≥5.6), tumors, significant vascular disease, stroke, inflammation, etc.) based on the neuropathological assessment.
4. The absence of history suggestive of familial AD (autosomal dominant mutations)

In the case of agreement with all the above-stated inclusion criteria, patients of all ages were included in the study.

One-centimeter thick sections were excised from one of the hemispheres. Dissected tissues were frozen rapidly and were later kept at -80ºC until further use for biochemical investigations. The other hemisphere was fixed by immersion in 4% buffered formalin for three weeks. Neuropathological and morphological characterizations were made later.

2.2.2 Pathological profiles

Non-demented control samples included in the study belonged to Braak stage I – II. Brain cortex samples for Alzheimer's subtypes were only included in the study if there were no co-pathologies. Braak stages (disease progression) in both spAD and rpAD were comparable and ranged from stage III to VI. The DLB cohort also included samples without any co-pathology (Braak stages I – III). Likewise, cortex samples from the sCJD (subtypes) cohort had pure prion pathologies. However, some brain samples included in rDLB, DFTL and SVD showed mixed pathologies. rDLB samples contained

co-existing AD pathology, tauopathy, progressive supranuclear palsy (PSP), and argyrophilic grain disease (AGD). Cerebral cortex samples from a DFTL cohort also showed features of motor neuron disease (MND) and TDP-43 pathology. All the SVD samples showed higher stages of AD pathology. Hippocampal sclerosis was also seen in one of the samples from the SVD cohort. Details of the studied cohorts are discussed in annexure data Table 14 to Table 16.

There were no significant differences in the age distribution of pathological cohorts included in the study (Figure 8 and Figure 9A). When compared, post-mortem intervals among the studied cohorts were also not significantly different from each other. Figure 9.B details the comparison of PMI in the studied cohorts. An overview of the sample cohorts is provided in Figure 8, and complete sample details are provided in the annexure (Table 14-Table 16).

2.2.3 Ethics statement

Samples were handled following the local legislation (Ley de la Investigación Biomédica 2013 and Real DecretoBiobancos, 2014). The Creutzfeldt-Jakob disease (sCJD) cohort was obtained after the approval of local ethics committees at the University Medical Center, Göttingen.

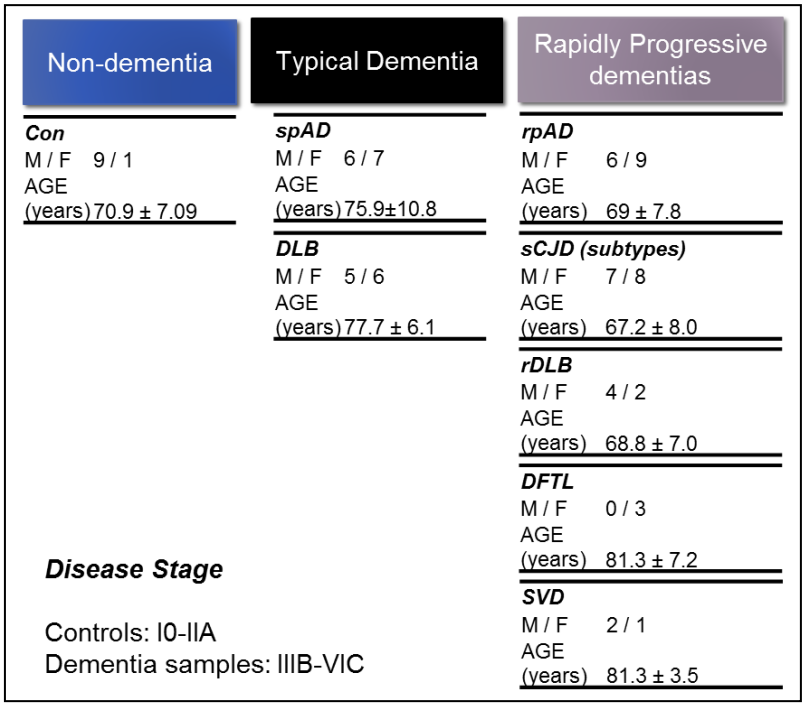

Figure 8: Summary of frontal cortex cohorts used in current study. The details of the cohort are given in the annexure (**Table 14-Table 16**).

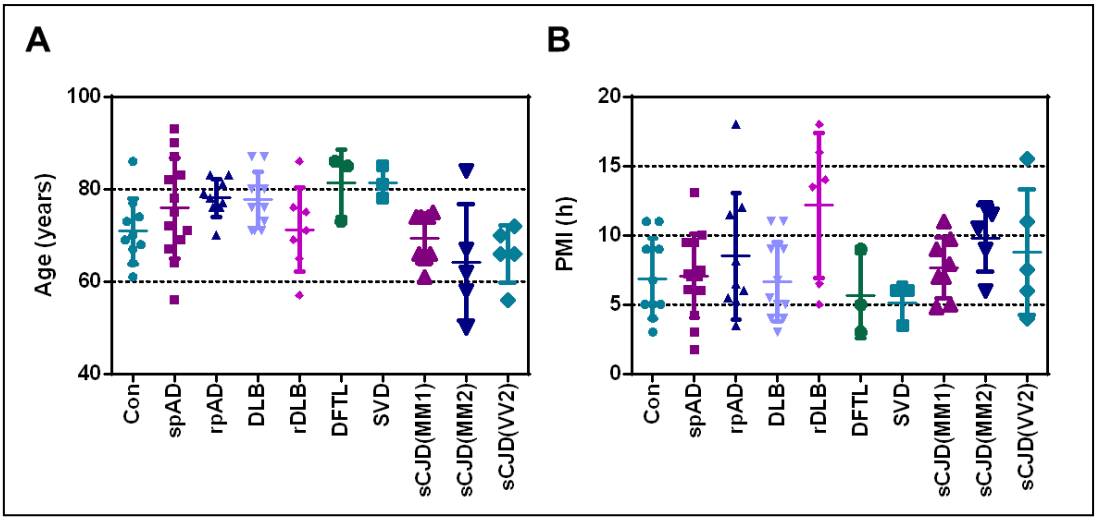

Figure 9: Sample cohorts used in the study A) Comparison of ages of the diverse pathological cohorts used in the study. B) Graph presents a comparison of post-mortem intervals to the time of autopsies.

2.2.4 Protein extraction

For immunoblotting and whole proteome mass spectrometric analysis, tissue slices were homogenized using a steel beads tissue disruptor (Qiagen), in ice-cold lysis buffer I to a final concentration of 10% w/v and were replenished with protease and phosphatase inhibitor cocktails (Roche). Homogenates were incubated at 4°C overnight. After ultracentrifugation at 40,000 xg at 4°C for 30 min (Beckman Coulter ultracentrifuge), supernatants were taken and used further for downstream applications.

Protein extractions performed otherwise are mentioned in the respective section, i.e. density gradient centrifugation, subcellular protein enrichments, and proteinase K digestion.

2.2.5 Protein concentration estimation

The protein concentration of homogenates was determined using the Bradford assay (Bio-Rad). Dye reagent concentrate (Bio-rad) was diluted with ddH_2O to prepare the working solution. The working solution of the dye was then filtered through Whatman filter paper before use. Bovine serum albumin (BSA) standards of serial concentrations were prepared in ddH_2O with the concentrations ranging from 0-1 mg/mL. Protein samples with unknown concentration were diluted 1:10 or 1:20 before measurements. Protein standards or diluted samples were mixed with Bradford working solution following the kit instructions and were incubated for 10 min at room temperature (RT). Absorbance of the samples was measured at 595 nm. Absorbance measurements of

standards were used for calculating the standard curve, which in turn was used for estimating the unknown protein concentrations.

2.2.6 SDS-PAGE and immunoblot analysis

Bi-phasic gels, with a 4% stacking gel and a 12% resolving gel were used for separating proteins based on their molecular weights. Isolates containing equal protein amounts were mixed with the corresponding volume of 4x Laemmli buffer and were heated to 95°C for 5 minutes in a thermomixer. Samples were loaded onto the gels along with suitable molecular weight protein marker (Bio-rad dual color precision plus protein standards). Electrophoresis was carried out at 100 V, until the loading dye reached the bottom of the resolving gel. Running buffer (1x) was prepared by diluting 10x running buffer stock. To resolve the density variant fractions, ready to use 26 well criterion TGX, 4-12% gradient gels (Bio-Rad) were used instead.

Relative protein expressions were assessed by immunoblotting. Resolved proteins were blotted onto PVDF or nitrocellulose membrane (0.2 µm pore size) from the gel, using semi-dry transfer at 14 V for 1 h. Transfer buffer (1x) was prepared with 20% methanol to use with PVDF and without methanol to use with nitrocellulose membranes. After transfer, blots were blocked for 1 h at RT, using either 5% fat-free milk or 2.5% BSA depending on the antibody to be probed.

After having been blocked, the blots were incubated with primary antibodies of different specificities and dilutions (see Table 1) overnight at 4°C. Membranes were then washed with TBS-T (1x) and incubated with the respective horse radish peroxidase (HRP)-conjugated secondary antibody (see Table 2) for 1 h at RT. Immunoreactivity was detected after immersing the membranes in enhanced chemiluminescence (ECL) solution, followed by scanning using a Bio-Rad Chemidoc imaging system.

2.2.7 Co-immunoprecipitation from frontal cortex lysates

PrP^C interacting proteins were isolated using Dynabeads protein G bead (Thermo Fischer scientific) bound to mouse monoclonal anti-prion (SPI Bio). To attach antibody molecules to protein G beads, the beads were prepared by washing with 1x PBS and twice with 0.3% CHAPS. The antibody was incubated to bind to protein G beads at manufacturer-recommended dilution for 20 min at 4°C on a tube rotator. Unbound antibody was removed by separating beads on the magnet. Cortex protein isolates were

then introduced at a concentration of 1 µg/µL to antibody-bound beads overnight at 4°C on a tube rotator. Unbound protein/complexes were taken out by pelleting protein G beads on the magnet. Beads were then washed four times with 0.3% CHAPS and transferred to a new tube to avoid non-specific elution of proteins bound to the tube wall. Proteins captured by antibody bound to Protein G beads were eluted either by denaturation of beads in 2x Laemmli buffer at 95°C for 5 min or by incubating beads with glycine buffer (50 mM, pH 2.5) for 2 min at RT in a tube rotator (eluates after glycine elution were neutralized with 1 M Tris, pH 9). The eluates were further used for immunoblotting and mass spectrometric identifications.

2.2.8 Sub-cellular (extracellular, intracellular and membrane) proteins enrichment

Differentially enriched protein fractions, i.e. i) extracellular proteins, ii) intracellular proteins, iii) membrane protein fractions, and iv) formic-acid-soluble protein aggregates, were isolated from human cortical tissues from patients with spAD, rpAD and non-demented control cases to investigate the distribution of PrP^C in the cerebral environment. These differential enrichments were prepared by following a previously described protocol (Sherman & Lesné, 2011). Briefly, frozen cortex sections, weighing ~150 mg, were taken in 500 µL of ice-cold NP-40 lysis buffer. Tissues were then initially homogenized mechanically using a 1 mL syringe without a needle (5 repeats), followed by passing the homogenates through the syringe after attachment of a 20-gauge needle 5 times. Soluble components (mostly extracellular proteins, EC) were separated by centrifugation at 800 xg for 10 min at 4°C and transferred to a new tube. Following extraction of extracellular proteins, pellets were re-suspended in 500 µL of ice-cold TNT lysis buffer by passing the mixture through a 1 mL-pipette, 8 to10 times, to obtain a homogenous mixture. Soluble components mostly intracellular (IC) proteins were separated by centrifugation at 16,100 ×g for 90 min at 4°C and stored for later use. Following extraction of IC proteins, the resultant pellets were dissolved in 750 µL of RIPA buffer to extract membrane-bound proteins (MB). Pellets were homogenized thoroughly using a 1 mL-pipette (with 30 repeats) and thereafter vortexed for 20s. Homogenates resulting were then incubated at 4°C for 15 min on a rotating platform to enhance chemical lysis followed by centrifugation at 16,100 xg, 4°C for 90 min to separate the membrane-bound protein-enriched fraction (MB). Following removal of membrane-associated proteins, resultant pellets were solubilized in 40 µL of freshly

prepared formic acid by passing the mix through a 1 mL pipette 15 times. Mixtures were then vortexed and incubated for 30 min at RT with agitation at 1,200 rpm. Homogenates were then supplemented in 760 µL of 1M Tris HCl (pH 8), followed by centrifugation at 16,100 xg for 90 min at 4°C. The supernatant was collected as formic-acid-enriched fraction (FA). To remove any insoluble components, all enriched fractions (EC, IC, MB, and FA) were centrifuged again at 16,100 ×g at 4°C for 90 min. Resultant minute pellets were discarded and supernatants were used for further biochemical analysis. Formic-acid-enriched fractions were concentrated by vacuum centrifugation (to improve protein concentrations, volume was reduced to half). Lysis buffers, i.e. NP-40, TNT and RIPA lysis buffers, were filtered using a 0.2 µm syringe filter and were supplemented with protease and phosphate-inhibitors cocktail prior to use.

2.2.9 Sucrose-gradient ultracentrifugation

For the segregation of density variants of proteins, rate zonal centrifugation was applied to cerebral cortex homogenates derived from patients with rpAD, spAD, and CJD subtypes as well as to age-matched controls. Sucrose-density-gradient centrifugation was carried out following the protocol already described (Cohen et al., 2015; Zafar, Younas, et al., 2018). Frontal cortex homogenates, 10% w/v in tissue lysis buffer I, were prepared using microbeads homogenizer. Homogenates were then clarified by centrifugation at 500 xg for 5 min, and 400 µL were carefully layered onto the top of 10 – 45% sucrose gradients. Gradients were manually prepared in thin wall polyallomer tubes (13 x 51 mm, Beckman) by layering sucrose solutions at different dilutions from bottom to top. Sucrose serial dilutions (10, 15, 20, 25, 30, 35, 40, 45% w/v) were prepared in PBS-1% N-lauryl sarkosyl (pH 7.4). To avoid variation among the replicates in an experiment, all the gradients were prepared with the same buffer batch at the same time. For the preparation of sucrose gradients in the thin wall polyallomer tubes, the tubes (sucrose layers) were frozen for 10min at -80°C after addition of each sucrose layer. The next layer was then added over the previous frozen layer, to avoid mixing of sucrose serial dilutions, the method was modified from a previously described protocol (Luthe, 1983). Gradients were then allowed to thaw overnight at 4°C before use. Ultracentrifugation was performed at 50,000 rpm for 73 min at 5°C in an Optima TL 60 floor ultracentrifuge (Beckman Coulter) equipped with a Beckman Coulter SW-55ti rotor. These conditions correspond to the adjusted proportionality constant k = 58.7 and angular velocity v = 5236 rad/s. Thereafter, twenty density variant

fractions, 200 µL each, were collected carefully from top to bottom in separate tubes from each sample.

2.2.10 Preparation of protein and peptide pools from high-density gradient fractions

Equal volumes of same density gradient fractions originating from the frontal cortices (n=6) of different patients from each pathological cohort were pooled together to proceed to co-immunoprecipitation and mass spectrometric analysis.

2.2.11 Co-immunoprecipitation of density variant fractions

To study the unique interactomics signature of density variant species of PrP^C oligomers, high throughput co-immunoprecipitation was employed. Density variant fractions were replenished with the phosphatase and protease-inhibitor cocktails, before the co-immunoprecipitation assay was carried out. High throughput Co-IP kits (catch and release HT immunoprecipitation kit, Cat. No.17-501, Merck) were used for the sake of assay homogeneity. High-density fractions were employed for Co-IP according to the manufacturer's instructions. Together with the fractions, lysate-only controls, antibody-only controls and whole lysate control were also included in the assay.

2.2.12 Proteinase K digestion

Protein homogenates prepared in Lysis buffer II (10% w/v) containing 200 µg of proteins were treated with proteinase K (PK) at a concentration of 50 µg/mL. Protein digestion was carried out at 37°C for 1 h, with the thermomixer set at 300 rpm orbital shaking. The digestion process was terminated by heating the samples at 65°C for 15 min. The digested samples were then boiled with adjusted volumes of 4x Laemmli buffer. Cooled-down samples were then used for SDS-PAGE together with the PK-untreated samples (as negative controls).

2.2.13 Silver staining

After a thorough washing in ddH_2O, the gels were incubated in a fixative solution for a minimum of 1 h. Fixed gels were then incubated with 50% ethanol for 20 min followed by incubation in 30% ethanol for another 20 min. Gels were then sensitized with sensitization buffer for 1 min (with gentle shaking) and incubated in silver-staining solution for 20 min while being shaken. Thereafter, the gels were washed in ddH_2O for 1 min

to remove excess stain. Gels were then incubated in the developing buffer until the required contrast was obtained (usually 5 min). The developing process was stopped by the addition of the fixative solution to the gel. Gels were washed and stored in 5% acetic acid for later use.

2.2.14 Real-time quaking-induced cyclic amplification (RT-QuIC)

Real-time quaking is a fluorometry-based assay for the determination of prion seeding activity. The method relies on the use of recombinant PrP peptide substrate to amplify the PrP seed from biological samples, i.e. brain tissue homogenate in our case. Aggregated PrP seed binds with the thioflavin-T (Th-T) dye giving a fluorescence signal, hence establishing the measurement basis of the assay. RT-QuIC reaction buffer (85 µL) was seeded with freshly prepared brain homogenates. Brain homogenates (10% w/v) were prepared in PBS (pH 7.4) supplemented with protease and phosphatase-inhibitor cocktails. Samples were further diluted in PBS with a dilution factor of 10^{-3}. Reactions were carried out in 96-well optical bottom black plates. After having been sealed, the plates were incubated in the FLOUROStar optima fluorometer at 42°C for 80 h with intermittent shaking cycles (1 min, double orbital shaking, 600 rpm), followed by 1 min rest. Fibrillation kinetics were assessed by measuring Th-T fluorescence intensity at 450 nm every 30 min.

2.2.15 Staining of cryopreserved and formalin-fixed paraffin-embedded (FFPE) tissues

Frozen tissue sections were affixed to the chuck of the cryotome using tissue tec (OCT). The complete process was performed without the tissue being allowed to thaw. Tissue sections of 5 µm thickness were obtained and were carefully transferred from the cryotome platform to glass slides. Tissue sections on glass slides were fixed by immersion in methanol for 9 min followed by immersion in acetone for 1 min.

For paraffin-embedded blocks, frontal cortex sections were taken from buffered formalin-fixed hemispheres and were dehydrated in serial ethanol dilutions (10% - 100%), replaced by xylene, and the sections were embedded in paraffin. Sections of 2-5 µm thickness were cut using a sliding microtome and were mounted on glass slides after having been flattened on the water surface in a water bath set at 37°C. For further immunofluorescent preparations, sections were dewaxed by incubating the slides at 63°C, followed by incubation with xylene and rehydration by immersing in

alcohol serial dilutions (100%-95%-80%-50%) for 5 min each, with a final incubation in water for 5 min. Antigen retrieval was achieved by cooking the sections in citrate buffer (pH 6.0) for 1 h, followed by 30 min cooling and 1 h washing with tap water. Sections were exposed to UV-A and UV-B for 20 min followed by incubation with Sudan Black, 0.1% in 25% EtOH for 20 min as a countermeasure to autofluorescence. Slides were then washed in 1x PBS. Tissue sections were permeabilized with 0.2% Triton X-100 in 1x PBS, followed by a 30 min blocking using blocking buffer with 10% FBS and 1% BSA in 1x PBS. Blocking was followed by the primary antibody (diluted in 1% BSA-PBS) incubation at 4°C overnight. Amyloid plaques were visualized using mouse anti-Aβ antibodies (6E10 + 4G8; 1:100 in antibody diluent), Tau tangles were visualized using rabbit anti-Tau (1:100), and rabbit anti-Tau phospho-(S199 + S202) (1:100) antibodies. The co-localization of G2L2 and the interacting partners was analyzed using rabbit anti-growth arrest specific 2 like 2 (1:100), mouse anti-PrP SAF70 antibody (1:100), rabbit anti-end binding protein 1 (1:100), mouse anti-actin-beta antibody (1:100) and mouse anti-tubulin-alpha antibody (1:100). After having been washed with PBS, slides were incubated for 60 min with corresponding Alexa-488 and Alexa-546 labeled secondary antibodies. For the nuclear staining, slides were incubated with TO-PRO-3 iodide (1:1000 dilution in PBS) for 10min at RT. Finally, coverslips were mounted on the glass slides with Fluoromount-G and were stored at 4°C prior to confocal scanning. All the steps were carried out in a dark, humid chamber.

2.2.16 Confocal laser scanning and image quantification

Confocal laser scanning microscopy was carried out using an SPE laser-scanning microscope (Leica, Germany; 543 and 633 nm helium-neon and 488 nm argon excitation wavelengths) using a 63x/1.25 oil immersion lens for the localization of PrP^C and other interacting proteins. Resulting individual images were separately analyzed for co-localization using the ImageJ (WCIF plugin) software. For two-color analysis, images were obtained using a dynamic range of 12 bits per pixel. Threshold Mander's overlap coefficient and Pearson's linear correlation coefficient (*rP*) values were calculated to quantify fluorescence channel correlations and illustrate the strength and direction of the linear relationship between two fluorescence channels. Additionally, intensity correlation analysis (ICA) was carried out for the channel intensities. The ICA analysis is based on a comparison of intensities of signal A or B along the product of the differences from the mean (PDM: product of the difference of each pixel A and B intensities

from their respective means as previously described (Li et al., 2004)). The resulting plots emphasize the high intensity stained pixels and allow the identification of protein pairs that vary in synchrony (positive PDM values), randomly (around 0), or independently (negative PDM values) within the cell.

2.2.17 Mass spectrometry-spectral counting

2.2.17.1 Peptide digestion and extraction

Either frontal cortex homogenates (50 µg protein per sample), density variant fractions (30 µL) or Co-IP eluates from density variant fractions (30 µL each) were loaded onto 4-12% NuPAGE Novex Bis-Tris Mini gels (Invitrogen) and run into the gel for 1 cm. Following Coomassie staining, the protein-stained gel areas were excised, diced, and washed in ddH_2O. After having been washed, the gel slices were reduced with reducing buffer (10 mM DTT in 100 mM NH_4HCO_3) by being incubated for 30 min at 56°C, followed by alkylation with alkylation buffer (55 mM IAA in 100 mM NH_4HCO_3) at RT in the dark for 60 min. Gel slices were then incubated in acetonitrile (ACN) for 15 min and dried in a SpeedVac to remove excess solvent. Dried gel slices were stored at -20°C before further use (Atanassov & Urlaub, 2013). For mass spectrometric identification of Co-IP from whole brain homogenates, the eluates were loaded on to 12% SDS polyacrylamide gels and gel electrophoresis continued until the loading dye had reached the bottom. Gels were then silver-stained, and the silver-stained bands were excised and processed for the peptide extraction with the protocol detailed above.

2.2.17.2 Peptide identification

Peptide mixtures were concentrated on a reversed phase-C18 precolumn (20 mm x 0.15 mm ID, self-packed with Reprosil-Pur 120 C18-AQ 3 µm material). Separation was achieved on a reversed phase-C18 nanoflow chromatography (Picofrit column, 0.075 mm ID × 200 mm (New Objective, Woburn, USA)) using a 60 min linear gradient (5-35% acetonitrile vs. 0.1% formic acid gradient), at a flow rate of 240 nL/min on an Easy nLC-1000 nanoflow chromatography system (Thermo Fisher Scientific, Dreieich, Germany). Eluents were analyzed on a Q Exactive hybrid quadrupole/orbitrap mass spectrometry system instructed by Excalibur v2.4 software (Thermo Fisher Scientific). A top10 method in the Data Dependent Acquisition mode was implemented to carry out the analysis. Raw2MSM v1.17 software (Max Planck Institute for Biochemistry, Martinsried, Germany) was used to extract tandem mass spectra for database

searching. MS/MS spectra were evaluated using Mascot (Matrix Science, London, UK; version 2.4.1) instructed to search for UniProt/SwissProt *Homo sapiens* reference proteome (revision 02-2017, 92,928 entries) with mass tolerances of 5 ppm for precursors and 0.02 Da for fragments, respectively. Methionine oxidation was considered as a variable post-translational modification (PTM) and cysteine carbamidomethylation as a fixed modification. Up to two missed cleavages were allowed. For validation of MS/MS based peptide and protein identifications, Scaffold software v4.8.4 (Proteome Software, Portland/OR, USA) was used. Peptide identifications were accepted if established at greater than 95.0% confidence, while a minimum of two confident peptide identifications and a confidence threshold of 99.0% was required for protein identifications.

2.2.18 SWATH-MS (Sequential Windowed Acquisition of All Theoretical Fragment Ion Mass Spectra)-based global proteomics

2.2.18.1 Library preparation

For the generation of a peptide library, equal amount aliquots from each sample were pooled to a total amount of 80 µg and separated into eight fractions using a reversed phase spin column (Pierce High pH Reversed-Phase Peptide Fractionation Kit, Thermo Fisher Scientific).

Peptides resulting from tryptic digestion were analyzed on an Eksigent nanoLC425 nanoflow chromatography system associated hybrid triple TripleTOF 5600+, quadrupole-TOF mass spectrometer (equipped with a Nanospray III ion source). Parameters for ionization were set as follows: ionspray voltage 2400 V, interface heater temperature 150°C, and sheath gas setting 12. Analyst TF 1.7.1 software build 1163 (AB Sciex) was used to instruct the system. Peptides were dissolved in loading buffer (2% acetonitrile, 0.1% formic acid in water) to a final concentration of 0.3 µg/µL. For each analysis, 1.5 µg of digested protein were concentrated on a self-packed precolumn (0.15 mm ID x 20 mm, Reprosil-Pur120 C18-AQ 5 µm, Dr. Maisch, Ammerbuch-Entringen, Germany), followed by separation on an analytical RP-C18 column (0.075 mm ID x 250 mm, Reprosil-Pur 120 C18-AQ, 3 µm, Dr. Maisch) using a 100 min linear gradient of 5%-35 % acetonitrile-0.1% formic acid at a flow rate of 300 nL/min. Qualitative LC-MS/MS analysis was performed using a Top30 data-dependent acquisition method with an MS survey scan of *m/z* 380–1250 accumulated for 250 ms at a

resolution of 35,000 full width at half maximum (FWHM). MS/MS scans of *m/z* 180–1500 were accumulated for 100 ms at a resolution of 17,500 FWHM and a precursor isolation width of 0.7 FWHM, resulting in a total cycle time of 3.4 s. Precursors ions with a threshold MS intensity of more than 200 cps and with charge states 2+, 3+, and 4+ were selected for MS/MS, and the dynamic exclusion time of 15 s was set. MS/MS activation was achieved by CID by the manufacturer's default rolling collision energy settings using nitrogen as a collision gas. Two technical replicates per reversed phase fraction were analyzed to construct a spectral library.

2.2.18.2 Quantitative SWATH measurement

For quantitative SWATH analysis, MS/MS data were acquired using 100 variable size windows (Zhang et al., 2015) across the 400-1200 *m/z* range. Fragments were produced using rolling collision energy settings for charge state 2+, and fragments acquired over an *m/z* range of 180–1500 for 40 ms per segment. Including a 250 ms survey scan, this resulted in an overall cycle time of 4.3 s. Two replicate injections were acquired for each biological sample. Protein identification was achieved using ProteinPilot Software version 5.0 build 4769 (AB Sciex) at "thorough" settings. A total of 152,341 MS/MS spectra from the combined qualitative analyses were searched against the UniProtKB *Homo sapiens* reference proteome (revision 02-2017, 92,928 entries) augmented with a set of 51 known common laboratory contaminants to identify 1,756 proteins at a false discovery rate (FDR) of 1%. Spectral library generation and SWATH peak extraction were achieved in PeakView Software version 2.1 build 11041 (AB Sciex) using the SWATH quantitation microApp version 2.0 build 2003. Following retention time correction on endogenous peptides spanning the entire retention time range, peak areas were extracted using information from the MS/MS library at an FDR of 1% (Lambert et al., 2013). The resulting peak areas were then summed to peptide and finally protein area values, which were used for further statistical analysis.

2.2.19 Statistical analysis

Graphpad Prism 6.0 was used for basic statistical analysis. For immunoblotting, densitometric analysis of western blots and 1-DE gels was carried out using Lab image (version 2.7.1 Kapelan, Leipzig, Germany) software. Results in the current study were obtained from four independent experiment sets and are expressed as mean ± S.E.M (standard error of the mean). For prion protein-interactome identification (Co-IP mass

spectrometric analysis) of frontal cortex lysates, MS/MS readings were carried out in duplicates for four biological replicates for each disease subtype and non-demented controls (n=4). Likewise, interactome of high-density prion oligomers was carried out by Co-IP mass spectrometric analysis of IP eluates in technical replicates (n=2). Global proteomic profiling of high-density fraction pools by mass spectrometric spectrum counting was also performed in technical replicates (n=3). Principle component analysis, z-score normalizations and one-way ANOVA were carried out using Perseus (version: 1.6.1.3). For hierarchical clustering, gplots R-package was used. Statistical significance was considered for p-value < 0.05. No adjustments for multiple testing were performed in this pilot study.

2.2.20 Bioinformatic analysis

UniProt/SwissProt database (release 02/14 filtered for *Homo sapiens* entries) was used for functional enrichment of the detected proteins from the MS/MS analysis. Protein candidates from high-density fraction datasets and global proteome datasets were manually grouped in modules, based on the UniProt/SwissProt database annotations, representing a singular physiological category for proteomics

Pathway enrichment analysis of HDP-ligands was performed using the Bioconductor clusterProfiler package (Yu, Wang, Han, & He, 2012). Reactome pathway database for *Homo sapiens* was used as a reference database (Fabregat et al., 2018).

Protein-protein interactions were structurally visualized by *in silico* analysis using a web-based tool, the ZDOCK server-version 3.0 (Pierce et al., 2014; Pierce, Hourai, & Weng, 2011). Three-dimensional reference structures for the proteins studied were taken from a protein databank (Berman, Henrick, & Nakamura, 2003).

3 Results

Diseases are usually outcomes of multiplex physiological variations at biochemical and metabolic strata. Minor differences even in these physio-alterations result in the broad spectrum of variability even in a single disease giving rise to subtypes.

Likewise, differences have been discussed for the progression rate amongst patients with Alzheimer's disease, leading to the classification of non-genetic sporadic LOAD cases in two categories, i.e. classical cases (abbreviated as spAD in the study) with a disease span of ~8 years and cases with a higher progression rate and shorter survival time ~4 years (abbreviated as rpAD in the study). In the current study, we aim to define the mechanistic differences behind the variation in the progression rate.

3.1 Characterization of the rpAD cohort

The present experimental study included the characterization of the progression rate variants of the AD, using established hallmarks and signal transduction pathways, utilizing a multitude of techniques including histochemistry, immunoblotting analysis, and SWATH-MS mass spectrometry.

3.1.1 Localization of amyloid plaques and Tau tangles

Alzheimer's subtype specific pathological features were studied using immunofluorescence microscopy to identify differences between plaque profiles and Tau tangles typical for sporadic and rapid Alzheimer's cases.

3.1.1.1 Amyloid plaques

Anti-amyloid β antibodies (6E10 and 4G8) were used together to visualize the amyloid plaques. Microscopic visualization of amyloid plaques revealed a difference in the pathological presentation. A trend towards decrease in the Aβ-plaque diameter was observed in the rpAD cortical sections compared to that of spAD. In rpAD cortices, a significant increase in the frequency of Aβ plaques was observed in comparison to the typical amyloid presentation in spAD cases (Figure 10).

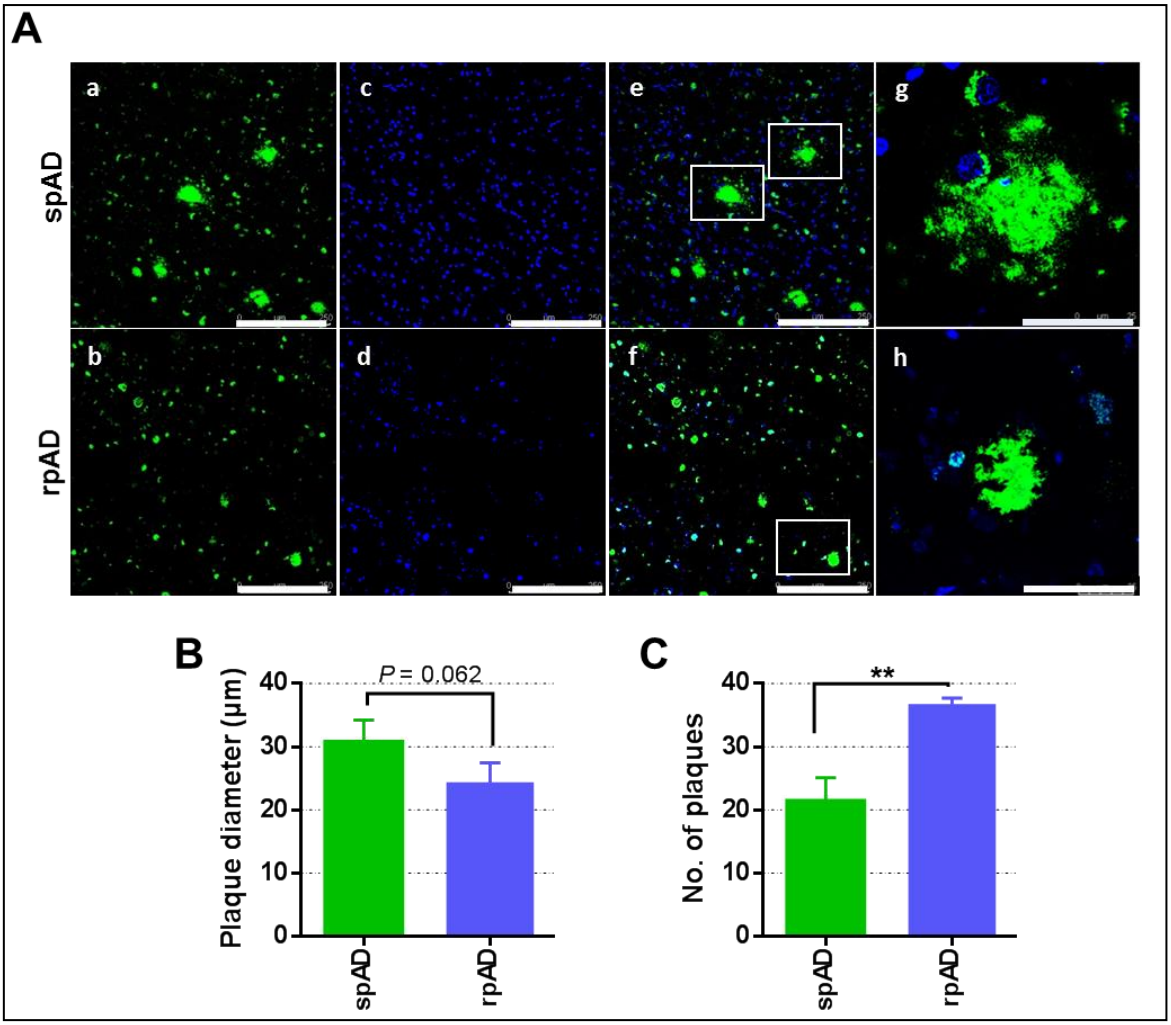

Figure 10: Characteristic presentation of amyloid plaques in spAD and rpAD frontal cortex tissues. A) Amyloid beta localization was visualized by using anti-amyloid β antibodies (4G8 and 6E10 mixture) shown in A.a and A.b for spAD and rpAD respectively. A.c and A.d correspond to the nuclear stain for spAD and rpAD respectively. A.e and A.f show merge images for both channel and A.g and A.h show the higher magnification micrographs for spAD and rpAD, respectively. Frontal cortex tissues from spAD showed typical plaque structure, whereas a higher number of smaller plaque populations was observed in frontal cortex tissues from rpAD. B-C) Statistical analysis was performed using cortical sections from rpAD (n=3) and spAD (n=3) patients, p-values were calculated using Student *t* -test. Counting f Aβ plaques was performed in the randomly selected regions of interest with length and width measuring 200 µm each. Scale bars in sections a-f = 250 µm and scale bars in sections g, h = 50 µm. *p < 0.05, **p < 0.005,

3.1.1.2 Tau tangles

Neurofibrillary Tau tangles (NFTs) constitute one of the highly differentiating pathological features of Alzheimer's disease. The NFTs form because of an accumulation of abnormally hyperphosphorylated Tau protein in neurons. To study NFTs, frontal cortex sections were immune-stained using anti-Tau and anti-pTau (S199 + S202) antibodies, separately.

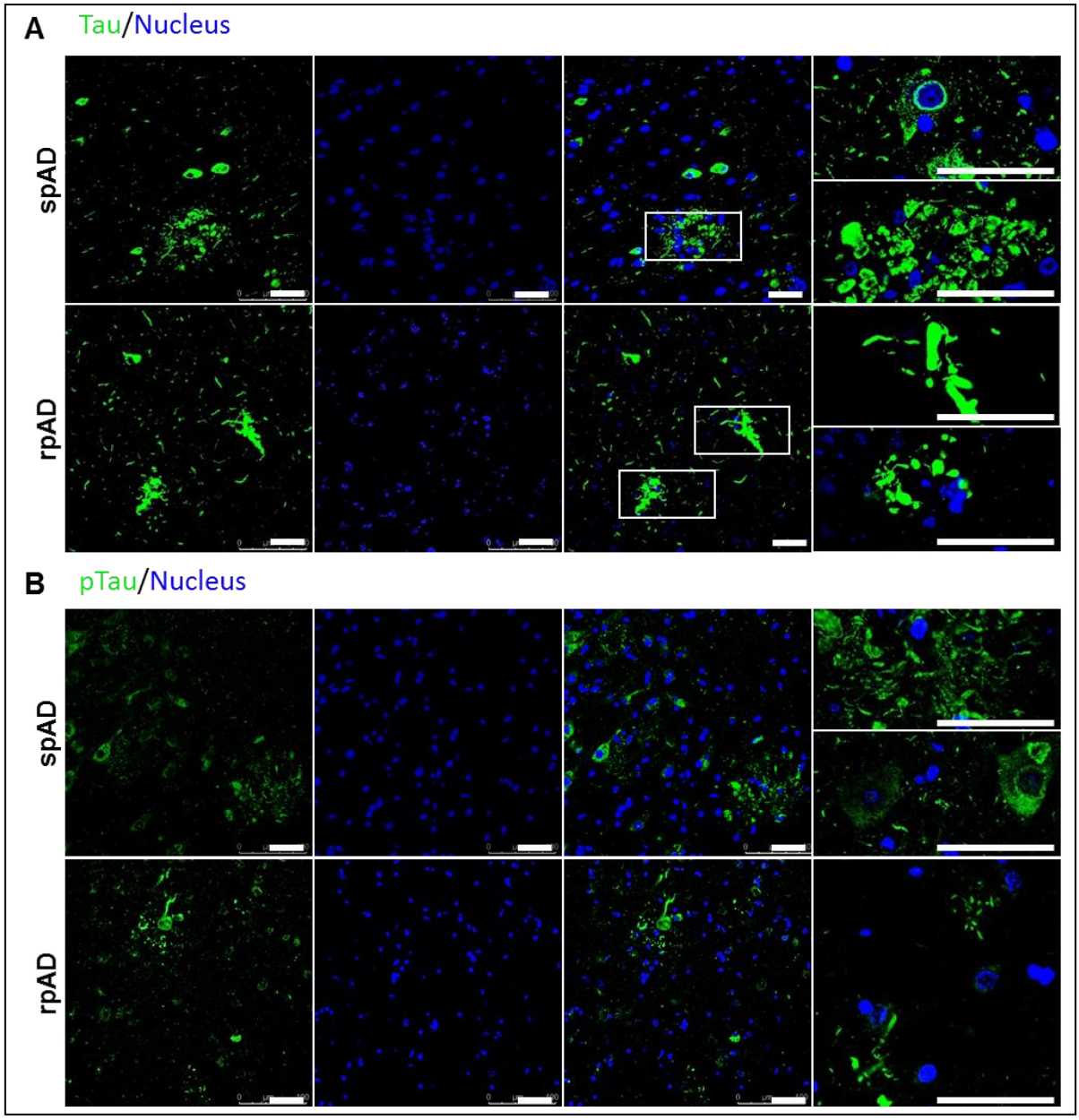

Figure 11: Localization of Tau and hyperphosphorylated Tau in Alzheimer's subtypes. Distribution of neurofibrillary tangles was assessed in the frontal cortex of rpAD and spAD brain cortex, using anti-Tau antibody (A) and anti-Tau phospho-(S199, S202) antibody (B). Scale bars correspond to 50 µm. No significant differences could be seen in the distribution and size between spAD and rpAD frontal cortices. Statistical significance was calculated using Student *t*-test.

Immunofluorescence microscopy for Tau revealed no significant differences in the NFT profiles, although, a trend was observed towards relatively smaller NFT clusters in the rpAD when compared to spAD cortices. Likewise, no significant differences were observed between NFT profiles for spAD and rpAD frontal cortices, when observed after immunolocalization using anti-p-Tau antibody. And a similar trend towards smaller sized NFT populations was observed in rpAD cases (Figure 11).

3.1.2 Expressions of amyloid-β and hyperphosphorylated Tau

The pathological development of senile plaques and Tau tangles associated with the AD is a result of differential APP cleavage, resulting in higher concentrations of amyloid-β species, and a higher degree of hyperphosphorylated Tau protein, respectively. Expression of total Tau, p-Tau, and amyloid-β was biochemically assessed using immunoblot analysis to estimate differences between the groups of rpAD and spAD patients. The densitometric analysis revealed no significant difference in the total amounts of Tau, p-Tau and the ratio of p-Tau to Tau, although a non-significant relative decrease in Tau phosphorylation could be noted for rpAD cases (Figure 12, A&C). Various low molecular weight amyloid-β oligomers, including dimers, trimers, hexamers, and dodecamers (Aβ-56*, a 56 kD species) were quantified in rpAD, spAD and controls. However, no significant differences in expression could be identified among the three groups (Figure 12, B).

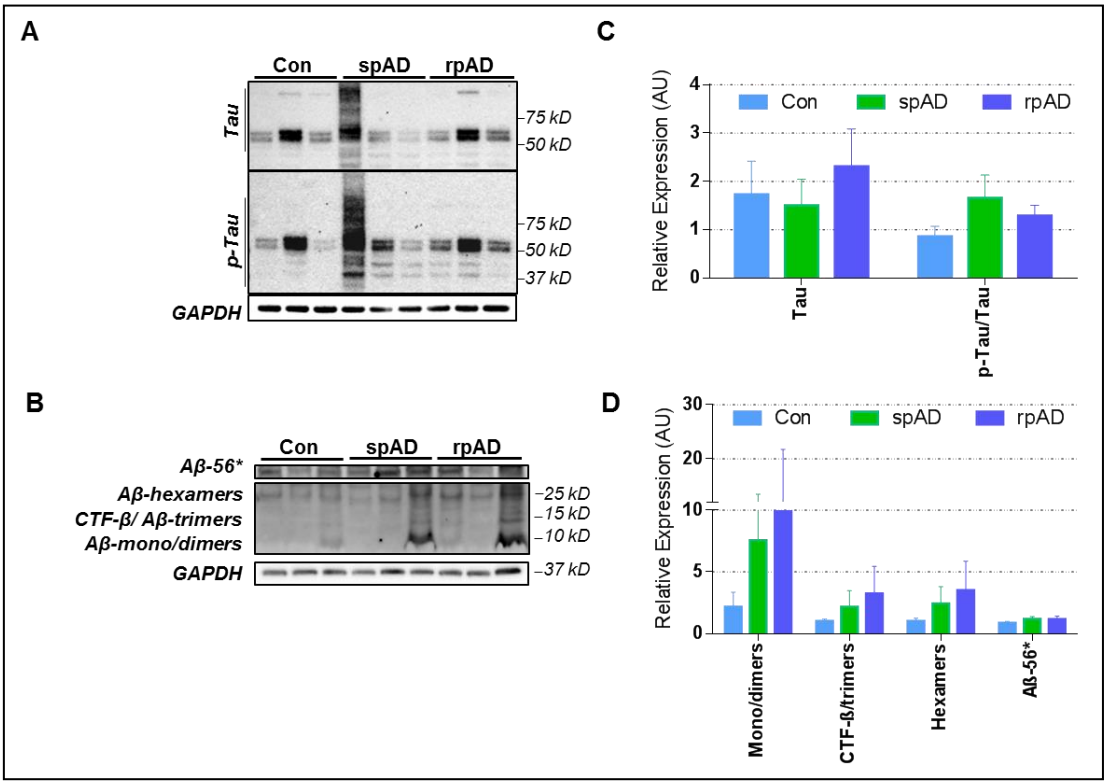

Figure 12: Expression of Total Tau, p-Tau, and Amyloid-β. Expression of Tau, phospho-Tau (S199) and amyloid-β was assessed in frontal cortex (FC) of rapidly progressive Alzheimer's (rpAD) samples in comparison to age-matched sporadic Alzheimer's disease (spAD) patients and non-dementia controls. A) Representative blots for Tau, p-Tau. B) Representative immunoblots for various amyloid-β species. C-D) Densitometric analysis for the immunoblots for spAD cases n=7, rpAD cases n=7 and controls n=7, showed no significant differences in the levels of Tau, pTau, and amyloid beta oligomer species. Statistical significances were calculated using one-way ANOVA and intergroup comparisons were made with Tukey post-hoc analysis. GAPDH was used as a loading control. Aβ:

amyloid-beta, CTF-β: C-terminal fragment-β of the amyloid precursor protein, Aβ-56*: dodecamer of Aβ at 56 kDa.

3.1.3 Differential kinome

Protein kinases are major contributors in the regulation of cellular machinery. Alterations in many kinases and their respective signal transduction pathways have been linked to neurodegeneration in general and Alzheimer's disease as well. We investigated extracellular signal-regulated kinases 1/2 (ERK 1/2), protein kinase B (AKT), mitogen-activated protein kinases p38 (p38), nuclear factor kappa-light-chain-enhancer of activated B cells (NFkB), glycogen synthase kinase 3-β (GSK3B) and respective phosphorylated forms using immunoblotting. The expression of calcium/calmodulin-dependent protein kinase type II (KCC2), myosin light chain kinase (MYLK), dual specificity mitogen-activated protein kinase-kinase 4 (MP2K4), pyruvate kinase PKM (KPYM), phosphatidylinositol 5-phosphate 4-kinase type-2 alpha (PI42A), protein kinase C (KPC), mitogen-activated protein kinase 1 (MK01) and proto-oncogene tyrosine-protein kinase Src (SRC) was assessed using SWATH-MS (DIA MSMS analysis).

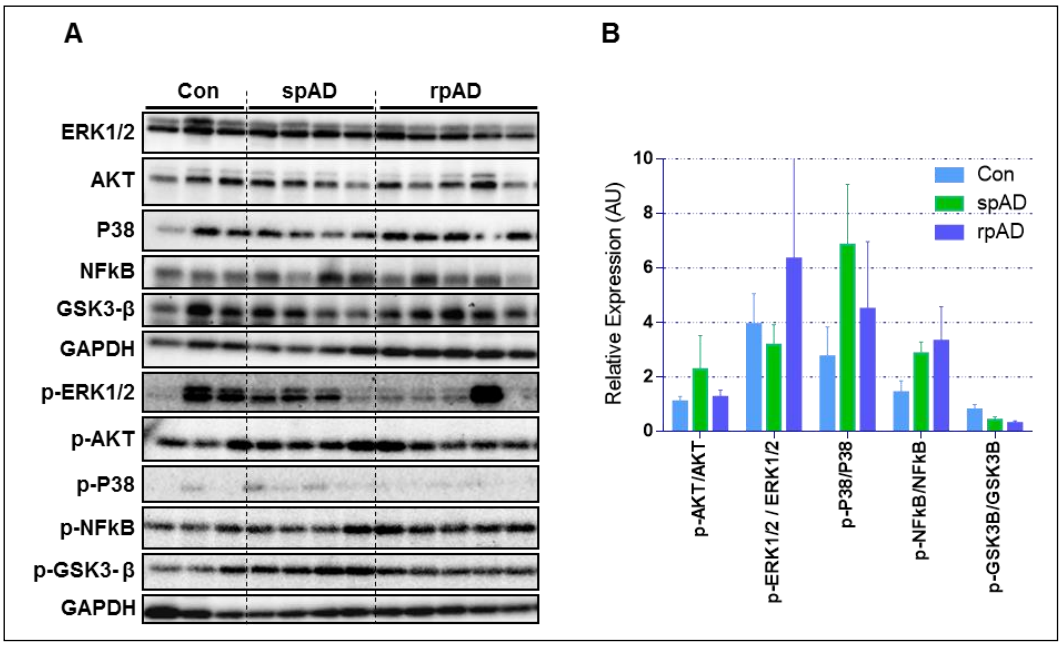

Figure 13: Expression regulation of kinases with known relevance to neurodegenerative diseases. A) Representative immunoblots for the expression of AKT, phospho-AKT, ERK, phospho-ERK, p38, phospho-p38, NFkB, phospho-NFkB, GSK3B and phospho-GSK3B were assessed from frontal cortex (FC) homogenates of rpAD patients in comparison to age and stage-matched spAD patients and controls. GAPDH was used as a loading control. B) Densitometric analysis based on rpAD samples (n=7), spAD patients (n=7) and controls (n=6), showed no significant differences in phosphorylated forms of the kinases mentioned. Statistical significance was calculated with one-way ANOVA followed by Tukey post-hoc test to compare all pairs of columns.

The kinases studied with immunoblot analysis showed no significant differences among the study groups for active (phosphorylated) ERK 1/2, AKT, p38, NFkB, and GSK3-β. The densitometric analysis for the immunoblots exhibits a vast variation among the sample cohorts used (Figure 13).

Total expression of CaMKII subunit gamma was found increased in the spAD compared to both rpAD and non-dementia controls in the SWATH-MS analysis. No observable significant differences were seen in MYLK, MP2K4, KPYM, PI424, KPC, MK01 and SRC kinases expression (Figure 14).

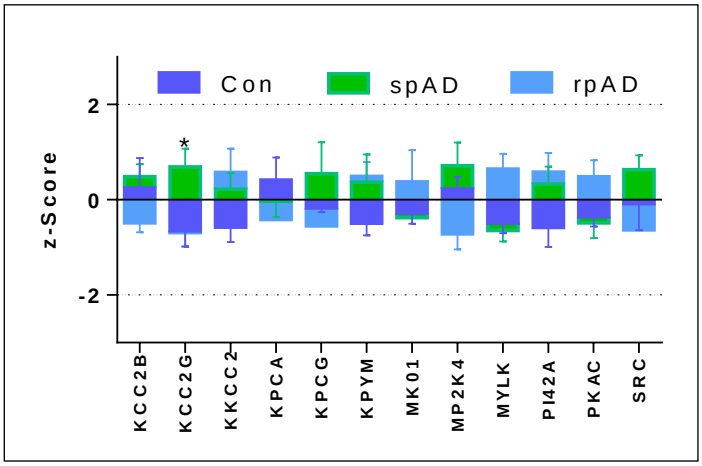

Figure 14: Expression analysis of selected kinases using SWATH-MS. MYLK, MP2K4, KPYM, PI42A, KPC, KCC2, MK01 and SRC were assessed using SWATH-MS. Relative quantitation of selected candidates did not reveal any significant differences among spAD (n=3), rpAD (n=3) and controls (n=3) except for increased KCC2G expression in spAD. Statistical significance was calculated with one-way ANOVA followed by Tukey post-hoc test to compare all paired interactions. *p < 0.05.

3.2 Differential regulation of prion protein metabolism

Alzheimer's disease cases with rapid progression have been shown to have higher levels of low molecular weight oligomeric species of amyloid-β oligomers. Prion protein becomes an interesting candidate for the study, due to its involvement in the sequestering of amyloid-β oligomers. We analyzed the expression of total prion protein (PrP) and relative expression of glycosylated variants, the distribution of PrP in extracellular and intracellular environments in cerebral cortex samples, followed by a study of conformation variants of PrP and respective protein ligands.

3.2.1 Subtype-specific alterations in PrP expression

PrP^C exists in three isoforms, namely di-glycosylated (DG), monoglycosylated (MG) and un-glycosylated (UG). Total PrP expression in the groups of the rpAD, spAD and

controls was estimated by immunoblot using SAF70 anti-PrP antibody (epitope 155-161 aa-residues). Total PrP^C expression exhibited no significant differences among AD subtypes and controls in our cohort. Conversely, a decrease in total PrP has been reported in Alzheimer's cases (Whitehouse et al., 2013). After normalizing expression of each glycoform to the respective total PrP expression, a small, but consistent and statistically significant decrease in DG-PrP expression was observed in rpAD group.

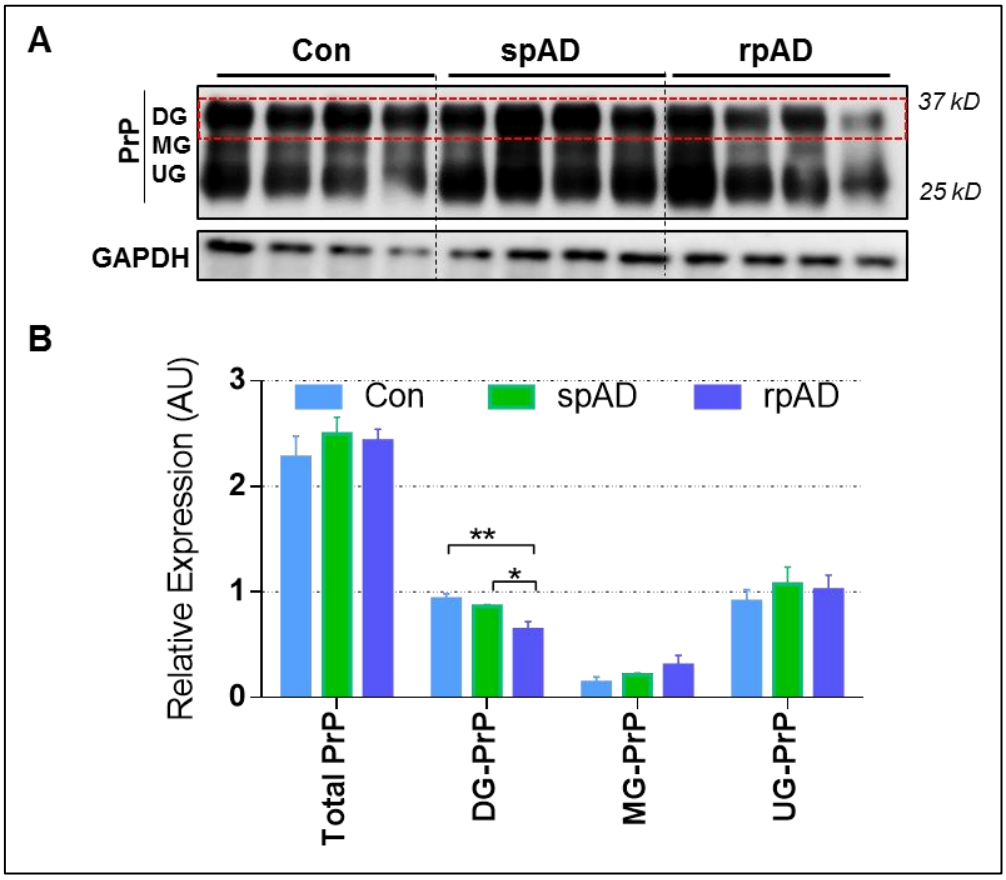

Figure 15: Differential expression of di-glycosylated PrP isoform. A) PrP expression was measured in spAD and rpAD using anti-PrP SAF70 antibody for immunoblotting and GAPDH as a loading control. B) Densitometry analysis from four independent immunoblotting experiments using control (n=10), spAD (n=15), and rpAD (n=8) cases. Statistical significance was calculated with one-way ANOVA followed by Tukey post-hoc test for inter-group comparisons. *p < 0.05, **p < 0.001; DG, di-glycosylated isoforms; MG, mono-glycosylated isoforms; UG, un-glycosylated isoforms.

Lowest expression was seen in rpAD cases, followed by spAD. The relative expression levels of MG-PrP and UG-PrP were not significantly different among the study cohorts.

3.2.2 Differential localization of PrP isoforms in cerebral tissue

Relative expression of PrP^C was analyzed in enrichment fractions of extracellular, cytosolic and membrane-bound proteins. A significant decrease was observed in the

levels of extracellular PrP isoforms in both AD subtypes in comparison with controls. Intergroup comparison of rpAD and spAD showed a significant reduction in Ex-PrP levels in rpAD. The rpAD cases also showed a statistically significant decrease in PrP levels in the cytosolic enriched proteins. However, there were no significant intergroup differences in the PrP^C from membrane enriched proteins. In the extracellular enrichment fragment, a lower abundance of DG-PrP was also observed (Figure 16).

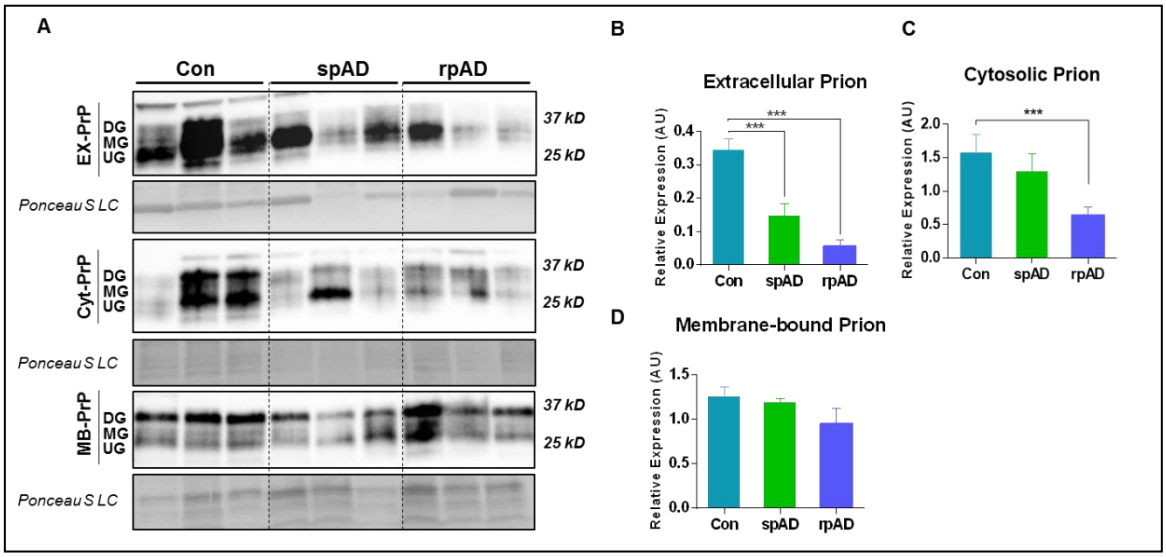

Figure 16: Decrease in shed-PrP in extracellular enrichment fraction. Expression of prion protein was assessed using anti-PrP antibody (SAF70) in homogenates enriched for extracellular, cytosolic and membrane-bound proteins, represented as EX-PrP, Cyt-PrP, and MB-PrP, respectively. B & C) Densitometric analysis from four independent immunoblotting experiments using controls (n=6), spAD (n=6), and rpAD (n=6) cases. Data are shown as average ± SEM in graphs. Statistical significance was calculated with one-way ANOVA followed by the Tukey post-hoc test for intergroup comparisons. DG, di-glycosylated isoforms; MG, mono-glycosylated isoforms; UG, un-glycosylated isoforms; *p < 0.05, **p < 0.005, ***p < 0.001.

Subtype-specific differential cellular localization of PrP^C was also seen in rpAD frontal cortex tissues. A significant degree of PrP^C-nuclear co-localization was seen in the neuronal cells from cerebral cortices of Alzheimer's disease cases. The extent of PrP^C-nuclear localization was seen to be significantly higher in rpAD cases when compared to spAD cases, represented by the overlap of nuclear and PrP channels in ICA (intensity correlation analysis) and channel co-localization-scatter plots (Figure 17).

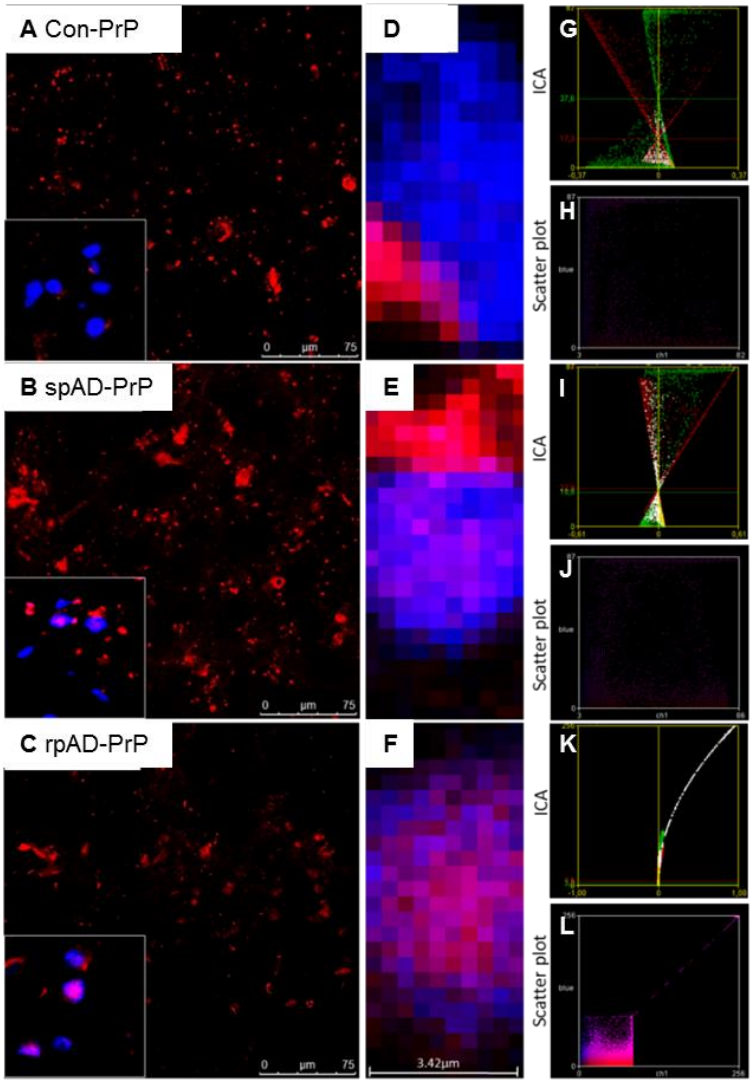

Figure 17: Characteristically distinct PrP^C-Nuclear localization in spAD and rpAD human brains. A-C) Colocalization of PrP^C and nuclear stains in the frontal cortex brain region in controls (A), spAD (B), and rpAD (C) patients, is shown using SAF70 anti-PrP antibody. Corresponding higher magnification areas (D-F) show higher extent of nuclear and PrP overlap in rpAD. G, I, and K) ICA plots for Con, spAD and rpAD respectively. A greater degree of overlap/colocalization can be seen between the PrP and nuclear channels in the rpAD ICA plot. H, J, and L) Representative correlation plots corresponding to Con, spAD and rpAD, respectively. Highest channel overlap can be observed in the scatter plot for rpAD (L). Scale bars in A-C: 75 µm, in D-F: 3.5 µm.

3.2.3 Characteristic PrP^C interactome identification in spAD and rpAD human brains

PrP-interacting proteins were isolated from rpAD, spAD and control frontal cortex tissues using Protein G coupled to super magnetic Dynabeads® after binding anti-prion SAF70 and SAF32 antibodies, separately. Co-IP eluates were resolved on SDS-PAGE, stained silver (Figure 18) and whole lanes from spAD, rpAD, and control eluate were excised, and peptides were extracted with tryptic in-gel digestion. Proteins were

identified with ESI/Q-TOF MS/MS. Among the identified PrP-interacting proteins, both known and novel PrP-interacting partners could be observed (Table 12), listing fifteen proteins as interacting partners of PrP. Two of these interactors, namely histone H2B type 1- B (H2B-1B) and zinc alpha-2 protein (ZAG), were uniquely found with PrP isolated from rpAD cases. However, three proteins, i.e., tubulin beta 2C, synaptojanin-1, and synaptopodin, showed no potential interaction with the PrP isoform from spAD and rpAD cases and appeared to bind to PrP specifically in the controls. Interestingly, one protein, namely myelin P2, was solely isolated as the binding partner with the PrP isoform in spAD samples. Four interacting proteins, i.e., peroxiredoxin 1, four-and-half LIM domains protein 1, transketolase variant (fragment), and the basic myelin protein, were found in both spAD and rpAD cases. Furthermore, four PrP binding proteins, ribonuclease UK114, fructose-bisphosphate aldolase A and lysozyme C, were found in common in the AD and non-demented healthy controls; and lastly, synapsin-1 and myelin proteolipid peptide were found to interact with PrP in all cases.

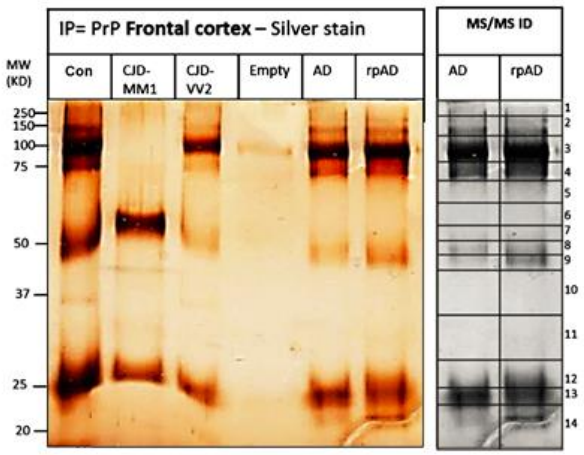

Figure 18: Characteristic PrP interactome identification in spAD and rpAD human brains. PrP-interacting partners isolated from spAD, rpAD, and control cases by using SAF32 and SAF70 PrP Protein G coupled to magnetic Dynabeads. The bands were excised, digested in-gel, and proteins were identified by ESI/Q-TOF MS/MS mass spectrometry.

Table 12: List of prion protein-interacting proteins in rpAD and spAD as determined by ESI/MS analysis

No.	Protein Name	Disease Specific occur-rence	Uniprot Acc. No.	Locali-zation (Uni-Prot)	Relevance (AD)	Relevance (Prion)	PrP lig-and
1	Histone H2B type 1-B	rpAD	P33778	Nu	Known (X. Yu, Caltagarone, Smith, & Bow-ser, 2005)	Known (Medici, Peana, Nurchi, & Zoroddu, 2013)	Novel
2	Zinc alpha-2 protein	rpAD	P25311	Nu, Pm, Ee	Known (Roher et al., 2009)	Novel	Novel
3	Peroxiredoxin–1	rpAD and spAD	Q06830	Nu, C, Ee	Known (Cum-ming, Dar-gusch, Fischer, & Schubert, 2007; S. H. Kim, Fountou-lakis, Cairns, & Lubec, 2001; Krap-fenbauer, En-gidawork, Cairns, Fountoulakis, & Lubec, 2003; Lee et al., 2011; Ro-her et al., 2009)	Known (Zafar et al., 2011)	Known (Zafar et al., 2011)
4	Four and a half LIM domains protein 1	rpAD and spAD	Q13642	C, Nu, Pm, Fa	Known (Wild-ing, McGrath, Bonne, & Mitchell, 2014)	Known (Wilding et al., 2014)	Known (J. Satoh et al., 2009)
5	Transketolase variant (Frag-ment)	rpAD and spAD	Q53EM5	-	Known (Pao-letti & Mocali, 1991; Paoletti, Mocali, Marchi, Sorbi, & Piacentini, 1990)	Known (Lonsdale, 2015)	Novel
6	Myelin basic protein	rpAD and spAD	P02686	Mm, Cs	Known (Selkoe *et al.*, 1981; Zhan *et al.*, 2015)	Known (Patzig et al., 2011; Tsutsui, Hahn, Johnson, Ali, & Jirik, 2008)	Novel
7	Myelin P2	spAD	P02689	C, Ee, Ms	Known (Cout-tas et al., 2016)	Known (Shearin & Bessen, 2014)	Novel

No.	Protein Name	Disease Specific occur-rence	Uniprot Acc. No.	Locali-zation (Uni-Prot)	Relevance (AD)	Relevance (Prion)	PrP lig-and
8	Tubulin, beta 2C	Cont.	Q8IZ29	C	Known (Takano et al., 2013; Zahid, Khan, Oeller-ich, Ahmed, & Asif, 2014)	Known (Zafar *et al.*, 2011; Schmitz *et al.*, 2014)	Known (Zafar et al., 2011)
9	Synaptojanin – 1	Cont.	O43426	C, Cp	Known (Martin et al., 2014)	Known (Zampieri, Legname, Segrè, & Altafini, 2011)	Novel
10	Synaptopodin	Cont.	Q8N3V7	C, Ck, Cj	Known (Ar-nold et al., 2013; Counts, Alldred, Che, Ginsberg, & Mufson, 2014; Reddy et al., 2005)	Novel	Novel
11	Ribonuclease UK114	spAD and Cont.	P52758	C, Nu	Known (Hoos et al., 2013)	Known (Tribouil-lard-Tanvier, Carroll, Moore, Striebel, & Chesebro, 2012)	Novel
12	Fructose-bisphosphate aldolase A	spAD and Cont.	P04075	C	Known (Chang, Etheridge, Dodd, & Nouwens, 2014; Zahid et al., 2014)	Known (Jang et al., 2008; Sultana et al., 2007; Zafar et al., 2014)	Known (Zafar et al., 2011)
13	Lysozyme C	spAD and Cont.	P61626	S, Ee	Known (Helm-fors et al., 2015)	Known (Nyström & Ham-marström, 2015)	Novel
14	Synapsin-1	all	P17600	Cj, Ga, Sv	Known (Reddy et al., 2005) (Arnold et al., 2013) (Counts et al., 2014)	Known (Ferrer, Ri-vera, Blanco, & Martí, 1999; Os-borne et al., 2016; Williams & Bate, 2016)	Known (Spiel-haupter & Schätzl, 2001)

15	Myelin proteolipid protein	all	P60201	Ms, Pm	Known (Barker et al., 2014; Miners, Palmer, & Love, 2016; Thomas, Miners, & Love, 2015)	Novel	Known (Radovanovic, 2005)

rpAD, rapid progressive Alzheimer's disease; spAD, sporadic Alzheimer's disease; Cont, controls (non-demented); Nu, nucleus; Pm, plasma membrane; Ee, extracellular exosome; C, cytoplasm; Ms, myelin sheath; Fa, focal adhesion; Mm, myelin membrane; Cs, cytoplasmic side; Cm, cell membrane; Cp, clathrin coat of coated pit; Cj, cell junction, Ck, cytoskeleton; S, secreted; Ga, Golgi apparatus; Sv, synaptic vesicle. The localization of proteins and accession number are assigned as in the ExPASy protein database and Uniprot database, respectively. Relevance for AD, prion and PrP ligand were also established by a UniProt database search.

3.2.4 Confirmation of unique rpAD-specific PrP interactors

Among the identified PrP-binding proteins, interactions of zinc alpha-2 glycoprotein and peroxiredoxin-1 were confirmed by reverse IP experiments, followed by immunoblotting. The ZAG-PrP binding, specific for rpAD cases and PRDX1-PrP binding specific for both sporadic and rapidly progressive forms were confirmed by Co-IP using Anti-ZAG and Anti-PRDX1 antibodies followed by immunoblotting (Figure 19).

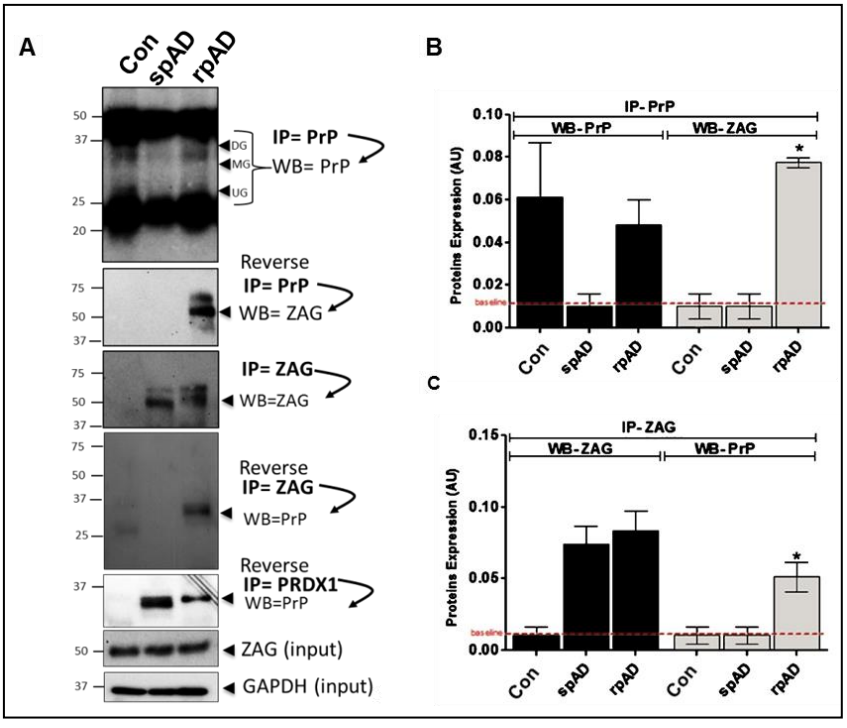

Figure 19: Reverse-IP and immunoblot verification of PrP-ZAG interaction. A) IP eluates were immunoblotted against PrP and ZAG by using specific monoclonal antibodies. ZAG and GAPDH immunoblotting analysis in spAD, rpAD, and control samples were used as loading controls. B and C) correspond to densitometry analysis from four independent (± SEM) IP eluate immunoblotting experiments with controls (n=10), spAD (n=10), and rpAD (n=10). The significance was calculated with one-way ANOVA and Tukey post-hoc test ($*p < 0.05$).

The possible interaction of PrP and ZAG was also corroborated by co-immunofluorescence using ZAG and PrP specific antibodies in frontal cortices from rpAD patients. Image analysis using ICA (intensity correlation analysis) revealed a high overlap between the channel intensities of PrP and ZAG in rpAD (Figure 20. A). We also confirmed *in silico* the probability of PrP^{C}-ZAG interaction using ZDOCK 3.0 (Figure 20. B). ZDOCK 3.0 relies on the crystalline structures of proteins and calculates the biochemical feasibility of interaction between specific proteins of interest.

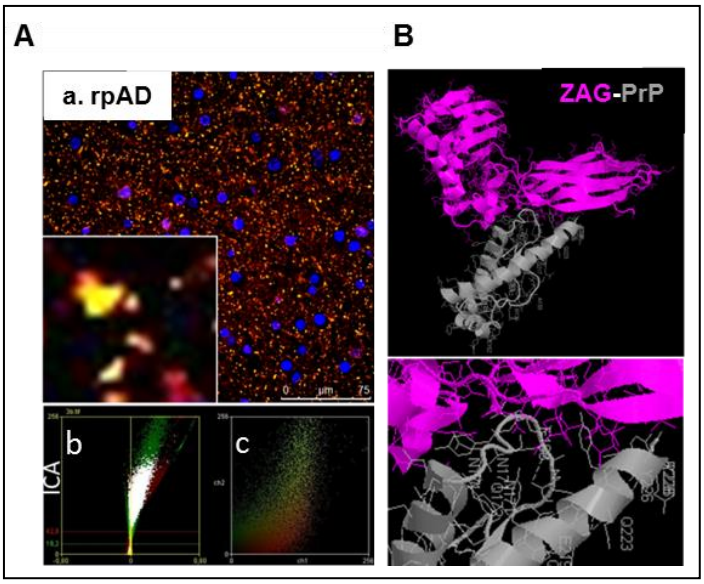

Figure 20: Subtype-specific colocalization of PrP^{C} and ZAG in frontal cortex region. A.a) Representative micrograph showing co-localization of PrP and ZAG in the frontal cortex of rpAD brain tissues using SAF70 anti-prion antibody (red signal) and ZAG antibody (green signal). Higher magnification shows overlapping (yellow signal) of PrP and ZAG in the frontal cortex brain region of rpAD brains. ICA plot (A.b) and scatter plot (A.c) also illustrate the interaction between PrP and ZAG in rpAD brain samples. B) *In Silico* prediction of protein-protein interaction between PrP and ZAG shows PrP (grey) and ZAG (pink) interacting sites by ZDOCK 3.0, and the molecule represents its corresponding centered orientation.

3.3 Identification of disease-specific PrP oligomers

The differences between the disease subtype-specific PrP-interactome lead us to hypothesize the possibility of various subtype-specific PrP oligomers, as PrP is known for the conformational instability in transmissible spongiform encephalopathies, and for its potential to oligomerize (C. Kim et al., 2011). To study the disease-specific variants, we relied on the density gradient centrifugation using (10-45%) sucrose, 1% sarkosyl-PBS-step gradient. Centrifugation was carried out at 50,000 rpm, 5°C, after loading 10% homogenate to the top of gradients. We also included the sporadic

Creutzfeldt Jakob disease (sCJD) frontal cortex samples as positive controls to the study. The experiment design is shown in the figure below (Figure 21).

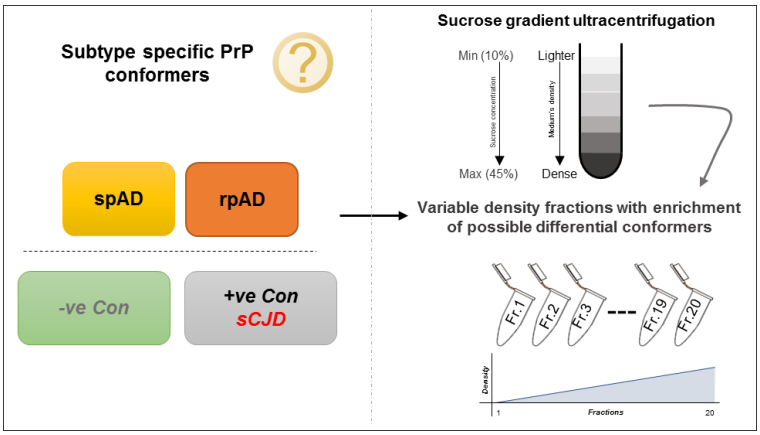

Figure 21: Experimental setup for isolation and characterization of disease-specific PrP conformers. Density gradient centrifugation using (10-45%) sucrose, 1% sarkosyl-PBS-step gradient was used for the separation of density variants. Centrifugation was carried out at 50,000 rpm at 5°C. Twenty density fractions were taken from top to bottom (lighter to dense) and were used for downstream biochemical assays and analyses.

From the immunoblotting of high-density fractions, we were able to identify the differential high-density PrP (HDP) oligomers in high-density fractions specific for rpAD, resembling that of sCJD PrP conformers. These HDPs were identified in the high-density fractions ranging between fraction thirteen and seventeen in rpAD cases (Figure 22).

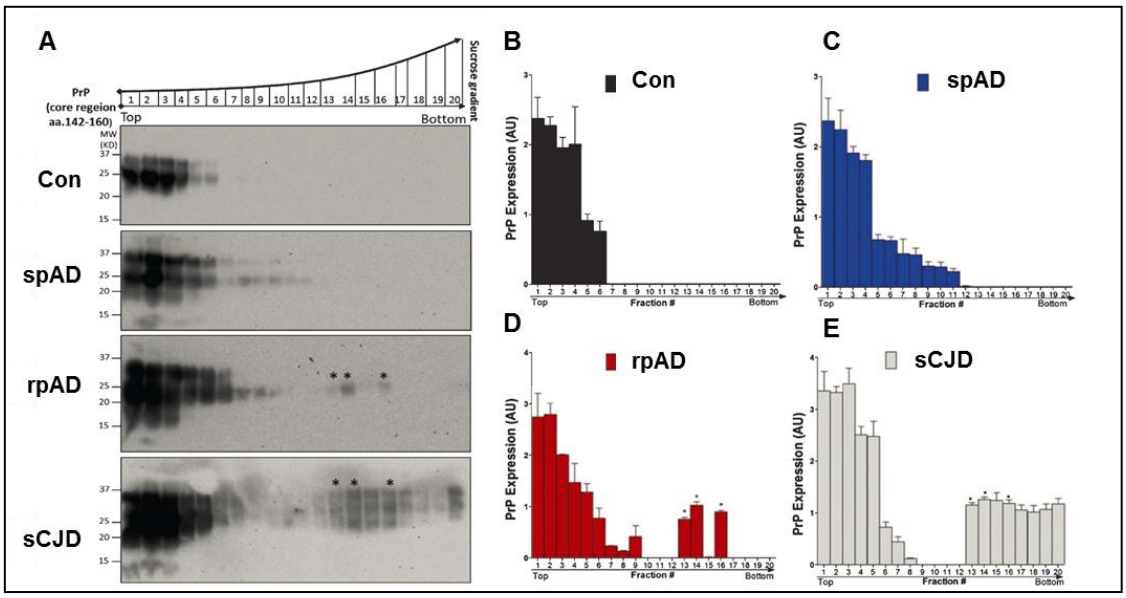

Figure 22: Resolution of characteristic density variant PrP oligomers by sedimentation centrifugation in sucrose gradient in spAD and rpAD human brain frontal cortices. A) The gradient fractionation profile of PrP particles from spAD, rpAD, sCJD and controls after separation by ultracentrifugation in a sucrose gradient. Fractions collected from the top of the tubes were immunoblotted using anti-PrP (SAF70) antibody. B-E)

Densitometric analysis from four independent immunoblotting experiments (average ± SEM). The significance was calculated with one-way ANOVA and Tukey's post-hoc test (*p < 0.05). AU are arbitrary units. Each blot contains twenty fractions from only one sample.

Results demonstrated PrP presence as detected in all the density fractions of sCJD cortex lysates. An overall outlook of PrP presence in disease subtypes is summarized in Figure 23.

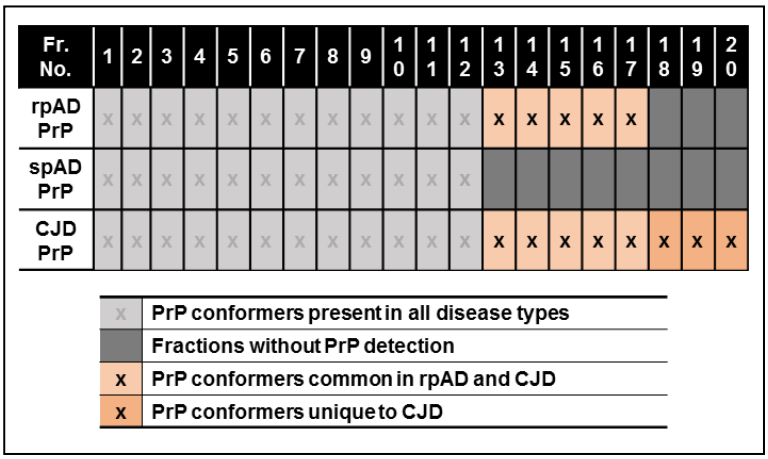

Figure 23: Profile of high density PrP (HDP) oligomer occurrence in cortical isolates of rpAD, spAD, and sCJD. HDP oligomers were uniquely detected from the density fractions 13 to 17 in rpAD subtype, overlapping with the HDPs from CJD.

3.3.1 Proteinase-K (PK) resistance and absence of seeding activity

Due to the overlap of sCJD and rpAD high-density PrP conformers, it could be assumed that the PrP conformers from rpAD may attain some properties of sCJD PrP, leading to the formation of high-density oligomers. Hence, we analyzed the PK resistance and the prion seeding activity in brain frontal cortex homogenates. We also assessed the seeding potential of PrP conformers in the rpAD-specific high-density fractions. PK-resistant PrP species could not be identified from the AD subtypes and the control cohorts.

In the Th-T based, real-time quaking-induced cyclic amplification (RT-QuIC) assay, no prion seeding activity was seen in the brain frontal cortex lysates in spAD, rpAD, and controls in comparison to that of sCJD. Corresponding observed relative fluorescence units (RFU) values were lower than the cut-off i.e. 2.0×10^4. For the sCJD samples, we could observe the typical RT-QuIC curve (Figure 24).

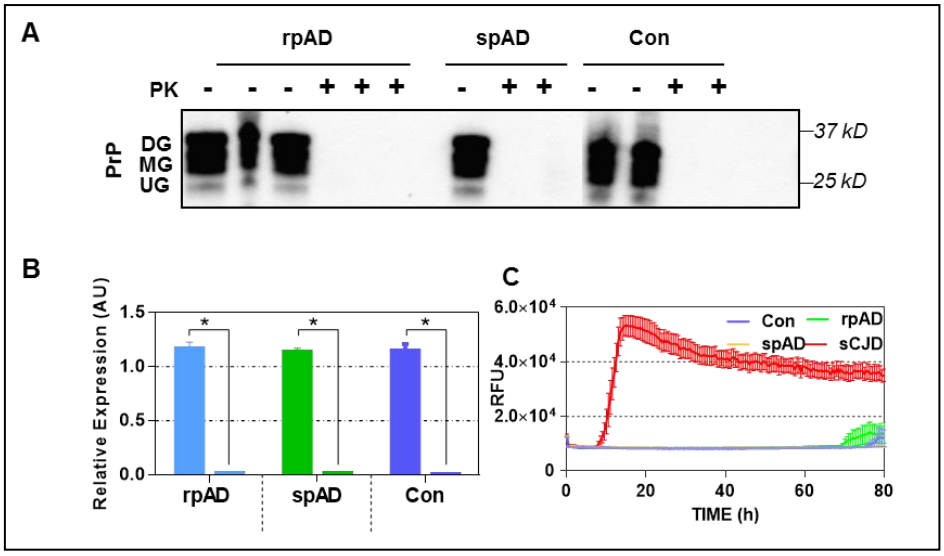

Figure 24: PK resistance and prion seeding activity in rpAD. A) Proteinase-K (PK) digestion was carried out for brain cortical homogenates from rpAD, spAD and control groups. PrP signal was detected via immunoblotting using anti-prion (SAF70) antibody. Brain homogenates in wells indicated with (-) were not treated with PK, conversely wells marked with (+) contain brain homogenates after PK digestion. No PK resistance was identified from the sporadic and rapidly progressive Alzheimer's frontal cortex samples. B) Densitometric analysis was carried out from four independent immunoblotting experiments including rpAD (n=6), spAD (n=7) and controls (n=9) groups. Data are represented as average ± SEM. The significance was calculated with pairwise t-test between the PK-treated and untreated frontal cortex lysates (*p < 0.001). C) Prion seeding activity, from the frontal cortex lysates of rpAD (n=6), spAD (n=7) and controls (n=9) was measured against that of sporadic Creutzfeldt-Jakob disease (sCJD) (n=5), using real-time quaking induced cyclic amplification. The rpAD samples exhibited no seeding activity like spAD and control cohorts.

Likewise, no prion seeding was detected in the high-density prion (HDP) variants from rpAD, but the HDPs from sCJD samples resulted in almost typical RT-QuIC curves (Figure 25).

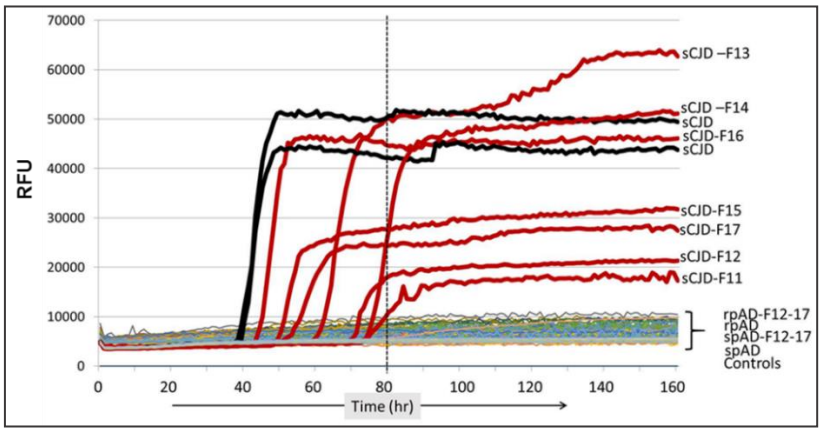

Figure 25: Absence of seeding activity in high-density PrP (HDP) oligomers isolated from rpAD. Prion seeding activity, from the high-density fractions after the density gradient ultracentrifugation of frontal cortex lysates from spAD (n=7), rpAD (n=6) and controls (n=9) was assessed against sCJD frontal cortex lysates, using RT-QuIC. High-density Prion protein species that were uniquely present in rpAD samples were not positive for the seeding potential.

3.4 Proteomic characterization of disease subtype-specific high-density fractions

To analyze the overall subtype-specific proteomic profile in high-density fractions, density fractions ranging from fraction 12 to 17 were pooled using six biological replicates for each disease subtype separately, except for sCJD-VV2, where experiments with 5 biological replicates were performed (fraction 12 of all biological replicates from the same group were pooled, similarly, the rest of the fraction pools were also prepared). Resultant peptide pools were subjected to high-resolution MS/MS analysis (Figure 26).

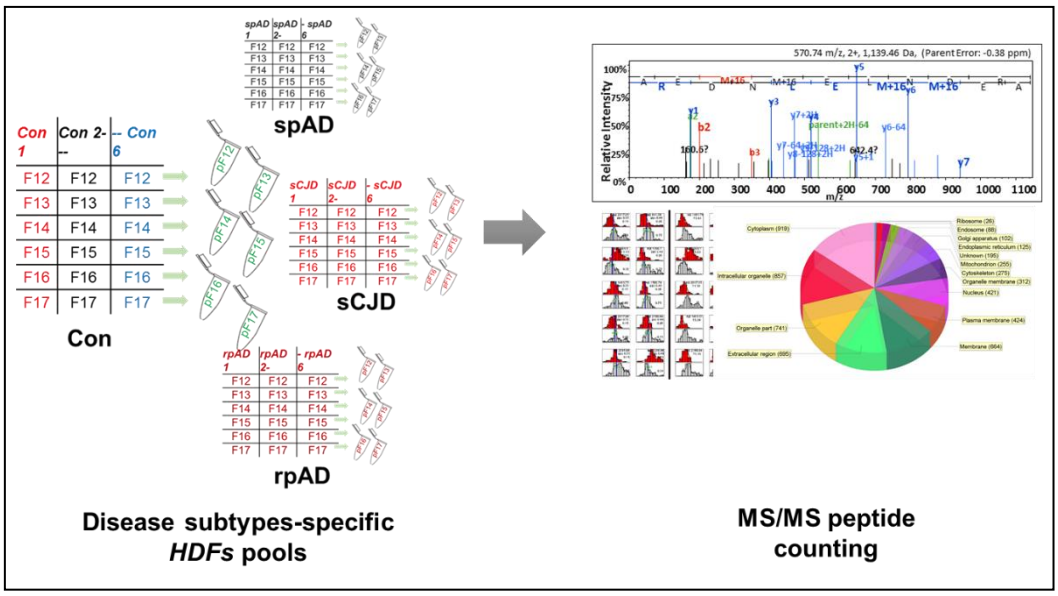

Figure 26: Preparation of subtype-specific pools of high-density fractions and downstream high-resolution MS/MS analysis.

In total, 1212 proteins were identified at decoy FDR <1%, with a protein threshold of 99% and a minimum of 2 peptides. Peptide counts for the high-density fraction pools showed a gradual decrease from fractions twelve to seventeen in rpAD and controls. However, in the case of AD subtypes and sCJD subtypes, the decline in the peptide counts was not uniform. In spAD, the overall peptide counts remained steady in fractions fifteen to seventeen, and in sCJD subtypes, the peptide counts rose again, the fractions ranging from fifteen to seventeen showing the higher concentration of high-density proteins (Figure 27).

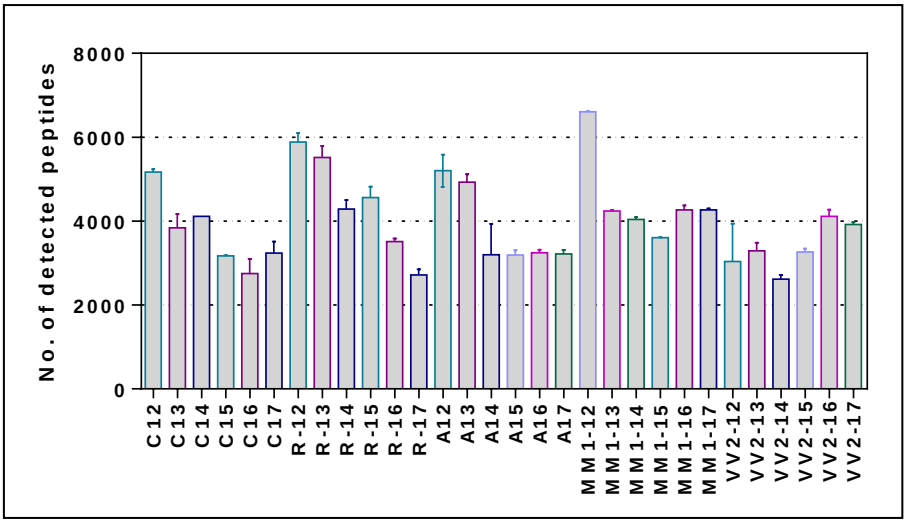

Figure 27: Dynamic range of detected peptides in the high-density fraction pools of disease subtypes. Sample pools were prepared from HDFs of rpAD (n=6), spAD (n=6) and sCJD-MM1 (n=6), sCJD-VV2 (n=5), and controls (n=6). MS/MS analysis was carried out in triplicates for each pool of high-density fractions. C12 to C17: HDF pool-12 to 17 from Con; A12 to A17: HDF pool-12 to 17 from spAD; R12 to R17: HDF pool-12 to 17 from rpAD, MM1-12 to MM1-17: HDF pool-12 to 17 from sCJD-MM1, and VV2-12 to VV2-17: HDF pool-12 to 17 from sCJD-VV2.

3.4.1 Disease subtype-specific clustering

Spectral counts for each high-density fraction proteome were normalized by the total spectra reads detected for the respective fraction, to overcome the protein loading variations in the mass spectrometric analysis. Averaged normalized spectral counts were then used to perform hierarchical clustering analysis, based on dissimilarity based-agglomerative clustering. As an outcome of clustering analysis, we were able to differentiate the disease subtype-specific clusters for controls and spAD, separate from the rpAD and sCJD subtypes. The cluster profiles of controls and spAD fractions showed close resemblance. However, the intergroup resemblance of sCJD subtype-specific fractions was also high. The rpAD fraction proteomes presented the group separate from the rest, suggesting the differential abundances of protein species (Figure 28).

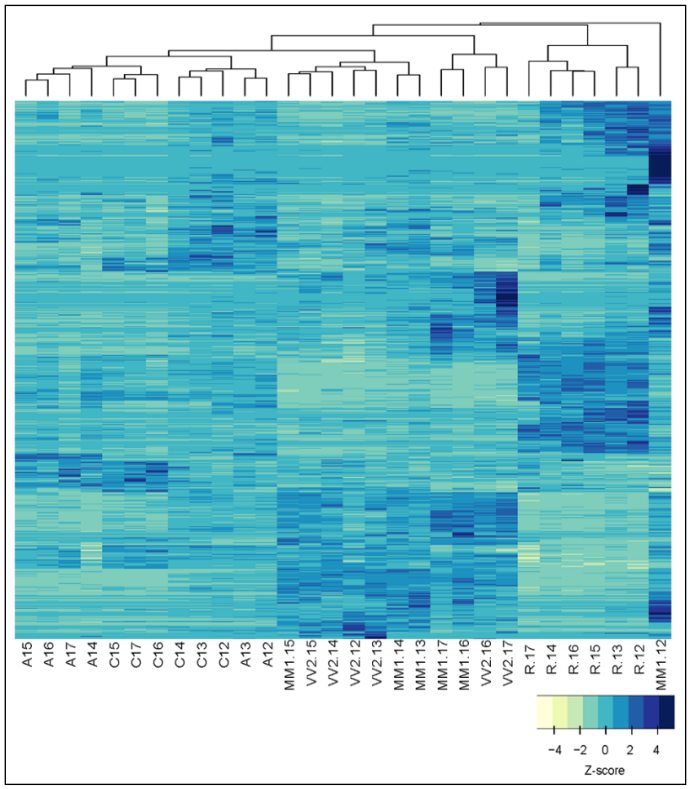

Figure 28: Hierarchical clustering defining the inter-closeness of subtype-specific high-density fractions. Clustering was performed using dissimilarity based-agglomerative grouping as an index of distance measurement. C12 to C17: HDF pool-12 to 17 from Con; A12 to A17: HDF pool-12 to 17 from spAD; R12 to R17: HDF pool-12 to 17 from rpAD, MM1-12 to MM1-17: HDF pool-12 to 17 from sCJD-MM1, and VV2-12 to VV2-17: HDF pool-12 to 17 from sCJD-VV2.

Principle component analysis, using the averaged normalized spectral counts of HDF proteomes, also resulted in the clustering that resembled the clustering pattern obtained via dissimilarity based-agglomerative clustering. The HDFs from rpAD pools clustered separately from that of spAD, controls, and sCJD. Small differences among the HDFs of CJD-MM1 and that of CJD-VV2, clustered them close together except for MM1-12. Like hierarchical clustering, (Figure 29 A).

Principle component loadings (Figure 29 B) gave an interesting insight that the protein candidates that mainly contributed to differentiation of the HDFs, belonged to the cytoskeletal system.

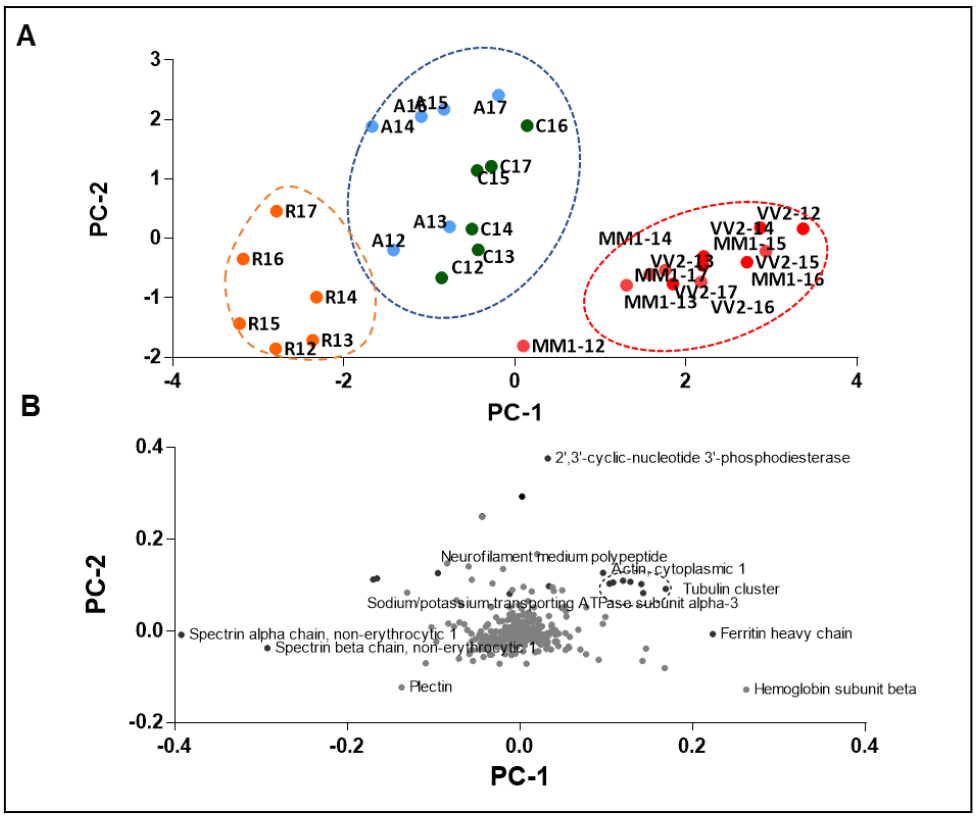

Figure 29: Subtype-specific relationships between disease variants defined by proteomic signatures of HDFs. A) Graphical representation of the degree of closeness between the disease-specific HDFs as determined by PCA. B) Graphical presentation of principle component loadings for PC-1 (principle component-1) and PC-2 (principle component-2). C12 to C17: HDF pool-12 to 17 from Con; A12 to A17: HDF pool-12 to 17 from spAD; R12 to R17: HDF pool-12 to 17 from rpAD, MM1-12 to MM1-17: HDF pool-12 to 17 from sCJD-MM1, and VV2-12 to VV2-17: HDF pool-12 to 17 from sCJD-VV2.

3.4.2 Subtype-specific reference global proteome

To verify the fact that the proteomic alterations in HDFs result from differential distribution in the density gradients and are not due to differences in expression, we included a comparative global proteomic dataset using sequential windowed acquisition of all theoretical mass spectra (SWATH-MS) for frontal cerebral cortices of rpAD (n=3), spAD (n=3), DLB (n=3) and controls (n=3). Rapid progressive dementia with Lewy bodies (n=3), DFTL (n=3) and SVD (n=3) were also included in the SWATH-MS based proteomics as positive controls of rpAD. In total, 1548 proteins were detected at 1% FDR in the global proteomics dataset, and their corresponding SWATH-MS values were measured for protein quantification and statistical/bioinformatic analyses.

3.4.3 Evaluated physiological domains

From the HDFs' proteomic dataset, proteins of related physiological activities were grouped together in modules to assess the respective biological aspects in disease

subtypes. From the perspective of neurodegeneration, we narrowed down our study to proteopathic proteins, cellular protein degradation machinery, ras-related proteins, cytoskeleton, and chaperones.

3.4.3.1 Proteopathic burden

Neurodegenerative disorders are associated with proteopathies (diseases arising due to conformational transition in certain proteins leading to subtle functional variations). Proteopathic proteins were detected in abundance in the HDFs. Overall, the expression of proteopathic proteins was the highest in sCJD (MM1 and VV2) HDFs, followed by those of rpAD (Figure 30).

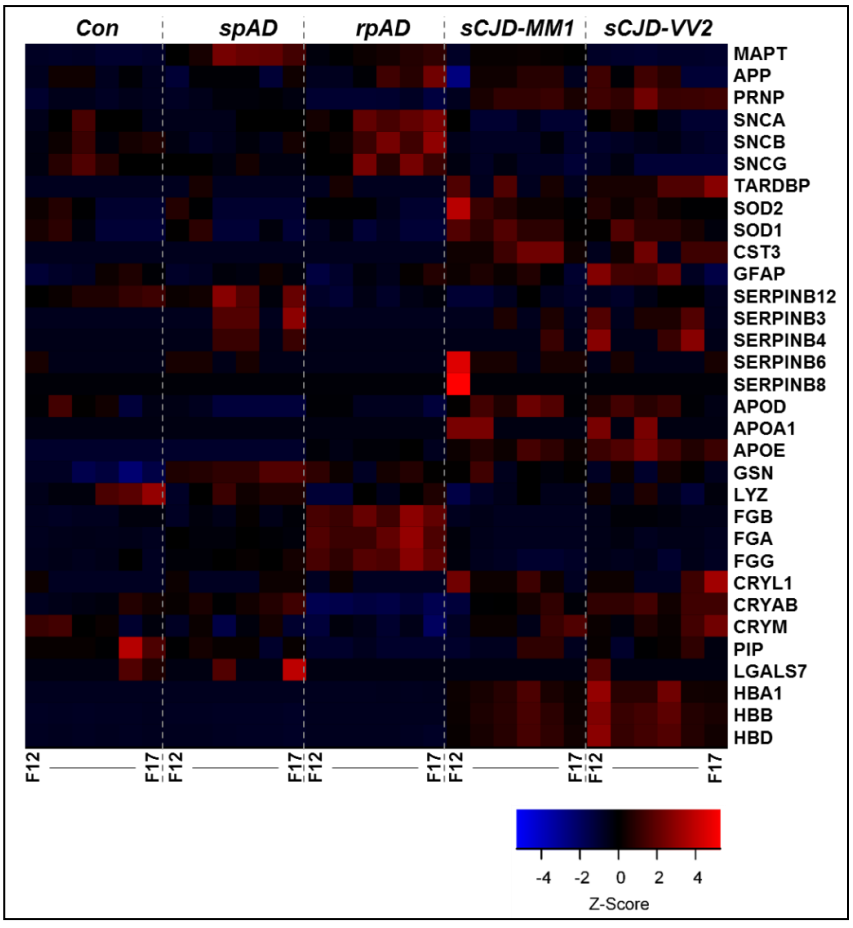

Figure 30: Elevated proteopathic burden in rpAD in comparison to that of spAD. The proteopathic proteins are found to be most abundant in the sCJD-specific HDFs, followed by rpAD-HDFs. A discrete trend in the HDF levels of proteopathic proteins was observed, with highest expression in sCJD-subtypes and lowest in Con. F12–F17: HDF pool 12 to 17.

The sCJD fractions showed high relative abundances for most of the detected proteins, including glial cell fibrillary acidic protein (GFAP), serpins, apolipoprotein isoforms, lambda-crystallin homolog (CRYL1), alpha-crystallin B chain (CRYAB) and

hemoglobin subunits (HBA, HBB, and HBD). Interestingly, certain proteins were specifically abundant in rpAD-HDFs including synuclein isoforms and fibrinogen chains compared to that of spAD, sCJD and controls (Figure 30).

In the SWATH-MS proteomic dataset, no significant differences were detected in the expression levels of respective proteins, showing that the variations in the HDFs' proteome do not result from native subtype-specific alterations of these proteins. Only GFAP was found to be significantly natively upregulated in rpAD samples in comparison to spAD, controls and other rapid dementias included in SWATH-MS-based global proteomics (Figure 31). There was no significant difference in the abundance of GFAP in HDFs of rpAD, spAD and controls, suggesting the involvement of GFAP in other physiological functions.

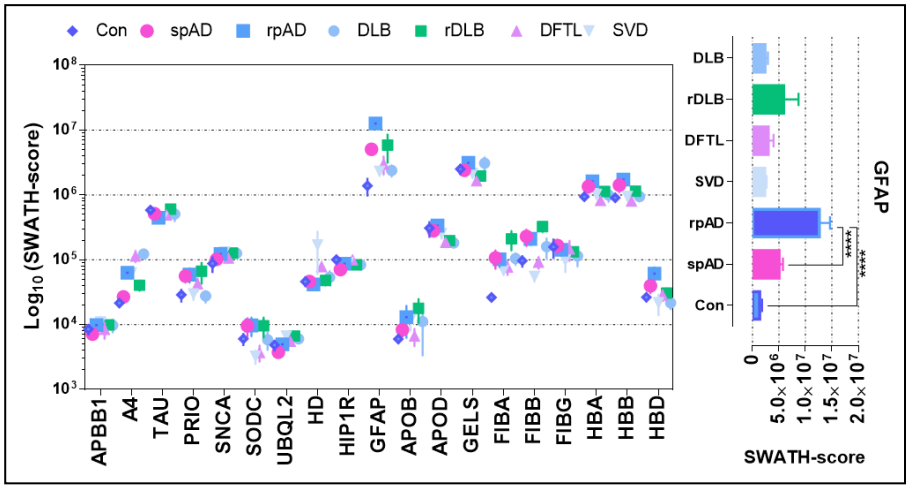

Figure 31: Expression of disease-specific proteopathic proteins. Expression of proteopathic proteins as estimated by SWATH-MS-based global proteomics for spAD (n=3), rpAD (n=3), DLB (n=3), rDLB (n=3), D-FTL (n=3), SVD (n=3), and controls (n=3).

3.4.3.2 Protein degradation machinery

Proteins associated with protein degradation machinery were also detected in the HDFs proteome and a certain trend could be seen in their inter-group abundances. The peptide counts of ubiquitin-60S ribosomal protein L40 (UBA52), polyubiquitin-B (UBB) and ubiquitin-40S ribosomal protein S27a (RPS27A) domains were observed to be significantly decreased in rpAD HDFs in comparison to spAD fractions, where it was lowest in controls followed by sCJD subtype HDFs. Ubiquitin-like modifier-activating enzyme (UBA1) and ubiquitin carboxyl-terminal hydrolase 5 (USP5) appeared to be abundant in the rpAD-specific HDFs. Proteasomal subunits appeared to be least

abundant in rpAD-specific HDFs. However, HDF levels of proteasomal subunits are significantly higher in sCJD subtype in comparison to AD-subtypes (Figure 32, A).

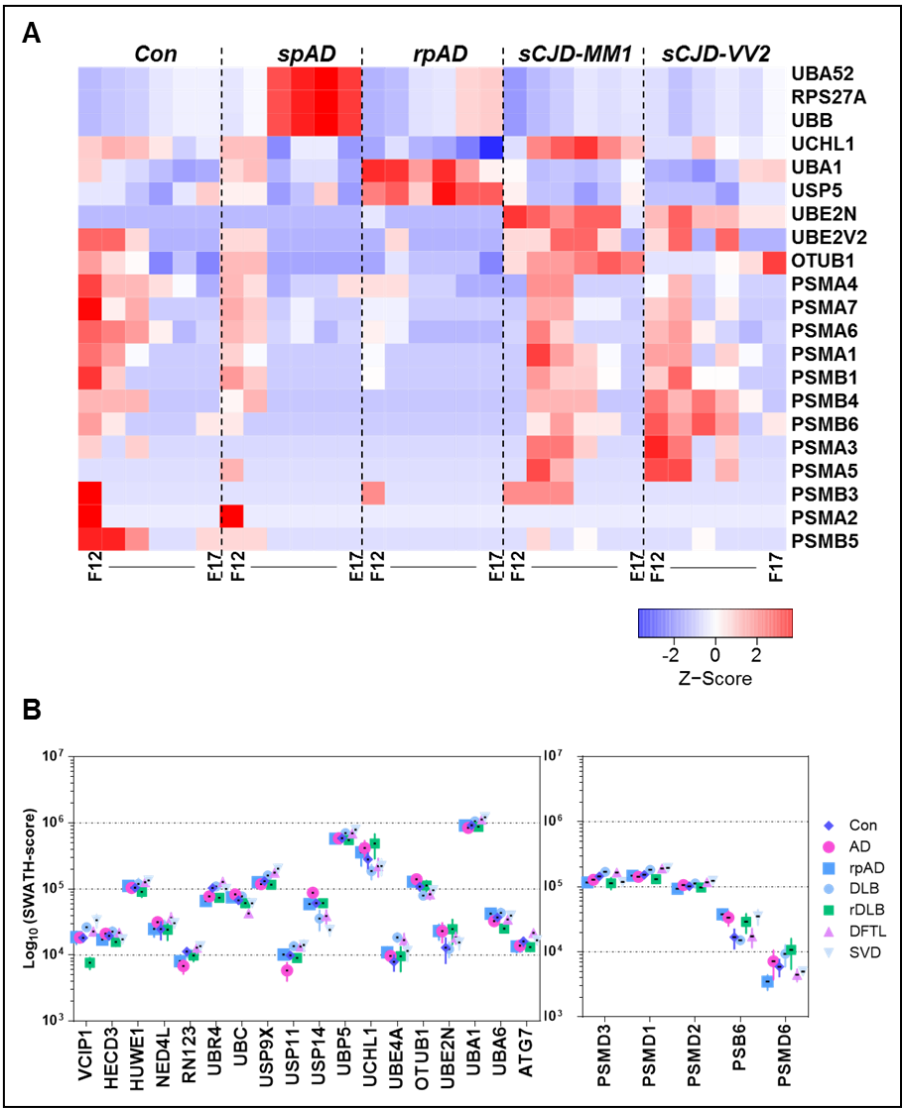

Figure 32: Dysregulations of protein degradation machinery. A) Heatmap representing the differences in relative concentrations (z-scores) of proteins associated with ubiquitin and proteasomal regulation. B) Global proteome expression levels of ubiquitin and proteasomal proteins (expression estimated by SWATH-MS) for spAD (n=3), rpAD (n=3), DLB (n=3), rDLB (n=3), D-FTL (n=3), SVD (n=3), and controls (n=3). F12–F17: HDF pool 12 to 17.

In global proteome, we could detect multiple ubiquitin-associated proteins and proteasomal subunits, but there were no significant differences in the expressions of the detected proteins (Figure 32. B).

3.4.3.3 Ras-related proteins

Multiple ras-related proteins including rab proteins, rap proteins, and ral proteins were detected in the HDFs. A highly differentiating profile was observed in the HDFs of the

subtypes studied. Significantly high levels of ras-related proteins were observed predominantly in the sCJD-subtype-specific fractions in comparison to controls and AD subtypes. However, levels of ras-related proteins in rpAD HDFs were found to be significantly decreased (Figure 33.A).

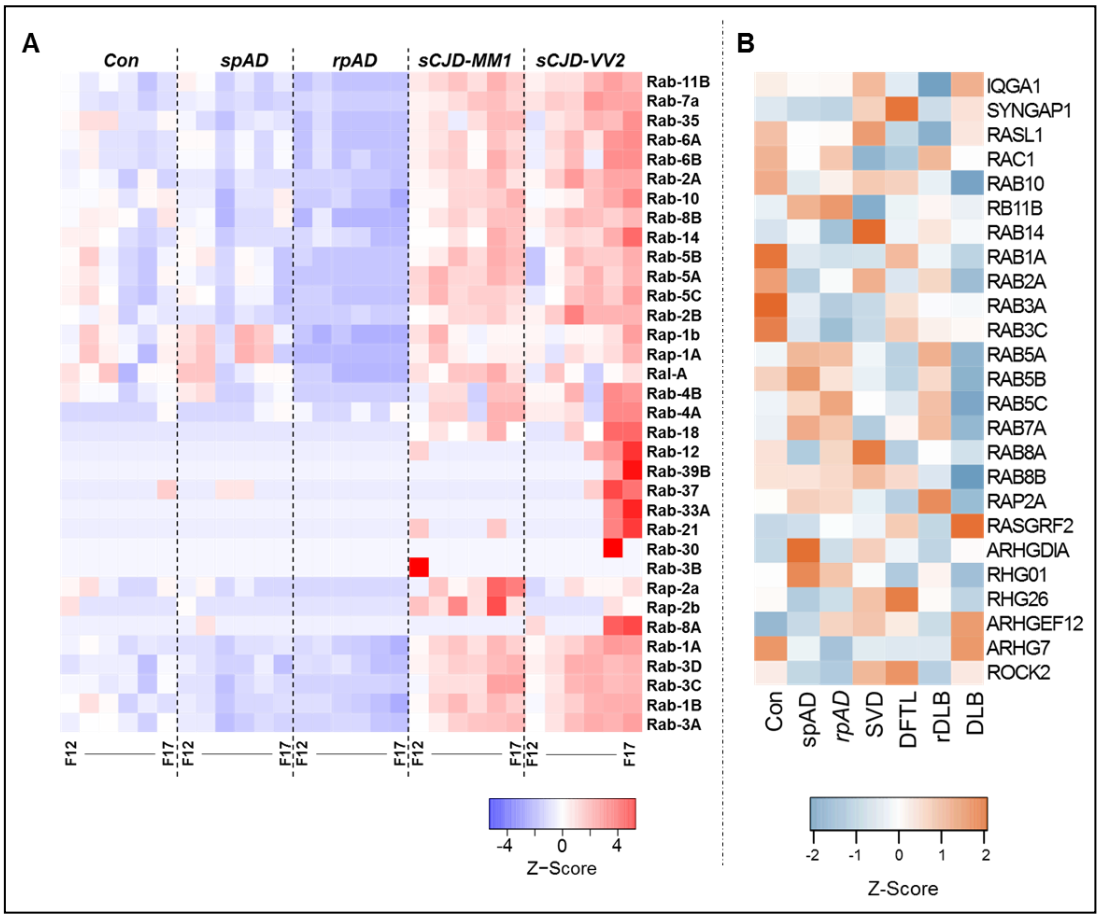

Figure 33: Profile alterations of ras-related proteins. A) differential expression levels of ras-related proteins in subtype-specific HDFs (relative expression is represented as Z-score). B) global proteome validation in frontal cortex samples for spAD (n=3), rpAD (n=3), DLB (n=3), rDLB (n=3), D-FTL (n=3), SVD (n=3), and controls (n=3), respectively. F12–F17: HDF pool-12 to 17.

For most SWATH-MS-quantified ras-related proteins, there were no significant differences among the compared dementia subtypes. Highly significant differences were only observed for ras/rap GTPase-activating protein SynGAP (SYNGAP1), with a significant increase observed in DFTL and SVD in comparison to other groups. Likewise, expression of ras-related protein Rab3A was found significantly reduced in rpAD in comparison to controls, DFTL, rDLB, and DLB. Expression of Rab3C was observed to be significantly decreased in spAD, rpAD, and SVD, compared to Con, but no significant differences were seen between rpAD and other rapid dementia subtypes. Overall,

rpAD exhibited a proteomic profile of ras-related proteins very similar to that of spAD (Figure 33. B).

3.4.3.4 Cytoskeletal proteins

Several cytoskeleton-associated proteins were quantified with MS/MS quantification in HDFs and SWATH-MS global proteome. Levels of tubulin subunits were observed to be significantly reduced in rpAD HDFs compared to other groups. A significant decrease was also seen for the levels of the neurofilament subunits, actin and actin-binding proteins in rpAD HDFs levels. Conversely, significantly higher levels of microtubule-associated proteins (MAP1A, MAP1B, and MAP2), flaming (FLNA), filaggrin (FLG) and plectin (PLEC) were observed in rpAD HDFs compared to sCJD-specific HDFs (Figure 34). Among the cytoskeletal proteins from global proteome data, expression of actin G (ACTG) was found to be significantly increased in rpAD compared to controls, whereas no significant differences were observed between the spAD and rpAD. ACTG expression was observed to be significantly decreased in SVD and DFTL compared to rpAD.

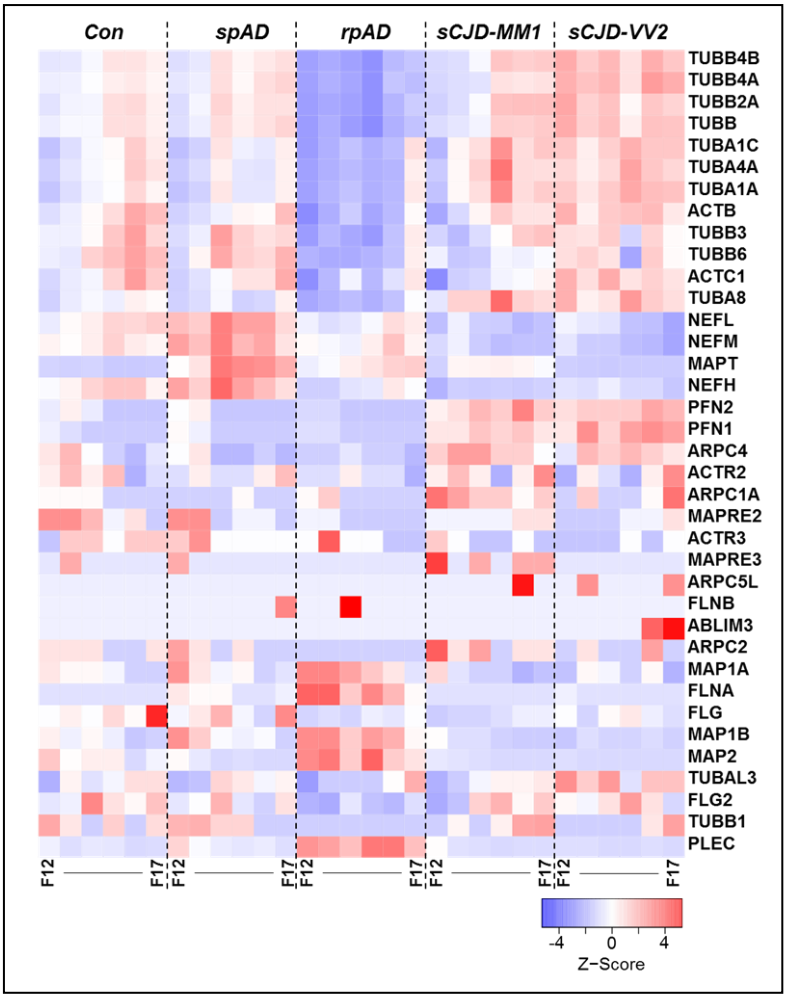

Figure 34: Variations in cytoskeletal proteins in high-density fractions. The relative abundance of cytoskeletal proteins in HDFs detected using high-resolution MS/MS analysis is represented as Z-score. Significant lowering of cytoskeletal proteins was seen in rpAD-specific HDFs. F12–F17: HDF pool 12 to 17.

Contactin 1 (CNTN1) expression was also found significantly higher in SVD and DFTL compared to rpAD, whereas no differences were seen in CNTN1 expression between rpAD and rDLB. Expression of tubulin alpha 1a (TBA1A) was observed to be significantly higher in rpAD compared to other rapid dementia brain cortex samples, i.e. DFTL, SVD, and r-DLB. Likewise, expression of TBA4A was differentially higher in rpAD compared to Con, DLB, DFTL, and SVD. A highly significant decrease, in contrast, was observed in the rpAD expression of septin-B in comparison to that of SVD, DFTL, and DLB. Overall, the pattern of cytoskeletal proteins in global proteomics data was similar in spAD and rpAD, but the other rapidly progressive dementia samples showed an opposite trend of regulation to corresponding proteins (Figure 35).

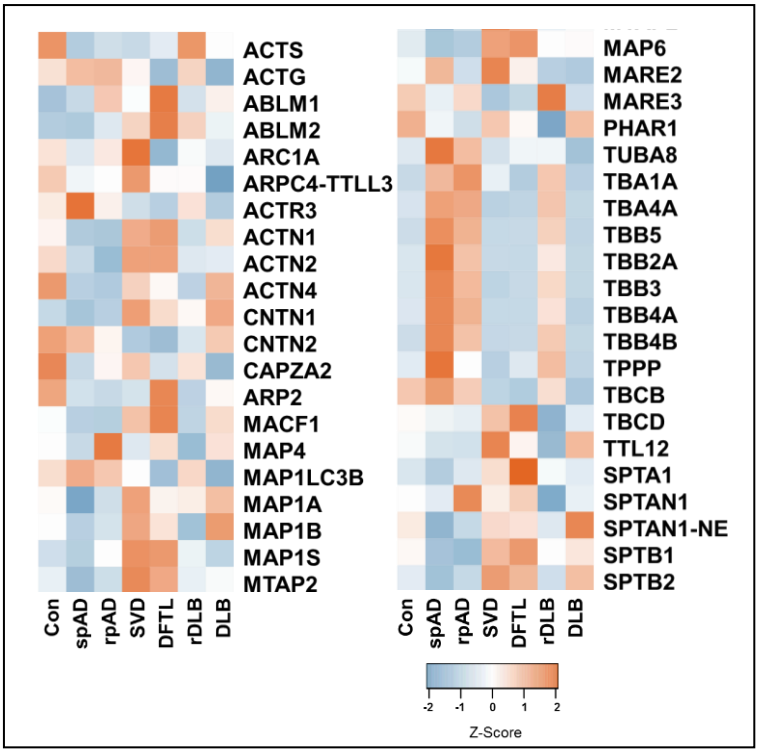

Figure 35: Expression differences of cytoskeletal-(associated) proteins as determined by the SWATH-MS. Heatmaps represent the relative protein expression indicated as Z-scores for spAD (n=3), rpAD (n=3), DLB (n=3), rDLB (n=3), D-FTL (n=3), SVD (n=3), and controls (n=3).

3.4.3.5 Subtype-specific changes in chaperones

Differential regulations were also observed in subtype-specific chaperone levels in the HDFs. In the rpAD HDFs, a significant increase was observed in MS-quantified chaperones, compared to controls, AD and sCJD subtypes (Figure 36.A). In the global proteomic SWATH-MS dataset, most of the detected chaperones did not show statistically significant intergroup differences, except for the 60 kD heat shock protein (CH60), heat shock protein 70 kD (HSP70) and heat shock cognate 71 kD protein (HSP7C). For the CH60, a significant decrease was observed in comparison to that of spAD and controls, however, the expression was even lower in other rapid dementias included in the study.

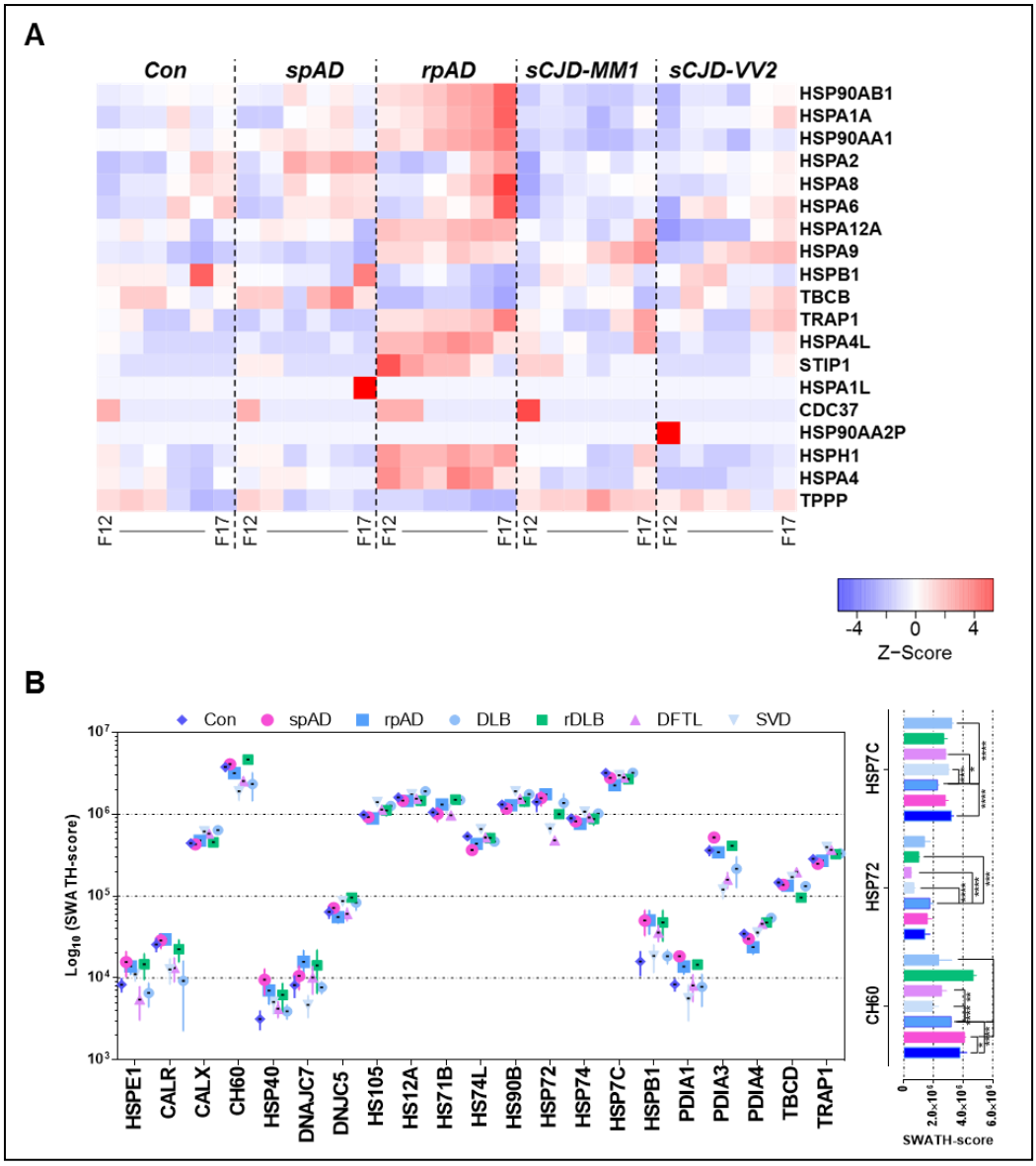

Figure 36: Differential chaperone expression levels in HDFs. A) Heatmap represents the relative levels of chaperones in high-density fractions (indicated as Z-score). Significant increase in the HDF expressions of chaperones was seen in rpAD-HDFs B) Baseline relative expression levels of chaperones (expression estimated by SWATH-MS) for spAD (n=3), rpAD (n=3), DLB (n=3), rDLB (n=3), D-FTL (n=3), SVD (n=3), and controls (n=3). F12 to F17: HDF pool 12 to 17.

A statistically significant increase was seen in the levels of HSP72 in rpAD in comparison to the other groups in the proteomic dataset. Whereas, the rpAD expression of HSP7C was also observed to be lowered, in comparison to other groups (Figure 36.B).

3.5 Identification of binding interactors for high-density prion oligomers (HDPs)

A high throughput co-immunoprecipitation assay was carried out, using an anti-prion SAF-70 antibody, with the aim of defining the interactome of high-density prion (HDP)

oligomers, and to establish whether HDP oligomers interfere with the proteins from previously described protein groups. Co-IP was carried out from the same protein pools of high-density fractions, as used for the high-resolution MS/MS analysis of HDFs. The experimental setup is described below (Figure 37.A).

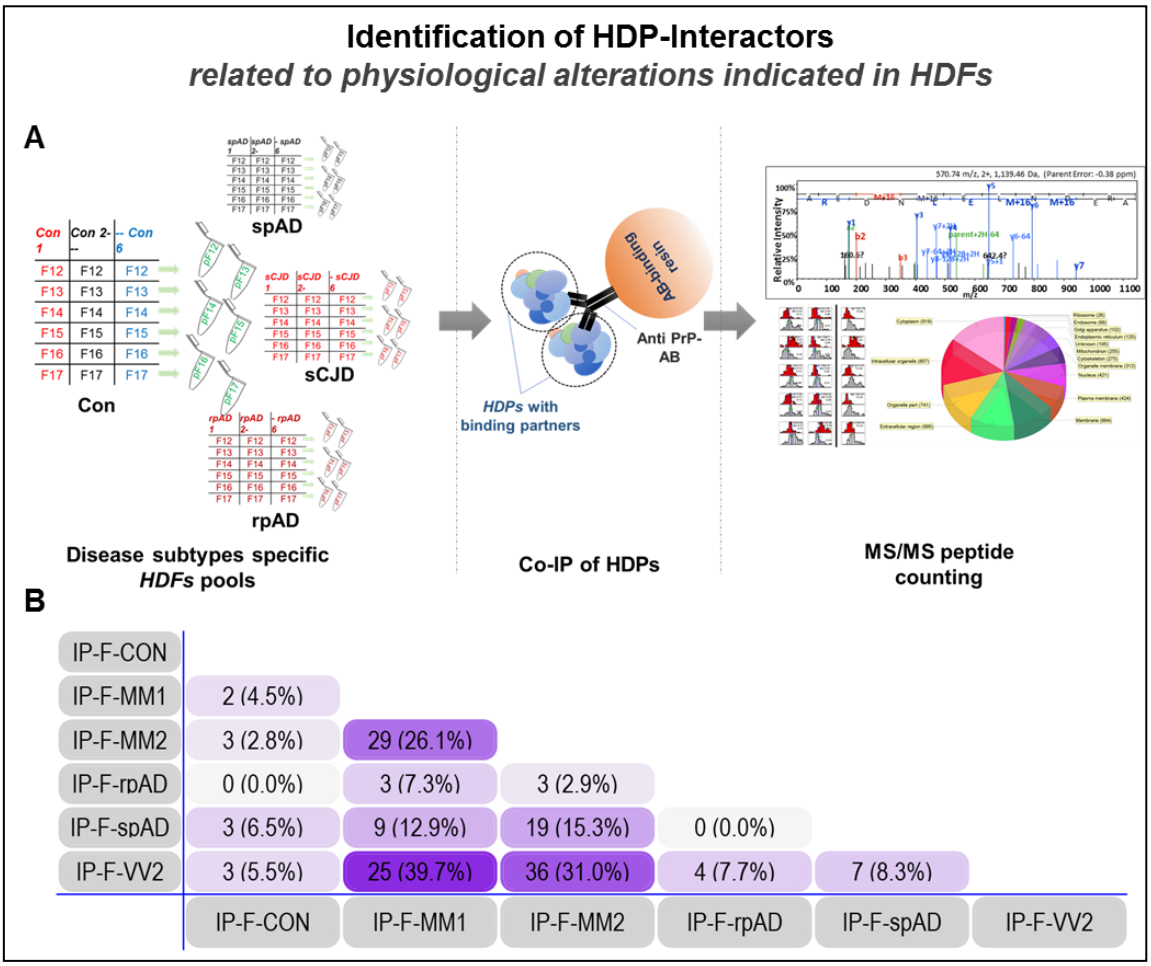

Figure 37: Disease subtype-specific binding interactors of high-density prion oligomers. A) Illustration showing the experimental setup for performance of t the co-immunoprecipitation. B) Numerical Venn-diagram showing the overlap of subtype-specific HDP interactors. IP-F-Con: high-density PrP (HDP) interactors in control HDFs pools from 12-17 (collectively), IP-F-spAD: HDP interactors in spAD HDFs pools from 12-17, IP-F-rpAD: HDP interactors in rpAD HDFs pools from 12-17, IP-F-MM1: HDP interactors in sCJD-MM1 HDFs pools from 12-17, IP-F-VV2: HDP interactors in sCJD-VV2 HDFs pools from 12-17IP-F-MM2: HDP interactors in sCJD-MM2 HDFs pools from 12-17.

3.5.1 Rapidly progressive Alzheimer's disease-specific high-density PrP interactors

Interestingly, the HDP interactomes of controls and spAD subtypes had no interactors in common with the rpAD-specific interactors of HDPs. However, some of the HDP interactors from rpAD HDFs were also commonly found as the interactors of HDP conformers from sCJD subtypes.

Table 13: HDP-binding interactors in rpAD high-density fractions.

No.	IDs	UniProt Acc. No.	Protein name	Occurrence	Subcellular location	Disease Relevance
1	KCC2B	Q13554	Calcium/calmodulin-dependent protein kinase type II subunit beta	**rpAD-F12**, sCJD-MM1-F13, 17, sCJD-MM2-F16, 17, sCJD-VV2-F16, 17	C, Ck, Ce, Sr, Sy	Alzheimer's disease (Bubber, Haroutunian, Fisch, Blass, & Gibson, 2005)
2	KCC2D	Q13557	Calcium/calmodulin-dependent protein kinase type II subunit delta	**rpAD-F12**, sCJD-MM1-F13, 17, sCJD-MM2-F16, 17, sCJD-VV2-F16, 17	Cm, Sl	
3	EPDR1	Q9UM22	Mammalian ependymin-related protein 1	**rpAD-F12**, sCJD-MM1-F13-16, sCJD-MM2-F13-16, sCJD-VV2-F12, 14, 15	S	Unknown
4	DIRA2	Q96HU8	GTP-binding protein Di-Ras2	**rpAD-F13**, **15** sCJD-VV2-F17	Cm	Unknown
5	G2L2	Q8NHY3	GAS2-like protein 2	**rpAD-F16**	C, Ck	Unknown
6	1433S	P31947	14-3-3 protein sigma	**rpAD-F17**, sCJD-VV2-F17	C, Nu, S	Parkinson's disease (Yacoubian et al., 2010), Alzheimer's disease, Creutzfeldt Jakob disease (Llorens et al., 2017), Epilepsy (Schindler, Heverin, & Henshall, 2006)

F12 to F17: HDF pool-12 to 17, Ce: centrosome, Sy: Synapse, Sr: sarcoplasmic reticulum, C: Cytoplasm, Ck: cytoskeleton, Nu: Nucleus, S: Secreted, Cm: Cell membrane, Sl: Sarcolemma, Ly: Lysosomes, Mc: Mitochondrion, Syo: Synaptosome, Cj: Cell junction, C V: cytoplasmic vesicles, Ga: Golgi apparatus, Pm: phagosome membrane, Px: peroxisome, Em: Endosome membrane, Cp: Cell projection, Gc: growth cone, Ms: Melanosome, Er: Endoplasmic reticulum and La: Lipid-anchor. The localization of proteins and accession number are assigned as in ExPASy protein database and Uniprot database, respectively.

Three interactors, namely mammalian ependymin-related protein 1 (EPDR1), CaMKII subunit beta (CAMK2B) and CaMKII subunit delta (CAMK2D) were commonly found interacting with HDPs in IP-F-rpAD and sCJD fractions i.e. IP-F-MM1, IP-F-MM2 and IP-F-VV2. IP-F-VV2 and IP-rpAD also shared another common interactor namely GTP-binding protein Di-Ras2 (DIRA2) (Figure 37.B, Table 13).

Though the spectrum of rpAD-specific HDP-interactors was not broad, the interactors identified belonged to diverse cellular activities. In total, six interactors could be identified, either uniquely present in rpAD-specific HDFs or commonly between rpAD and

sCJD subtype-specific fractions. Calcium/calmodulin-dependent protein kinase type II (CaMKII) has been previously reported to be relevant in Alzheimer's disease, however, the disease relevance of ependymin-related protein 1, GTP-binding protein Di-Ras2 and GAS2-like protein 2 have not been reported so far, in curated databases (Table 13). Subtype unique HDP interactors and HDP interactors commonly occurring in samples from spAD and sCJD subtypes are discussed in the supplementary data section 6.1, Table 19, Table 20 and Table 21.

3.5.2 The physiological coherence of subtype-specific high-density PrP binding proteins

The pathway enrichment analysis of HDP interactors resulted in an interesting outcome. No overlap could be observed in PrP interactors from spAD and rpAD HDFs. On the contrary, the physiological pathways shown for the rpAD also appeared to be affected in sCJD subtypes, suggesting a similar involvement of HDPs in the pathophysiology of the two diseases (Figure 38).

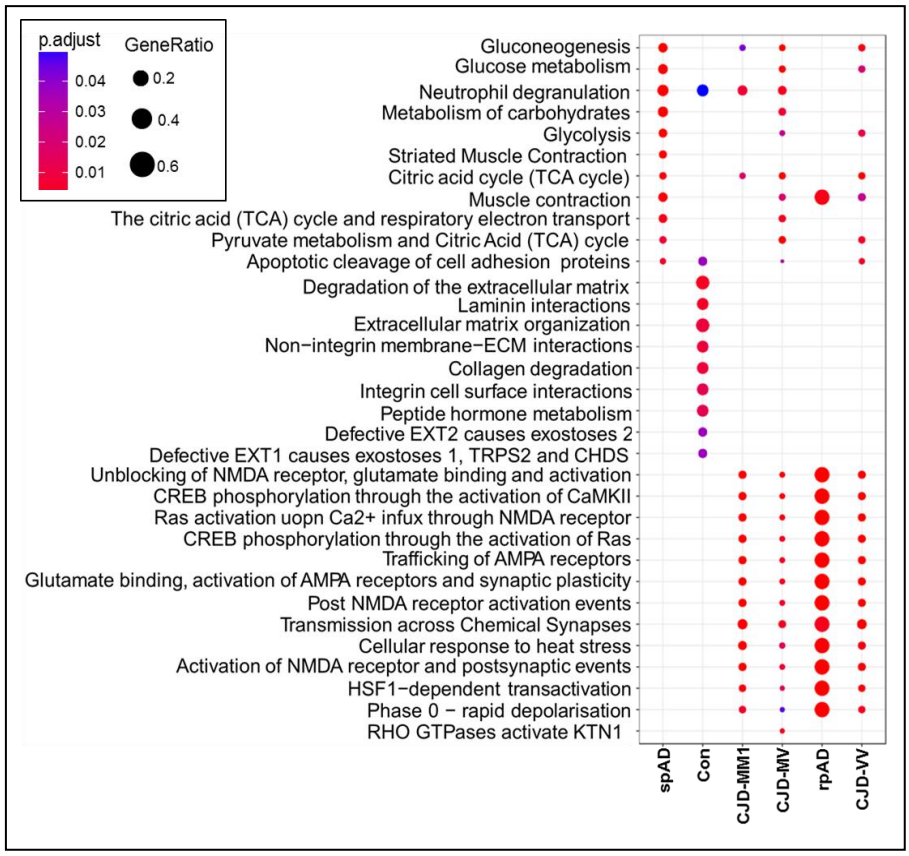

Figure 38: Enrichment analysis of subtype-specific HDP interactors, based on Reactome-pathway database. The graphical presentation exhibits adjusted *p*-values for corresponding pathways, calculated using cluster profiler package in R-statistical language.

3.6 *Growth arrest-specific 2-like 2 (G2L2) and potential interaction to HDPs*

Out of the candidates identified as HDP interactors in rpAD, growth arrest-specific 2-like 2 (G2L2) was selected for further functional verification. G2L2 was selected, because it is a unique interactor to rpAD-specific HDPs and for its essential role in the cytoskeletal integrity (actin-microtubule assemblage), as the prior MS/MS analysis of HDFs had also indicated differential cytoskeletal anomalies among the disease subtypes. G2L2 is reported to play a role in the co-alignment of actin filaments and microtubules bundles, by cross-linking the two together. This cross-linking is assisted by the end-binding protein-1 (EB-1) in the actin filaments (Stroud et al., 2014). To study G2L2 comprehensively, the proteins associated with the physiology of G2L2 including EB-1, tubulin and actin were also tested in the study.

3.6.1 Expression of G2L2 and associated proteins in Alzheimer's subtypes

Immunoblotting-based expression analysis of brain frontal cortex protein isolates showed no significant differences in the expression of G2L2 between the AD-subtypes and Con. Likewise, no significant differences in expression could be seen for EB-1, tubulin-α, and actin-β (Figure 39).

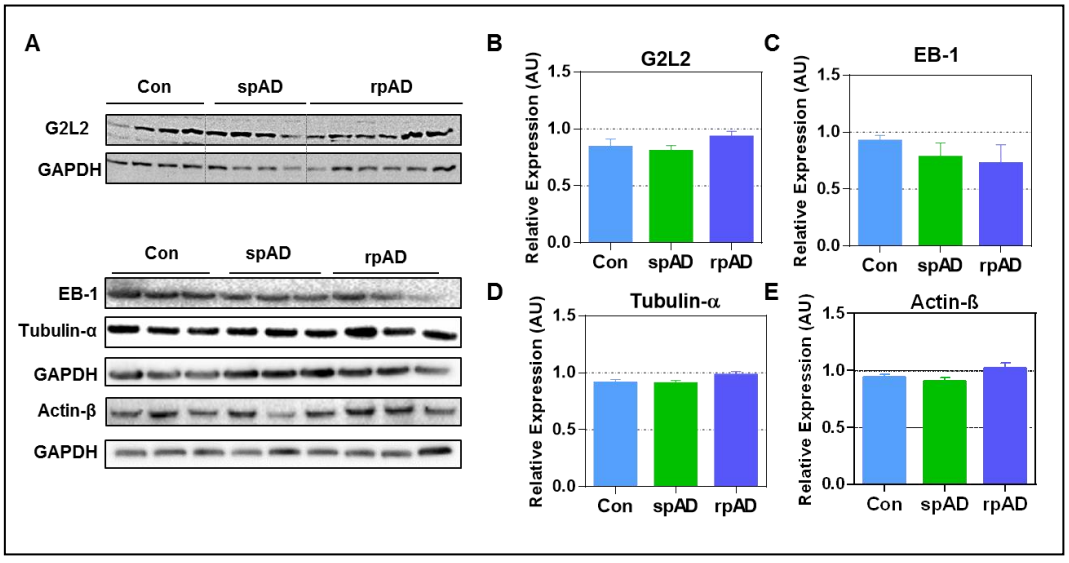

Figure 39: Expression regulation of G2L2 and associated proteins. A) Immunoblots showing the expression levels of G2L2, EB-1, tubulin-α, and actin-β. B-E) Densitometric analysis for G2L2, EB-1, tubulin, and actin, carried out using immunoblots for spAD (n=7), rpAD (n=7) and controls (n=6), in three independent experiments. No significant expression differences could be found for the G2L2 and associated proteins. Statistical significance was calculated with one-way ANOVA followed by Tukey post-hoc test to compare all pairs of columns.

3.6.2 Colocalization of G2L2 and associated proteins in brain frontal cortex

After not having been able to identify differences in expression, we investigated the colocalization patterns of G2L2 with PrP and EB-1, tubulin-α, and actin-β in AD-subtypes and controls. Tubulin-α and actin-β colocalization was also visualized for assessment of the functional integrity the cytoskeletal system.

3.6.2.1 Neuronal co-localization of G2L2 and PrP

By comparing the colocalization patterns of G2L2 and PrP, a certain subtype-specific trend was apparent. Immuno-histological observations were made from the grey matter areas of the frontal cortices from the controls and AD subtypes. The highest level of colocalization between PrP^C and G2L2 was observed in frontal cortex tissues of rpAD (Figure 40.p) followed by spAD (Figure 40. j) cortical sections.

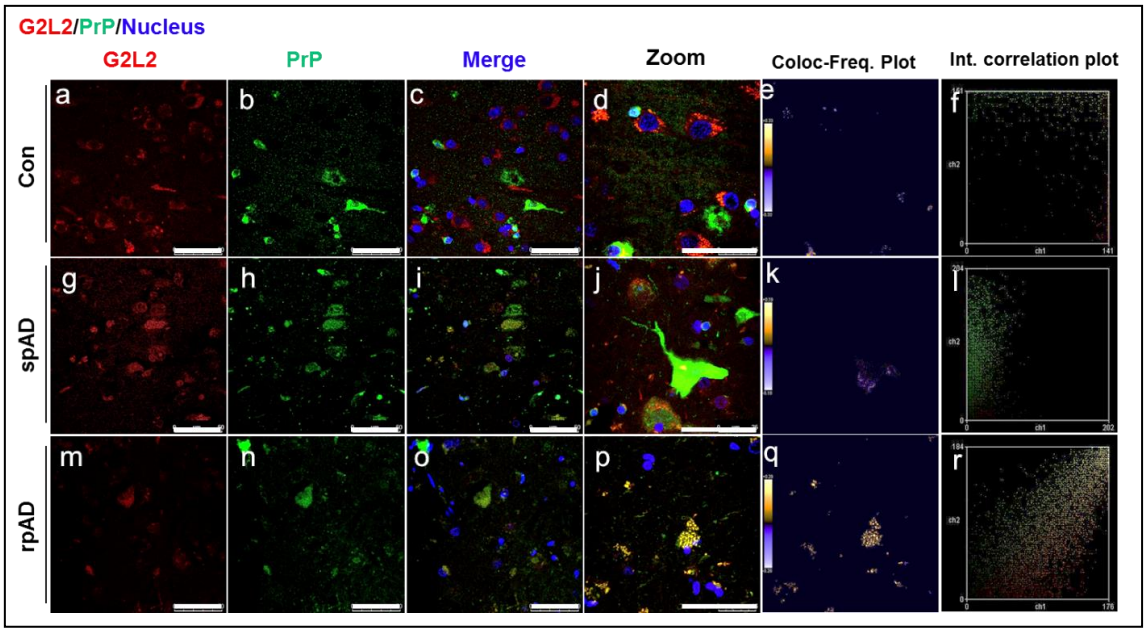

Figure 40: Characteristic colocalization of G2L2 and PrP in rpAD, spAD and control brains. Brain frontal cortex sections of rpAD (n=3), spAD (n=3) and controls (n=3) were stained using anti-G2L2 and anti-PrP (SAF70) antibodies. Scale bars = 50µm. Colocalization frequency plots (panels e, k, q) and correlation plots (panel f, l, r) were prepared using intensity correlation analysis plug-in in ImageJ.

Intensity correlation analysis (ICA) of channel intensities was performed for PrP^C and G2L2 channels to quantitatively define the colocalization. Colocalization frequency plots (shown in Figure 40, e, k, and q) and the channel intensity correlation plots (Figure 40, f, l and r) also represent the highest G2L2-PrP^C colocalization in rpAD followed by spAD and controls, respectively. Threshold Mander's coefficient (tM) and Pearson correlation (*rP*) coefficient values were also calculated for the channel intensities. The

value of tM1 shows the overlap of G2L2 channel pixels to PrP^C channel pixels, which is significantly higher in rpAD than in spAD. On the other hand, tM2 (representing the overlap of PrP^C channel pixels to G2L2 channel pixels) is also significantly higher in rpAD than in spAD. High *rP*-values show that there is a strong correlation between the PrP and G2L2 in colocalization areas (Figure 41).

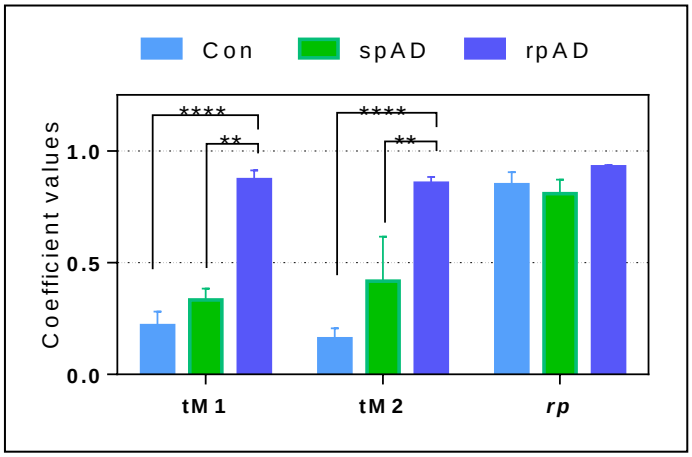

Figure 41: Correlation coefficients for colocalization of G2L2 and PrP in frontal cortex of rpAD, spAD and control frontal cortex tissues. Brain frontal cortex sections of rpAD (n=3), spAD (n=3) and controls (n=3) were stained using anti-G2L2 and anti-PrP (SAF70) antibodies. Threshold correlation coefficient values were calculated using intensity correlation plugin in ImageJ from micrographs scanned at 630x magnification. Statistical significance was calculated using one-way ANOVA. Tukey post-hoc test was used to calculate the intergroup statistical differences. **p < 0.005; ***p < 0.001

3.6.2.2 G2L2 and EB-1 binding

We hypothesized that the interaction of HDP oligomers with G2L2 (shown in Figure 40) may interfere with the interaction of G2L2 and EB-1, necessary for the downstream control of actin-tubulin integrity.

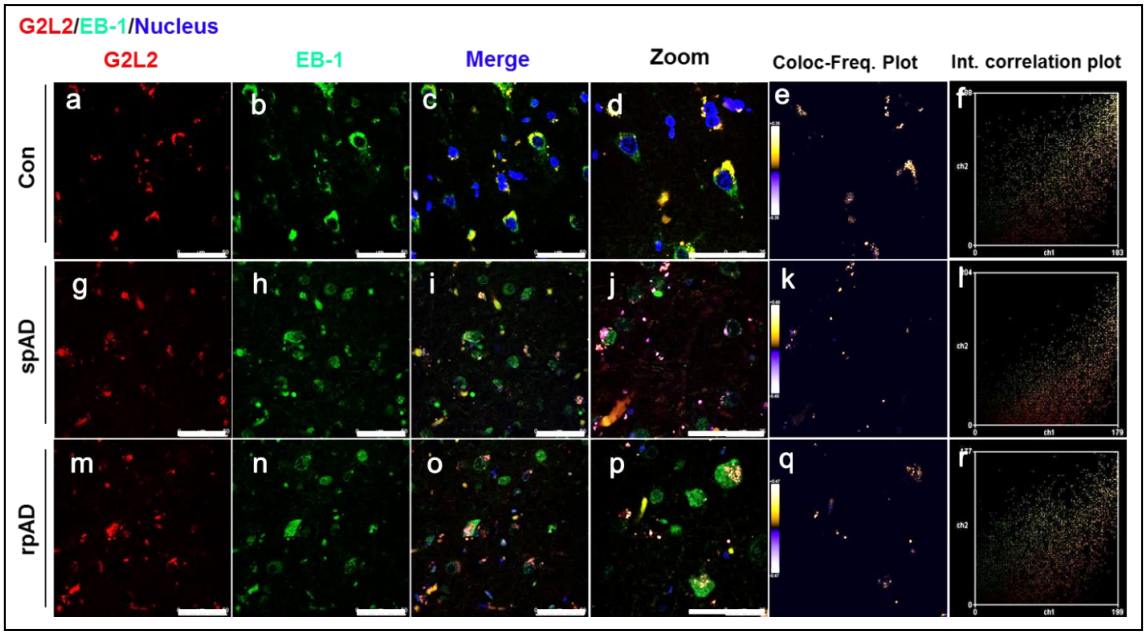

Figure 42: Characteristic colocalization of G2L2 and EB-1 in the frontal cortex of AD and control brains. Brain frontal cortex sections of rpAD (n=3), spAD (n=3) and controls (n=3) were stained using anti-G2L2 and anti-EB-1 antibodies. Scale bars = 50 µm. Colocalization frequency plots (shown in e, k, and q) and correlation plots (f, l, r) were prepared using intensity correlation analysis plug-in in ImageJ.

A significant decrease in G2L2 and EB-1 colocalization was observed in the frontal cortex brain tissues of rpAD compared to spAD cortical sections and controls. Intensity correlation analysis (ICA) of channel intensities was performed for EB-1 and G2L2 channels to quantitatively define the colocalization extent. Colocalization frequency plots (shown in Figure 42 e, k, and q) and the channel intensity correlation plots (Figure 42 f, l and r) also show the colocalization to be minimum in rpAD followed by the higher overlap in spAD and maximum in control frontal cortex tissues. Significantly decreased G2L2 (tM1) and tM2 (EB-1) values in rpAD in comparison with those of spAD represent the lower degree of colocalization in rpAD. A strong correlation between the EB-1 and G2L2 channels is represented by high *rP* values, in the areas of channel colocalization (Figure 43).

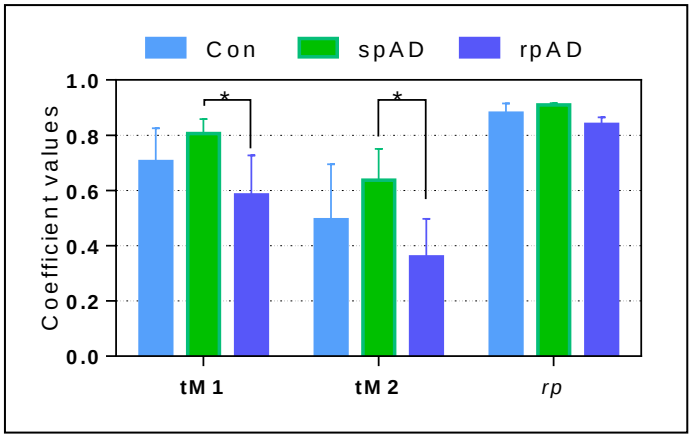

Figure 43: Correlation coefficients for colocalization of G2L2and EB-1 in frontal cortex of rpAD, spAD, and controls. Brain frontal cortex sections of rpAD (n=3), spAD (n=3) and controls (n=3), were stained using anti-G2L2 and anti-EB -1 antibodies. Threshold correlation coefficient values were calculated using the intensity correlation plugin in ImageJ from micrographs scanned at 630x magnification. Statistical significance was calculated using one-way ANOVA. Tukey post-hoc test was used to calculate the intergroup statistical differences. *p < 0.05

3.6.2.3 G2L2/tubulin-α colocalization

To study the hypothesized disruption in G2L2 and tubulin-α integrity under the influence of HDPs, we studied the colocalization of G2L2 and tubulin-α in frontal cortex tissues of AD subtypes.

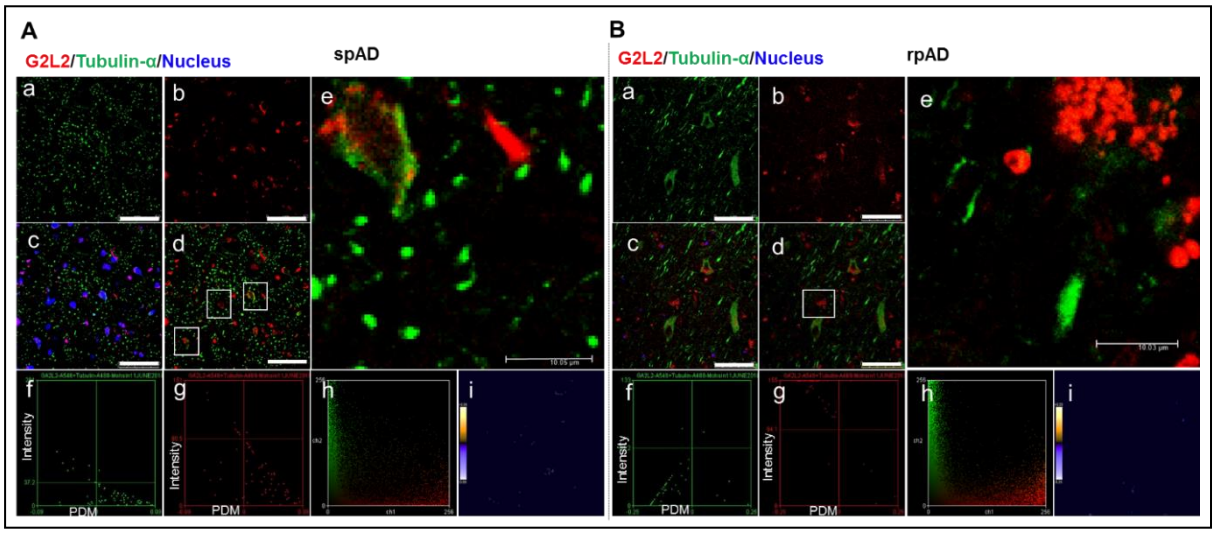

Figure 44: G2L2 and tubulin-α localization in the frontal cortex of rpAD and spAD brains. Brain frontal cortex sections of rpAD (n=3) and spAD (n=3) were stained using anti-G2L2 and anti-tubulin-α antibodies. Scale bars in panels A.a -A.d and panels B.a -B.d measure 50 µm and 10 µm in Ae and Be. ICA plots (panels A.f-g and B.f-g), colocalization frequency plots (panels A.i and B.i) and correlation plots (panel A.h and B.h) were prepared using intensity correlation analysis plug-in in ImageJ.

Scanning laser micrographs showed a low degree of colocalization for G2L2 and tubulin-α in the cortical gray matter area of rpAD and spAD brain sections. Colocalization

frequency plots (Figure 42 e, k, and q) and the channel intensity correlation plots (Figure 44, A.h and Figure 44, B.h) represent the low level of colocalization in both rpAD and spAD. Values of tM1 (G2L2) and tM2 (tubulin-α) did not show any significant differences (Figure 45).

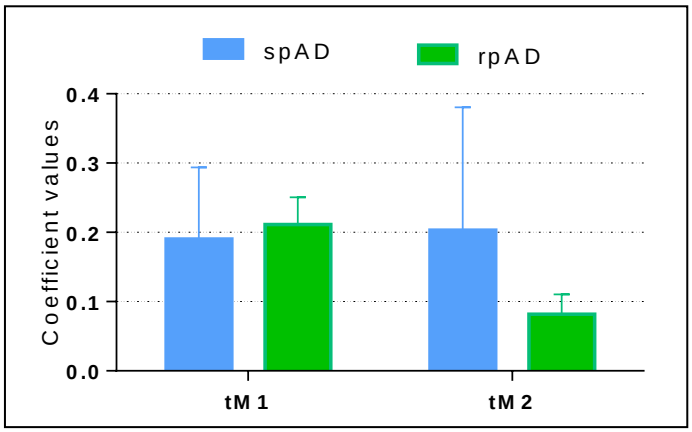

Figure 45: Correlation coefficients for colocalization of G2L2 and tubulin-α in the frontal cortex of rpAD and spAD. Frontal cortex section from rpAD (n=3) and spAD (n=3) were stained with anti-G2L2 and anti-tubulin antibodies. Threshold coefficient values were calculated using the intensity correlation plugin in ImageJ from micrographs scanned at 630x magnification. Statistical significance was calculated using one-way ANOVA.

3.6.2.4 G2L2/actin-β colocalization

We could not establish any significant difference in the colocalization between the actin and G2L2 in frontal cortex gray matter areas of spAD and rpAD brain tissues. Distant distribution of channel-intensities in the correlation plots in (Figure 46 A, panel h and Figure 46 B, panel h) represent the non-existent colocalization between G2L2 and actin. Likewise, the colocalization-frequency calculations showed a very low extent of colocalization in the two channels only in spAD sections (Figure 46 A, panel i and Figure 46 B, panel i).

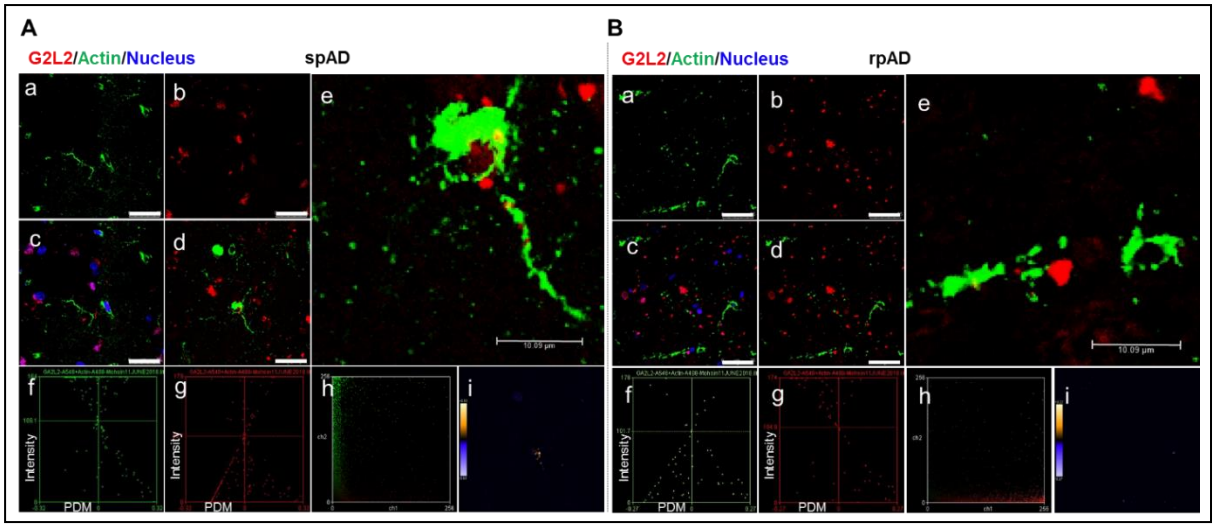

Figure 46: G2L2 and actin-β distribution in the frontal cortex of rpAD and spAD brains. Brain frontal cortex sections of rpAD (n=3) and spAD (n=3), were stained using anti-G2L2 and anti-actin-β antibodies. Scale bars in panels A.a-A.d and B.a-Bd measure 50 µm and 10 µm in panel A.e and B.e. ICA plots (panels A.f-g and B.f-g), colocalization frequency plots (shown in panels A.i and B.i) and correlation plots (panel A.h and B.h) were prepared using Intensity correlation analysis plug-in in ImageJ.

3.6.2.5 Actin-β/tubulin-α integration

Probable disruptions in actin-tubulin co-alignment were also studied using confocal laser scanning microscopy. Frontal cortex sections (5 µm thick) were stained for tubulin-α and actin-β and were scanned for the confocal z-sections, and later used for the construction of three-dimensional images.

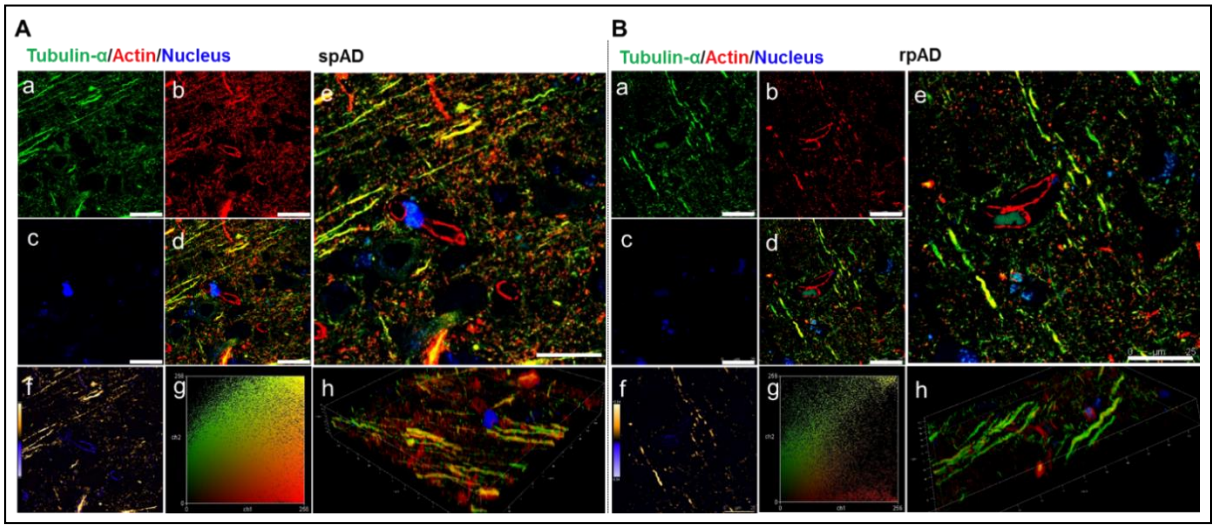

Figure 47: Actin-β and tubulin-α colocalization in the frontal cortex of AD-subtypes. Brain frontal cortex sections of rpAD (n=3) and spAD (n=3), were stained using anti-tubulin-α and anti-actin-β antibodies. A.e and B.e represent region of interests at higher magnification. A.h and B.h represent three-dimensional reconstruct from the z-sections. Scale bars in panels A.a-A.d and B.a-B.d correspond to 50 µm and 25 µm in panel A.e and B.e. Colocalization frequency plots (panels A.f and B.f) and correlation plots (panel A.g and B.g) were prepared using Intensity correlation analysis plug-in in ImageJ.

A more pronounced actin-tubulin colocalization was observed in the spAD samples in comparison to rpAD (Figure 47 A, panel e and Figure 47 B, panel e) shown also by the colocalization-frequency plots (Figure 47 A, panel f and Figure 47 B, panel f). Likewise, in correlation plots calculated for the actin and tubulin channels, we could also see significantly higher overlap between the channel intensities (Figure 47 A, panel g and Figure 47 B, panel g). Three-dimensional reconstructs from the z-sections show longer stretches of filaments with actin-tubulin colocalization in spAD compared to rpAD with higher actin and tubulin channel overlap (Figure 47 A, panel h and Figure 47 B, panel h).

4 Discussion

Alzheimer's disease is the most commonly occurring dementia of the elderly, constituting up to 75% of all dementias either exhibited as an independent entity or occurring as comorbidity disease. Typically, Alzheimer's disease is a slowly progressive disease with either spontaneous development of characteristic symptoms in sporadic cases, or due to an associated mutation in presenilin 1, 2 and APP. Over the past few decades, some atypical AD cases have been reported, with a rapid cognitive decline of >6 MMSE points a year and a shorter post-diagnostic survival, spanning ~4 years. The aim of the current study was to characterize the mechanisms leading to progression rate variations in AD. The study was based on brain frontal cortices from rpAD and spAD, sCJD subtypes (MM1, MM2 and VV2), DLB, rDLB, SVD, and DFTL. Frontal cortex tissues were selected to carry out the experimentation, as the cortical pathology in neurodegenerative disease marks the end stages of the disease (Braak & Braak, 1991). The study focuses on many aspects linked to Alzheimer's disease including basic pathological alterations, changes in the kinome involved in the neurodegenerative diseases and primarily the metabolism of prion protein and biochemical and physiological characterization of the rpAD-unique PrP-oligomers.

4.1 Amyloid plaques and Tau tangles

We were able to identify slight differences in the development of amyloid plaques. The amyloid plaques in the rpAD frontal cortex were observed at higher frequencies but they were rather small in rpAD in comparison to other subtypes. However, non-significant differences were seen for Tau tangle frequency and size in the rpAD when compared to spAD cases. Biochemically, we could not identify any subtype-specific differences in the expression of Aβ and Tau levels, nor in the phosphorylation of Tau. Conformation variants of Aβ oligomers have been extensively studied by many groups. Human brain derived Aβ has been used in some studies to seed synthetic Aβ and resultant differential species have been further examined for structural differences (Lu et al., 2013; Qiang, Yau, Lu, Collinge, & Tycko, 2017). Likewise, work from Cohen et al. (2016) has exhibited the structural variation in the Aβ species persisting between spAD and rpAD. Biophysically divergent species of Aβ have also been described by Rasmussen et al., with the spAD and FAD cases. In the study, classification of Aβ species was based on respective interactions with luminescent-conjugated

oligophenes (LCOs). An association between different Aβ-conformational variants and disease subtypes including spAD and FAD with mutations including *APP* V717I, *PSEN1* A431E, *PSEN1* F105L, *PSEN1* E280A cases, was observed in the study. Surprisingly, age-dependent variation in Aβ-conformation was also noted in a mouse model, (Rasmussen et al., 2017). However, the mechanistic details of these discrepancies in Aβ conformation remain unclear.

The increase in the plaque and tangle frequencies in our cohort can be inferred as the higher degree of failure in the control mechanisms checking the oligomers in brain interstices. Failure in the conversion of soluble oligomers to insoluble fibrils/plaques may be the cause of a higher number of smaller sized plaques and tangles. Differential signal transduction and prion protein metabolism were investigated further to reveal the mechanism leading to amyloid profiles.

4.2 Differential signal transduction

Differential signal transduction has been associated with neurodegenerative disease. Specifically AD has diverse associative variations in signaling events, including Wnt signaling (Inestrosa & Varela-Nallar, 2014), MAPK signaling (Kim & Choi, 2015), p38 MAPK signaling (Munoz & Ammit, 2010), NFkB signaling (Li, Long, He, Belshaw, & Scott, 2015), AMPK signaling (Godoy, Rios, Zolezzi, Braidy, & Inestrosa, 2014) and Fyn signaling (Um & Strittmatter, 2013). Furthermore, a battery of kinases, including Fyn, AKT, PKA, CaMKII, Cdk5, MAPK and MARK, is responsible for Tau phosphorylation (Querfurth & LaFerla, 2010). In the current study, we aimed to differentiate specific signal transduction pathways involved in the pathological events and most importantly progression rate differences. Kinases including AKT, ERK, p38, NFkB, GSK3-β, MYLK, MP2K4, KPYM, PI424, KPC, CaMKII, MK01, and SRC, were studied for the total expression and expression of phosphorylated forms. Only CaMKII subunit B was observed to be up-regulated in the spAD cortex compared to rpAD and Con. CaMKII is known for its Tau-phosphorylation activity (Ghosh & Giese, 2015). Up-regulation of CaMKII-B can be considered responsible for the slightly higher (though non-significant) phosphorylation of Tau in spAD. Interestingly, the differences in kinase expression profiles between the Alzheimer's subtype and the control cohort were also not significant, suggesting that it then may well be associated with changes originating due to aging in control brain samples.

4.3 Prion protein metabolism (differential glycoforms and distribution)

In recent years, PrP^C has been shown to interact with amyloid-β species (Dohler et al., 2014). Cell surface PrP^C is reported to act as a receptor for oligomers resulting in neurotoxicity (Zhou & Liu, 2013). On the other hand, shed-PrP (sPrP) promotes the fibrilization of extracellular Aβ oligomers (Altmeppen et al., 2012). Moreover, earlier studies from Jiri Safar's group have established that there is a distinct increase in the low molecular weight species of Aβ oligomers in rpAD cases in comparison to spAD (Cohen et al., 2015). We hypothesized that the differences in the Aβ oligomer-induced neurotoxicity is a contributing factor to progression rate variations in AD subtypes and the cause of this increased population of low molecular weight oligomers reflects alterations in PrP metabolism. Expression analysis revealed a significant decrease in the di-glycosylated isoform of PrP (DG-PrP), although no significant differences were observed in the total PrP. Variations in the DG-PrP have already been reported, in the context of prion strain variations (Aguzzi, Heikenwalder, & Polymenidou, 2007; Khalili-Shirazi et al., 2005; Neuendorf et al., 2004), but the mechanism leading to such differences the glycosylation patterns have not been understood. Some studies show the data with a decrease in extracellular shedding of PrP^C as a result of a decrease in DG-PrP (Linsenmeier et al., 2018). Therefore, we checked the distribution of extracellular PrP in our cohort and established a significant decrease in the shed-PrP. Interestingly, we found a significant decrease in the extracellular PrP. We also saw a higher nuclear accumulation of PrP (Zafar, Shafiq, et al., 2017). A previous study from Say et al., (2007) suggests that the perinuclear presence of PrP might arise due to the recycling of plasma membrane to the nucleus (Say & Hooper, 2007). However, nuclear colocalization of PrP and histone has been verified in a study by Strom et al., (2011). Prion protein has also been reported to localize in the nucleus under genotoxic conditions acting as a strong activator of DNA repair via the central base excision repair enzyme, the AP endonuclease. (Bravard et al., 2015). From the above-mentioned debate and corresponding results from our study, we think that the disrupted localization of PrP in the brain tissue interferes with the amyloid sequestering, hence a higher number of toxic lower molecular weight oligomers are available in rpAD cases in comparison to spAD. An overview of ongoing cellular events is shown in Figure 48.

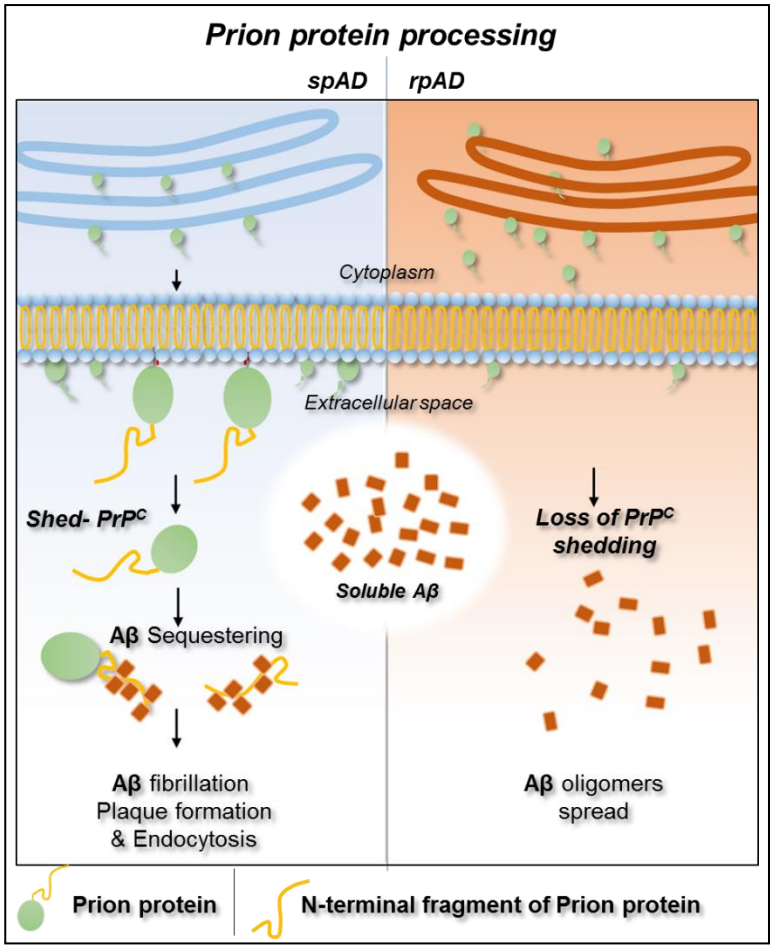

Figure 48: Prion protein shedding in AD-subtypes. Shedding of prion protein is proportional to the degree of glycosylation in PrP (Linsenmeier et al., 2018). Extracellular levels of prion protein have been found decreased in rpAD frontal cortices. Less extracellular PrP results in the decreased sequestering of Aβ oligomers, resulting in rapid spread in rpAD, hence a higher neurotoxicity.

4.4 Subtype-specific PrP^C interactors

Prion protein has been actively studied for its binding interactors with the aim of understanding the underlying physiological aspects. Prion protein interacts with the ligands belonging to three major molecular categories, namely metal ions, single molecular interactors, and multimolecular complexes. The octapeptide region of surface PrP^C is often reported to interact with divalent metal ions, particularly Cu^{2+} (Brown et al., 1997), Ni^{2+}, Zn^{2+} and Fe^{2+} (Jackson et al., 2001) leading to conformational changes, in turn activating N-methyl-D-aspartic acid receptors (NMDA) (Singh, Das, Singh, & Mohan, 2010). The PrP-metal associations have also been discussed as a control mechanism of oxidative stress (Singh et al., 2010). Prion protein is also reported to interact with other proteins and RNA molecules. Well-established-prion protein interactors include synuclein-α (De Cecco & Legname, 2018), 14-3-3 isoforms (Di

Fede et al., 2007; Richard et al., 2003; Satoh, Onoue, Arima, & Yamamura, 2005), cytoskeletal proteins, including synapsin 1b (Spielhaupter & Schätzl, 2001), glial cell fibrillary acidic protein (Dong et al., 2008), tubulin isoforms (Nieznanski, Nieznanska, Skowronek, Osiecka, & Stepkowski, 2005; Osiecka et al., 2009), microtubule-associated protein-MAPT (Wang et al., 2008), stress-inducible protein 1 (Ostapchenko et al., 2013), Rab7a and lactate dehydrogenase (Zafar et al., 2014), RNA binding proteins, and some other proteins including growth factor receptor-bound protein 2, b-cell lymphoma 2 protein, nuclear factor erythroid 2-related factor 2, casein kinase 2 (Nieznanski, 2010).

In the current study, we have characterized subtype-specific PrP interactors in Alzheimer's disease. Histone H2B2 and zinc alpha 2 glycoprotein (ZAG) have been identified as novel PrP interacting proteins from rapidly-progressive forms of the AD. One protein, myelin P2, was isolated as the sole binding partner to the PrP isoform in spAD samples. We also identified PrP interacting proteins for both subtypes of Alzheimer's disease studied including transketolase, myelin basic protein, peroxiredoxin-1, and four and a half LIM domains protein 1. Interestingly, physiological relevance for the ZAG and histone H2B2 was established earlier, for the Alzheimer's and PrP function. ZAG is a protein with multiple reported functions, including lipid mobilization, and ribonuclease activity (Hassan, Waheed, Yadav, Singh, & Ahmad, 2008; Lei, Arany, Tyring, Brysk, & Brysk, 1998), and was previously reported for an increase in expression in serum of Alzheimer's disease patients; but the physiological significance of increased expression has not been discussed (Shen et al., 2017). Histone interaction with the prion protein has been previously reported, with a suggestive role in transcriptional control (Rousset, Leturque, & Thenet, 2016; Strom et al., 2011). Among the interactors commonly present in AD-subtypes, peroxiredoxin-1 plays a protective role in cell redox stress (Kang et al., 1998). Four and a half LIM domains protein 1 is involved in cell morphogenesis (Sato K et al., 2016). Transketolase isoform functions as a phosphate-adding enzyme acting over sugars and is important in mammalian glycolysis. Myelin basic protein has a role in myelination and brain development (Nye et al., 1995). Though functional outcomes of subtype-specific PrP^C interactions have yet to be established. We recognized that the differences in interactors might be a result of various types of PrP conformers. To this end, for the next phase of the study we focused on the isolation and characterization of PrP oligomers in varying molecular weight ranges.

4.5 Prion protein oligomers in rpAD

Multiple PrP conformers have been previously described in the association of transmissible spongiform diseases in animals and humans (Cracco et al., 2017; Imran & Mahmood, 2011; Kitamoto & Tateishi, 1994). In recent years, many studies have focused on the existence of soluble PrP oligomers of varying molecular weights, as the toxic mediators of disease (Cracco et al., 2017; Haass & Selkoe, 2007; Haldiman et al., 2013; C. Kim et al., 2011, 2012). However, AD has not previously been associated with variant PrP oligomer populations. In the current study, we examined density variant PrP oligomers in AD frontal cortices. Frontal cortex tissues from sCJD were used as positive controls. We were able to identify unique assemblies of PrP associated specifically with the rpAD and sCJD in high-density fractions, suggesting an overlap of properties between the prion oligomers of rpAD and sCJD-subtypes. However, no similarities between the rpAD- and sCJD-specific PrP oligomers could be established in proteinase-K digestion assays or the seeding activity assay (via real-time quaking-induced cyclic amplification). Presence of HDP oligomers in rpAD can specifically be indicative in two different domains; firstly, the loss of function with the PrP conformers resulting in their malfunction due to the inability to perform normal physiological functions, secondly, gain of function with higher neurotoxicity directly induced by the PrP oligomers.

4.6 Differentially distributed proteins in high-density fractions

High-resolution MS/MS analysis of HDFs was carried out to study the subtype-specific protein expression. Differential mass spectrometric analysis when compared to baseline global proteome (SWATH-MS based), highlighted rpAD-specific alterations in certain physiological domains, including ubiquitin, proteasomal subunits, ras-related proteins, chaperones, and the cytoskeletal machinery, as well as a higher over-all proteopathic burden.

4.6.1 Proteopathic proteins and protein degradation machinery

High-density fractions of the sCJD subtypes showed the highest levels of proteopathic proteins followed by the rpAD HDFs, except for serpins. Serpin levels were significantly higher in spAD compared to that of rpAD. The increased levels of proteopathic proteins in HDFs are indicative, to a higher degree of dysregulation, of protein

degradation machinery as well as an increase in molecular events that promote the polymerization of the proteopathic proteins; alterations in these physiological domains associated with rpAD and sCJD could also be observed in the HDF proteomic profiles. Experimentally, we observed a differential distribution of ubiquitin and proteasomal subunits. Levels of ubiquitin subunits were significantly reduced in rpAD fractions compared to controls and spAD HDFs. Similar decreased expression levels were also observed for sCJD HDFs. However, highest levels of proteasomal subunits were found in sCJD HDFs, in contrast to rpAD HDFs, where the HDF levels of proteasomal subunits were found significantly decreased. The protein degradation machinery (proteasomal subunits and ubiquitin isoforms) has already been discussed as the control mechanism for the removal of misfolded proteins (Checler and Vincent, 2002; Klaips, Jayaraj & Hartl, 2018). Synaptic aggregates of hyperphosphorylated Tau have also been associated with pathophysiological alterations of the ubiquitin-proteasome axis (Tai et al., 2012). The decrease in the proteasomal abundance in the rpAD-specific fractions is indicative of the relatively higher proteopathic burden in rpAD and the presence of rpAD unique PrP oligomers. We considered that the increase in sCJD proteasomal subunits is related to the higher abundance of the proteopathic proteins.

4.6.2 Ras-related proteins

Rab-GTPases have been reported generally to take part in vesicle formation, vesicular transport in both endocytic, exocytic pathways and membrane trafficking (Bucci, Thomsen, Nicoziani, McCarthy, & van Deurs, 2000). However, unique subsidiary roles are assigned to specific ras-related proteins. Rab11 has been reported for its role in the expression control of potassium channels and Cav1.2 calcium channel (Best et al., 2011; Delisle et al., 2009). Ras-related protein Rab14, through its interaction with FAM116, modulates the subcellular distribution of ADAM10 in migrating cells (Linford et al., 2012). Involvement of Rab7a along with the PrP in the vesicular transport has been well characterized previously (Zafar et al., 2011). Rab21 has been shown to regulate integrin trafficking necessary for cytokinesis. In our study, levels of ras-related proteins were observed to be significantly higher in the HDFs from sCJD subtypes compared to AD subtypes and controls. Contrary to our expectation, the differential HDF levels of ras-related proteins point more towards variant pathological events in action in rpAD than those of sCJD. Increase in the sCJD-HDF levels can be an indication of a higher expression of ras-related proteins in sCJD subtypes. As ras-related

proteins are described to be associated with the vesicles, Golgi complex and ER in many studies (Plutner et al., 1990; Tisdale et al., 1992; Zafar et al., 2011; Banton et al., 2014; Zheng et al., 2015), we also argue that the higher HDF levels of ras-related proteins in sCJD subtypes correspond to higher levels of membrane vesicles as well as Golgi and ER fragments, due to higher neurodegenerative damage.

4.6.3 Cytoskeletal components

The cytoskeleton provides the basic framework of shape, support and, most importantly, the transport process within the cell. Defects in cytoskeletal proteins lead to interrupted transport, and these are major features in neurodegenerative disorders (Brunden, Lee, Smith, Trojanowski, & Ballatore, 2017; Gartz Hanson et al., 2016; Matamoros & Baas, 2016; Swanger, Mattheyses, Gentry, & Herskowitz, 2015). Decreased levels of tubulin in rpAD HDFs showed that cytoskeletal proteins are indicative of worse damage to the cytoskeletal system, as previously described (Richter-Landsberg, 2008; Tas & Kapitein, 2018). The decrease in the tubulin integrity marks the involvement of pathways linked predominantly to rpAD, compared to spAD. PrP^C was reported previously to inhibit microtubule synthesis, through its direct interaction with tubulin (Nieznanski, Podlubnaya, & Nieznanska, 2006). Uniquely identified PrP oligomers in rpAD can be associated with tubulin sequestration, resulting in a higher degree of microtubule damage. In our study, the decrease in the HDF levels of tubulin in rpAD is accompanied by higher levels of microtubule-associated proteins (MAP1 and MAP2). This increase of MAPs in HDFs is indicative of a higher degree of MAPs being sequestered in the tangles as described previously (Harada et al., 1994; Wang & Mandelkow, 2016). MAPs sequestration also correlates with the loss of microtubule integrity in the rpAD cortices. Higher levels of the cytoskeletal proteins in sCJD HDFs indicate involvement of a different set of mechanisms. As the tubulin-PrP interaction has been previously investigated by many authors (Nieznanski et al., 2005, 2006; Osiecka et al., 2009; Scott-McKean et al., 2016), we argue that the higher levels of these cytoskeletal proteins (tubulin isoforms and microtubule-associated proteins) persists due to the high levels of HDPs.

4.6.4 Chaperones

Chaperones are involved in various cellular activities regarding the preservation of the three-dimensional conformation of proteins, by ensuring their correct folding,

preventing their misfolding in the first place, and/or by refolding the misfolded proteins. These general functions are shared by all the chaperones (Mayer, 2013; Radons, 2016). Some specific activities include regulating parkin protein translocation to the mitochondria (Hasson et al., 2013), scaffolding for the spliceosomes and inflammatory signaling (Triantafilou, Triantafilou, & Dedrick, 2001; Yahata et al., 2000). In the presence of Aβ oligomers, chaperones molecules, including HSP70, clusterin (Clu) and α_2-macroglobin (α_2M), are reported to accumulate in areas of oligomerization to prevent the spread of toxic oligomers (Mannini et al., 2012). Clu and α_2M are also reported to inhibit the permeation of α-syn oligomers through the lipid membranes (Whiten et al., 2018). The higher abundance of chaperones and associated proteins in rpAD HDFs indicates a possible positive feedback mechanism, to overcome the protein misfolding in rpAD high-density fractions. Most probably, the reduction in the chaperones in sCJD is suggestive of an increase in the protein misfolding extent in sCJD cases.

4.7 Interactors of high-density prion (HDP) oligomers

Diverse sets of prion protein interactors were identified from subtype-specific HDFs. A lower count of rpAD-specific HDP interactors was identified in comparison to that of sCJD. The sCJD tissues exhibit a wide spectrum of PrP/PrP^{Sc} oligomers, as previously reported (Cracco et al., 2017; C. Kim et al., 2011, 2012), compared to that of rpAD (Zafar, Shafiq, et al., 2017). This diversity of PrP/PrP^{Sc} oligomers in the sCJD pathology can be a potential reason for the relatively diverse interactome in sCJD PrP oligomers. There was no overlap of HDP interactors of rpAD to either spAD or control samples, assuring the subtype-specific occurrence of the PrP species in rpAD. Common interactors between the rpAD and sCJD datasets suggest the presence of common PrP oligomers. Proteins interacting with the prion oligomers in rpAD included calcium/calmodulin-dependent protein kinase type II subunit beta and delta, mammalian ependymin-related protein 1, GTP-binding protein Di-Ras2, GAS2-like protein 2, and 14-3-3 protein. All the interactors, except the GAS2-like protein, were part of the HDP interactomes in rpAD and those of sCJD. Calcium/calmodulin-dependent protein kinase type II regulates Ca^{2+} mediated effects in neurons, it is also responsible for the actin reorganization in bundles leading to the development of the dendritic spines (Stephenson et al., 2017). GTP-binding Di-Ras2 is a Ras GTPase and has been reported to be involved in cell morphogenesis. G2L2 has been reported to play a role in actin-tubulin communication (Goriounov, 2003). The protein 14-3-3 sigma is a diverse

protein with many known interactions, and is involved in p53, protein kinase C, and AKT/mTOR signaling (Yang, Dicker, Chen, & El-Deiry, 2008). There is strong evidence in the literature for the involvement of 14-3-3 isoforms in various neurodegenerative diseases particularly prion dementias and Alzheimer's disease, where 14-3-3 isoforms are found associated with PrP^{Sc} and Aβ plaques (Richard et al., 2003; Jun-ichi Satoh et al., 2005; Wang et al., 2008). Physiological outcomes of novel interactions of these proteins with the PrP oligomers have yet to be described. Thus, it may be justified to include G2L2 for further investigation, particularly for its role in actin-tubulin intercommunication.

4.7.1 G2L2 and cytoskeletal machinery

Actin and tubulin interlinking and communication is necessary for the proper function of the cellular transport system, morphogenesis, repair and many other related functions in the cells. Actin-tubulin communication is mainly controlled by the spectraplakins, via their ability to bind actin and tubulin, as well as multiple spectrin and plakin domains (Suozzi, Wu, & Fuchs, 2012). Many diseases have been related to the malfunction of spectraplakins (Sonnenberg & Liem, 2007). Likewise, the family of growth arrest-specific (GAS) proteins and growth arrest-specific like (GASL) proteins have been connected to the same function of actin-tubulin linking, but the functional orchestration has not been well established (Goriounov, 2003). Other than cytoskeletal maintenance, GAS proteins also play a role in apoptosis and inhibition of cell division (Brancolini, Benedetti, & Schneider, 1995; Brancolini & Schneider, 1994). Surprisingly, a mutation in the G2L2 protein is reported to enhance the chances of Alzheimer development (Jian et al., 2016). A comprehensive experimental account on the GAS and GASL proteins was provided by Stroud and coworkers (2014), proposing a model where growth-specific like 1 (G2L1) and growth-specific like 2 (G2L2) are suggested to control microtubular stability via attachment to end-binding protein-1 (EB-1). The interaction of the G2L2 and EB-1 to the tubulin is also reported to account for the stability of the microtubules (Stroud et al., 2014).

In our study, we described a subtype-specific colocalization of PrP oligomers to G2L2 in rapidly progressive Alzheimer's disease. Correspondingly, we found a decrease in G2L2 and EB-1 colocalization. We considered that the HDPs specifically found in the

rpAD possess a tendency to recruit and bind G2L2. This HDP-G2L2 interaction is negatively correlated to G2L2 and EB-1 binding.

Hence, the disturbance in the G2L2/EB-1/tubulin systems leads to a malfunction in actin-assisted microtubule growth in the neurons. The shortening in the actin-tubulin colocalization fibers specifically noted in frontal cortices of rpAD patients can also be an outcome of the disturbance of G2L2/EB-1/tubulin. A putative mechanism of HDP oligomers interacting with the cytoskeletal system is shown in Figure 49.

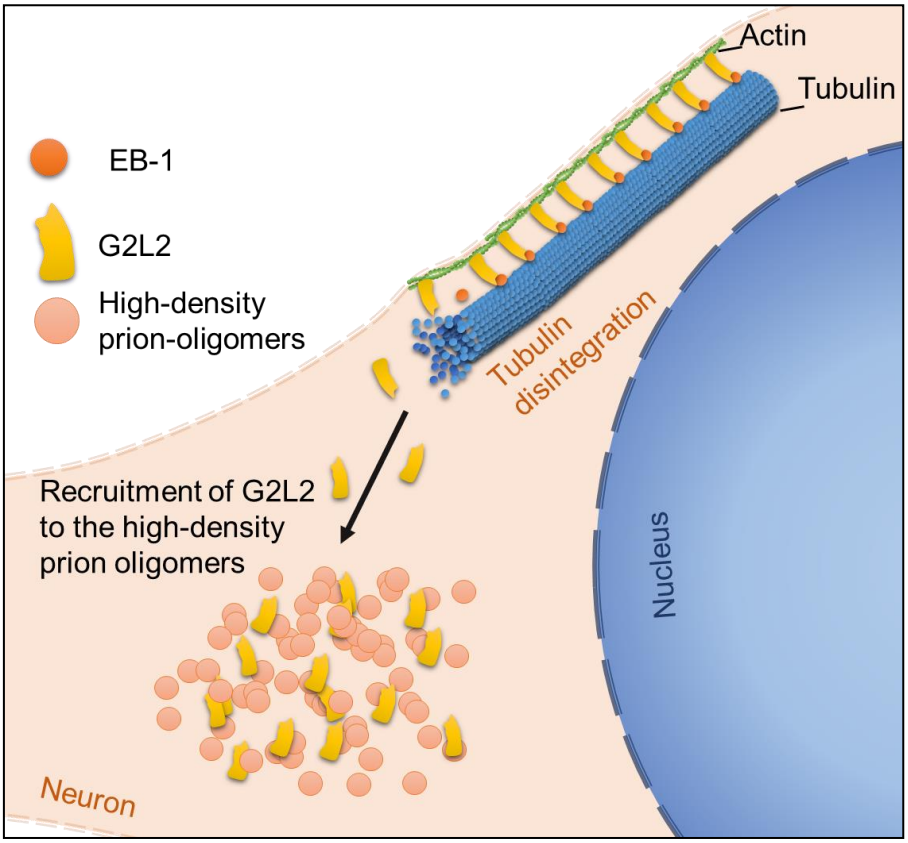

Figure 49: Recruitment of G2L2 to the high-density prion-oligomers. The recruitment of G2L2 towards the HDPs results in the loss of its binding to EB-1, affecting the actin-guided microtubule (MT) integrity.

Considering the extreme size of neurons, there is need of a robust transport system in the neuron to build up a connection between the cell body and neural processes, for various types of neuronal cargo including organelles, vesicles, cell signaling molecules, RNA molecules, neurotransmitter receptors, and adhesion molecules (Hirokawa, Niwa, & Tanaka, 2010; Maday, Twelvetrees, Moughamian, & Holzbaur, 2014). The actin-guided MT growth also imparts a critical role to the structural stability of neurons including kinesin-based axon differentiation/polarization (Hirokawa et al., 2010; Hoogenraad & Bradke, 2009; Maday et al., 2014), MAPs-assisted axon growth

(Dent, Gupton, & Gertler, 2011; Prokop, 2013), and finally the morphodynamics of dendritic spines (Hirokawa et al., 2010; Hoogenraad & Bradke, 2009; Maday et al., 2014). With any malfunctioning in the MT system, neurons suffer from a variety of degenerative events.

4.8 Conclusion

Results of our study have helped in defining multiple pathological layers that contribute to the variation of progression rates in Alzheimer's disease. Based on our results, we can state that the dysregulation of PrP^C glycosylation and extracellular shedding leads to a reduction in Aβ sequestering, a phenomenon keeping check on the extension of Aβ spread. The binding of PrP to ZAG in rpAD (as indicated by interactomics) also indicates the number of PrP molecules available for Aβ sequestering. Likewise, histone H2B2 and PrP interaction and nuclear localization of PrP point towards the pathological variations in PrP trafficking in rpAD. On the other hand, the presence of PrP oligomers and higher levels of high-density proteopathic proteins in rpAD compared to spAD, indicate landmark changes in protein degradation metabolism in neurons. Proteomic signature of high-density fractions obtained in velocity gradient centrifugation shows a higher degree of cytoskeletal damage associated with rpAD, together with a differential metabolism of ras-related proteins. Cytoskeletal damage was also highlighted by the rpAD-specific interaction of G2L2 with PrP oligomers (found in the interactome of HDFs). Finally, confocal laser scanning microscopy did not exclude the possibility that the interaction of HDPs with G2L2 results in the loss of G2L2 attachment to EB-1. This loss of G2L2 and EB-1 may interfere with actin-guided microtubular e growth, resulting in neuronal growth abnormalities specifically associated with rpAD. The outcomes of the study are summarized in the overview (Figure 50). HDP interaction with G2L2 and resulting cytoskeletal changes can be interesting for future investigations.

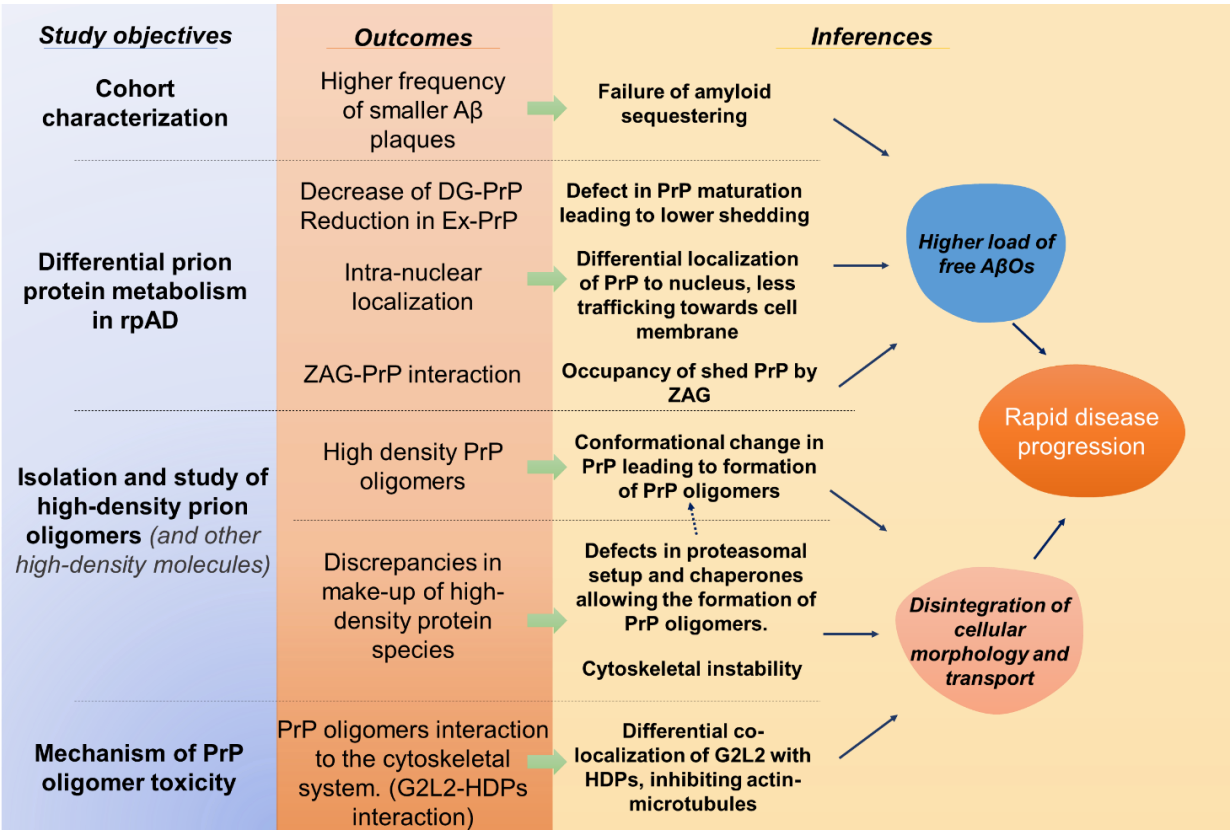

Figure 50: Overview of pathophysiology in rpAD resulting from our study. Rapid progression rate in the rpAD cases can be attributed to multiple homeostatic events. Changes in prion protein shedding, cellular distribution and presumably the occupancy by ZAG in extracellular space results in decreased Aβ-sequestration, hence increasing the extent of neurotoxicity. Conformational changes in prion protein result in the oligomerization of PrP in rpAD cases, resulting oligomers pose the threat of neurotoxicity by interfering with the cytoskeletal machinery of neurons and promoting the process of neurodegeneration.

5 Summary

Alzheimer's disease is the most commonly occurring dementia of the elderly, comprising up to 75% of all the neurodegenerative disorders. Alzheimer's disease (AD) typically exhibits a slow progression rate, resulting in an average disease span of eight years. Classically, AD exists predominantly as two subtypes, the first group are cases with spontaneous onset, namely sporadic cases; whereas the second group, the familial Alzheimer's disease (FAD), result due to mutations in presenilin 1, 2 and amyloid precursor protein (APP) genes. Over the past few decades, some atypical cases have been reported with a higher degree of pathological severity and rapid progression rates, i.e. with a decline of >6 MMSE points per year and a shorter post-diagnostic time (average of four years).

The present study was undertaken to identify and characterize the mechanisms involved in the progression rate variations in Alzheimer's disease subtypes, using human frontal cerebral cortex samples from rapidly progressive AD (rpAD), sporadic (spAD), sporadic Creutzfeldt Jakob disease (sCJD), dementia with Lewy bodies with typical (DLB) and rapid progression (rDLB), rapid progressive cases with vascular dementia (SVD) and dementia with frontotemporal lobar degeneration (DFTL). We have focused on multiple aspects associated with Alzheimer's disease including basic pathological alterations, signal transduction pathways involved in the neurodegenerative diseases, the metabolism of prion protein and biochemical and physiological characterization of the rpAD-unique PrP-oligomers.

Microscopic examination of pathological hallmarks revealed a decrease in amyloid plaque diameters, with a significantly higher frequency in cortices of rpAD patients compared to spAD. However, no significant differences were recognized in Tau tangles in the AD subtype. We could not identify any significant differences in amyloid-β and Tau/p-Tau expressions in rpAD- and spAD-subtypes.

Signal transduction pathways were assessed by expression analyses of a battery of kinases (and active forms) using immunoblot analysis and SWATH-MS-based quantification, and a slight increase in the CaMKII subunit gamma was observed in spAD in comparison to both controls and rapidly progressive cases of Alzheimer's disease.

Due to the involvement of prion protein in Aβ oligomer sequestering, we focused on the differential metabolism of prion protein (PrP) in Alzheimer's subtypes. A significant

decrease was noted in the di-glycosylated isoform of prion protein (DG-PrP) in rapid progressive AD cases, along with a decrease in the extracellular PrP levels. The reduction in the levels of both DG-PrP and extracellular PrP can be linked to the disturbance in the amyloid-sequestering activity of prion protein and a consequent higher load of free toxic oligomers. A higher PrP-nuclear localization was also observed in rpAD frontal cortex tissues that can be associated with a higher genotoxicity. In addition, we were able to observe subtype-specific differences among PrP interactomes, with histone-2 B2 and ZAG specifically interacting with prion protein in rpAD frontal cortices, suggesting the presence of differential prion variants in Alzheimer subtypes.

High-density variants of prion proteins (HDP) were uniquely observed in the rpAD frontal cortices. No PK-resistance and PrP-seeding activity could be observed from the identified HDPs. We could identify a rpAD-specific differential higher load of proteopathic proteins, disturbances in the protein degradation machinery, cytoskeletal disfigurations, relative abundance of chaperones and differential metabolism of Ras-related proteins (utilizing high-resolution mass spectrometry analysis of high-density fractions and SWATH-MS-based global proteomics).

From the co-immunoprecipitation of high-density prion oligomers, we identified a rpAD-unique interactor, GAS2-like protein 2 (G2L2), together with the interactors commonly found among rpAD and sCJD high-density prion interactors, including calcium/calmodulin-dependent protein kinase type II subunits beta and delta, mammalian ependymin-related protein 1, GTP-binding protein Di-Ras2 and 14-3-3 protein sigma. Due to involvement in actin-tubulin dynamics, and its unique interaction with rpAD high-density prion oligomers, GAS2-like protein 2 was further studied along with associated proteins. The G2L2 serves as a linker protein between the tubulin bundles and actin filaments to stabilize the microtubules via attachment to end binding protein-1. A significantly more pronounced colocalization of G2L2 and PrP was seen in the frontal cortex tissues of rapidly progressive AD cases, with an associated decrease in the colocalization of G2L2 and end binding protein-1 (EB-1). A decrease in the actin-β and tubulin-α co-localization was also noted in frontal cortex tissues of AD cases with rapid progression.

Based on the results, we confirm that prion protein metabolism plays an important role in the progression rate of Alzheimer’s disease. The dysregulation of PrP maturation

leads to impairment of oligomer sequestration. Formation of PrP oligomers and their downstream intervention with cell signaling and cytoskeletal organization promotes the faster progression in rapidly progressive Alzheimer' disease cases. Furthermore, the interaction of G2L2 with PrP oligomers targets the actin-tubulin stability and actin-directed microtubular growth and can be considered an interesting target for future studies.

6 Annexure

Table 14: Patient details of non-demented controls, Alzheimer's disease and dementia with Lewy bodies cohorts.

No.	Patient ID	Gender	Age	Disease duration(y)	Braak stages (AD)	Post-mortem Interval (h)
1	rpAD1	Male	70	<4	VI/C	11:30
2	rpAD2	Male	76	<4	VI/C	6:30
3	rpAD3	Female	76	<4	VI/C	18:00
4	rpAD4	Female	77	<4	IV/A	12:00
5	rpAD5	Male	78	<4	V/C	3:30
6	rpAD6	Female	79	<4	V	5:30
7	rpAD7	Female	81	<4	III/B	6:00
8	rpAD8	Male	83	<4	VI/C	5:30
9	rpAD9	Male	83	<4	V/C	8:20
10	spAD1	Female	56	>4	V/C	7:00
11	spAD2	Male	64	>4	II/A	6:00
12	spAD3	Female	67	>4	III/C	6:10
13	spAD4	Male	69	>4	III/0	13:10
14	spAD5	Female	71	>4	III/0	7:15
15	spAD6	Female	72	>4	V/C	9:30
16	spAD7	Female	75	>4	V/C	4:15
17	spAD8	Male	78	>4	V/C	9:30
18	spAD9	Female	82	>4	VI/B	1:45
19	spAD10	Male	83	>4	III/0	7:25
20	spAD11	Male	87	>4	V/C	7:05
21	spAD12	Female	90	>4	IV/A	9:55
22	spAD13	Female	93	>4	V/C	3:00
23	DLB1	Female	71	>4	II	5:03
24	DLB2	Female	87	>4	-	5:00
25	DLB3	Male	76	>4	III	9:00
26	DLB4	Male	71	>4	-	5:03
27	DLB5	Female	87	>4	II	11:00
28	DLB6	Male	83	>4	II	6:45
29	DLB7	Male	80	>4	III	4:03
30	DLB8	Female	76	>4	III	9:00
31	DLB9	Male	73	>4	I	3:03
32	DLB10	Female	80	>4	II	11:00
33	DLB11	Female	71	>4	III	4:00
34	Cont 1	Male	69	–	II/A	5:03
35	Cont 2	Male	68	–	I/0	5:03
36	Cont 3	Female	64	–	I/0	9:00
37	Cont 4	Male	67	–	I/0	5:03
38	Cont 5	Male	74	–	II/A	11:00
39	Cont 6	Male	86	–	II/A	6:45
40	Cont 7	Female	73	–	I/0	4:03
41	Cont 8	Male	70	–	I/A	9:00
42	Cont 9	Male	61	–	I/0	3:03
43	Cont 10	Male	77	–	I/A	11:00

Table 15: List of samples exhibiting a rapid neurodegeneration, but pathologically different in comparison to Alzheimer's disease samples.

No.	Patient ID	Gender	Age	Disease duration (y)	Diagnosis	Post-mortem Interval (h)
1	rDLB1	Male	57	<4	DLB	14:00
2	rDLB2	Male	65	<4	DLB + PSP some features	16:00
3	rDLB3	Male	69	<4	DLB+ AGD +PSP + Tauopathy	18:00
4	rDLB4	Male	71	<4	DLB Neocortical	5:00
5	rDLB5	Female	75	<4	DLB neocortical + ADIII	13:30
6	rDLB6	Male	76	<4	DLB neocortical + AD VIC	6:30
7	DFTL1	Female	73	<4	DFTL + Motor Neuron Disease + TDP-43	5:00
8	DFTL2	Female	85	<4	AD V + DLFT + TDP-43 +MND	9:00
9	DFTL3	Female	86	<4	DFTL + TDP-43 + Motor Neuron Disease	3:00
10	SVD1	Female	81	<4	SVD + AD III B	6:00
11	SVD2	Female	85	<4	SVD + AD IV + Hippocampal Sclerosis	6:00
12	SVD3	Male	78	<4	SVD + AD V (INCIP) B/C	3:30

Table 16: **Patient details of Creutzfeldt-Jakob disease cohort.**

No.	ID	Gender	Age	Disease duration (y)	Genotype	Post-mortem Interval (h)
1	sCJD (MM1)1	Male	65	<1	MM/MV1	9:45
2	sCJD (MM1)2	Female	74	<1	MM/MV1	7:50
3	sCJD (MM1)3	Male	61	<1	MM/MV1	7:00
4	sCJD (MM1)4	Female	66	<1	MM/MV1	5:05
5	sCJD (MM1)5	Female	74	<1	MM/MV1	11:00
6	sCJD (MM1)6	Male	74	<1	MM/MV1	4:50
7	sCJD (MM1)7	Male	75	<1	MM1	9:00
8	sCJD (MM1)8	Female	66	<1	MM1	7:00
9	sCJD (MM2)1	Male	62	<1	MM/MV1+2	11:30
10	sCJD (MM2)2	Female	84	<1	MM/MV2C	12:00
11	sCJD (MM2)3	Male	67	<1	MM2 C	9:00
12	sCJD (MM2)4	Female	58	<1	MV2	10:30
13	sCJD (MM2)5	Male	50	<1	CJD (NO SUBTYPING)	6:00
14	sCJD (VV2)1	Male	56	<1	VV2	7:30
15	sCJD (VV2)2	Male	66	<1	VV2	15:30
16	sCJD (VV2)3	Female	70	<1	VV2	11:00
17	sCJD (VV2)4	Female	72	<1	VV2	6:00
18	sCJD (VV2)5	Female	66	<1	VV2	4:00

6.1 Interacting partners of high-density prion (HDP) oligomers

Table 17: Subtype-specific interactors of HDPs from density variable fraction pools of controls, rpAD, spAD and sCJD variants.

	High Density Fractions					
	F12	***F13***	***F14***	***F15***	***F16***	***F17***
Con	CATD	PKP1		CTNB1		PCLO
	SHRM3	CTNB1				CTNB1
		SHRM3				PGBM
		LAMP1				CO4A2
						ITIH2
spAD	TPIS	ACON	ZGPAT	IDHP	ACON	TITIN
	ACON	PKP1	ACON			TPIS
	PCLO	CTNB1	CTNB1			MYPC3
	PIGR	CALL5	PKP1			PFKAP
	FKAP	GGCT	TITIN			MPCP
	LCN1	IDHP	IDHP			ACON
	DMBT1	LCN1	TPIS			GTR1
	MPCP	DMBT1	GGCT			MYH10
	GTR1	MPCP	GTR1			ENOB
	MUC5A	CYTM	PCLO			IDHP
	ELNE	MYH16	CATD			ALDOC
	SG1D1		MDHM			PCLO
	TRFE		CALL5			ENPL
	MUC5B		PFKAP			MDHC
	CAP7		G6PI			MYL3
	SG2A1		MPCP			ANXA6
	PERM					MYL4
						ATP6
						VINC
						ATPO
rpAD	KCC2B	DIRA2		DIRA2	PKP1	1433S
	KCC2D	PKP1			GA2L2	
	EPDR1					
MM1	FRIH	SLPI	EPDR1	PPT1	SYN1	SYN1
	ASAH1	LCN1	PPT1	CATD	SYN2	SYN2
	CATD	TPP1	TPP1	EPDR1	CALL5	PACN1
	TPP1	PPT1	FRIH		COF1	COF1
	CO1A2	FRIH	CATD		EPDR1	STMN1
	SYN1	DMBT1	ASAH1		CATD	CRYM
	PKP1	EPDR1			LCN1	NSF
	A4	KCC2B			COF2	COF2
		KCC2G			PPT1	TPIS
		PCLO			A4	IDH3A

	F12	*F13*	*F14*	*F15*	*F16*	*F17*
		PKP1				A4
		ASAH1				ENPL
		DHX15				PROF2
						NFL
						CBR1
						KCC2B
						KCC2D
						KCC2G
						GRP75
						TPPP
						TCPQ
						MDHM
						1433E
						HNRPK
	1433E	PKP1	PIGR	PPT1	SYN1	SYN1
	COF1	EPDR1	BPIB1	CATD	SYN2	NSF
	ENPL	TPP1	SYN1	EPDR1	NSF	SYN2
	MDHC	CALL5	SYN2		PACN1	PACN1
	CH10	CATD	EPDR1		CRYM	CRYM
	IDHP	ACON	PPT1		KCC2B	KCC2B
	MYL3	PPT1	CATD		KCC2G	KCC2D
	PROF1	SYN1	TPP1		COF1	KCC2G
	SERPH	FRIH	GGCT		COF2	COF1
	COF2	CTNB1	SYPL1		IDH3A	TPIS
	DEST	KLK7	SLPI		KCC2D	TPPP
	ENOB				TPP1	COF2
	PRDX6				SEPT3	COR1A
	EZRI				ACON	SEPT3
	MOES				PCLO	CISY
	RADI				EPDR1	ACON
	ANXA5				PKP1	UCHL1
	SET				CATD	STX1B
	GSTP1				PHF24	IDH3A
	FABPH				SUCB1	PHF24
	HSPB7					MDHM
	ACON					A4
	PFKAP					PRIO
	RAN					NFL
	PDIA3					CNRP1
	KCRM					GRP75
	TPIS					CATD
	IDH3A					LEG1
	FRIH					SCRN1
MV	MDHM					PROF2

	F12	*F13*	*F14*	*F15*	*F16*	*F17*
	ANXA6					UBA1
	G6PI					AINX
	GDIB					PRDX5
	CALX					GDIR1
	CALR					GBB5
	PGM1					TPP1
	CISY					EFTU
	GRP75					ARF4
	PPT1					RAC1
	CATD					CDC42
	MYL4					RTN1
	AN32A					TBCB
	AATC					
	CALU					
	KLC1					
	PKP1					
	TPP1					
	CTNB1					
	GDIR1					
	CALL5					
	ALDH2					
	LIS1					
	UGPA					
	ARP2					
	CAPZB					
	FUMH					
	RS3					
	PDK1					
	RS19					
	MYL9					
	NP1L4					
	RET1					
	ALDOB	PPT1	EPDR1	SYN1	SYN1	SYN1
	FRIH		FRIH	PRIO	SYN2	CRYM
	EPDR1		CATD	SYN2	PRIO	SYN2
	PPT1		TPP1	PCLO	NSF	NSF
	CTNB1		SYN1	COF1	CRYM	PRIO
	CATD		PPT1	COF2	KCC2B	PACN1
			CTNB1	EPDR1	COF1	COF1
			WWC3	PPT1	TPIS	TPIS
				PKP1	SCRN1	SCRN1
				TIF1B	COF2	COF2
					UBA1	ALDOC
VV2					PROF2	PROF2

	F12	*F13*	*F14*	*F15*	*F16*	*F17*
					SEPT3	NFL
					KCC2D	CBR1
					KCC2G	KCC2B
					PACN1	UBA1
					COR1A	COR1A
					AINX	AINX
					CISY	STX1B
					IDH3A	SEPT3
					ACON	NFM
					GRP75	SEPT9
					NFL	CISY
					STX1B	IDH3A
					SEPT9	PA1B3
					PA1B3	CNRP1
					TPPP	DEST
					PRDX5	DIRA2
					TCPQ	GDIA
					PSD3	AT1B1
					DHPR	

Table 18: List of subtype-specific HDP interactors from spAD, rpAD and sCJD.

IDs	Uniprot Acc. No.	Protein name	Prion protein interaction	Disease Relevance
1433E	P62258	14-3-3 protein epsilon	Novel	Parkinson's disease (Yacoubian et al., 2010), Alzheimer's disease, Creutzfeldt Jakob disease (Llorens et al., 2017), Epilepsy (Schindler et al., 2006)
1433S	P31947	14-3-3 protein sigma	Novel	
A4	P05067	Amyloid beta A4 protein	Known (Smith & Strittmatter, 2017)	Alzheimer disease (Querfurth & LaFerla, 2010)
AATC	P17174	Aspartate aminotransferase, cytoplasmic	Novel	
ACON	Q99798	Aconitate hydratase, mitochondrial	Novel	Infantile cerebellar-retinal degeneration (Spiegel et al., 2012)
AINX	Q16352	Alpha-internexin	Novel	
ALDH2	P05091	Aldehyde dehydrogenase, mitochondrial	Novel	
ALDOB	P05062	Fructose-bisphosphate aldolase B	Known (Zafar et al., 2011)	
ALDOC	P09972	Fructose-bisphosphate aldolase C	Novel	

IDs	Uniprot Acc. No.	Protein name	Prion protein interaction	Disease Relevance
AMPL	P28838	Cytosol aminopeptidase	Novel	
AN32A	P39687	Acidic leucine-rich nuclear phosphoprotein 32 family member A	Novel	
ANXA5	P08758	Annexin A5	Known (Zafar et al., 2011)	Recurrent Pregnancy loss, , 3 (Bogdanova et al., 2007)
ANXA6	P08133	Annexin A6	Novel	
ARF4	P18085	ADP-ribosylation factor 4	Novel	
ARP2	P61160	Actin-related protein 2	Novel	
ASAH1	Q13510	Acid ceramidase	Novel	Farber lipogranulomatosis (Muramatsu et al., 2002), Alzheimer's disease (Huang et al., 2004)
AT1B1	P05026	Sodium/potassium-transporting ATPase subunit beta-1	Novel	
ATP6	P00846	ATP synthase subunit a	Novel	Neuropathy, ataxia, and retinitis pigmentosa (Cha et al., 2015)
ATPO	P48047	ATP synthase subunit O, mitochondrial	Novel	
BPIB1	Q8TDL5	BPI fold-containing family B member 1	Novel	
CALL5	Q9NZT1	Calmodulin-like protein 5	Novel	
CALR	P27797	Calreticulin	Novel	Alzheimer's disease (Lin, Cao, & Gao, 2014)
CALU	O43852	Calumenin	Novel	
CALX	P27824	Calnexin	Known (W. Wang et al., 2010)	
CAP7	P20160	Azurocidin	Novel	
CAPZB	P47756	F-actin-capping protein subunit beta	Novel	
CATD	P07339	Cathepsin D	Novel	Creutzfeldt-Jakob-disease (Kovacs et al., 2010)
CBR1	P16152	Carbonyl reductase [NADPH] 1	Novel	
CDC42	P60953	Cell division control protein 42 homolog	Novel	Takenouchi-Kosaki syndrome (Takenouchi, Kosaki, Niizuma, Hata, & Kosaki, 2015)
CH10	P61604	10 kDa heat shock protein, mitochondrial	Novel	
CISY	O75390	Citrate synthase, mitochondrial	Novel	
CNRP1	Q96F85	CB1 cannabinoid receptor-interacting protein 1	Novel	
CO1A2	P08123	Collagen alpha-2(I) chain	Novel	Ehlers-Danlos syndrome 7B (Weil, D'Alessio, Ramirez, & Eyre, 1990)
CO4A2	P08572	Collagen alpha-2(IV) chain	Novel	Stroke (Jeanne et al., 2012)

IDs	Uniprot Acc. No.	Protein name	Prion protein interaction	Disease Relevance
COF1	P23528	Cofilin-1	Known (Zafar et al., 2011)	Creutzfeldt-Jakob-disease (Zafar, Younas, et al., 2017)
COF2	Q9Y281	Cofilin-2	Novel	
COPZ1	P61923	Coatomer subunit zeta-1	Novel	
COR1A	P31146	Coronin-1A	Novel	
CRYM	Q14894	Ketimine reductase mu-crystallin	Novel	Autosomal dominant, 40 deafness (Abe et al., 2003)
CTNB1	P35222	Catenin beta-1	Novel	Colorectal cancer (Abe et al., 2003)
CYTM	Q15828	Cystatin-M	Novel	Parkinsonism and Alzheimer's disease (Ii, Ito, Kominami, & Hirano, 1993)
DEST	P60981	Destrin	Novel	
DHPR	P09417	Dihydropteridine reductase	Novel	Hyperphenylalaninemia associated with neurological disorders (Dianzani et al., 1993)
DHX15	O43143	Pre-mRNA-splicing factor ATP-dependent RNA helicase DHX15	Novel	
DIRA2	Q96HU8	GTP-binding protein Di-Ras2	Novel	
DMBT1	Q9UGM3	Deleted in malignant brain tumors 1 protein	Novel	Glioma (Takito et al., 1999)
EFTU	P49411	Elongation factor Tu, mitochondrial	Novel	Combined oxidative phosphorylation deficiency 4 (Valente et al., 2007)
ELNE	P08246	Neutrophil elastase	Novel	Cyclic haematopoiesis (Horwitz, Benson, Person, Aprikyan, & Dale, 1999)
ENOB	P13929	Beta-enolase	Novel	Glycogen storage disease 13 (Comi et al., 2001)
ENPL	P14625	Endoplasmin	Novel	
EPDR1	Q9UM22	Mammalian ependymin-related protein 1	Novel	
EZRI	P15311	Ezrin	Novel	
FRIH	P02794	Ferritin heavy chain	Known (Comi et al., 2001)	Creutzfeldt-Jakob-disease (Comi et al., 2001)
FUMH	P07954	Fumarate hydratase, mitochondrial	Novel	
G6PI	P06744	Glucose-6-phosphate isomerase	Novel	Hemolytic anemia, non-spherocytic, due to glucose phosphate isomerase deficiency (Comi et al., 2001)
G2L2	Q8NHY3	GAS2-like protein 2	Novel	

IDs	Uniprot Acc. No.	Protein name	Prion protein interaction	Disease Relevance
GBB5	O14775	Guanine nucleotide-binding protein subunit beta-5	Novel	Intellectual developmental disorder with cardiac arrhythmia (Comi et al., 2001)
GDIA	P31150	Rab GDP dissociation inhibitor alpha	Novel	Creutzfeldt-Jakob-disease (Gawinecka et al., 2012)
GDIB	P50395	Rab GDP dissociation inhibitor beta	Novel	
GDIR1	P52565	Rho GDP-dissociation inhibitor 1	Novel	Nephrotic syndrome 8 (NPHS8)
GGCT	O75223	Gamma-glutamylcyclotransferase	Novel	
GRP75	P38646	Stress-70 protein, mitochondrial	Novel	Anemia, sideroblastic, 4 (Schmitz-Abe et al., 2015)
GSTP1	P09211	Glutathione S-transferase P	Novel	
GTR1	P11166	Solute carrier family 2, facilitated glucose transporter member 1	Novel	Creutzfeldt-Jakob-disease (Gawinecka et al., 2012)
HNRPK	P61978	Heterogeneous nuclear ribonucleoprotein K	Novel	Au-Kline syndrome (Au et al., 2015)
HSPB7	Q9UBY9	Heat shock protein beta-7	Novel	
IDH3A	P50213	Isocitrate dehydrogenase [NAD] subunit alpha, mitochondrial	Novel	Alzheimer's disease (Bubber et al., 2005)
IDHP	P48735	Isocitrate dehydrogenase [NADP], mitochondrial	Novel	Alzheimer's disease (Bubber et al., 2005)
ITIH2	P19823	Inter-alpha-trypsin inhibitor heavy chain H2	Novel	
KCC2B	Q13554	Calcium/calmodulin-dependent protein kinase type II subunit beta	Novel	
KCC2D	Q13557	Calcium/calmodulin-dependent protein kinase type II subunit delta	Novel	
KCC2G	Q13555	Calcium/calmodulin-dependent protein kinase type II subunit gamma	Novel	Alzheimer's disease (Bubber et al., 2005)
KCRM	P06732	Creatine kinase M-type	Novel	
KLC1	Q07866	Kinesin light chain 1	Novel	
KLK7	P49862	Kallikrein-7	Novel	
LAMP1	P11279	Lysosome-associated membrane glycoprotein 1	Novel	
LCN1	P31025	Lipocalin-1	Novel	
LEG1	P09382	Galectin-1	Novel	
LEG3	P17931	Galectin-3	Known (Bubber et al., 2005)	
LIS1	P43034	Platelet-activating factor acetylhydrolase IB subunit alpha	Novel	Lissencephaly 1 (Bubber et al., 2005)
LYG2	Q86SG7	Lysozyme g-like protein 2	Novel	
MDHC	P40925	Malate dehydrogenase, cytoplasmic	Novel	

IDs	Uniprot Acc. No.	Protein name	Prion protein interaction	Disease Relevance
MDHM	P40926	Malate dehydrogenase, mitochondrial	Known (Zafar et al., 2011)	Creutzfeldt-Jakob-disease (Gawinecka et al., 2013)
MIF	P14174	Macrophage migration inhibitory factor	Novel	
MOES	P26038	Moesin	Novel	
MPCP	Q00325	Phosphate carrier protein, mitochondrial	Novel	
MUC5A	P98088	Mucin-5AC	Novel	
MUC5B	Q9HC84	Mucin-5B	Novel	
MYH10	P35580	Myosin-10	Novel	Associated with severe intellectual disability, microcephaly, and feeding difficulties as well as cerebral atrophy (Hamdan et al., 2014)
MYH16	Q9H6N6	Putative uncharacterized protein MYH16	Novel	
MYL3	P08590	Myosin light chain 3	Known	Creutzfeldt-Jakob-disease (Zafar et al., 2015)
MYL4	P12829	Myosin light chain 4	Novel	
MYL9	P24844	Myosin regulatory light polypeptide 9	Novel	
MYPC3	Q14896	Myosin-binding protein C, cardiac-type	Novel	
NDKB	P22392	Nucleoside diphosphate kinase B	Novel	
NFL	P07196	Neurofilament light polypeptide	Novel	Prion diseases (Inga Zerr et al., 2018), familial Alzheimer's disease (Weston et al., 2017)
NFM	P07197	Neurofilament medium polypeptide	Novel	Neurofilamentopathy (Weston et al., 2017)
NP1L4	Q99733	Nucleosome assembly protein 1-like 4	Novel	
NSF	P46459	Vesicle-fusing ATPase	Novel	
PA1B3	Q15102	Platelet-activating factor acetylhydrolase IB subunit gamma	Novel	
PACN1	Q9BY11	Protein kinase C and casein kinase substrate in neurons protein 1	Novel	
PCLO	Q9Y6V0	Protein piccolo	Novel	
PDIA3	P30101	Protein disulfide-isomerase A3	Novel	Prion disease (Weston et al., 2017)f
PDK1	Q15118	[Pyruvate dehydrogenase (acetyl-transferring)] kinase isozyme 1, mitochondrial	Novel	
PERM	P05164	Myeloperoxidase	Novel	
PFKAP	Q01813	ATP-dependent 6-phosphofructokinase, platelet type	Novel	

IDs	Uniprot Acc. No.	Protein name	Prion protein interaction	Disease Relevance
PGBM	P98160	Basement membrane-specific heparan sulfate proteoglycan core protein	Novel	
PGM1	P36871	Phosphoglucomutase-1	Novel	
PHF24	Q9UPV7	PHD finger protein 24	Novel	
PIGR	P01833	Polymeric immunoglobulin receptor	Novel	
PKP1	Q13835	Plakophilin-1	Novel	
PPT1	P50897	Palmitoyl-protein thioesterase 1	Novel	Ceroid lipofuscinosis, neuronal, 1 (CLN1)
PRDX5	P30044	Peroxiredoxin-5, mitochondrial	Novel	
PRDX6	P30041	Peroxiredoxin-6	Novel	Prion disease (Weston et al., 2017)
PRIO	P04156	Major prion protein	Known (Linden et al., 2008)	(Glatzel, Stoeck, Seeger, Lührs, & Aguzzi, 2005) Prion spongiform encephalopathies in human and animals
PROF1	P07737	Profilin-1	Novel	Amyotrophic lateral sclerosis 18 (Wu et al., 2012)
PROF2	P35080	Profilin-2	Novel	Creutzfeldt-Jakob-disease (Gawinecka et al., 2013)
PSD3	Q9NYI0	PH and SEC7 domain-containing protein 3	Novel	
RAC1	P63000	Ras-related C3 botulinum toxin substrate 1	Novel	
RADI	P35241	Radixin	Novel	
RAN	P62826	GTP-binding nuclear protein Ran	Novel	
RET1	P09455	Retinol-binding protein 1	Novel	
RS19	P39019	40S ribosomal protein S19	Novel	
RS3	P23396	40S ribosomal protein S3	Novel	
RSSA	P08865	40S ribosomal protein SA	Novel	
RTN1	Q16799	Reticulon-1	Novel	
S10A3	P33764	Protein S100-A3	Novel	
SCRN1	Q12765	Secernin-1	Novel	
SEPT3	Q9UH03	Neuronal-specific septin-3	Novel	
SEPT9	Q9UHD8	Septin-9	Novel	
SERPH	P50454	Serpin H1	Novel	
SET	Q01105	Protein SET	Novel	
SG1D1	O95968	Secretoglobin family 1D member 1	Novel	
SG2A1	O75556	Mammaglobin-B	Novel	
SHRM3	Q8TF72	Protein Shroom3	Novel	
SLPI	P03973	Antileukoproteinase	Novel	

IDs	Uniprot Acc. No.	Protein name	Prion protein interaction	Disease Relevance
STMN1	P16949	Stathmin	Novel	
STX1B	P61266	Syntaxin-1B	Novel	Generalized epilepsy with febrile seizures plus 9 (Schubert et al., 2014)
SUCB1	Q9P2R7	SuccinateCoA ligase [ADP-forming] subunit beta, mitochondrial	Novel	
SYN1	P17600	Synapsin-1	Known (Zafar, Shafiq, et al., 2017)	Epilepsy X-linked, with variable learning disabilities and behavior disorders (Schubert et al., 2014)
SYN2	Q92777	Synapsin-2	Novel	Schizophrenia (Schubert et al., 2014)
SYPL1	Q16563	Synaptophysin-like protein 1	Novel	
TBCB	Q99426	Tubulin-folding cofactor B	Novel	
TCPQ	P50990	T-complex protein 1 subunit theta	Novel	
TIF1B	Q13263	Transcription intermediary factor 1-beta	Novel	
TITIN	Q8WZ42	Titin	Novel	
TPIS	P60174	Triosephosphate isomerase	Novel	
TPP1	O14773	Tripeptidyl-peptidase 1	Novel	Ceroid lipofuscinosis, neuronal, 2 (Schubert et al., 2014)
TPPP	O94811	Tubulin polymerization-promoting protein	Known (Schubert et al., 2014)	
TRFE	P02787	Serotransferrin	Novel	
TRXR1	Q16881	Thioredoxin reductase 1, cytoplasmic	Novel	
UBA1	P22314	Ubiquitin-like modifier-activating enzyme 1	Novel	
UCHL1	P09936	Ubiquitin carboxyl-terminal hydrolase isozyme L1	Novel	Parkinson disease (Leroy et al., 1998; Liu, Fallon, Lashuel, Liu, & Lansbury, 2002), Alzheimer's disease (Setsuie & Wada, 2007)
UGPA	Q16851	UTP-glucose-1-phosphate uridylyltransferase	Novel	
VINC	P18206	Vinculin	Novel	
VSIG8	Q5VU13	V-set and immunoglobulin domain-containing protein 8	Novel	
WWC3	Q9ULE0	Protein WWC3	Novel	
ZGPAT	Q8N5A5	Zinc finger CCCH-type with G patch domain-containing protein	Novel	

Certain HDP interactors were commonly present between the spAD-HDFs and sCJD-HDFs i.e. nine common interactors between CJD-MM1 and spAD HDFs, likewise, nineteen common interactors for CJD-MM2 HDPs and seven from that of sCJD-VV2 were also found in spAD-HDFs. The number of HDP-interactors for the sCJD-subtypes was higher compared to that of controls, spAD and rpAD and the degree of intergroup overlap between the HDP-interactors from sCJD subtypes was also the highest, presumably due to pathological similarities among the prion strains (Table 17 and Table 18). Aldolase C was commonly identified between HDPs of spAD and VV2. Catenin beta-1 and aconitase hydratase were commonly present between the spAD, VV2 and MM2 HDFs. Four proteins, namely protein piccolo, plakophilin-1, cathepsin D and triosephosphate isomerase were found commonly interacting with HDPs between the HDFs of spAD, CJD-MM1, CJD-VV2 and CJD-MM2 (Figure 51).

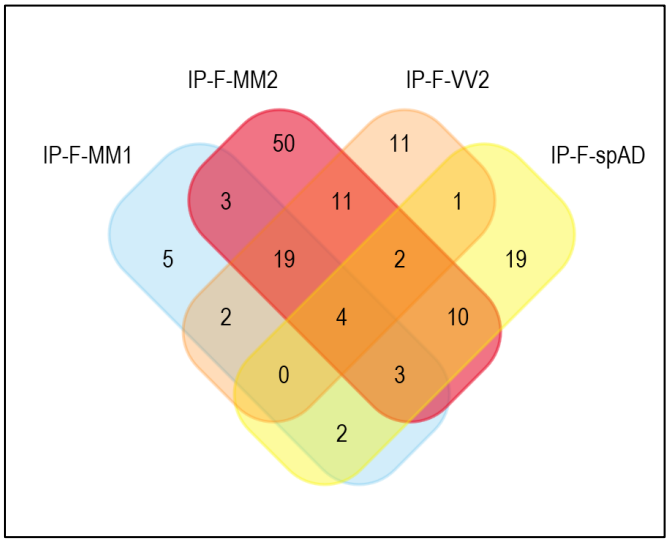

Figure 51: Venn diagram showing the degree of overlap of HDP-interactors from the high-density fractions of spAD and CJD-subtypes. IP-F-spAD: HDP interactors in spAD HDFs pools from 12-17, IP-F-MM1: HDP interactors in sCJD-MM1 HDFs pools from 12-17, IP-F-VV2: HDP interactors in sCJD-VV2 HDFs pools from 12-17IP-F-MM2: HDP interactors in sCJD-MM2 HDFs pools from 12-17.

Three proteins including calmodulin-like protein 5, endoplasmin and malate dehydrogenase, mitochondrial, were found in the HDFs of spAD, CJD-MM1 and CJD-MM2. Three HDP-interactors, antileukoproteinase, amyloid precursor proteins and 14-3-3E were found in the HDFs from sCJD-MM1 and sCJD-MM2 subtypes (Figure 51). The high density PrP interactors commonly expressed in all sCJD-subtypes are listed below together with their disease relevance, and corresponding HDFs (Table 19).

Table 19: High density PrP (HDP) interactors commonly found in the HDFs of sCJD-subtypes.

IDs	Uniprot. Acc. No.	Identified Proteins	Subcellular location	Prion protein-interaction	Involvement in disease	HDFs occurrence
TPP1	O14773	Tripeptidyl-peptidase 1	Ly	Novel	Ceroid lipofuscinosis, neuronal, 2 (Schubert et al., 2014)	sCJD-MM1:F12 toF14, sCJD-MM2:F12 toF14, F16, F17 sCJD-VV2:F14
FRIH	P02794	Ferritin heavy chain		Known (Comi et al., 2001)	Creutzfeldt-Jakob-disease (Comi et al., 2001)5	sCJD-MM1:F12 toF14, sCJD-MM2:F12, F13, sCJD-VV2:F12, F13
EPDR1	Q9UM22	Mammalian ependymin-related protein 1	S	Novel		sCJD-MM1:F13 to F16, sCJD-MM2:F13 toF16, F17, sCJD-VV2:F12, F14, F15
PPT1	P50897	Palmitoyl-protein thioesterase 1	Ly	Novel	Ceroid lipofuscinosis, neuronal, 1 (Vesa et al., 1995)	sCJD-MM1:F13 toF16, sCJD-MM2:F12 toF15, sCJD-VV2:F12
SYN1	P17600	Synapsin-1	Cj, Sy. Ga	Known (Zafar, Shafiq, et al., 2017)	Epilepsy X-linked, with variable learning disabilities and behavior disorders (Schubert et al., 2014)	sCJD-MM1:F12, F16, F17, sCJD-MM2:F13, F14, F16, F17, sCJD-VV2:F14 to F17
SYN2	Q92777	Synapsin-2	Cj, Sy.	Novel	Schizophrenia (Schubert et al., 2014)	sCJD-MM1:F16, F17 sCJD-MM2:F14, F16, F17 sCJD-VV2:F15 toF17
PACN1	Q9BY11	Protein kinase C and casein kinase substrate in neurons protein 1	Cy, Cp,Cj, Sy, Syo, Cp,	Novel		sCJD-MM1:F17 sCJD-MM2:F16, F17, sCJD-VV2:F15, F17
COF1	P23528	Cofilin-1	Nu, Cy, Ck, Cp	Known (Zafar et al., 2011)	Creutzfeldt-Jakob-disease (Zafar, Younas, et al., 2017)	sCJD-MM1:F16, F17 sCJD-MM2:F12, F16, F17, sCJD-VV2:F16, F17
CRYM	Q14894	Ketimine reductase mu-crystallin	Cy	Novel	Autosomal dominant, 40 deafness (Abe et al., 2003)	sCJD-MM1:F17, sCJD-MM2:F16, F17, sCJD-VV2:F16, F17

IDs	Uniprot. Acc. No.	Identified Proteins	Subcellular location	Prion protein-interaction	Involvement in disease	HDFs occurrence
NSF	P46459	Vesicle-fusing ATPase	Cy	Novel		sCJD-MM1:F17, sCJD-MM2:F16, F17, sCJD-VV2:F16, F17
COF2	Q9Y281	Cofilin-2	Nu matrix cy, Ck	Novel		sCJD-MM1:F16, F17, sCJD-MM2:F12, F16, F17, sCJD-VV2:F15, F17
IDH3A	P50213	Isocitrate dehydrogenase [NAD] subunit alpha, mitochondrial	Mc	Novel	Alzheimer's disease (Bubber et al., 2005)	sCJD-MM1:F17 sCJD-MM2:F12, F16, F17 sCJD-VV2:F16, F17
PROF2	P35080	Profilin-2	Cy, Ck.	Novel	Creutzfeldt-Jakob-disease (Gawinecka et al., 2013)	sCJD-MM1:F17, sCJD-MM2:F17, sCJD-VV2:F16, F17
NFL	P07196	Neurofilament light polypeptide (NF-L)		Novel	Prion diseases (Inga Zerr et al., 2018), familial Alzheimer's disease (Weston et al., 2017)	sCJD-MM1:F17 sCJD-MM2:F17, sCJD-VV2:F16, 17
KCC2G	Q13555	Calcium/calmodulin-dependent protein kinase type II subunit gamma	Sr membrane	Novel	Alzheimer's disease (Bubber et al., 2005)	sCJD-MM1:F13, F17 sCJD-MM2:F16, F17 sCJD-VV2:F16
GRP75	P38646	Stress-70 protein, mitochondrial	Mc, Nu, nucleolus	Novel		sCJD-MM1:F17, sCJD-MM2:F12, F17 sCJD-VV2:F16
TPPP	O94811	Tubulin polymerization-promoting protein	Cy, Ck. Nu. Localizes to glial Lewy bodies	Novel	Known (Schubert et al., 2014)	sCJD-MM1:F17, sCJD-MM2:F17, sCJD-VV2:F16

F12 to F17: HDF pool-12 to 17Ce: centrosome, Sy: Synapse, Sr: sarcoplasmic reticulum, C: Cytoplasm, Ck: cytoskeleton, Nu: Nucleus, S: Secreted, Cm: Cell membrane, Sl: Sarcolemma, Ly: Lysosomes, Mc: Mitochondrion, Syo: Synaptosome, Cj: Cell junction, C V: cytoplasmic vesicles, Ga: Golgi apparatus, Pm: phagosome membrane, Px: peroxisome, Em: Endosome membrane, Cp: Cell projection, Gc: growth cone, Ms: Melanosome, Er: Endoplasmic reticulum and La: Lipid-anchor. The localization of proteins and accession number are assigned as in the ExPASy protein database and Uniprot data base, respectively. Relevance with AD, prion and PrP ligand were established by Uniprot database search as well.

Likewise, eleven proteins were uniquely identified in two sCJD subtype (i.e. MV and VV2)-specific HDFs. Reported PrP interaction, disease involvement and specific occurrence in subtype-specific HDFs are enlisted in Table 20.

Table 20: High density PrP (HDP) interactors commonly detected between the high-density fractions of sCJD-MM2 and sCJD-VV2 subtypes.

No.	IDs	Entry	Protein names	Subcellular location	PrP-interaction	Involvement in disease	Occurrence in subtype-specific fractions
1	DEST	P60981	Destrin (Actin-depolymerizing factor)		Novel		sCJD-MM2:F12, sCJD-VV2:F17
2	COR1A	P31146	Coronin-1A	C, Ck, C, C V, Pm	Novel		sCJD-MM2:F12, sCJD-VV2:F16, F17
3	SEPT3	Q9UH03	Neuronal-specific septin-3	C, Ck, Cj, Sy	Novel		sCJD-MM2:F16, 17, sCJD-VV2:F16, F17
4	CISY	O75390	Citrate synthase, mitochondrial	Mc	Novel		sCJD-MM2:F12. 17, sCJD-VV2:F16, 17
5	STX1B	P61266	Syntaxin-1B	Nu, C, Ck, Ce	Novel	Generalized epilepsy with febrile seizures plus 9 (Schubert et al., 2014)	sCJD-MM2:F17, sCJD-VV2:F16, 17
6	PRIO	P04156	Major prion protein (PrP)	Cm; Ga, Nu	Known (Linden et al., 2008)	Transmissible spongiform encephalopathies (Kuru, CJD, FFI and GSS), Alzheimer's disease (Glatzel et al., 2005)	sCJD-MM2:F17, sCJD-VV2:F15 to F17
7	CNRP1	Q96F85	CB1 cannabinoid receptor-interacting protein 1		Novel		sCJD-MM2:F17, sCJD-VV2:F17
8	SCRN1	Q12765	Secernin-1	C	Novel		sCJD-MM2:F17, sCJD-VV2:F16, 17
9	UBA1	P22314	Ubiquitin-like modifier-activating enzyme 1	C, Mc, Nu	Novel		sCJD-MM2:F17, sCJD-VV2:F16, 17
10	AINX	Q16352	Alpha-internexin		Novel		sCJD-MM2:F17, sCJD-VV2:F16, 17

11	PRDX5	P30044	Peroxiredoxin-5, mitochon-drial	Mc, C, Px	Novel		sCJD-MM2:F17, sCJD-VV2:F16

F12 to F17: HDF pool-12 to 17. Ce: centrosome, Sy: Synapse, Sr: sarcoplasmic reticulum, C: Cytoplasm, Ck: cytoskeleton, Nu: Nucleus, S: Secreted, Cm: Cell membrane, Sl: Sar-colemma, Ly: Lysosomes, Mc: Mitochondrion, Syo: Synaptosome, Cj: Cell junction, C V: cytoplasmic vesicles, Ga: Golgi apparatus, Pm: phagosome membrane, Px: peroxisome, Em: Endosome membrane, Cp: Cell projection, Gc: growth cone, Ms: Melanosome, Er: Endoplasmic reticulum and La: Lipid-anchor. The localization of proteins and accession number are assigned as in ExPASy protein database and Uniprot data base respectively. Relevance with AD, prion and PrP ligand were established by Uniprot database search as well.

Certain HDP-interactors were unique to certain subtype-specific high-density fractions from each disease subtype cohort. The disease relevance and reported interaction to PrP are detailed in Table 21. We could also identify three interactors common to the controls and spAD HDFs including cathepsin D (CTSD), catenin beta-1 (CTNNB1) and protein piccolo (PCLO).

Table 21: Subtype-specific interactors for high-density protein conformers, uniquely identified from respective high-density fractions (HDFs).

HDFs	IDs	Uniprot Acc. No.	Protein names	Subcellu-lar loca-tion	PrP-inter-action	Involvement in disease
CON-F13	LAMP1	P11279	Ly-associated mem-brane glycoprotein 1	Cm, Em, Ly	Novel	
CON-F17	CO4A2	P08572	Collagen alpha-2(IV) chain	S	Novel	Stroke (Jeanne et al., 2012)
	ITIH2	P19823	Inter-alpha-trypsin inhibi-tor heavy chain H2	S	Novel	
	PGBM	P98160	Basement membrane-specific heparan sulfate proteoglycan core pro-tein	S	Novel	
spAD-F12	CAP7	P20160	Azurocidin	C	Novel	
	ELNE	P08246	Neutrophil elastase		Novel	
	MUC5A	P98088	Mucin-5AC	S	Novel	
	MUC5B	Q9HC84	Mucin-5B	S	Novel	
	PERM	P05164	Myeloperoxidase	Ly	Novel	
	SG1D1	O95968	Secretoglobin family 1D member 1	S	Novel	
	SG2A1	O75556	Mammaglobin-B		Novel	
	TRFE	P02787	Serotransferrin	S	Novel	
spAD-F13	CYTM	Q15828	Cystatin-M	S	Novel	Parkinsonism and Alz-heimer's dis-ease (Ii et al., 1993)
	MYH16	Q9H6N6	Putative uncharacterized protein MYH16		Novel	

HDFs	IDs	Uniprot Acc. No.	Protein names	Subcellular location	PrP-interaction	Involvement in disease
spAD-F 14	ZGPAT	Q8N5A5	Zinc finger CCCH-type with G patch domain-containing protein	Nu	Novel	
spAD-F 17	ATP6	P00846	ATP synthase subunit a	Mc	Novel	Neuropathy, ataxia, and retinitis pigmentosa (Cha et al., 2015)
	ATPO	P48047	ATP synthase subunit O, mitochondrial	Mc	Novel	
	MYH10	P35580	Myosin-10 (Cellular myosin heavy chain, type B)	Cp	Novel	Intellectual disability, microcephaly, cerebral atrophy (Hamdan et al., 2014)
	MYPC3	Q14896	Myosin-binding protein C, cardiac-type		Novel	Cardiomyopathy, familial hypertrophic 4
	VINC	P18206	Vinculin	Cm, Cj, C, Ck	Novel	Cardiomyopathy, dilated 1W
rpAD-F 16	G2L2	Q8NHY3	GAS2-like protein 2	C, Ck	Novel	
rpAD-F 17	1433S	P31947	14-3-3 protein sigma	C, Nu, S	Novel	
sCJD-MM1-F12	CO1A2	P08123	Collagen alpha-2(I) chain	S	Novel	
sCJD-MM1-F 13	DHX15	O43143	Pre-mRNA-splicing factor ATP-dependent RNA helicase DHX15	Nu	Novel	
sCJD-MM1-F 17	HNRPK	P61978	Heterogeneous nuclear ribonucleoprotein K	C, Nu, Cp	Novel	Au-Kline syndrome (Au et al., 2015)
	STMN1	P16949	Stathmin (Leukemia-associated phosphoprotein p18)	C, Ck.	Novel	
sCJD-MM2-F12	AATC	P17174	Aspartate aminotransferase, cytoplasmic	C	Novel	
	ALDH2	P05091	Aldehyde dehydrogenase, mitochondrial	Mc matrix.	Novel	
	AN32A	P39687	Acidic leucine-rich nuclear phosphoprotein 32 family member A	Nu, C, ER	Novel	
	ANXA5	P08758	Annexin A5		Known (Zafar et al., 2011)	
	ARP2	P61160	Actin-related protein 2	C, Ck, Cp	Novel	
	CALR	P27797	Calreticulin	ER, C, S, Cell surface, Sr	Novel	Alzheimer's disease (Lin et al., 2014)

	IDs	Uniprot Acc. No.	Protein names	Subcellular location	PrP-interaction	Involvement in disease
	CALU	O43852	Calumenin	ER membrane, Ga, S, Sr lumen	Novel	
	CALX	P27824	Calnexin	ER membrane	Known (Wang et al., 2010)	
	CAPZB	P47756	F-actin-capping protein subunit beta	C, Ck	Novel	
	CH10	P61604	10 kDa heat shock protein, mitochondrial	Mc matrix	Novel	
	EZRI	P15311	Ezrin	Cm, Cp C, Ck	Novel	
	FABPH	P05413	Fatty acid-binding protein, heart	C	Novel	
	FUMH	P07954	Fumarate hydratase, mitochondrial	Mc, C	Novel	Fumarase deficiency
	GDIB	P50395	Rab GDP dissociation inhibitor beta	C	Novel	
	GSTP1	P09211	Glutathione S-transferase P	C	Novel	
	HSPB7	Q9UBY9	Heat shock protein beta-7	C, Nu, Cajal body	Novel	
	KCRM	P06732	Creatine kinase M-type	C	Novel	
	KLC1	Q07866	Kinesin light chain 1	Cp, Gc, C V, C, Ck	Novel	
	LIS1	P43034	Platelet-activating factor acetylhydrolase IB subunit alpha	C, Ck. C, Ck, Ce. C, Ck, Nu	Novel	Lissencephaly 1 (Bubber et al., 2005)
	MOES	P26038	Moesin	Cm, C, Ck, Cp	Novel	Immunodeficiency 50
	MYL9	P24844	Myosin regulatory light polypeptide 9		Novel	
	NP1L4	Q99733	Nucleosome assembly protein 1-like 4	Nu, C	Novel	
	PDIA3	P30101	Protein disulfide-isomerase A3	ER	Novel	Prion disease (Weston et al., 2017)
	PDK1	Q15118	[Pyruvate dehydrogenase	Mc	Novel	
	PGM1	P36871	Phosphoglucomutase-1	C	Novel	
	PRDX6	P30041	Peroxiredoxin-6	C, Ly	Novel	Prion disease (Weston et al., 2017)
	PROF1	P07737	Profilin-1	C, Ck.	Novel	Amyotrophic lateral sclerosis 18

	IDs	Uniprot Acc. No.	Protein names	Subcellular location	PrP-interaction	Involvement in disease
	RADI	P35241	Radixin	Cm, C, Ck, Cp	Novel	Deafness, autosomal recessive, 24
	RAN	P62826	GTP-binding nuclear protein Ran	Nu, C, Ms	Novel	
	RET1	P09455	Retinol-binding protein 1	C	Novel	
	RS19	P39019	40S ribosomal protein S19	Nu	Novel	
	RS3	P23396	40S ribosomal protein S3	C, Nu, Mc, C, Ck,	Novel	
	SERPH	P50454	Serpin H1	ER	Novel	
	SET	Q01105	Protein SET	C, ER, Nu	Novel	
	UGPA	Q16851	UTP-glucose-1-phosphate uridylyltransferase	C	Novel	
sCJD-MM2-F13	KLK7	P49862	Kallikrein-7	S	Novel	
sCJD-MM2-F14	BPIB1	Q8TDL5	BPI fold-containing family B member 1	S	Novel	
	SYPL1	Q16563	Synaptophysin-like protein 1	C, Ms	Novel	
sCJD-MM2-F16	SUCB1	Q9P2R7	Succinate-CoA ligase	Mc	Novel	
sCJD-MM2-F17	ARF4	P18085	ADP-ribosylation factor 4	Ga, M	Novel	
	CDC42	P60953	Cell division control protein 42 homolog	Cm, Ck, Ce	Novel	Takenouchi-Kosaki syndrome (Takenouchi et al., 2015)
	EFTU	P49411	Elongation factor Tu, mitochondrial	Mc	Novel	Combined oxidative phosphorylation deficiency 4 (Valente et al., 2007)
	GBB5	O14775	Guanine nucleotide-binding protein subunit beta-5	Membrane	Novel	Intellectual developmental disorder with cardiac arrhythmia (Comi et al., 2001)
	LEG1	P09382	Galectin-1 (Gal-1)	S	Novel	
	IDs	**Uniprot Acc. No.**	**Protein names**	**Subcellular location**	**PrP-interaction**	**Involvement in disease**

	RAC1	P63000	Ras-related C3 botulinum toxin substrate 1	Cm, La, Ms, C	Novel	Mental retardation, autosomal dominant 48
	RTN1	Q16799	Reticulon-1	ER	Novel	
	TBCB	Q99426	Tubulin-folding cofactor B	C, Ck	Novel	
	UCHL1	P09936	Ubiquitin carboxyl-terminal hydrolase isozyme L1	C, ER	Novel	Parkinson disease (Leroy et al., 1998; Y. Liu et al., 2002), Alzheimer's disease (Setsuie & Wada, 2007)
sCJD-VV2-F12	ALDOB	P05062	Fructose-bisphosphate aldolase B	C, Ck, Ce	Known (Zafar et al., 2011)	
sCJD-VV2-F14	WWC3	Q9ULE0	Protein WWC3		Novel	
sCJD-VV2-F15	TIF1B	Q13263	Transcription intermediary factor 1-beta	Nu	Novel	
sCJD-VV2-F16	DHPR	P09417	Dihydropteridine reductase		Novel	Hyperphenylalaninemia associated with neurological disorders (Dianzani et al., 1993)
	PSD3	Q9NYI0	PH and SEC7 domain-containing protein 3	Cm, Cj, Sy	Novel	
sCJD-VV2-F17	AT1B1	P05026	Sodium/potassium-transporting ATPase subunit beta-1	Cm, Sl	Novel	
	GDIA	P31150	Rab GDP dissociation inhibitor alpha (Rab GDI alpha)	C, Ga	Novel	Creutzfeldt-Jakob-disease (Gawinecka et al., 2012)
	NFM	P07197	Neurofilament medium polypeptide (NF-M)		Novel	Neurofilamentopathy (Weston et al., 2017)

F12 to F17: HDF pool-12 to 17, Ce: centrosome, Sy: Synapse, Sr: sarcoplasmic reticulum, C: Cytoplasm, Ck: cytoskeleton, Nu: Nucleus, S: Secreted, Cm: Cell membrane, Sl: Sarcolemma, Ly: Lysosomes, Mc: Mitochondrion, Syo: Synaptosome, Cj: Cell junction, C V: cytoplasmic vesicles, Ga: Golgi apparatus, Pm: phagosome membrane, Px: peroxisome, Em: Endosome membrane, Cp: Cell projection, Gc: growth cone, Ms: Melanosome, Er: Endoplasmic reticulum and La: Lipid-anchor. The localization of proteins and accession number are assigned as in the ExPASy protein database and Uniprot data base, respectively. Relevance with AD, prion and PrP ligand were also established by Uniprot database search.

7 Bibliography

Abe S, Katagiri T, Saito-Hisaminato A, Usami S, Inoue Y, Tsunoda T, Nakamura Y. Identification of CRYM as a candidate responsible for nonsyndromic deafness, through cDNA microarray analysis of human cochlear and vestibular tissues. *Am J Hum Genet*. 2003; 72(1): 73-82.

Aguzzi A, Heikenwalder M, Polymenidou M. Insights into prion strains and neurotoxicity. *Nat Rev Mol Cell Biol.* 2007; 8(7): 552-61.

Aksamit AJ Jr, Preissner CM, Homburger HA. Quantitation of 14-3-3 and neuron-specific enolase proteins in CSF in Creutzfeldt-Jakob disease. *Neurology*. 2001; 57(4): 728-30.

Altmeppen HC, Prox J, Puig B, Kluth MA, Bernreuther C, Thurm D, Jorissen E, Petrowitz B, Bartsch U, De Strooper B, Saftig P, Glatzel M. Lack of a-disintegrin-and-metalloproteinase ADAM10 leads to intracellular accumulation and loss of shedding of the cellular prion protein *in vivo. Mol Neurodegener*. 2011; 6:36.

Altmeppen HC, Puig B, Dohler F, Thurm DK, Falker C, Krasemann S, Glatzel M. Proteolytic processing of the prion protein in health and disease. *Am J Neurogener Dis.* 2012; 1(1): 15-31

Alzheimer, A. Über eine eigenartige Erkrankung der Hirnrinde. *Allg Zeitschr f Psychiatrie u Psych-Gerichtl Med*. 1907; 64(64): 146–8.

Andreasen N, Vanmechelen E, Vanderstichele H, Davidsson P, Blennow K. Cerebrospinal fluid levels of total-tau, phospho-tau and A beta 42 predicts development of Alzheimer's disease in patients with mild cognitive impairment. *Acta Neurol Scand Suppl.* 2003; 179: 47-51.

Arevalo-Rodriguez I, Smailagic N, Roqué I Figuls M, Ciapponi A, Sanchez-Perez E, Giannakou A, Pedraza OL, Bonfill Cosp X, Cullum S. Mini-Mental State Examination (MMSE) for the detection of Alzheimer's disease and other dementias in people with mild cognitive impairment (MCI). *Cochrane Database Syst Rev*. 2015; (3): CD010783.

Arnold SE, Louneva N, Cao K, Wang LS, Han LY, Wolk DA, Negash S, Leurgans SE, Schneider JA, Buchman AS, Wilson RS, Bennett DA. Cellular, synaptic, and

biochemical features of resilient cognition in Alzheimer's disease. *Neurobiol Aging*. 2013; 34(1): 157-68.

Atanassov I, Urlaub H. Increased proteome coverage by combining PAGE and peptide isoelectric focusing: comparative study of gel-based separation approaches. *Proteomics*. 2013; 13(20): 2947-55.

Au PYB, You J, Caluseriu O, Schwartzentruber J, Majewski J, Bernier FP, Ferguson M; Care for Rare Canada Consortium, Valle D, Parboosingh JS, Sobreira N, Innes AM, Kline AD. GeneMatcher aids in the identification of a new malformation syndrome with intellectual disability, unique facial dysmorphisms, and skeletal and connective tissue abnormalities caused by de novo variants in HNRNPK. *Hum Mutat.* 2015; 36(10): 1009-14.

Ba M, Li X, Ng KP, Pascoal TA, Mathotaarachchi S, Rosa-Neto P, Gauthier S; Alzheimer's Disease Neuroimaging Initiative. The prevalence and biomarkers' characteristic of rapidly progressive Alzheimer's disease from the Alzheimer's Disease Neuroimaging Initiative database. *Alzheimers Dement* (N. Y.). 2017; 3(1): 107-113.

Banton MC, Inder KL, Valk E, Rudd CE, Schneider H. Rab8 binding to immune cell-specific adaptor LAX facilitates formation of trans-Golgi network-proximal CTLA-4 vesicles for surface expression. *Mol Cell Biol*. 2014; 34(8): 1486-99.

Barker R, Ashby EL, Wellington D, Barrow VM, Palmer JC, Kehoe PG, Esiri MM, Love S. Pathophysiology of white matter perfusion in Alzheimer's disease and vascular dementia. *Brain*. 2014; 137(Pt 5): 1524-32.

Basler K, Oesch B, Scott M, Westaway D, Wälchli M, Groth DF, McKinley MP, Prusiner SB, Weissmann C. Scrapie and cellular PrP isoforms are encoded by the same chromosomal gene. *Cell.* 1986; 46(3): 417-28.

Bayer TA, Cappai R, Masters CL, Beyreuther K, Multhaup G. It all sticks together-the APP-related family of proteins and Alzheimer's disease. *Mol Psychiatry.* 1999; 4(6): 524-8.

Berman H, Henrick K, Nakamura H. Announcing the worldwide Protein Data Bank. *Nat Struct Biol.* 2003; 10(12): 980.

Best JM, Foell JD, Buss CR, Delisle BP, Balijepalli RC, January CT, Kamp TJ. Small GTPase Rab11b regulates degradation of surface membrane L-type Cav1.2 channels. *Am J Physiol Cell Physiol.* 2011; 300(5): C1023-33.

Bogdanova N, Horst J, Chlystun M, Croucher PJ, Nebel A, Bohring A, Todorova A, Schreiber S, Gerke V, Krawczak M, Markoff A. A common haplotype of the annexin A5 (ANXA5) gene promoter is associated with recurrent pregnancy loss. *Hum Mol Genet.* 2007; 16(5): 573-8.

Braak H, Braak E. Neuropathological stageing of Alzheimer-related changes. *Acta Neuropathol.* 1991; 82(4): 239-59.

Braak H, Del Tredici K. Alzheimer's pathogenesis: is there neuron-to-neuron propagation? *Acta Neuropathol*. 011; 121(5): 589-95.

Brancolini C, Benedetti M, Schneider C. Microfilament reorganization during apoptosis: the role of Gas2, a possible substrate for ICE-like proteases. *EMBO J.* 1995; 14(21): 5179-90.

Brancolini C, Schneider C. Phosphorylation of the growth arrest-specific protein Gas2 is coupled to actin rearrangements during Go→G1 transition in NIH 3T3 cells. *J Cell Biol.* 1994; 124(5): 743-56.

Bravard A, Auvré F, Fantini D, Bernardino-Sgherri J, Sissoëff L, Daynac M, Xu Z, Etienne O, Dehen C, Comoy E, Boussin FD, Tell G, Deslys JP, Radicella JP. The prion protein is critical for DNA repair and cell survival after genotoxic stress. *Nucleic Acids Res.* 2015; 43(2): 904-16.

Brettschneider J, Del Tredici K, Lee VM, Trojanowski JQ. Spreading of pathology in neurodegenerative diseases: a focus on human studies. *Nat Rev Neurosci*. 2015; 16(2): 109-20.

Brown DR, Qin K, Herms JW, Madlung A, Manson J, Strome R, Fraser PE, Kruck T, von Bohlen A, Schulz-Schaeffer W, Giese A, Westaway D, Kretzschmar H. The cellular prion protein binds copper *in vivo*. *Nature*. 1997; 390(6661): 684-7.

Brunden KR, Lee VM, Smith AB 3rd, Trojanowski JQ, Ballatore C. Altered microtubule dynamics in neurodegenerative disease: Therapeutic potential of microtubule-stabilizing drugs. *Neurobiol Dis.* 2017; 105: 328-335.

Bubber P, Haroutunian V, Fisch G, Blass JP, Gibson GE. Mitochondrial abnormalities in Alzheimer brain: mechanistic implications. *Ann Neurol.* 2005; 57(5): 695-703.

Bucci C, Thomsen P, Nicoziani P, McCarthy J, van Deurs B. Rab7: a key to lysosome biogenesis. *Mol Biol Cell.* 2000; 11(2): 467-80.

Cali I, Castellani R, Alshekhlee A, Cohen Y, Blevins J, Yuan J, Langeveld JP, Parchi P, Safar JG, Zou WQ, Gambetti P. Co-existence of scrapie prion protein types 1 and 2 in sporadic Creutzfeldt-Jakob disease: its effect on the phenotype and prion-type characteristics. *Brain.* 2009; 132(Pt 10): 2643-58.

Campana V, Sarnataro D, Zurzolo C. The highways and byways of prion protein trafficking. *Trends Cell Biol*. 2005;15(2): 102-11.

Casadei VM, Ferri C, Calabrese E, Grimaldi LM, Franceschi M, Veglia F, Licastro F, Mariani C. Prion protein gene polymorphism and Alzheimer's disease: one modulatory trait of cognitive decline? *J Neurol Neurosurg Psychiatry*. 2001; 71(2): 279-80.

Cha MY, Cho HJ, Kim C, Jung YO, Kang MJ, Murray ME, Hong HS, Choi YJ, Choi H, Kim DK, Choi H, Kim J, Dickson DW, Song HK, Cho JW, Yi EC, Kim J, Jin SM, Mook-Jung I. Mitochondrial ATP synthase activity is impaired by suppressed O-GlcNAcylation in Alzheimer's disease. *Hum Mol Genet*. 2015 ;24(22): 6492-504.

Chang RY, Etheridge N, Dodd PR, Nouwens AS. Targeted quantitative analysis of synaptic proteins in Alzheimer's disease brain. *Neurochem Int*. 2014; 75: 66-75.

Checler F, Vincent B. Alzheimer's and prion diseases: distinct pathologies, common proteolytic denominators. *Trends Neurosci*. 2002; 25(12): 616-20.

Choi EM, Geschwind MD, Deering C, Pomeroy K, Kuo A, Miller BL, Safar JG, Prusiner SB. Prion proteins in subpopulations of white blood cells from patients with sporadic Creutzfeldt-Jakob disease. *Lab Invest*. 2009; 89(6): 624-35.

Cleary JP, Walsh DM, Hofmeister JJ, Shankar GM, Kuskowski MA, Selkoe DJ, Ashe KH. Natural oligomers of the amyloid-beta protein specifically disrupt cognitive function. *Nat Neurosci*. 2005; 8(1): 79-84.

Cohen M, Appleby B, Safar JG. Distinct prion-like strains of amyloid beta implicated in phenotypic diversity of Alzheimer's disease. *Prion*. 2016; 10(1):9-17.

Cohen ML, Kim C, Haldiman T, ElHag M, Mehndiratta P, Pichet T, Lissemore F, Shea M, Cohen Y, Chen W, Blevins J, Appleby BS, Surewicz K, Surewicz WK, Sajatovic M, Tatsuoka C, Zhang S, Mayo P, Butkiewicz M, Haines JL, Lerner AJ, Safar JG. Rapidly progressive Alzheimer's disease features distinct structures of amyloid-β. *Brain.* 2015; 138(Pt 4): 1009-22.

Collinge J, Whittington MA, Sidle KC, Smith CJ, Palmer MS, Clarke AR, Jefferys JG. Prion protein is necessary for normal synaptic function. *Nature.* 1994; 370(6487): 295-7.

Combarros O, Sánchez-Guerra M, Llorca J, Alvarez-Arcaya A, Berciano J, Peña N, Fernández-Viadero C. Polymorphism at codon 129 of the prion protein gene is not associated with sporadic AD*. Neurology.* 2000; 55(4): 593-5.

Comi GP, Fortunato F, Lucchiari S, Bordoni A, Prelle A, Jann S, Keller A, Ciscato P, Galbiati S, Chiveri L, Torrente Y, Scarlato G, Bresolin N. Beta-enolase deficiency, a new metabolic myopathy of distal glycolysis*. Ann Neurol.* 2001; 50(2): 202-7.

Cooper DM, Crossthwaite AJ. Higher-order organization and regulation of adenylyl cyclases. *Trends Pharmacol Sci*. 2006; 27(8): 426-31.

Counts SE, Alldred MJ, Che S, Ginsberg SD, Mufson EJ. Synaptic gene dysregulation within hippocampal CA1 pyramidal neurons in mild cognitive impairment. *Neuropharmacology.* 2014; 79: 172-9.

Couttas TA, Kain N, Suchowerska AK, Quek LE, Turner N, Fath T, Garner B, Don AS. Loss of ceramide synthase 2 activity, necessary for myelin biosynthesis, precedes tau pathology in the cortical pathogenesis of Alzheimer's disease. *Neurobiol Aging.* 2016; 43: 89-100.

Cracco L, Notari S, Cali I, Sy MS, Chen SG, Cohen ML, Ghetti B, Appleby BS, Zou WQ, Caughey B, Safar JG, Gambetti P. Novel strain properties distinguishing sporadic prion diseases sharing prion protein genotype and prion type. *Sci Rep.* 2017; 7: 38280.

Crum RM, Anthony JC, Bassett SS, Folstein MF. Population-based norms for the Mini-Mental State Examination by age and educational level. *JAMA.* 1993; 269(18): 2386-91.

Cumming RC, Dargusch R, Fischer WH, Schubert D. Increase in expression levels and resistance to sulfhydryl oxidation of peroxiredoxin isoforms in amyloid beta-resistant nerve cells. *J Biol Chem*. 2007; 282(42): 30523-34.

de Calignon A, Polydoro M, Suárez-Calvet M, William C, Adamowicz DH, Kopeikina KJ, Pitstick R, Sahara N, Ashe KH, Carlson GA, Spires-Jones TL, Hyman BT. Propagation of tau pathology in a model of early Alzheimer's disease. *Neuron*. 2012; 73(4): 685-97.

De Cecco E, Legname G. The role of the prion protein in the internalization of α-synuclein amyloids. *Prion*. 2018; 12(1): 23-27.

De Santi S, de Leon MJ, Rusinek H, Convit A, Tarshish CY, Roche A, Tsui WH, Kandil E, Boppana M, Daisley K, Wang GJ, Schlyer D, Fowler J. Hippocampal formation glucose metabolism and volume losses in MCI and AD. *Neurobiol Aging*. 2001; 22(4): 529-39.

De Strooper B, Iwatsubo T, Wolfe MS. Presenilins and γ-secretase: structure, function, and role in Alzheimer Disease. *Cold Spring Harb Perspect Med*. 2012; 2(1): a006304.

Dekker LV, Palmer RH, Parker PJ. The protein kinase C and protein kinase C related gene families. *Curr Opin Struct Biol*. 1995; 5(3): 396-402.

Del Bo R, Scarlato M, Ghezzi S, Martinelli-Boneschi F, Fenoglio C, Galimberti G, Galbiati S, Virgilio R, Galimberti D, Ferrarese C, Scarpini E, Bresolin N, Comi GP. Is M129V of PRNP gene associated with Alzheimer's disease? A case-control study and a meta-analysis. *Neurobiol Aging*. 2006; 27(5): 770.e1-770.e5.

Delisle BP, Underkofler HA, Moungey BM, Slind JK, Kilby JA, Best JM, Foell JD, Balijepalli RC, Kamp TJ, January CT. Small GTPase determinants for the Golgi processing and plasmalemmal expression of human ether-a-go-go related (hERG) K+ channels. *J Biol Chem*. 2009; 284(5): 2844-53.

Dent EW, Gupton SL, Gertler FB. The growth cone cytoskeleton in axon outgrowth and guidance. *Cold Spring Harb Perspect Biol*. 2011; 3(3). pii: a001800.

Dermaut B, Croes EA, Rademakers R, van den Broeck M, Cruts M, Hofman A, van Duijn CM, van Broeckhoven C. *PRNP* Val129 homozygosity increases risk for

early-onset Alzheimer's disease. *Ann Neurol*. 2003; 53(3): 409-12.

Di Fede G, Giaccone G, Limido L, Mangieri M, Suardi S, Puoti G, Morbin M, Mazzoleni G, Ghetti B, Tagliavini F. The epsilon isoform of 14-3-3 protein is a component of the prion protein amyloid deposits of Gerstmann-Sträussler-Scheinker disease. *J Neuropathol Exp Neurol*. 2007; 66(2): 124-30.

Dianzani I, Howells DW, Ponzone A, Saleeba JA, Smooker PM, Cotton RG. Two new mutations in the dihydropteridine reductase gene in patients with tetrahydrobiopterin deficiency. *J Med Genet*. 1993; 30(6): 465-9.

Dohler F, Sepulveda-Falla D, Krasemann S, Altmeppen H, Schlüter H, Hildebrand D, Zerr I, Matschke J, Glatzel M. High molecular mass assemblies of amyloid-β oligomers bind prion protein in patients with Alzheimer's disease. *Brain*. 2014; 137(Pt 3): 873-86.

Dong CF, Wang XF, Wang X, Shi S, Wang GR, Shan B, An R, Li XL, Zhang BY, Han J, Dong XP. Molecular interaction between prion protein and GFAP both in native and recombinant forms *in vitro*. *Med Microbiol Immunol*. 2008;197(4):361-8.

Drummond E, Nayak S, Faustin A, Pires G, Hickman RA, Askenazi M, Cohen M, Haldiman T, Kim C, Han X, Shao Y, Safar JG, Ueberheide B, Wisniewski T. Proteomic differences in amyloid plaques in rapidly progressive and sporadic Alzheimer's disease. *Acta Neuropathol*. 2017; 133(6): 933-954.

Fabregat A, Jupe S, Matthews L, Sidiropoulos K, Gillespie M, Garapati P, Haw R, Jassal B, Korninger F, May B, Milacic M, Roca CD, Rothfels K, Sevilla C, Shamovsky V, Shorser S, Varusai T, Viteri G, Weiser J, Wu G, Stein L, Hermjakob H, D'Eustachio P. The Reactome Pathway Knowledgebase. *Nucleic Acids Res*. 2018; 46(D1): D649-D655.

Ferreira LK, Busatto GF. Neuroimaging in Alzheimer's disease: current role in clinical practice and potential future applications. *Clinics (Sao Paulo)*. 2011; 66 Suppl 1:19-24.

Ferrer I, Rivera R, Blanco R, Martí E. Expression of proteins linked to exocytosis and neurotransmission in patients with Creutzfeldt-Jakob disease. *Neurobiol Dis*. 1999; 6(2): 92-100.

Fluharty BR, Biasini E, Stravalaci M, Sclip A, Diomede L, Balducci C, La Vitola P, Messa M, Colombo L, Forloni G, Borsello T, Gobbi M, Harris DA. An N-terminal fragment of the prion protein binds to amyloid-β oligomers and inhibits their neurotoxicity *in vivo*. *J Biol Chem.* 2013; 288(11)

Förstl H, Kurz A. Clinical features of Alzheimer's disease. *Eur Arch Psychiatry Clin Neurosci*. 1999; 249(6): 288-90.

Frost B, Diamond MI. Prion-like mechanisms in neurodegenerative diseases. *Nat Rev Neurosci*. 2010; 11(3): 155-9.

Fuhrmann M, Bittner T, Mitteregger G, Haider N, Moosmang S, Kretzschmar H, Herms J. Loss of the cellular prion protein affects the Ca^{2+} homeostasis in hippocampal CA1 neurons. *J Neurochem*. 2006; 98(6): 1876-85.

Gambetti P, Kong Q, Zou W, Parchi P, Chen SG. Sporadic and familial CJD: classification and characterisation. *Br Med Bull*. 2003; 66: 213-39.

Gartz Hanson M, Aiken J, Sietsema DV, Sept D, Bates EA, Niswander L, Moore JK. Novel α-tubulin mutation disrupts neural development and tubulin proteostasis. *Dev Biol*. 2016; 409(2): 406-19.

Gawinecka J, Cardone F, Asif AR, De Pascalis A, Wemheuer WM, Schulz-Schaeffer WJ, Pocchiari M, Zerr I. Sporadic Creutzfeldt-Jakob disease subtype-specific alterations of the brain proteome: impact on Rab3a recycling. *Proteomics*. 2012; 12(23-24): 3610-20.

Gawinecka J, Nowak M, Carimalo J, Cardone F, Asif AR, Wemheuer WM, Schulz-Schaeffer WJ, Pocchiari M, Zerr I. Subtype-specific synaptic proteome alterations in sporadic Creutzfeldt-Jakob disease. *J Alzheimers Dis*. 2013; 37(1): 51-61.

GBD 2015 Disease and Injury Incidence and Prevalence Collaborators. Global, regional, and national incidence, prevalence, and years lived with disability for 310 diseases and injuries, 1990-2015: a systematic analysis for the Global Burden of Disease Study 2015. *Lancet*. 2016; 388(10053): 1545-602.

Ghosh A, Giese KP. Calcium/calmodulin-dependent kinase II and Alzheimer's disease. *Mol Brain*. 2015; 8(1): 78.

Giannakopoulos P, Hof PR, Bouras C. Alzheimer's disease with asymmetric atrophy

of the cerebral hemispheres: morphometric analysis of four cases. *Acta Neuropathol*. 1994; 88(5): 440-7.

Glatzel M, Stoeck K, Seeger H, Lührs T, Aguzzi A. Human prion diseases: molecular and clinical aspects. *Arch Neurol*. 2005; 62(4): 545-52.

Godoy JA, Rios JA, Zolezzi JM, Braidy N, Inestrosa NC. Signaling pathway cross talk in Alzheimer's disease. *Cell Commun Signal*. 2014; 12: 23.

Goedert M, Clavaguera F, Tolnay M. The propagation of prion-like protein inclusions in neurodegenerative diseases. *Trends Neurosci*. 2010; 33(7): 317-25.

Goedert M, Jakes R. Mutations causing neurodegenerative tauopathies. *Biochim Biophys Acta*. 2005; 1739(2-3): 240-50.

Goedert M, Masuda-Suzukake M, Falcon B. Like prions: the propagation of aggregated tau and α-synuclein in neurodegeneration. *Brain*. 2017; 140(2): 266-78.

Golanska E, Hulas-Bigoszewska K, Rutkiewicz E, Styczynska M, Peplonska B, Barcikowska M, Bratosiewicz-Wasik J, Liberski PP. Polymorphisms within the prion (PrP) and prion-like protein (Doppel) genes in AD. *Neurology*. 2004; 62(2): 313-5.

Gómez-Isla T, Hollister R, West H, Mui S, Growdon JH, Petersen RC, Parisi JE, Hyman BT. Neuronal loss correlates with but exceeds neurofibrillary tangles in Alzheimer's disease. *Ann Neurol*. 1997; 41(1): 17-24.

Goriounov D, Leung CL, Liem RK. Protein products of human Gas2-related genes on chromosomes 17 and 22 (hGAR17 and hGAR22) associate with both microfilaments and microtubules. *J Cell Sci*. 2003; 116(Pt 6): 1045-58.

Green AJ, Thompson EJ, Stewart GE, Zeidler M, McKenzie JM, MacLeod MA, Ironside JW, Will RG, Knight RS. Use of 14-3-3 and other brain-specific proteins in CSF in the diagnosis of variant Creutzfeldt-Jakob disease. *J Neurol Neurosurg Psychiatry*. 2001; 70(6): 744-8.

Haass C, Selkoe DJ. Soluble protein oligomers in neurodegeneration: lessons from the Alzheimer's amyloid beta-peptide. *Nat Rev Mol Cell Biol*. 2007; 8(2): 101-12.

Haldiman T, Kim C, Cohen Y, Chen W, Blevins J, Qing L, Cohen ML, Langeveld J,

Telling GC, Kong Q, Safar JG. Co-existence of distinct prion types enables conformational evolution of human PrPSc by competitive selection. *J Biol Chem*. 2013; 288(41): 29846-61.

Hämäläinen A, Pihlajamäki M, Tanila H, Hänninen T, Niskanen E, Tervo S, Karjalainen PA, Vanninen RL, Soininen H. Increased fMRI responses during encoding in mild cognitive impairment. *Neurobiol Aging*. 2007; 28(12): 1889-903.

Hamdan FF, Srour M, Capo-Chichi JM, Daoud H, Nassif C, Patry L, Massicotte C, Ambalavanan A, Spiegelman D, Diallo O, Henrion E, Dionne-Laporte A, Fougerat A, Pshezhetsky AV, Venkateswaran S, Rouleau GA, Michaud JL. De novo mutations in moderate or severe intellectual disability. *PLoS Genet*. 2014; 10(10): e1004772.

Harada A, Oguchi K, Okabe S, Kuno J, Terada S, Ohshima T, Sato-Yoshitake R, Takei Y, Noda T, Hirokawa N. Altered microtubule organization in small-calibre axons of mice lacking tau protein. *Nature*. 1994; 369(6480): 488-91.

Haraguchi T, Fisher S, Olofsson S, Endo T, Groth D, Tarentino A, Borchelt DR, Teplow D, Hood L, Burlingame A, Lycke E, Kobata A, Prusiner SB. Asparagine-linked glycosylation of the scrapie and cellular prion proteins. *Arch Biochem Biophys*. 1989; 274(1): 1-13.

Harris JA, Devidze N, Verret L, Ho K, Halabisky B, Thwin MT, Kim D, Hamto P, Lo I, Yu GQ, Palop JJ, Masliah E, Mucke L. Transsynaptic progression of amyloid-β-induced neuronal dysfunction within the entorhinal-hippocampal network. *Neuron*. 2010; 68(3): 428-41.

Hassan MI, Waheed A, Yadav S, Singh TP, Ahmad F. Zinc alpha 2-glycoprotein: a multidisciplinary protein. *Mol Cancer Res*. 2008; 6(6): 892-906.

Hasson SA, Kane LA, Yamano K, Huang CH, Sliter DA, Buehler E, Wang C, Heman-Ackah SM, Hessa T, Guha R, Martin SE, Youle RJ. High-content genome-wide RNAi screens identify regulators of parkin upstream of mitophagy. *Nature*. 2013; 504(7479): 291-5.

He Q, Meiri KF. Isolation and characterization of detergent-resistant microdomains responsive to NCAM-mediated signaling from growth cones. *Mol Cell Neurosci*.

2002; 19(1): 18-31.

He Y, Zheng MM, Ma Y, Han XJ, Ma XQ, Qu CQ, Du YF. Soluble oligomers and fibrillar species of amyloid β-peptide differentially affect cognitive functions and hippocampal inflammatory response. *Biochem Biophys Res Commun*. 2012; 429(3-4): 125-30.

Hegde RS, Mastrianni JA, Scott MR, DeFea KA, Tremblay P, Torchia M, DeArmond SJ, Prusiner SB, Lingappa VR. A transmembrane form of the prion protein in neurodegenerative disease. *Science*. 1998; 279(5352): 827-34.

Hegde RS, Voigt S, Lingappa VR. Regulation of protein topology by trans-acting factors at the endoplasmic reticulum. *Mol Cell*. 1998; 2(1): 85-91.

Helmfors L, Boman A, Civitelli L, Nath S, Sandin L, Janefjord C, McCann H, Zetterberg H, Blennow K, Halliday G, Brorsson AC, Kågedal K. Protective properties of lysozyme on β-amyloid pathology: implications for Alzheimer disease. *Neurobiol Dis*. 2015; 83: 122-33.

Herms J, Tings T, Gall S, Madlung A, Giese A, Siebert H, Schürmann P, Windl O, Brose N, Kretzschmar H. Evidence of presynaptic location and function of the prion protein. *J Neurosci*. 1999; 19(20): 8866-75.

Herms JW, Korte S, Gall S, Schneider I, Dunker S, Kretzschmar HA. Altered intracellular calcium homeostasis in cerebellar granule cells of prion protein-deficient mice. *J Neurochem*. 2000; 75(4): 1487-92.

Hirokawa N, Niwa S, Tanaka Y. Molecular motors in neurons: transport mechanisms and roles in brain function, development, and disease. *Neuron*. 2010; 68(4): 610-38.

Hof PR, Bouras C, Constantinidis J, Morrison JH. Balint's syndrome in Alzheimer's disease: specific disruption of the occipito-parietal visual pathway. *Brain Res*. 1989; 493(2): 368-75.

Hoogenraad CC, Bradke F. Control of neuronal polarity and plasticity-a renaissance for microtubules? *Trends Cell Biol*. 2009; 19(12): 669-76.

Hoos MD, Richardson BM, Foster MW, Everhart A, Thompson JW, Moseley MA, Colton CA. Longitudinal study of differential protein expression in an Alzheimer's

mouse model lacking inducible nitric oxide synthase. *J Proteome Res*. 2013; 12(10): 4462-77.

Horwitz M, Benson KF, Person RE, Aprikyan AG, Dale DC. Mutations in ELA2, encoding neutrophil elastase, define a 21-day biological clock in cyclic haematopoiesis. *Nat Genet*. 1999; 23(4): 433-6.

Huang Y, Tanimukai H, Liu F, Iqbal K, Grundke-Iqbal I, Gong CX. Elevation of the level and activity of acid ceramidase in Alzheimer's disease brain. *Eur J Neurosci*. 2004; 20(12): 3489-97.

Humpel C. Identifying and validating biomarkers for Alzheimer's disease. *Trends Biotechnol*. 2011; 29(1): 26-32.

Ii K, Ito H, Kominami E, Hirano A. Abnormal distribution of cathepsin proteinases and endogenous inhibitors (cystatins) in the hippocampus of patients with Alzheimer's disease, parkinsonism-dementia complex on Guam, and senile dementia and in the aged. *Virchows Arch A Pathol Anat Histopathol*. 1993; 423(3): 185-94.

Ikonomovic MD, Klunk WE, Abrahamson EE, Mathis CA, Price JC, Tsopelas ND, Lopresti BJ, Ziolko S, Bi W, Paljug WR, Debnath ML, Hope CE, Isanski BA, Hamilton RL, DeKosky ST. Post-mortem correlates of *in vivo* PiB-PET amyloid imaging in a typical case of Alzheimer's disease. *Brain*. 2008; 131(Pt 6): 1630-45.

Imran M, Mahmood S. An overview of animal prion diseases. *Virol J*. 2011; 8:493.

Inestrosa NC, Varela-Nallar L. Wnt signaling in the nervous system and in Alzheimer's disease. *J Mol Cell Biol*. 2014; 6(1): 64-74.

Iqbal K, Liu F, Gong CX, Grundke-Iqbal I. Tau in Alzheimer disease and related tauopathies. *Curr Alzheimer Res*. 2010; 7(8): 656-64.

Jack CR Jr, Petersen RC, Xu Y, O'Brien PC, Smith GE, Ivnik RJ, Tangalos EG, Kokmen E. Rate of medial temporal lobe atrophy in typical aging and Alzheimer's disease. *Neurology*. 1998; 51(4): 993-9.

Jackson GS, Murray I, Hosszu LL, Gibbs N, Waltho JP, Clarke AR, Collinge J. Location and properties of metal-binding sites on the human prion protein. *Proc Natl Acad Sci U. S. A.*. 2001; 98(15): 8531-5.

Jang B, Kim E, Choi JK, Jin JK, Kim JI, Ishigami A, Maruyama N, Carp RI, Kim YS, Choi EK. Accumulation of citrullinated proteins by up-regulated peptidylarginine deiminase 2 in brains of scrapie-infected mice: a possible role in pathogenesis. *Am J Pathol*. 2008; 173(4): 1129-42.

Jayaratnam S, Khoo AK, Basic D. Rapidly progressive Alzheimer's disease and elevated 14-3-3 proteins in cerebrospinal fluid. *Age Ageing*. 2008; 37(4): 467-9.

Jeanne M, Labelle-Dumais C, Jorgensen J, Kauffman WB, Mancini GM, Favor J, Valant V, Greenberg SM, Rosand J, Gould DB. COL4A2 mutations impair COL4A1 and COL4A2 secretion and cause hemorrhagic stroke. *Am J Hum Genet*. 2012; 90(1): 91-101.

Jian X, Bis JC, Kunkle BW, Hamilton KL, Beecham GW, Bush WS., Salerno W, Lancour D, Ma Y, Chen Y, DeStefano AL, Dupius J, Boerwinkle E, Schellenberg GD, Naj AC, Seshadri S, Fornage M, Farrer LA. Rare deleterious and loss-of-function variants in OPRL1 and GAS2L2 contribute to the risk of late-onset Alzheimer's disease: Alzheimer's disease sequencing project case-control study. *Alzheimer's & Dementia.* 2016; 12(7): P163

Johnson KA, Fox NC, Sperling RA, Klunk WE. Brain imaging in Alzheimer disease. *Cold Spring Harb Perspect Med*. 2012; 2(4): a006213.

Johnson KA, Gregas M, Becker JA, Kinnecom C, Salat DH, Moran EK, Smith EE, Rosand J, Rentz DM, Klunk WE, Mathis CA, Price JC, Dekosky ST, Fischman AJ, Greenberg SM. Imaging of amyloid burden and distribution in cerebral amyloid angiopathy. *Ann Neurol*. 2007; 62(3): 229-34.

Jucker M, Walker LC. Pathogenic protein seeding in Alzheimer disease and other neurodegenerative disorders. *Ann Neurol*. 2011; 70(4): 532-40.

Kalia LV, Kalia SK, McLean PJ, Lozano AM, Lang AE. α-synuclein oligomers and clinical implications for parkinson disease. *Ann Neurol*. 2013; 73(2): 155-69.

Kamenetsky M, Middelhaufe S, Bank EM, Levin LR, Buck J, Steegborn C. Molecular details of cAMP generation in mammalian cells: a tale of two systems. *J Mol Biol*. 2006; 362(4): 623-39.

Kandel, E. R., Schwatrz, J. H., Jessel, T. M., Siegelbaum, S. A., & Hudspeth, A. J.

(Eds.). Chapter 59: The aging brian. Principles of Neural Science (5th ed.). 2013. p: 1337. New York: McGraw-Hill Companies.

Kang SW, Chae HZ, Seo MS, Kim K, Baines IC, Rhee SG. Mammalian peroxiredoxin isoforms can reduce hydrogen peroxide generated in response to growth factors and tumor necrosis factor-alpha. *J Biol Chem*. 1998; 273(11): 6297-302.

Karch CM, Goate AM. Alzheimer's disease risk genes and mechanisms of disease pathogenesis*. Biol Psychiatry*. 2015; 77(1): 43-51.

Khalili-Shirazi A, Summers L, Linehan J, Mallinson G, Anstee D, Hawke S, Jackson GS, Collinge J. PrP glycoforms are associated in a strain-specific ratio in native PrPSc. *J Gen Virol*. 2005; 86(Pt 9): 2635-44.

Kim C, Haldiman T, Cohen Y, Chen W, Blevins J, Sy MS, Cohen M, Safar JG. Protease-sensitive conformers in broad spectrum of distinct PrPSc structures in sporadic Creutzfeldt-Jakob disease are indicator of progression rate. *PLoS Pathog*. 2011; 7(9): e1002242.

Kim C, Haldiman T, Surewicz K, Cohen Y, Chen W, Blevins J, Sy MS, Cohen M, Kong Q, Telling GC, Surewicz WK, Safar JG. Small protease sensitive oligomers of PrPSc in distinct human prions determine conversion rate of PrP(C). *PLoS Pathog*. 2012; 8(8): e1002835.

Kim EK, Choi EJ. Compromised MAPK signaling in human diseases: an update. *Arch Toxicol*. 2015; 89(6): 867-82.

Kim J, Holtzman DM. Prion-like behavior of amyloid-beta. *Science*. 2010 12; 330(6006): 918-9.

Kim SH, Fountoulakis M, Cairns N, Lubec G. Protein levels of human peroxiredoxin subtypes in brains of patients with Alzheimer's disease and Down syndrome. *J Neural Transm Suppl*. 2001; (61): 223-35.

Kitamoto T, Tateishi J. Human prion diseases with variant prion protein. *Philos Trans R Soc Lond B Biol Sci*. 1994; 343(1306): 391-8.

Klaips CL, Jayaraj GG, Hartl FU. Pathways of cellular proteostasis in aging and disease. *J Cell Biol*. 2018; 217(1): 51-63.

Kovacs GG, Sanchez-Juan P, Ströbel T, Schuur M, Poleggi A, Nocentini S, Giannattasio C, Belay G, Bishop M, Capellari S, Parchi P, Gelpi E, Gal A, Bakos A, Molnar MJ, Heinemann U, Zerr I, Knight RS, Mitrova E, van Duijn C, Budka H. Cathepsin D (C224T) polymorphism in sporadic and genetic Creutzfeldt-Jakob disease. *Alzheimer Dis Assoc Disord*. 2010; 24(1): 104-7.

Krapfenbauer K, Engidawork E, Cairns N, Fountoulakis M, Lubec G. Aberrant expression of peroxiredoxin subtypes in neurodegenerative disorders. *Brain Res*. 2003; 967(1-2): 152-60.

Kwong KK, Belliveau JW, Chesler DA, Goldberg IE, Weisskoff RM, Poncelet BP, Kennedy DN, Hoppel BE, Cohen MS, Turner R. Dynamic magnetic resonance imaging of human brain activity during primary sensory stimulation. *Proc Natl Acad Sci U. S. A*. 1992; 89(12): 5675-9.

LaFerla FM, Green KN, Oddo S. Intracellular amyloid-beta in Alzheimer's disease. *Nat Rev Neurosci*. 2007; 8(7): 499-509.

Lambert JP, Ivosev G, Couzens AL, Larsen B, Taipale M, Lin ZY, Zhong Q, Lindquist S, Vidal M, Aebersold R, Pawson T, Bonner R, Tate S, Gingras AC. Mapping differential interactomes by affinity purification coupled with data-independent mass spectrometry acquisition. *Nat Methods*. 2013; 10(12): 1239-45.

Laurén J, Gimbel DA, Nygaard HB, Gilbert JW, Strittmatter SM. Cellular prion protein mediates impairment of synaptic plasticity by amyloid-beta oligomers. *Nature*. 2009; 457(7233): 1128-32.

Lee YJ, Goo JS, Kim JE, Nam SH, Hwang IS, Choi SI, Lee HR, Lee EP, Choi HW, Kim HS, Lee JH, Jung YJ, Kim HJ, Hwang DY. Peroxiredoxin I regulates the component expression of γ-secretase complex causing the Alzheimer's disease. *Lab Anim Res*. 2011; 27(4): 293-9.

Lehéricy S, Baulac M, Chiras J, Piérot L, Martin N, Pillon B, Deweer B, Dubois B, Marsault C. Amygdalohippocampal MR volume measurements in the early stages of Alzheimer disease. *AJNR Am J Neuroradiol*. 1994; 15(5): 929-37.

Lei G, Arany I, Tyring SK, Brysk H, Brysk MM. Zinc-alpha 2-glycoprotein has ribonuclease activity. *Arch Biochem Biophys*. 1998; 355(2): 160-4.

Leroy E, Boyer R, Auburger G, Leube B, Ulm G, Mezey E, Harta G, Brownstein MJ, Jonnalagada S, Chernova T, Dehejia A, Lavedan C, Gasser T, Steinbach PJ, Wilkinson KD, Polymeropoulos MH. The ubiquitin pathway in Parkinson's disease. *Nature*. 1998; 395(6701): 451-2.

Lesné SE, Sherman MA, Grant M, Kuskowski M, Schneider JA, Bennett DA, Ashe KH. Brain amyloid-β oligomers in ageing and Alzheimer's disease. *Brain*. 2013; 136(Pt 5): 1383-98.

Lewis V, Hooper NM. The role of lipid rafts in prion protein biology. *Front Biosci* (Landmark Ed). 2011 ; 16: 151-68.

Li Q, Lau A, Morris TJ, Guo L, Fordyce CB, Stanley EF. A syntaxin 1, Galpha(o), and N-type calcium channel complex at a presynaptic nerve terminal: analysis by quantitative immunocolocalization. *J Neurosci*. 2004; 24(16): 4070-81.

Li X, Long J, He T, Belshaw R, Scott J. Integrated genomic approaches identify major pathways and upstream regulators in late onset Alzheimer's disease. *Sci Rep*. 2015; 5: 12393.

Lin Q, Cao Y, Gao J. Serum calreticulin is a negative biomarker in patients with Alzheimer's disease. *Int J Mol Sci*. 2014; 15(12): 21740-53.

Linden R, Martins VR, Prado MA, Cammarota M, Izquierdo I, Brentani RR. Physiology of the prion protein. *Physiol Rev*. 2008; 88(2): 673-728.

Linford A, Yoshimura S, Nunes Bastos R, Langemeyer L, Gerondopoulos A, Rigden DJ, Barr FA. Rab14 and its exchange factor FAM116 link endocytic recycling and adherens junction stability in migrating cells. *Dev Cell*. 2012; 22(5): 952-66.

Linsenmeier L, Mohammadi B, Wetzel S, Puig B, Jackson WS, Hartmann A, Uchiyama K, Sakaguchi S, Endres K, Tatzelt J, Saftig P, Glatzel M, Altmeppen HC. Structural and mechanistic aspects influencing the ADAM10-mediated shedding of the prion protein. *Mol Neurodegener*. 2018; 13(1): 18.

Liu CC, Liu CC, Kanekiyo T, Xu H, Bu G. Apolipoprotein E and Alzheimer disease: risk, mechanisms and therapy. *Nat Rev Neurol*. 2013; 9(2): 106-18.

Liu P, Reed MN, Kotilinek LA, Grant MK, Forster CL, Qiang W, Shapiro SL, Reichl JH, Chiang AC, Jankowsky JL, Wilmot CM, Cleary JP, Zahs KR, Ashe KH.

Quaternary Structure Defines a Large Class of Amyloid-β Oligomers Neutralized by Sequestration. *Cell Rep*. 2015; 11(11): 1760-71.

Liu Y, Fallon L, Lashuel HA, Liu Z, Lansbury PT Jr. The UCH-L1 gene encodes two opposing enzymatic activities that affect alpha-synuclein degradation and Parkinson's disease susceptibility. *Cell*. 2002; 111(2): 209-18.

Llorens F, Schmitz M, Ferrer I, Zerr I. CSF biomarkers in neurodegenerative and vascular dementias. *Prog Neurobiol*. 2016; 138-140: 36-53.

Llorens F, Schmitz M, Knipper T, Schmidt C, Lange P, Fischer A, Hermann P, Zerr I. Cerebrospinal Fluid Biomarkers of Alzheimer's Disease Show Different but Partially Overlapping Profile Compared to Vascular Dementia. *Front Aging Neurosci*. 2017; 9: 289.

Lonsdale D. Thiamine and magnesium deficiencies: keys to disease. *Med Hypotheses*. 2015; 84(2): 129-34.

Lopez O.L., D. S. T. (2008). Clinical symptoms in Alzheimer’s disease. Handbook of Clinical Neurology, 89, 207–216.

Lu JX, Qiang W, Yau WM, Schwieters CD, Meredith SC, Tycko R. Molecular structure of β-amyloid fibrils in Alzheimer's disease brain tissue. *Cell*. 2013; 154(6): 1257-68.

Luthe DS. A simple technique for the preparation and storage of sucrose gradients. *Anal Biochem*. 1983; 135(1): 230-2.

Maday S, Twelvetrees AE, Moughamian AJ, Holzbaur EL. Axonal transport: cargo-specific mechanisms of motility and regulation. *Neuron*. 2014; 84(2): 292-309.

Mann UM, Mohr E, Chase TN. Rapidly progressive Alzheimer's disease. *Lancet.* 1989; 2(8666): 799.

Mannini B, Cascella R, Zampagni M, van Waarde-Verhagen M, Meehan S, Roodveldt C, Campioni S, Boninsegna M, Penco A, Relini A, Kampinga HH, Dobson CM, Wilson MR, Cecchi C, Chiti F. Molecular mechanisms used by chaperones to reduce the toxicity of aberrant protein oligomers. *Proc Natl Acad Sci U. S. A..* 2012; 109(31): 12479-84.

Markesbery WR. Oxidative stress hypothesis in Alzheimer's disease. *Free Radic Biol Med.* 1997; 23(1): 134-47.

Martin SB, Dowling AL, Lianekhammy J, Lott IT, Doran E, Murphy MP, Beckett TL, Schmitt FA, Head E. Synaptophysin and synaptojanin-1 in Down syndrome are differentially affected by Alzheimer's disease. *J Alzheimers Dis*. 2014; 42(3): 767-75.

Matamoros AJ, Baas PW. Microtubules in health and degenerative disease of the nervous system. *Brain Res Bull*. 2016; 126(Pt 3): 217-225.

Mayer MP. Hsp70 chaperone dynamics and molecular mechanism. *Trends Biochem Sci.* 2013; 38(10): 507-14.

Medici S, Peana M, Nurchi VM, Zoroddu MA. The involvement of amino acid side chains in shielding the nickel coordination site: an NMR study. *Molecules*. 2013; 18(10): 12396-414.

Melo RC, Morgan E, Monahan-Earley R, Dvorak AM, Weller PF. Pre-embedding immunogold labeling to optimize protein localization at subcellular compartments and membrane microdomains of leukocytes. *Nat Protoc*. 2014; 9(10): 2382-94.

Mendez MF. Early-Onset Alzheimer Disease. *Neurol Clin.* 2017; 35(2): 263-281

Meredith SC. Protein denaturation and aggregation: Cellular responses to denatured and aggregated proteins*. Ann N Y Acad Sci*. 2005; 1066: 181-221

Miners JS, Palmer JC, Love S. Pathophysiology of Hypoperfusion of the Precuneus in Early Alzheimer's Disease. *Brain Pathol*. 2016; 26(4): 533-41.

Mirra SS, Heyman A, McKeel D, Sumi SM, Crain BJ, Brownlee LM, Vogel FS, Hughes JP, van Belle G, Berg L. The Consortium to Establish a Registry for Alzheimer's Disease (CERAD). Part II. Standardization of the neuropathologic assessment of Alzheimer's disease. *Neurology*. 1991; 41(4): 479-86.

Montine TJ, Phelps CH, Beach TG, Bigio EH, Cairns NJ, Dickson DW, Duyckaerts C, Frosch MP, Masliah E, Mirra SS, Nelson PT, Schneider JA, Thal DR, Trojanowski JQ, Vinters HV, Hyman BT; National Institute on Aging; Alzheimer's Association. National Institute on Aging-Alzheimer's Association guidelines for the neuropathologic assessment of Alzheimer's disease: a practical approach. *Acta*

Neuropathol. 2012; 123(1): 1-11.

Morris JC, Heyman A, Mohs RC, Hughes JP, van Belle G, Fillenbaum G, Mellits ED, Clark C. The Consortium to Establish a Registry for Alzheimer's Disease (CERAD). Part I. Clinical and neuropsychological assessment of Alzheimer's disease. *Neurology.* 1989; 39(9): 1159-65.

Mueller SG, Schuff N, Yaffe K, Madison C, Miller B, Weiner MW. Hippocampal atrophy patterns in mild cognitive impairment and Alzheimer's disease. *Hum Brain Mapp.* 2010; 31(9): 1339-47.

Mungas D. In-office mental status testing: a practical guide. *Geriatrics*. 1991; 46(7): 54-8, 63, 66.

Munoz L, Ammit AJ. Targeting p38 MAPK pathway for the treatment of Alzheimer's disease. *Neuropharmacology*. 2010; 58(3): 561-8.

Muramatsu T, Sakai N, Yanagihara I, Yamada M, Nishigaki T, Kokubu C, Tsukamoto H, Ito M, Inui K. Mutation analysis of the acid ceramidase gene in Japanese patients with Farber disease. *J Inherit Metab Dis*. 2002; 25(7): 585-92.

Murray ME, Graff-Radford NR, Ross OA, Petersen RC, Duara R, Dickson DW. Neuropathologically defined subtypes of Alzheimer's disease with distinct clinical characteristics: a retrospective study. *Lancet Neurol*. 2011; 10(9): 785-96.

Musicco M, Palmer K, Salamone G, Lupo F, Perri R, Mosti S, Spalletta G, di Iulio F, Pettenati C, Cravello L, Caltagirone C. Predictors of progression of cognitive decline in Alzheimer's disease: the role of vascular and sociodemographic factors. *J Neurol.* 2009; 256(8): 1288-95.

Neuendorf E, Weber A, Saalmueller A, Schatzl H, Reifenberg K, Pfaff E, Groschup MH. Glycosylation deficiency at either one of the two glycan attachment sites of cellular prion protein preserves susceptibility to bovine spongiform encephalopathy and scrapie infections. *J Biol Chem*. 2004; 279(51): 53306-16.

Newens AJ, Forster DP, Kay DW, Kirkup W, Bates D, Edwardson J. Clinically diagnosed presenile dementia of the Alzheimer type in the Northern Health Region: ascertainment, prevalence, incidence and survival. *Psychol Med*. 199; 23(3): 631-44.

Nieznanski K, Nieznanska H, Skowronek KJ, Osiecka KM, Stepkowski D. Direct interaction between prion protein and tubulin. *Biochem Biophys Res Commun*. 2005; 334(2): 403-11.

Nieznanski K. Interactions of prion protein with intracellular proteins: so many partners and no consequences? *Cell Mol Neurobiol*. 2010; 30(5): 653-66.

Nimmrich V, Grimm C, Draguhn A, Barghorn S, Lehmann A, Schoemaker H, Hillen H, Gross G, Ebert U, Bruehl C. Amyloid beta oligomers (A beta(1-42) globulomer) suppress spontaneous synaptic activity by inhibition of P/Q-type calcium currents. *J Neurosci.* 2008; 28(4): 788-97.

Novak P, Prcina M, Kontsekova E. Tauons and prions: infamous cousins? *J Alzheimers Dis*. 2011; 26(3): 413-30

Nye SH, Pelfrey CM, Burkwit JJ, Voskuhl RR, Lenardo MJ, Mueller JP. Purification of immunologically active recombinant 21.5 kDa isoform of human myelin basic protein. *Mol Immunol*. 1995; 32(14-15): 1131-41.

Nyström S, Hammarström P. Generic amyloidogenicity of mammalian prion proteins from species susceptible and resistant to prions. *Sci Rep*. 2015; 5: 10101.

O'Brien RJ, Wong PC. Amyloid precursor protein processing and Alzheimer's disease. *Annu Rev Neurosci*. 2011; 34: 185-204.

Oesch B, Westaway D, Wälchli M, McKinley MP, Kent SB, Aebersold R, Barry RA, Tempst P, Teplow DB, Hood LE, Stanley BP, Weissmann C. A cellular gene encodes scrapie PrP 27-30 protein. *Cell*. 1985; 40(4): 735-46.

Ogawa S, Lee TM, Nayak AS, Glynn P. Oxygenation-sensitive contrast in magnetic resonance image of rodent brain at high magnetic fields. *Magn Reson Med*. 1990; 14(1): 68-78.

Osborne C, West E, Nolan W, McHale-Owen H, Williams A, Bate C. Glimepiride protects neurons against amyloid-β-induced synapse damage. *Neuropharmacology*. 2016; 101: 225-36.

Osiecka KM, Nieznanska H, Skowronek KJ, Karolczak J, Schneider G, Nieznanski K. Prion protein region 23-32 interacts with tubulin and inhibits microtubule assembly. *Proteins*. 2009; 77(2): 279-96.

Ostapchenko VG, Beraldo FH, Mohammad AH, Xie YF, Hirata PH, Magalhaes AC, Lamour G, Li H, Maciejewski A, Belrose JC, Teixeira BL, Fahnestock M, Ferreira ST, Cashman NR, Hajj GN, Jackson MF, Choy WY, MacDonald JF, Martins VR, Prado VF, Prado MA. The prion protein ligand, stress-inducible phosphoprotein 1, regulates amyloid-β oligomer toxicity. *J Neurosci*. 2013; 33(42): 16552-64.

Paoletti F, Mocali A, Marchi M, Sorbi S, Piacentini S. Enhanced proteolytic activities in cultured fibroblasts of Alzheimer patients are revealed by peculiar transketolase alterations. *Biochem Biophys Res Commun*. 1990; 172(2): 396-401.

Paoletti F, Mocali A. Enhanced proteolytic activities in cultured fibroblasts of Alzheimer patients are revealed by peculiar transketolase alterations. *J Neurol Sci*. 1991; 105(2): 211-6.

Parkin ET, Watt NT, Hussain I, Eckman EA, Eckman CB, Manson JC, Baybutt HN, Turner AJ, Hooper NM. Cellular prion protein regulates beta-secretase cleavage of the Alzheimer's amyloid precursor protein. *Proc Natl Acad Sci U. S. A.*. 2007; 104(26): 11062-7.

Parton RG, Joggerst B, Simons K. Regulated internalization of caveolae. *J Cell Biol*. 1994; 127(5): 1199-215.

Patzig J, Jahn O, Tenzer S, Wichert SP, de Monasterio-Schrader P, Rosfa S, Kuharev J, Yan K, Bormuth I, Bremer J, Aguzzi A, Orfaniotou F, Hesse D, Schwab MH, Möbius W, Nave KA, Werner HB. Quantitative and integrative proteome analysis of peripheral nerve myelin identifies novel myelin proteins and candidate neuropathy loci. *J Neurosci*. 2011; 31(45): 16369-86.

Perani D. FDG-PET and amyloid-PET imaging: the diverging paths. *Curr Opin Neurol.* 2014; 27(4): 405-13.

Peterson A, Lantz MS; American Association for Geriatric Psychiatry. Is it Alzheimer's? Neuropsychological testing helps to clarify diagnostic puzzle. *Geriatrics*. 2001; 56(4): 58, 61.

Pham E, Crews L, Ubhi K, Hansen L, Adame A, Cartier A, Salmon D, Galasko D, Michael S, Savas JN, Yates JR, Glabe C, Masliah E. Progressive accumulation of amyloid-beta oligomers in Alzheimer's disease and in amyloid precursor protein

transgenic mice is accompanied by selective alterations in synaptic scaffold proteins. *FEBS J.* 2010; 277(14): 3051-67.

Pierce BG, Hourai Y, Weng Z. Accelerating protein docking in ZDOCK using an advanced 3D convolution library. *PLoS One*. 2011; 6(9): e24657.

Pierce BG, Wiehe K, Hwang H, Kim BH, Vreven T, Weng Z. ZDOCK server: interactive docking prediction of protein-protein complexes and symmetric multimers. *Bioinformatics.* 2014; 30(12): 1771-3.

Pieri L, Madiona K, Melki R. Structural and functional properties of prefibrillar α-synuclein oligomers. *Sci Rep.* 2016; 6: 24526.

Plutner H, Schwaninger R, Pind S, Balch WE. Synthetic peptides of the Rab effector domain inhibit vesicular transport through the secretory pathway. *EMBO J*. 1990; 9(8): 2375-83.

Pozueta A, Rodríguez-Rodríguez E, Vazquez-Higuera JL, Mateo I, Sánchez-Juan P, González-Perez S, Berciano J, Combarros O. Detection of early Alzheimer's disease in MCI patients by the combination of MMSE and an episodic memory test. *BMC Neurol*. 2011; 11: 78.

Prokop A. The intricate relationship between microtubules and their associated motor proteins during axon growth and maintenance. *Neural Dev*. 2013; 8: 17.

Prots I, Veber V, Brey S, Campioni S, Buder K, Riek R, Böhm KJ, Winner B. α-Synuclein oligomers impair neuronal microtubule-kinesin interplay. *J Biol Chem*. 2013; 288(30): 21742-54.

Prusiner SB, Groth DF, Bolton DC, Kent SB, Hood LE. Purification and structural studies of a major scrapie prion protein. *Cell*. 1984; 38(1): 127-34.

Prusiner SB, Scott MR, DeArmond SJ, Cohen FE. Prion protein biology. *Cell*. 1998; 93(3): 337-48.

Prusiner SB. Some speculations about prions, amyloid, and Alzheimer's disease. *N Engl J Med.* 1984; 310(10): 661-3.

Qiang W, Yau WM, Lu JX, Collinge J, Tycko R. Structural variation in amyloid-β fibrils from Alzheimer's disease clinical subtypes. *Nature.* 2017; 541(7636): 217-221.

Querfurth HW, LaFerla FM. Alzheimer's disease. *N Engl J Med.* 2010; 362(4): 329-44.

Radons J. The human HSP70 family of chaperones: where do we stand? *Cell Stress Chaperones*. 2016; (3): 379-404.

Radovanovic I, Braun N, Giger OT, Mertz K, Miele G, Prinz M, Navarro B, Aguzzi A. Truncated prion protein and Doppel are myelinotoxic in the absence of oligodendrocytic PrPC. *J Neurosci*. 2005; 25(19): 4879-88.

Rasmussen J, Mahler J, Beschorner N, Kaeser SA, Häsler LM, Baumann F, Nyström S, Portelius E, Blennow K, Lashley T, Fox NC, Sepulveda-Falla D, Glatzel M, Oblak AL, Ghetti B, Nilsson KPR, Hammarström P, Staufenbiel M, Walker LC, Jucker M. Amyloid polymorphisms constitute distinct clouds of conformational variants in different etiological subtypes of Alzheimer's disease. *Proc Natl Acad Sci U. S. A..* 2017; 114(49): 13018-13023.

Reddy PH, Mani G, Park BS, Jacques J, Murdoch G, Whetsell W Jr, Kaye J, Manczak M. Differential loss of synaptic proteins in Alzheimer's disease: implications for synaptic dysfunction. *J Alzheimers Dis*. 2005; 7(2): 103-17; discussion 173-80.

Reinwald S, Westner IM, Niedermaier N. Rapidly progressive Alzheimer's disease mimicking Creutzfeldt-Jakob disease. *J Neurol.* 2004; 251(8): 1020-2.

Reitz C, Mayeux R. Alzheimer disease: epidemiology, diagnostic criteria, risk factors and biomarkers. *Biochem Pharmacol*. 2014; 88(4): 640-51.

Richard M, Biacabe AG, Streichenberger N, Ironside JW, Mohr M, Kopp N, Perret-Liaudet A. Immunohistochemical localization of 14.3.3 zeta protein in amyloid plaques in human spongiform encephalopathies. *Acta Neuropathol.* 2003; 105(3): 296-302.

Richter-Landsberg C. The cytoskeleton in oligodendrocytes. Microtubule dynamics in health and disease. *J Mol Neurosci*. 2008; 35(1): 55-63.

Riemenschneider M, Klopp N, Xiang W, Wagenpfeil S, Vollmert C, Müller U, Förstl H, Illig T, Kretzschmar H, Kurz A. Prion protein codon 129 polymorphism and risk of Alzheimer disease. *Neurology.* 2004; 63(2): 364-6.

Roberson ED, Halabisky B, Yoo JW, Yao J, Chin J, Yan F, Wu T, Hamto P, Devidze N, Yu GQ, Palop JJ, Noebels JL, Mucke L. Amyloid-β/Fyn-induced synaptic,

network, and cognitive impairments depend on tau levels in multiple mouse models of Alzheimer's disease. *J Neurosci*. 2011; 31(2): 700-11.

Roher AE, Maarouf CL, Sue LI, Hu Y, Wilson J, Beach TG. Proteomics-derived cerebrospinal fluid markers of autopsy-confirmed Alzheimer's disease. *Biomarkers.* 2009; 14(7): 493-501.

Rombouts SA, Barkhof F, Veltman DJ, Machielsen WC, Witter MP, Bierlaagh MA, Lazeron RH, Valk J, Scheltens P. Functional MR imaging in Alzheimer's disease during memory encoding. *AJNR Am J Neuroradiol*. 2000; 21(10): 1869-75.

Roselli F, Tartaglione B, Federico F, Lepore V, Defazio G, Livrea P. Rate of MMSE score change in Alzheimer's disease: influence of education and vascular risk factors. *Clin Neurol Neurosurg*. 2009; 111(4): 327-30.

Rousset M, Leturque A, Thenet S. The nucleo-junctional interplay of the cellular prion protein: A new partner in cancer-related signaling pathways? *Prion.* 2016; 10(2): 143-52.

Rozemuller JM, Eikelenboom P, Stam FC. Role of microglia in plaque formation in senile dementia of the Alzheimer type. An immunohistochemical study. *Virchows Arch B Cell Pathol Incl Mol Pathol.* 1986; 51(3): 247-54.

Safar JG, Xiao X, Kabir ME, Chen S, Kim C, Haldiman T, Cohen Y, Chen W, Cohen ML, Surewicz WK. Structural determinants of phenotypic diversity and replication rate of human prions. *PLoS Pathog*. 2015; 11(4): e1004832.

Sarnataro D, Campana V, Paladino S, Stornaiuolo M, Nitsch L, Zurzolo C. PrP(C) association with lipid rafts in the early secretory pathway stabilizes its cellular conformation. *Mol Biol Cell.* 2004; 15(9): 4031-42.

Sato K, Kimura M, Sugiyama K, Nishikawa M, Okano Y, Nagaoka H, Nagase T, Kitade Y, Ueda H. Four-and-a-half LIM Domains 1 (FHL1) Protein Interacts with the Rho Guanine Nucleotide Exchange Factor PLEKHG2/FLJ00018 and Regulates Cell Morphogenesis. *J Biol Chem.* 2016; 291(48):25227-25238.

Satoh J, Obayashi S, Misawa T, Sumiyoshi K, Oosumi K, Tabunoki H. Protein microarray analysis identifies human cellular prion protein interactors. *Neuropathol Appl Neurobiol.* 2009; 35(1): 16-35.

Satoh J, Onoue H, Arima K, Yamamura T. The 14-3-3 protein forms a molecular complex with heat shock protein Hsp60 and cellular prion protein. *J Neuropathol Exp Neurol.* 2005; 64(10): 858-68.

Say YH, Hooper NM. Contamination of nuclear fractions with plasma membrane lipid rafts. *Proteomics*. 2007; 7(7): 1059-64.

Scahill RI, Schott JM, Stevens JM, Rossor MN, Fox NC. Mapping the evolution of regional atrophy in Alzheimer's disease: unbiased analysis of fluid-registered serial MRI. *Proc Natl Acad Sci U. S. A.*. 2002; 99(7): 4703-7.

Schaffer C, Sarad N, DeCrumpe A, Goswami D, Herrmann S, Morales J, Patel P, Osborne J. Biomarkers in the Diagnosis and Prognosis of Alzheimer's Disease. *J Lab Autom.* 2015; 20(5): 589-600.

Schindler CK, Heverin M, Henshall DC. Isoform- and subcellular fraction-specific differences in hippocampal 14-3-3 levels following experimentally evoked seizures and in human temporal lobe epilepsy. *J Neurochem*. 2006; 99(2): 561-9.

Schmidt C, Haïk S, Satoh K, Rábano A, Martinez-Martin P, Roeber S, Brandel JP, Calero-Lara M, de Pedro-Cuesta J, Laplanche JL, Hauw JJ, Kretzschmar H, Zerr I. Rapidly progressive Alzheimer's disease: a multicenter update. *J Alzheimers Dis*. 2012; 30(4): 751-6.

Schmidt C, Redyk K, Meissner B, Krack L, von Ahsen N, Roeber S, Kretzschmar H, Zerr I. Clinical features of rapidly progressive Alzheimer's disease. *Dement Geriatr Cogn Disord.* 2010; 29(4): 371-8.

Schmidt C, Wolff M, Weitz M, Bartlau T, Korth C, Zerr I. Rapidly progressive Alzheimer disease. *Arch Neurol.* 2011; 68(9): 1124-30.

Schmitt-Ulms G, Legname G, Baldwin MA, Ball HL, Bradon N, Bosque PJ, Crossin KL, Edelman GM, DeArmond SJ, Cohen FE, Prusiner SB. Binding of neural cell adhesion molecules (N-CAMs) to the cellular prion protein. *J Mol Biol*. 2001; 314(5): 1209-25.

Schmitz M, Zafar S, Silva CJ, Zerr I. Behavioral abnormalities in prion protein knockout mice and the potential relevance of PrP(C) for the cytoskeleton. *Prion.* 2014; 8(6): 381-6.

Schmitz-Abe K, Ciesielski SJ, Schmidt PJ, Campagna DR, Rahimov F, Schilke BA, Cuijpers M, Rieneck K, Lausen B, Linenberger ML, Sendamarai AK, Guo C, Hofmann I, Newburger PE, Matthews D, Shimamura A, Snijders PJ, Towne MC, Niemeyer CM, Watson HG, Dziegiel MH, Heeney MM, May A, Bottomley SS, Swinkels DW, Markianos K, Craig EA, Fleming MD. Congenital sideroblastic anemia due to mutations in the mitochondrial HSP70 homologue HSPA9. *Blood*. 2015; 126(25): 2734-8.

Schubert J, Siekierska A, Langlois M, May P, Huneau C, Becker F, Muhle H, Suls A, Lemke JR, de Kovel CG, Thiele H, Konrad K, Kawalia A, Toliat MR, Sander T, Rüschendorf F, Caliebe A, Nagel I, Kohl B, Kecskés A, Jacmin M, Hardies K, Weckhuysen S, Riesch E, Dorn T, Brilstra EH, Baulac S, Møller RS, Hjalgrim H, Koeleman BP; EuroEPINOMICS RES Consortium, Jurkat-Rott K, Lehman-Horn F, Roach JC, Glusman G, Hood L, Galas DJ, Martin B, de Witte PA, Biskup S, De Jonghe P, Helbig I, Balling R, Nürnberg P, Crawford AD, Esguerra CV, Weber YG, Lerche H. Mutations in STX1B, encoding a presynaptic protein, cause fever-associated epilepsy syndromes. *Nat Genet*. 2014; 46(12): 1327-32.

Scott-McKean JJ, Surewicz K, Choi JK, Ruffin VA, Salameh AI, Nieznanski K, Costa ACS, Surewicz WK. Soluble prion protein and its N-terminal fragment prevent impairment of synaptic plasticity by Aβ oligomers: Implications for novel therapeutic strategy in Alzheimer's disease. *Neurobiol Dis*. 2016; 91: 124-131.

Selkoe DJ, Brown BA, Salazar FJ, Marotta CA. Myelin basic protein in Alzheimer disease neuronal fractions and mammalian neurofilament preparations. *Ann Neurol*. 1981; 10(5): 429-36.

Sengupta A, Grundke-Iqbal I, Iqbal K. Regulation of phosphorylation of tau by protein kinases in rat brain. *Neurochem Res*. 2006; 31(12): 1473-80.

Setsuie R, Wada K. The functions of UCH-L1 and its relation to neurodegenerative diseases*. Neurochem Int*. 2007; 51(2-4): 105-11.

Shankar GM, Li S, Mehta TH, Garcia-Munoz A, Shepardson NE, Smith I, Brett FM, Farrell MA, Rowan MJ, Lemere CA, Regan CM, Walsh DM, Sabatini BL, Selkoe DJ. Amyloid-beta protein dimers isolated directly from Alzheimer's brains impair synaptic plasticity and memory. *Nat Med.* 2008; 14(8): 837-42.

Shearin H, Bessen RA. Axonal and transynaptic spread of prions. *J Virol*. 2014; 88(15): 8640-55.

Shen L, Liao L, Chen C, Guo Y, Song D, Wang Y, Chen Y, Zhang K, Ying M, Li S, Liu Q, Ni J. Proteomics Analysis of Blood Serums from Alzheimer's Disease Patients Using iTRAQ Labeling Technology. *J Alzheimers Dis*. 2017; 56(1): 361-378

Sherman, M. A., & Lesné, S. E. (2011). Alzheimer's Disease and Frontotemporal Dementia. (E. D. Roberson, Ed.) (Vol. 670). Totowa, NJ: *Humana Press*. https://doi.org/10.1007/978-1-60761-744-0

Simard AR, Soulet D, Gowing G, Julien JP, Rivest S. Bone marrow-derived microglia play a critical role in restricting senile plaque formation in Alzheimer's disease. *Neuron.* 2006; 49(4): 489-502.

Singh N, Das D, Singh A, Mohan ML. Prion protein and metal interaction: physiological and pathological implications. *Curr Issues Mol Biol.* 2010; 12(2): 99-107.

Smith LM, Strittmatter SM. Binding Sites for Amyloid-β Oligomers and Synaptic Toxicity. *Cold Spring Harb Perspect Med.* 2017; 7(5). pii: a024075.

Sonnenberg A, Liem RK. Plakins in development and disease. *Exp Cell Res*. 2007; 313(10): 2189-203.

Spiegel R, Pines O, Ta-Shma A, Burak E, Shaag A, Halvardson J, Edvardson S, Mahajna M, Zenvirt S, Saada A, Shalev S, Feuk L, Elpeleg O. Infantile cerebellar-retinal degeneration associated with a mutation in mitochondrial aconitase, ACO2. *Am J Hum Genet.* 2012; 90(3): 518-23.

Spielhaupter C, Schätzl HM. PrPC directly interacts with proteins involved in signaling pathways. *J Biol Chem*. 2001; 276(48): 44604-12.

Stephenson JR, Wang X, Perfitt TL, Parrish WP, Shonesy BC, Marks CR, Mortlock DP, Nakagawa T, Sutcliffe JS, Colbran RJ. A Novel Human CAMK2A Mutation Disrupts Dendritic Morphology and Synaptic Transmission, and Causes ASD-Related Behaviors. *J Neurosci*. 2017; 37(8): 2216-2233.

Stöckl MT, Zijlstra N, Subramaniam V. α-Synuclein oligomers: an amyloid pore? Insights into mechanisms of α-synuclein oligomer-lipid interactions. *Mol Neurobiol.* 2013; 47(2): 613-21.

Stoeck K, Schmitz M, Ebert E, Schmidt C, Zerr I. Immune responses in rapidly progressive dementia: a comparative study of neuroinflammatory markers in Creutzfeldt-Jakob disease, Alzheimer's disease and multiple sclerosis. *J Neuroinflammation.* 2014; 11: 170.

Stork PJ, Schmitt JM. Crosstalk between cAMP and MAP kinase signaling in the regulation of cell proliferation. *Trends Cell Biol.* 2002; 12(6): 258-66.

Strittmatter WJ, Roses AD. Apolipoprotein E and Alzheimer disease. *Proc Natl Acad Sci.* U. S. A.. 1995; 92(11): 4725-7.

Strom A, Wang GS, Picketts DJ, Reimer R, Stuke AW, Scott FW. Cellular prion protein localizes to the nucleus of endocrine and neuronal cells and interacts with structural chromatin components. *Eur J Cell Biol.* 2011; 90(5): 414-9.

Stroud MJ, Nazgiewicz A, McKenzie EA, Wang Y, Kammerer RA, Ballestrem C. GAS2-like proteins mediate communication between microtubules and actin through interactions with end-binding proteins. *J Cell Sci.* 2014; 127(Pt 12): 2672-82.

Stroylova YY, Kiselev GG, Schmalhausen EV, Muronetz VI. Prions and chaperones: friends or foes? *Biochemistry (Mosc).* 2014; 79(8): 761-75.

Stuermer CA, Langhorst MF, Wiechers MF, Legler DF, Von Hanwehr SH, Guse AH, Plattner H. PrPc capping in T cells promotes its association with the lipid raft proteins reggie-1 and reggie-2 and leads to signal transduction.*FASEB J.* 2004; 18(14): 1731-3.

Sultana R, Boyd-Kimball D, Cai J, Pierce WM, Klein JB, Merchant M, Butterfield DA. Proteomics analysis of the Alzheimer's disease hippocampal proteome. *J Alzheimers Dis*. 2007; 11(2): 153-64.

Sunyach C, Jen A, Deng J, Fitzgerald KT, Frobert Y, Grassi J, McCaffrey MW, Morris R. The mechanism of internalization of glycosylphosphatidylinositol-anchored prion protein. *EMBO J.* 2003; 22(14): 3591-601.

Suozzi KC, Wu X, Fuchs E. Spectraplakins: master orchestrators of cytoskeletal dynamics. *J Cell Biol.* 2012; 197(4): 465-75.

Swanger SA, Mattheyses AL, Gentry EG, Herskowitz JH. ROCK1 and ROCK2

inhibition alters dendritic spine morphology in hippocampal neurons. *Cell Logist.* 2016; 5(4): e1133266.

Tai HC, Serrano-Pozo A, Hashimoto T, Frosch MP, Spires-Jones TL, Hyman BT. The synaptic accumulation of hyperphosphorylated tau oligomers in Alzheimer disease is associated with dysfunction of the ubiquitin-proteasome system. *Am J Pathol.* 2012; 181(4): 1426-35.

Takano M, Yamashita T, Nagano K, Otani M, Maekura K, Kamada H, Tsunoda S, Tsutsumi Y, Tomiyama T, Mori H, Matsuura K, Matsuyama S. Proteomic analysis of the hippocampus in Alzheimer's disease model mice by using two-dimensional fluorescence difference in gel electrophoresis. *Neurosci Lett.* 2013; 534: 85-9.

Takenouchi T, Kosaki R, Niizuma T, Hata K, Kosaki K. Macrothrombocytopenia and developmental delay with a de novo CDC42 mutation: Yet another locus for thrombocytopenia and developmental delay. *Am J Med Genet A.* 2015; 167A (11): 2822-5.

Takito J, Yan L, Ma J, Hikita C, Vijayakumar S, Warburton D, Al-Awqati Q. Hensin, the polarity reversal protein, is encoded by DMBT1, a gene frequently deleted in malignant gliomas. *Am J Physiol.* 1999; 277(2): F277-89.

Tas RP, Kapitein LC. Exploring cytoskeletal diversity in neurons. *Science.* 2018; 361(6399): 231-232.

Taylor DR, Whitehouse IJ, Hooper NM. Glypican-1 mediates both prion protein lipid raft association and disease isoform formation. *PLoS Pathog.* 2009; 5(11): e1000666.

Thal DR, Rüb U, Orantes M, Braak H. Phases of A beta-deposition in the human brain and its relevance for the development of AD. *Neurology.* 2002; 58(12): 1791-800.

Thomas T, Miners S, Love S. Post-mortem assessment of hypoperfusion of cerebral cortex in Alzheimer's disease and vascular dementia. *Brain.* 2015; 138(Pt 4): 1059-69.

Tisdale EJ, Bourne JR, Khosravi-Far R, Der CJ, Balch WE. GTP-binding mutants of rab1 and rab2 are potent inhibitors of vesicular transport from the endoplasmic reticulum to the Golgi complex. *J Cell Biol.* 1992; 119(4): 749-61.

Tombaugh TN, McDowell I, Kristjansson B, & Hubley AM. Mini-Mental State Examination (MMSE) and the Modified MMSE (3MS): A psychometric comparison and normative data. *Psychological Assessment.* 1996; 8(1), 48-59.

Tosto G, Gasparini M, Brickman AM, Letteri F, Renie' R, Piscopo P, Talarico G, Canevelli M, Confaloni A, Bruno G. Neuropsychological predictors of rapidly progressive Alzheimer's disease. *Acta Neurol Scand.* 2015; 132(6): 417-22.

Triantafilou K, Triantafilou M, Dedrick RL. A CD14-independent LPS receptor cluster. Nat Immunol. 2001 Apr; 2(4): 338-45. Erratum in: *Nat Immunol* 2001; 2(7): 658.

Tribouillard-Tanvier D, Carroll JA, Moore RA, Striebel JF, Chesebro B. Role of cyclophilin A from brains of prion-infected mice in stimulation of cytokine release by microglia and astroglia *in vitro*. *J Biol Chem.* 2012; 287(7): 4628-39.

Tsutsui S, Hahn JN, Johnson TA, Ali Z, Jirik FR. Absence of the cellular prion protein exacerbates and prolongs neuroinflammation in experimental autoimmune encephalomyelitis. *Am J Pathol.* 2008; 173(4): 1029-41.

Turk E, Teplow DB, Hood LE, Prusiner SB. Purification and properties of the cellular and scrapie hamster prion proteins. *Eur J Biochem.* 1988; 176(1): 21-30.

Um JW, Strittmatter SM. Amyloid-β induced signaling by cellular prion protein and Fyn kinase in Alzheimer disease. *Prion*. 2013; 7(1): 37-41.

Usenovic M, Niroomand S, Drolet RE, Yao L, Gaspar RC, Hatcher NG, Schachter J, Renger JJ, Parmentier-Batteur S. Internalized Tau Oligomers Cause Neurodegeneration by Inducing Accumulation of Pathogenic Tau in Human Neurons Derived from Induced Pluripotent Stem Cells. *J Neurosci.* 2015; 35(42): 14234-50.

Valente L, Tiranti V, Marsano RM, Malfatti E, Fernandez-Vizarra E, Donnini C, Mereghetti P, De Gioia L, Burlina A, Castellan C, Comi GP, Savasta S, Ferrero I, Zeviani M. Infantile encephalopathy and defective mitochondrial DNA translation in patients with mutations of mitochondrial elongation factors EFG1 and EFTu. Am J Hum Genet. 2007 Jan; 80(1): 44-58. Epub 2006 Nov 15. Erratum in: *Am J Hum Genet.* 2007; 80(3): 580.

Vassallo N, Herms J, Behrens C, Krebs B, Saeki K, Onodera T, Windl O, Kretzschmar

HA. Activation of phosphatidylinositol 3-kinase by cellular prion protein and its role in cell survival. *Biochem Biophys Res Commun*. 2005; 332(1): 75-82.

Vassar R, Kuhn PH, Haass C, Kennedy ME, Rajendran L, Wong PC, Lichtenthaler SF. Function, therapeutic potential and cell biology of BACE proteases: current status and future prospects. *J Neurochem*. 2014; 130(1): 4-28.

Vesa J, Hellsten E, Verkruyse LA, Camp LA, Rapola J, Santavuori P, Hofmann SL, Peltonen L. Mutations in the palmitoyl protein thioesterase gene causing infantile neuronal ceroid lipofuscinosis. *Nature.* 1995; 376(6541): 584-7.

Walsh DM, Klyubin I, Fadeeva JV, Cullen WK, Anwyl R, Wolfe MS, Rowan MJ, Selkoe DJ. Naturally secreted oligomers of amyloid beta protein potently inhibit hippocampal long-term potentiation *in vivo*. *Nature.* 2002; 416(6880): 535-9.

Wang JZ, Xia YY, Grundke-Iqbal I, Iqbal K. Abnormal hyperphosphorylation of tau: sites, regulation, and molecular mechanism of neurofibrillary degeneration. *J Alzheimers Dis.* 2013; 33 Suppl 1: S123-39.

Wang W, Chen R, Luo K, Wu D, Huang L, Huang T, Xiao G. Calnexin inhibits thermal aggregation and neurotoxicity of prion protein. *J Cell Biochem.* 2010; 111(2): 343-9.

Wang XF, Dong CF, Zhang J, Wan YZ, Li F, Huang YX, Han L, Shan B, Gao C, Han J, Dong XP. Human tau protein forms complex with PrP and some GSS- and fCJD-related PrP mutants possess stronger binding activities with tau *in vitro*. *Mol Cell Biochem.* 2008; 310(1-2): 49-55.

Wang Y, Mandelkow E. Tau in physiology and pathology. *Nat Rev Neurosci.* 2016; 17(1): 5-21.

Weil D, D'Alessio M, Ramirez F, Eyre DR. Structural and functional characterization of a splicing mutation in the pro-alpha 2(I) collagen gene of an Ehlers-Danlos type VII patient. *J Biol Chem.* 1990; 265(26): 16007-11.

Weise J, Sandau R, Schwarting S, Crome O, Wrede A, Schulz-Schaeffer W, Zerr I, Bähr M. Deletion of cellular prion protein results in reduced Akt activation, enhanced postischemic caspase-3 activation, and exacerbation of ischemic brain injury. *Stroke.* 2006; 37(5): 1296-300.

Weston PSJ, Poole T, Ryan NS, Nair A, Liang Y, Macpherson K, Druyeh R, Malone IB, Ahsan RL, Pemberton H, Klimova J, Mead S, Blennow K, Rossor MN, Schott JM, Zetterberg H, Fox NC. Serum neurofilament light in familial Alzheimer disease: A marker of early neurodegeneration. *Neurology.* 2017; 89(21): 2167-2175.

Whitehouse IJ, Miners JS, Glennon EB, Kehoe PG, Love S, Kellett KA, Hooper NM. Prion protein is decreased in Alzheimer's brain and inversely correlates with BACE1 activity, amyloid-β levels and Braak stage. *PLoS One.* 2013; 8(4): e59554.

Whiten DR, Cox D, Horrocks MH, Taylor CG, De S, Flagmeier P, Tosatto L, Kumita JR, Ecroyd H, Dobson CM, Klenerman D, Wilson MR. Single-Molecule Characterization of the Interactions between Extracellular Chaperones and Toxic α-Synuclein Oligomers. *Cell Rep.* 2018; 23(12): 3492-3500.

Wilding BR, McGrath MJ, Bonne G, Mitchell CA. FHL1 mutants that cause clinically distinct human myopathies form protein aggregates and impair myoblast differentiation. *J Cell Sci.* 2014; 127(Pt 10): 2269-81.

Williams RS, Bate C. An *in vitro* model for synaptic loss in neurodegenerative diseases suggests a neuroprotective role for valproic acid via inhibition of cPLA2 dependent signalling. *Neuropharmacology.* 2016; 101: 566-75.

Wu CH, Fallini C, Ticozzi N, Keagle PJ, Sapp PC, Piotrowska K, Lowe P, Koppers M, McKenna-Yasek D, Baron DM, Kost JE, Gonzalez-Perez P, Fox AD, Adams J, Taroni F, Tiloca C, Leclerc AL, Chafe SC, Mangroo D, Moore MJ, Zitzewitz JA, Xu ZS, van den Berg LH, Glass JD, Siciliano G, Cirulli ET, Goldstein DB, Salachas F, Meininger V, Rossoll W, Ratti A, Gellera C, Bosco DA, Bassell GJ, Silani V, Drory VE, Brown RH Jr, Landers JE. Mutations in the profilin 1 gene cause familial amyotrophic lateral sclerosis.*Nature.* 2012; 488(7412): 499-503.

Wyss-Coray T. Inflammation in Alzheimer disease: driving force, bystander or beneficial response? *Nat Med.* 2006; 12(9): 1005-15.

Yacoubian TA, Slone SR, Harrington AJ, Hamamichi S, Schieltz JM, Caldwell KA, Caldwell GA, Standaert DG. Differential neuroprotective effects of 14-3-3 proteins in models of Parkinson's disease. *Cell Death Dis.* 2010; 1: e2.

Yahata T, de Caestecker MP, Lechleider RJ, Andriole S, Roberts AB, Isselbacher KJ, Shioda T. The MSG1 non-DNA-binding transactivator binds to the p300/CBP co-activators, enhancing their functional link to the Smad transcription factors.*J Biol Chem.* 2000; 275(12): 8825-34.

Yang W, Dicker DT, Chen J, El-Deiry WS. CARPs enhance p53 turnover by degrading 14-3-3sigma and stabilizing MDM2. *Cell Cycle*. 2008 Mar 1; 7(5): 670-82.

Yu G, Wang LG, Han Y, He QY. clusterProfiler: an R package for comparing biological themes among gene clusters. *OMICS.* 2012; 16(5): 284-7.

Yu X, Caltagarone J, Smith MA, Bowser R. DNA damage induces cdk2 protein levels and histone H2B phosphorylation in SH-SY5Y neuroblastoma cells. *J Alzheimers Dis.* 2005; 8(1): 7-21.

Zafar S, Asif AR, Ramljak S, Tahir W, Schmitz M, Zerr I. Anchorless 23-230 PrPC interactomics for elucidation of PrPC protective role. *Mol Neurobiol.* 2014; 49(3): 1385-99.

Zafar S, Schmitz M, Younus N, Tahir W, Shafiq M, Llorens F, Ferrer I, Andéoletti O, Zerr I. Creutzfeldt-Jakob Disease Subtype-Specific Regional and Temporal Regulation of ADP Ribosylation Factor-1-Dependent Rho/MLC Pathway at Pre-Clinical Stage. *J Mol Neurosci.* 2015; 56(2): 329-48

Zafar S, Shafiq M, Younas N, Schmitz M, Ferrer I, Zerr I. Prion Protein Interactome: Identifying Novel Targets in Slowly and Rapidly Progressive Forms of Alzheimer's Disease. *J Alzheimers Dis.* 2017; 59(1): 265-275.

Zafar S, von Ahsen N, Oellerich M, Zerr I, Schulz-Schaeffer WJ, Armstrong VW, Asif AR. Proteomics approach to identify the interacting partners of cellular prion protein and characterization of Rab7a interaction in neuronal cells. *J Proteome Res.* 2011; 10(7): 3123-35.

Zafar S, Younas N, Sheikh N, Tahir W, Shafiq M, Schmitz M, Ferrer I, Andréoletti O, Zerr I. Cytoskeleton-Associated Risk Modifiers Involved in Early and Rapid Progression of Sporadic Creutzfeldt - Jakob disease*. Mol Neurobiol.* 2018; 55(5): 4009-4029.

Zahid S, Khan R, Oellerich M, Ahmed N, Asif AR. Differential S-nitrosylation of proteins

in Alzheimer's disease. *Neuroscience.* 2014; 256: 126-36.

Zahn R, Liu A, Lührs T, Riek R, von Schroetter C, López García F, Billeter M, Calzolai L, Wider G, Wüthrich K. NMR solution structure of the human prion protein. *Proc Natl Acad Sci U. S. A..* 2000; 97(1): 145-50.

Zampieri M, Legname G, Segrè D, Altafini C. A system-level approach for deciphering the transcriptional response to prion infection. *Bioinformatics.* 2011 Dec 15; 27(24): 3407-14

Zerr I, Pocchiari M, Collins S, Brandel JP, de Pedro Cuesta J, Knight RS, Bernheimer H, Cardone F, Delasnerie-Lauprêtre N, Cuadrado Corrales N, Ladogana A, Bodemer M, Fletcher A, Awan T, Ruiz Bremón A, Budka H, Laplanche JL, Will RG, Poser S. Analysis of EEG and CSF 14-3-3 proteins as aids to the diagnosis of Creutzfeldt-Jakob disease. *Neurology.* 2000; 55(6): 811-5.

Zerr I, Schmitz M, Karch A, Villar-Piqué A, Kanata E, Golanska E, Díaz-Lucena D, Karsanidou A, Hermann P, Knipper T, Goebel S, Varges D, Sklaviadis T, Sikorska B, Liberski PP, Santana I, Ferrer I, Zetterberg H, Blennow K, Calero O, Calero M, Ladogana A, Sánchez-Valle R, Baldeiras I, Llorens F. Cerebrospinal fluid neurofilament light levels in neurodegenerative dementia: Evaluation of diagnostic accuracy in the differential diagnosis of prion diseases. *Alzheimers Dement.* 2018; 14(6): 751-763.

Zhan X, Jickling GC, Ander BP, Stamova B, Liu D, Kao PF, Zelin MA, Jin LW, DeCarli C, Sharp FR. Myelin basic protein associates with AβPP, Aβ1-42, and amyloid plaques in cortex of Alzheimer's disease brain. *J Alzheimers Dis.* 2015; 44(4): 1213-29.

Zhang Y, Bilbao A, Bruderer T, Luban J, Strambio-De-Castillia C, Lisacek F, Hopfgartner G, Varesio E. The Use of Variable Q1 Isolation Windows Improves Selectivity in LC-SWATH-MS Acquisition. *J Proteome Res*. 2015; 14(10): 4359-71.

Zheng H, Zheng W, Wu C, Yang J, Xi Y, Xie Q, Zhao X, Deng X, Lu G, Li G, Ebbole D, Zhou J, Wang Z. Rab GTPases are essential for membrane trafficking-dependent growth and pathogenicity in Fusarium graminearum. *Environ Microbiol*. 2015; 17(11): 4580-99.

Zhou J, Liu B. Alzheimer's disease and prion protein. *Intractable Rare Dis Res*. 2013; 2(2): 35-44.

8 Abbreviations

µl	Micro liter
µm	Micro meter
ACN	Acetonitrile
AD	Alzheimer’s disease
ADAM	A Disintegrin- And Metalloproteinase
$AgNO_3$	Silver nitrate
AKT / PKB	Protein kinase B
APOE	Apolipoprotein E
APP	Amyloid Precursor Protein
Aβ	amyloid-β
BACE1	beta-site APP cleaving enzyme 1
BSA	Bovine serum albumin
CA1	CA1 region of Hippocampus
CaMKII	Calcium/calmodulin-dependent protein kinase type II
cAMP	Cyclic adenosine monophosphate
CD2AP	CD2 Associated Protein
CERAD	Consortium to Establish a Registry for Alzheimer's Disease
Co-IP	Co-immunoprecipitation
CSF	Cerebrospinal fluid
ddH_2O	Double distilled water
DFTL	Dementia with fronto-temporal lobar degeneration
DIA	Data independent acquisition
DLB	Dementia with Lewy bodies
DSG2	Desmoglein 2
DTT	Dithiothreitol
EDTA	Ethylenediaminetetraacetic acid
eFAD	Early onset familial AD
EOAD	Early onset AD
ERK	Extracellular signal–regulated kinases
Erk	Extracellular signal–regulated kinases
ESI	Electrospray Ionization
FAD	Familial AD
G-CSF	Granulocyte-colony stimulating factor
GPI	Glycophosphatidyl Inositol
GSK3	Glycogen synthase kinase 3-β
HDFs	High Density Fractions
HDP	High density prions
HMW	High molecular weight
IAA	Iodoacetamide
IgG	Immunoglobulin G
IL-13	Interleukin 13
IL-6	Interleukin 6
JNK	C-Jun N-terminal kinases
KCC2	Calcium/calmodulin-dependent protein kinase type II

kD	Kilodalton
LMW	Low molecular weight
LOAD	Late onset AD
LTP	Long-term potentiation
MAPKs	Mitogen-activated protein kinases
MCI	Mild Cognitive Impairment
MCP-1	
MMSE	Mini-Mental State Examination
MS/MS	Mass spectrometry
MYLK	Myosin light chain kinase
$Na_2S_2O_3$	Sodium thiosulfate
NaCl	Sodium chloride
NFkB	Nuclear factor kappa-light-chain-enhancer of activated B cells
NFTs	Neurofibrillary tangles
NH_4HCO_3	Sodium bicarbonate
NP-40	Nonidet P-40
NrCAM	neuronal cell adhesion molecule
^oC	Degree Celsius
p38	Mitogen-activated protein kinases p38
PBS	Phosphate-buffer saline
PCA	Principle Component Analysis
PDM	Product difference of means
PKA	Protein kinase A
PKC	Protein kinase C
PLD3	Phospholipase D3,
PRNP	Prion protein coding gene
PrP	Prion protein
PrP^C	Physiological form of Prion Protein
PrP^{Sc}	Scrapie form of Prion Protein
PSEN1	Presenilin 1
PSEN2	Presenilin 2
p-Tau	Phosphorylated Tau
Q-TOF	Quadrupole-time-of-flight
rDLB	Rapidly progressive dementia with Lewy bodies
recPrP	Recombinant PrP
RFU	Relative fluorescence units
rP	Pearson's linear correlation coefficient
rpAD	Rapidly progressive Alzheimer’s disease
SAPK	stress-activated phospho-kinases
sAPPα	Shed-APP
sCJD	Sporadic Creutzfeldt-Jakob disease
SDS	Sodium dodecyl sulfate
SDS-PAGE	Sodium dodecyl sulfate- Polyacrylamide gel electrophoresis
spAD	Sporadic Alzheimer’s disease
SRC	Proto-oncogene tyrosine-protein kinase

SVD	Small vessel disease
SWATH-MS	Sequential window acquisition of all theoretical mass spectra- Mass spectrometry
$t_{1/2}$	Half life
Tau	Tubulin associated unit
TBS	Tris Buffer saline
TBST	TBS with 0.1% Tween
TEMED	Tetramethylethylenediamine
Th-T	Thioflavin-T
tM	Threshold Mander's coefficient
TNF	Tumor necrosis factor
TREM2	Triggering receptor expressed on myeloid cells 2
Tris	Tris(hydroxymethyl)aminomethane
TSEs	Transmissible Spongiform Encephalopathies

Acknowledgements

First of all, my heartiest gratitude to our group leader Prof. Dr. Inga Zerr. I have had a chance to work under her guidance for my MS thesis, and then to complete my PhD. I consider myself lucky to work with such a motivated and focused leader, during this time, she has influenced a lot, my critical thinking and my scientific attitude, with her inputs, helpful suggestions, and her encouragement. At the same time, the freedom she gave me to follow sundry approaches has also helped me to become a better scientist. I can't thank her enough for providing such an opportunity.

Likewise, I express my heartiest gratitude and respect towards my supervisor, Dr. Saima Zafar. She has been a good teacher, and a very good supervisor. She taught me to think for diverse approaches to resolve the problems. I thank her for involving me in this interesting project. Her encouragement, and support have been vital for developing my confidence.

I express my gratitude to my thesis committee members, Prof. Dr. Thomas Meyer and PD Dr. Michael Hoppert, for their supervision, support and contribution to my work. Their suggestions are highly appreciated.

I am very thankful to Dr. Berta Puig, Beata Szalay and Prof. Dr. Markus Glatzel for they have helped me in conducting a part of my PhD experimentation at the institute of neuropathology, University Medical Center, Eppendorf-Hamburg, during my lab rotation. Many thanks to Prof. Isidre Ferrer for providing the samples and helping to complete the study.

I would also like to thank Dr. Nadeem Sheikh, for his encouragement and support since my bachelor thesis. And, for providing me opportunities that led me to obtain my PhD position. I cannot thank him enough for his assistance. Then, I present my sincere thanks to Dr. Waqas Tahir, for his help in my start at UMG. His support and guidance in my research work are appreciable.

Special thanks to Neelam younas, for her technical and moral support, and for bearing my long boring scientific discussions. I present my thanks to other colleagues and friends of the prion lab, Dr. Matthias Schmitz, Dr. Franc Llorens, Dr. Katrin Ditmar, Dr. Maria Cramm, Dr. Amandeep, Aneeqa, Katrin Thüne, Tobias, Sussana, Angela, Nicco, Barbara, Vivi and Mandy for providing a good work environment and for their direct or indirect help. I am thankful to Dr. Raza Khan for his inputs in the statistics and bioinformatics analysis.

I also acknowledge the support of my good friends during my research blues; specially, Dr. Aamir Nadeem, Zaheer, Umair, Rabia bhabi, Umer, Dr. Shakil, Sidra, Raza, Awais and Abdul-Rehman.

I would like to gratefully appreciate the assistance of Maja Schneider-Dominco and Jolanthe Ehrlich for the whole duration at UMG.

After all, I owe a massive gratitude to my family back home, my brother Qasim bhai, sister Sumaira and specially Amma and Abba; for their immense love, appreciation, support and confidence in me all along.

MOHSIN SHAFIQ

Curriculum vitae

Mohsin Shafiq

Phone: (+49) 176 31658935 | E-mail:

Born **13/09/1989** | Nationality: **Pakistani**

Education

10/2014 – 10/2018 **PhD in Biology**

Georg-August-University Göttingen, Göttingen (Germany)

Dissertation

"Progression rate modifiers in Alzheimer's Disease"

Prion Research Group, Institute of Neurology, UMG, Göttingen

09/2011 – 07/2013 **M.S. Zoology** Masters degree in Science

University of the Punjab, Lahore (Pakistan)

Research Thesis

Cortical Brain specific differential proteome analysis in Experimental Autoimmune Encephalomyelitis

09/2007 – 08/2011 **B.S. Zoology** Bachelor degree in Science

University of the Punjab, Lahore (Pakistan)

Research Thesis

Effects of *Mentha piperita* (oil) on the hematology, serology, gene expression and microanatomy of liver in rats

Work Experience

07/2018 – Present **Researcher**

Institute for Neuropathology, University Medical Center, Eppendorf-Hamburg

09/2012 – 06/2018 **Research Assistant**

Department of Neurology, University Medical Center, Göttingen, Göttingen

09/2009 – 09/2012 **Research Assistant**

Cell and molecular biology lab, Dept. of Zoology, University of the Punjab, Lahore, Pakistan

Peer-reviewed publications

In-Prep

1. **Shafiq M**, Zafar S, Younas N, Noor A, Schmitz M, Puig, B, Jakob, M, Glatzel M, Andréoletti O, Zerr I, (2018), Proteinic interactors of high-density prion protein oligomers in rapidly progressive Alzheimer's disease, and their involvement in cytoskeletal degradation.
2. **Shafiq M**, Zafar S, Younas N, Noor A, Schmitz M, Puig, B, Jakob, M, Glatzel M, Andréoletti O, Zerr I, (2018), Differential amyloid sequestering in rapidly progressive Alzheimer's disease

Published

1. Zafar S, **Shafiq M**, Andréoletti O, Zerr I, Animal TSEs and public health: What remains of past lessons? PLoS Pathog. 2018, 14(2): e1006759. https://doi.org/10.1371/journal.ppat.1006759
2. Zafar S[§], **Shafiq M**[§], Younas N, Schmitz M, Ferre I, Zerr I. (2017) Prion protein interactome: identifying novel targets in slowly and rapidly progressive forms of Alzheimer's disease, Journal of Alzheimer's Disease. 59(1)
3. Zafar S, Younas N, Sheikh N, Tahir W, **Shafiq M**, Schmitz M, Ferre I, Andréoletti O, Zerr I. (2017) Cytoskeleton associated risk modifiers involved in early and rapid progression of sporadic Creutzfeldt-Jakob disease. Mol Neurobiol. 2017, https://doi.org/10.1007/s12035-017-0589-0
4. Zafar S, Younas N, Correia S, **Shafiq M**, Tahir W, Schmitz M, Ferrer I, Andréoletti O, Zerr I. (2016) Strain-Specific Altered Regulatory Response of Rab7a and Tau in Creutzfeldt-Jakob Disease and Alzheimer's Disease. Mol Neurobiol.54(1):697-709. doi: 10.1007/s12035-016-9694-8.
5. Zafar S, Schmitz M, Younus N, Tahir W, **Shafiq M**, Llorens F, Ferrer I, Andéoletti O, Zerr I. (2015) Creutzfeldt-Jakob Disease Subtype-Specific Regional and Temporal Regulation of ADP Ribosylation Factor-1-Dependent Rho/MLC Pathway at Pre-Clinical Stage." Journal of Molecular Neuroscience: 1-20.
6. Llorens F, Zafar S, Ansoleaga B, **Shafiq M**, Blanco R, Carmona M, Grau-Rivera, O, et al. (2015) Subtype and regional regulation of prion biomarkers in sporadic Creutzfeldt–Jakob disease. Neuropathology and applied neurobiology.

7. Llorens F, Kruse N, Schmitz M, **Shafiq M**, Gomes da Cunha JE, Gotzman N, Zafar S, et al. (2015) Quantification of CSF biomarkers using an electrochemiluminescence-based detection system in the differential diagnosis of AD and sCJD. Journal of neurology: 1-7.

Presentations

Progression rate modifiers in Alzheimer's disease - Seminar Presentation. Presented in **Deutsches Zentrum für Neurodegenerative Erkrankungen (DZNE),** September 28th, 2017. Göttingen

Progression rate modifiers in Alzheimer's disease - UPDATE. Presented in **Abschlusssymposium, Kompetenznetz Degenerative Demenz (KNDD),** June the 29th – 30th, 2017. Göttingen

Identification and characterization of slow and fast progressive AD modifiers. Presented in **Statuskolloquium, Kompetenznetz Degenerative Demenz (KNDD),** December the 13th-14th, 2016. Göttingen

Alzheimer's disease and corresponding progression rate modifiers, Seminar in **Department of Zoology, University of the Punjab, Lahore, Pakistan.** October the 21st , 2016. Lahore

Identification and characterization of slow and fast progressive AD modifiers. Presented in **Statuskolloquium, Kompetenznetz Degenerative Demenz (KNDD),** December the 9th and 10th, 2015, Bonn.

Identification and characterization of Large Fibrillar Amyloid plaques to Small Non-amyloid oligomeric forms in neurodegeneration. Presented in **Forschungskonferenz, Universitätsmedizin Göttingen. Abteilungen: Neurologie und Neuropathologie.** September the 5th, 2015. Göttingen.

Identification and characterization of Large Fibrillar Amyloid plaques to Small Non-amyloid oligomeric forms in neurodegeneration. Seminar presentation at **European Neuroscience institute (ENI)**, February the 17th, 2015, Göttingen.

Posters presented and contributed

Shafiq M, Zafar S, Younas N, Shcmitz M, Ferrer I, and Zerr I. Differential cerebral localization of prion protein in rapidly progressive Alzheimer's disease. Presented in Prion Conference, **2017,** Edinburgh, Scotland

Shafiq M, Zafar S, Younas N, Shcmitz M, Ferrer I, and Zerr I. Prion protein interactome: identifying novel targets in rapidly progressive Alzheimer's disease. Presented in Prion Conference, **2016,** Tokyo, Japan

Younas N, Zafar S, **Shafiq M**, Tahir W, Shcmitz M, Ferrer I, Andreoletti O, and Zerr I, Early response of Cofilin1 pathway in Creutzfeldt Jakob disease. Presented in Prion Conference. **2016** Tokyo, Japan

Shafiq M, Llorens F, Zafar S, and Zerr I. Alpha-Synuclein: A potential Cerebrospinal fluid biomarker for differentiation of CJD from AD. Presented in Prion Conference **2015, CSU, Fort Collins, USA**.

Llorens F, Zafar S, Ansoleaga B, **Shafiq M**, Blanco R, Carmona M, Gelpi E, Del rio JA, Zerr I, and Ferre I. Subtype and regional regulation of prion biomarkers in sporadic Creutzfeldt-jakob disease. Presented at Prion Conference, **2014,** Trieste.

Shafiq M, Zafar S, Schmitz M, Sheikh N and Zerr I. Temporal degradation of prion biomarkers and relative efficacy of different storage tubes. Presented at Prion Conference, **2013, Banff, Canada**.

Tahir W, Zafar S, Nessler S, Arora AD, **Shafiq M**, Schmitz M, Stadelmann C. and Zerr I. Characterization of truncated forms of cellular prion protein under inflammatory and demyelinating stress condition by proteomic analysis of the Spinal Cord. Presented at Prion Conference, **2013, Banff, Canada**